Winter 2011

Hydrogenation of nanostructured carbon, synthesis of organic semiconductors and progress towards synthesis of fullerenes and nanoribbons from polyaromatic hydrocarbons

Jeremy T. Kintigh
University of New Hampshire, Durham

HYDROGENATION OF NANOSTRUCTURED CARBON, SYNTHESIS OF ORGANIC SEMICONDUCTORS AND PROGRESS TOWARDS SYNTHESIS OF FULLERENES AND NANORIBBONS FROM POLYAROMATIC HYDROCARBONS

BY

JEREMY T. KINTIGH
Bachelor of Science in Chemistry, University of Massachusetts - Amherst, 2000

DISSERTATION

Submitted to the University of New Hampshire
in Partial Fulfillment of
the Requirements for the Degree of

Doctor of Philosophy
in
Chemistry

December, 2011

This dissertation has been examined and approved.

Dissertation Director, Prof. Glen P. Miller,
Director, Material Science Program
Professor, Department of Chemistry

Prof. Richard P. Johnson, Professor, Department of Chemistry

Prof. W. Rudolf Seitz, Professor, Department of Chemistry

Prof. Arthur Greenburg, Professor, Department of Chemistry

Prof. Dhandapani Venkataraman, Associate Professor,
Department of Chemistry, University of Massachusetts

Dec 8th, 2011
Date

Dedicated in loving memory

To

Elizabeth Lytle Kintigh

September 2nd, 1946 - January 30th, 2008

"Facts are stubborn things, and whatever may be our wishes, our inclinations, or the dictums of our passions, they cannot alter the state of facts and evidence."

-John Adams, 1770

ACKNOWLEDGEMENTS

First and foremost I would like to acknowledge my parents Dana and Elizabeth Kintigh who have been there throughout my life and were my guiding light during the darkest of times. Without their strength and commitment my journey would have been almost impossible. My brother Seth, my nephew Tyler, my many aunts, uncles and cousins have all supported me without hesitation for which I will forever be grateful. I thank all my friends, who are far too many to list; your friendship and generosity will never be forgotten. I would like to acknowledge my advisor Prof. Glen P. Miller whose patience and understanding has been vital for my success in his group and in the department. I would also like to acknowledge my committee Prof. Rudy Seitz, Prof. Arthur Greenberg, Prof. Richard Johnson and a special thanks to Prof. Dhandapani Venkataraman who was also my undergraduate advisor. I owe a great deal of thanks to Dr. Jennifer Hodgson who helped with calculations that are detailed in this thesis. Also, thanks to Jon Briggs for helping with the x-ray crystallography. Special thanks go to Randy Pierce and his guide dog The Mighty Quinn. His inspiration and perseverance has been nothing short of amazing and I am truly thankful for his friendship. My many thanks to Katharine Liu; we both shared far too much tragedy, but through supporting each other we were able to endure, grieve and grow. I would like to thank the Miller group past and present including Dr. Weimin Lin, Dr. Chandrani Pamanik,Ye Xi, Lei Zhou, Yushu Li, Shunfu Hu, Simka Ellis, Hao Geng, Joe Dunn, Dr. James Rainbolt, Dr. Andrew Athans, Dr. Ryan Kopreski and Dr. Weling Jia, Dr. Jung-Fu Liu, and Dr. Mikaël Jazdzyk.

TABLE OF CONTENTS

DEDICATION....iii

ACKNOWLEDGEMENTS....iv

LIST OF FIGURES....x

LIST OF SCHEMES....xiv

LIST OF TABLES....xvi

LIST OF NUMBERED STRUCTURES....xvii

ABSTRACT....xx

CHAPTER PAGE

CHAPTER 1: Introduction....1

1.1 Fullerenes....1

1.1.1 History of Fullerenes....1

1.1.2 Natural Occurrence of Fullerenes....2

1.1.3 Synthesis of Fullerenes....2

1.1.4 Hydrogenation of Fullerenes....3

1.2 Nanotubes....5

1.2.1 Discovery and Synthesis of Nanotubes....5

1.2.2 Hydrogenation of Nanotubes....8

1.3 Graphene....11

1.3.1 Nomenclature and Discovery....11
1.3.2 Discovery and Synthesis of Graphene....12
1.3.3 Hydrogenation of Graphene to Graphane....17
1.4 Acenes....20
1.4.1 Background on Acenes....20
1.4.2 Synthesis of Unsubstituted Acenes....22
1.4.3 Synthesis of Substituted Acenes....25

CHAPTER 2: Synthesis of Fulleranes and Hydrogenated SWNTs....30
2.1 Fulleranes....30
2.1.1 Background of Polyamine Hydrogenation of [60]Fullerene....30
2.1.2 Long Chain Polyamine Hydrogenation of [60]Fullerene and [70]Fullerene....33
2.1.3 Transition Metal Catalyzed Polyamine Hydrogenation of [60]Fullerene....37
2.1.4 Exploration of Mechanism/Unusual Amines for Hydrogenation..41
2.1.5 Proposed Synthesis of S_6-$C_{60}H_{24}$....47
2.2 Hydrogenated Single-Walled Nanotubes....51
2.2.1 Hydrogenation and Characterization of SWNTs....51

CHAPTER 3: Synthesis of Graphane....60
3.1 Graphane....60

3.1.1 Exfoliation of Graphene from Graphite and HOPG using high boiling Hydrocarbon Solvents....60

3.1.2 Hydrogenation and Exfoliation of bulk Graphite and HOPG....64

3.1.3 Characterization of Graphane....70

CHAPTER 4: Synthesis of Bisacenes, Periacenes and Thiaacenes....76

4.1 Bisacenes and Periacenes....76

4.1.1 Background....76

4.1.2 Synthesis of Unsubstiuted Bipentacene....78

4.1.3 Synthesis of Peripentacenequinone....83

4.1.4 Proposed Synthesis of Substituted Bipentacenes....86

4.1.5 Proposed Synthesis of Substituted Peripentacenes....90

4.2 Trithiacenes and Hexathiacenes....92

4.2.1 Background of Hexathiapentacene (HTP)....92

4.2.2 Synthesis and Characterization of Trithiaacenes....93

4.2.3 Proposed Synthesis of Substituted TTPO Derivatives....99

4.2.4 Progress Towards the Synthesis of Fused Bistrithiapentaceneones and Trithiaperipentaceneone....100

CHAPTER 5: Towards the rational synthesis of fullerenes and nanoribbons from hydrogenated polyaromatic hydrocarbons....103

5.1 Synthesis of Fullerenes....103

5.1.1 Towards the Synthesis of [60]Fullerene....103

5.2 Synthesis of Graphene Nanoribbons....108

5.2.1 Initial Discovery....108

5.2.2 Oligoperipentacenes as Graphene Nanoribbons....112

5.2.3 Attempted Synthesis of Soluble Nanoribbons....117

CHAPTER 6: Conclusion....127

CHAPTER 7: EXPERIMENTAL DATA....130

7.1 General Method....130

7.2 Solvents....131

7.3 Reagents....132

7.4 Synthesis....135

7.4.1 General Hydrogenation Synthesis....135

7.4.2 General Exfoliation Reaction....137

7.4.3 Test Reactions of [60]Fullerene with various amines....138

7.4.4 Small Molecule Organic Synthesis....142

REFERENCES....156

APPENDIX....S1

LIST OF FIGURES

Number Page

1 Structure of [60]fullerene....2

2 Top and side views of C_{3v} $C_{60}H_{18}$ fullerane with a crown-like structure....4

3 First images of MWNTs and SWNTs....5

4 Schematic of a flattened nanotubes surface illustrating zigzag (n,0), armchair (n,n), and chiral (C_h) nanotubes....6

5 Intensity comparison of hydrogenated SWNTs and hydrocarbons in SWNT samples....9

6 Graphite's structure....11

7 Idealized structure of graphite oxide (GO)....14

8 Structures of acenes....20

9 Numbering of Pentacene....21

10 ^{1}H NMR spectra of [70]fullerane ($CDCl_3$, ppm scale) produced after 1 week in boiling DET and 15 h in DET at 300 °C....35

11 LDI mass spectrum of a 1-phenylnaphthalene extract of Kratschmer-Huffman soot before hydrogenation....36

12 ^{1}H NMR spectrum (top, C_6D_6, ppm scale) and LDI mass spectrum (bottom) of [60]fullerane produced after 15 h in boiling PEH with 5 weight % Co added....38

13 ^{1}H NMR of the amination of [60]fullerenes from diproplyenetriamine....43

14 Proposed structure of S_6-$C_{60}H_{24}$.....47

15 ^{1}H-NMR spectra of the products from the [60]fullerenes/TETA reaction.....48

16 ^{13}C-NMR spectra of the products from the [60]fullerenes/TETA reaction.....49

17 HPLC profile for the separation of the products from the [60]fullerenes/TEPA reaction.....50

18 Comparison between H-SWNTs (left) and as purchased SWNTs (right) suspended in methanol.....54

19 TEM of nanotubes before hydrogenation (left) and after hydrogenation (right) (at 25000x).....55

20 TEM of SWNTs after thermal annealing in which bundling is clearly seen (at 160000x).....56

21 Raman spectra of SWNTs and H-SWNTs.....57

22 IR spectra of H-SWNTs in Fluorolube mull.....58

23 Examples of graphene from exfoliation with naphthalene (let) and adamantane (right) (scale of bar is 200 nm).....62

24 Examples of a multi-layer graphene nanoribbon produced from exfoliation by adamantane (scale of bar is 500 nm).....63

25 SEM images of bulk graphite before (left) and after (right) ball milling (scale of bar is 1 micrometer).....65

26 HRTEM images of nano-onions and MWNT formed from vibrational ball milling.....66

27 TEM images of bulk graphite after milling and hydrogenation containing multi-layered graphane and single sheet-graphane (left) and single-sheet graphane and

graphane nanoribbons (right) (scale of bar is 200 nanometers).....67

28 SEM image of graphane made from bulk graphite (Image taken by Dr. Yolanda Echegoyen).....68

29 TEM images of HOPG after hydrogenation and exfoliation containing multi-layered graphane (left, scale of bar is 2 micrometers) and single sheet-graphane (right) (scale of bar is 200 nanometers).....69

30 Microscope images and Raman spectra of (**a**) Graphene prepared by mechanical exfoliation ("Scotch Tape" method) of HOPG (**b**) Few-layer graphane from polyamine treated HOPG (**c**) Large particles of hydrogenated graphite from HOPG (**d**) Laser annealed hydrogenated graphite (Figures constructed by Dr. Bogdan Diaconescu).....71

31 Comparison of Raman spectra of graphene (blue) and graphane (red).....73

32 Hydrogenation of single layer graphene on Ru(0001). (Figures constructed by Dr. Bogdan Diaconescu).....75

33 X-Ray crystal structure of compound **4.3**.....80

34 UV/Vis spectrum of compound **4.5**.....81

35 Mass spectrum of bipentacene and its di-endoperoxide derivative.....82

36 Mass spectrometry of compound **4.8**.....84

37 UV/Vis spectrum of compound **4.8**.....85

38 Unit cell for the crystal structure of trithaipentaceneone (TTPO).....95

39 Head-to-Tail arrangement of TTPO and columnar stacking as observed in the x-ray crystal structure.....96

40 DFT NBO population analysis of TTPO at B3LYP/6-311+G(d,p) (Calculations performed by Dr. Jennifer Hodgson).....97

41 Thermal evaporation of **4.13** onto a SiO_2 wafer.....99

42 Drain-source current versus drain-source voltage behavior as a function of gate voltage.....99

43 Mass spectrometry of [60]fullerene/**5.6** reaction.....110

44 Laser desorption ionization mass spectrum of oligoperitetracenes or nanoribbons formed in the reaction between [60]fullerene and **5.6**. The 'n' indicates the number of tetracene repeat units in the nanoribbon.....112

45 Mass spectrometry of the pentacene nanoribbons from insoluble material in **5.8**/**5.10** reaction, 'n' indicates the number of pentacene repeat units in the nanoribbon.116

46 Examples of 'head-to-tail' substituted tetracene and pentacene nanoribbons.....119

47 Mass spectrum of soluble tetracene nanoribbons in the reaction between **5.16** and **5.18**. The 'n' indicates the number of tetracene repeat units in the nanoribbon.....124

48 Mass spectrum of soluble pentacene nanoribbons in the reaction between **5.17** and **5.19**. The 'n' indicates the number of pentacene repeat units in the nanoribbon.....125

LIST OF SCHEMES

Number		Page
1	Total synthesis of [60]fullerene	3
2	Generic scheme for a RF CVD process	7
3	Tetracene synthesis	22
4	Pentacene synthesis	23
5	Synthesis of hexacene and heptacene	24
6	Synthesis of octacene and nonacene	25
7	Synthesis of 6,13-diphenylpentacene	26
8	Substituted pentacenes with solution phase half-lives ($t_{½}$) in minutes	27
9	Examples of TIPS substituted hexacenes and heptacenes	28
10	Example of *tert*-butylphenyl thiol substituted heptacene	29
11	Structure of first soluble, persistent nonacene	29
12	Partial mechanism proposed for the polyamine hydrogenation of fullerene	32
13	Deuteration of [60]fullerene	33
14	Structure of Polyamines	33
15	Hydrogenation of [60]fullerene with polyamines	34
16	Hydrogenation of [60]fullerene with DETA in the presence of catalyst	40
17	Amination of fullerenes from polyamines and decylamine	42
18	Proposed hydrogen transfer mechanism for polyamine hydrogenation of [60]fullerene	46

19 Synthesis of graphene from high temperature hydrocarbon reaction.....61

20 Synthesis of TIPS-Bipentacene.....77

21 Synthesis of fused bispentacenequinone.....78

22 Synthesis of bipentacene.....79

23 Synthesis of Peripentacenequinone.....83

24 Synthesis of Fused Bipentacene.....86

25 Attempted synthesis of substituted bipentacene.....87

26 Proposed synthesis of substituted bisacenes.....89

27 Proposed synthesis substituted periacenes.....91

28 Synthesis of hexathiapentacene (HTP).....92

29 Resonance forms of hexathiapentacene (HTP).....93

30 Synthesis of Trithaipentaceneone (TTPO).....94

31 Proposed synthesis of substituted TTPO.....100

32 Synthesis of Fused Trithiabispentaceneone and Trithiaperipentaceneone.....102

33 Scott's total synthesis of [60]fullerene.....105

34 Our novel synthesis of decacyclene.....106

35 Proposed mechanism for decacyclene synthesis using acenaphthylene in the presence of catalytic acenaphthene.....107

36 Proposed synthesis of [60]fullerene using a partially hydrogenated PAH compound as free radical initiator.....108

37 Synthesis of 5,12-dihydrotetracene.....109

38 Synthesis of tetracene nanoribbons from tetracene and 5,12-dihydrotetracene..113

39 Synthesis of 6,13-dihydropentacene and pentacene.....114

40 Synthesis of pentacene nanoribbons from pentacene and 6,13-dihydropentacene....115

41 Synthesis of a small molecule precursor to a soluble acene....119

42 Synthesis soluble acenequinones....120

43 Synthesis of soluble acenes and dihydroacenes....121

44 Synthesis of soluble tetracene nanoribbons....123

LIST OF TABLES

Number Page

1 Approximate number of additions to large fullerenes during DET hydrogenation of 1-phenylnaphthalene extraction....37

2 Results of hydrogenation in the presence of transition metal catalyst....40

3 Reactions between [60]fullerene and substituted polyamines....44

4 Reactions between [60]fullerene and cyclic amines or cyclic polyamines....45

LIST OF COMPOUNDS

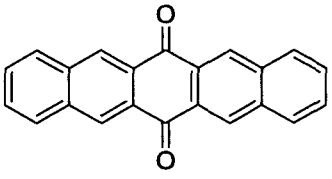

4.1

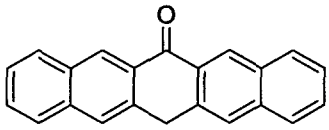

4.2

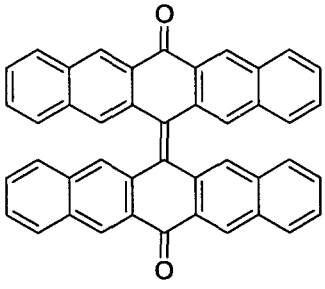

4.3

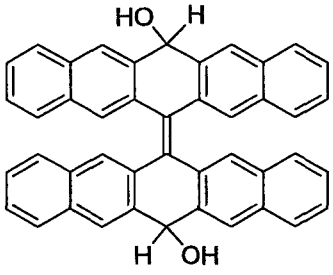

4.4

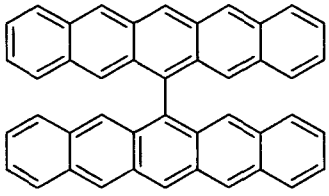

4.5

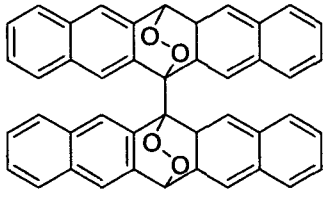

4.6

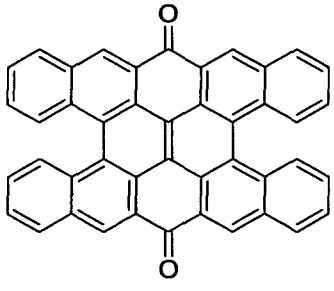

4.7

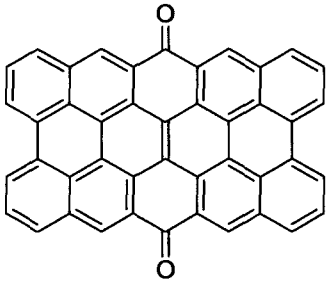

4.8

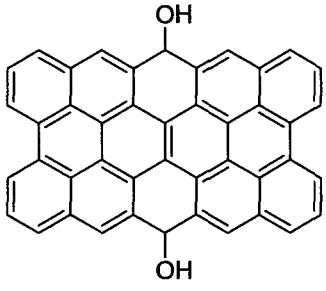

4.9

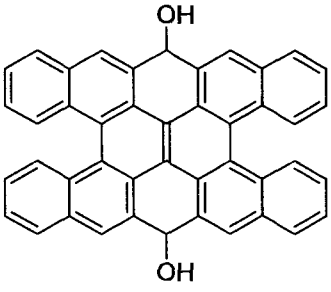

4.10

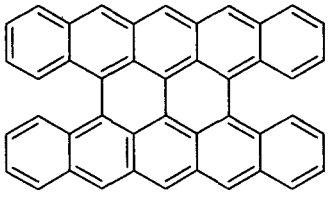

4.11

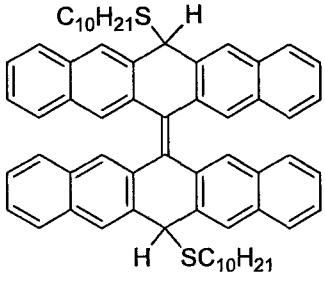

4.12

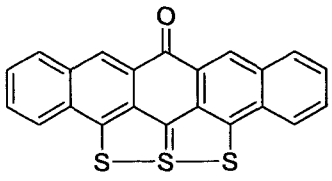

4.13

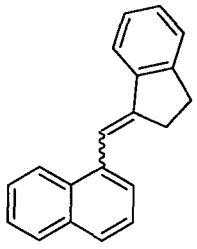

5.1

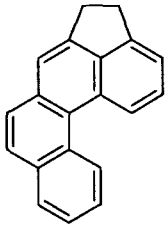

5.2

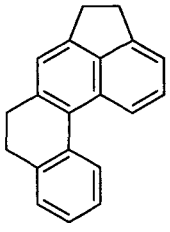

5.3

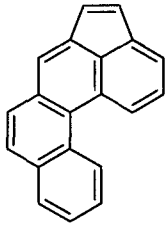

5.4

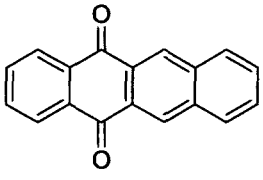

5.5

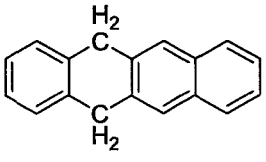

5.6

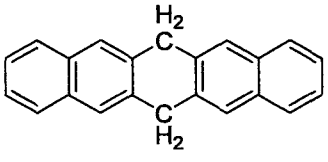

5.7

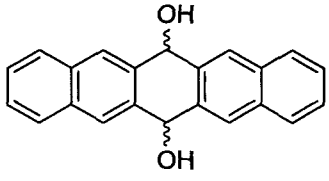

5.8

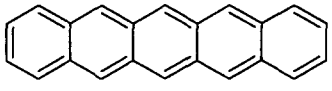

5.9

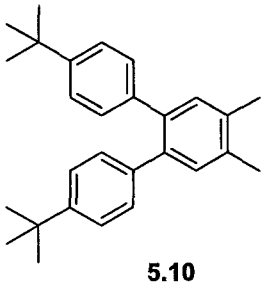

5.10

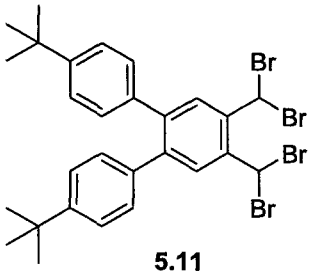

5.11

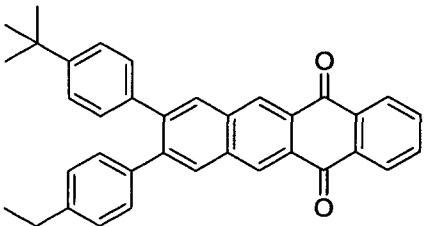

5.12

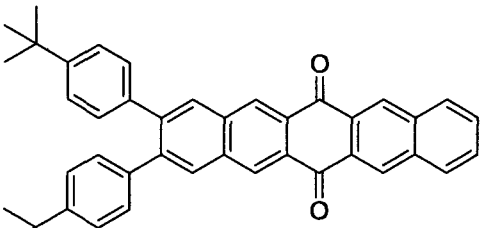

5.13

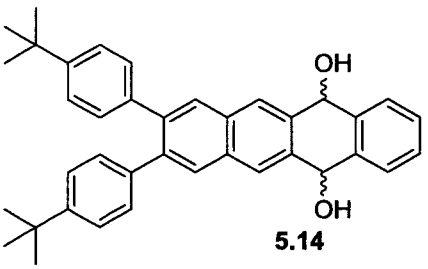

5.14

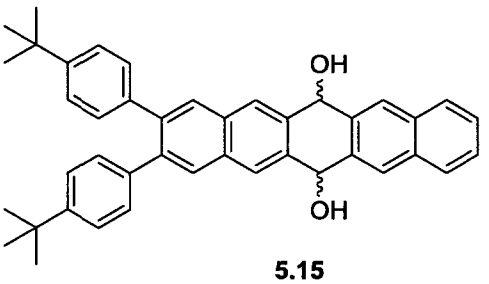

5.15

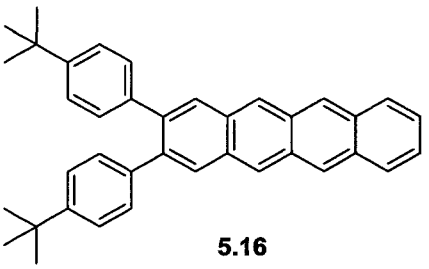

5.16

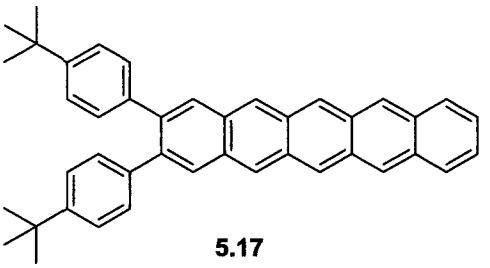

5.17

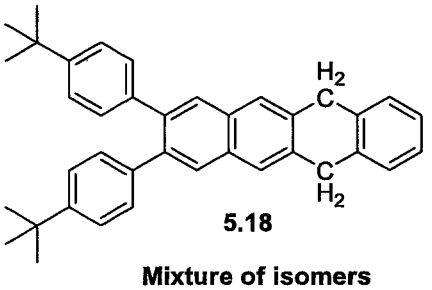

5.18

Mixture of isomers

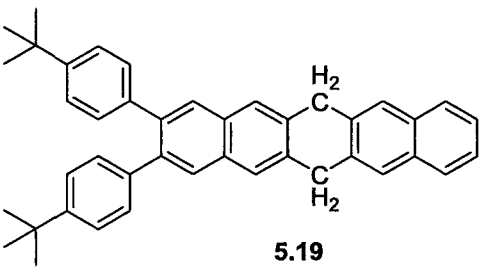

5.19

Mixture of Products

ABSTRACT

HYDROGENATION OF NANOSTRUCTURED CARBON, SYNTHESIS OF ORGANIC SEMICONDUCTORS AND PROGRESS TOWARDS SYNTHESIS OF FULLERENES AND NANORIBBONS FROM POLYAROMATIC HYDROCARBONS

By

Jeremy Kintigh

University of New Hampshire, December, 2011

The hydrogenation of carbon allotropes including fullerenes, nanotubes and graphene was investigated using polyamines as hydrogenation reagents. In each case, a rapid, scalable and reversible hydrogenation was observed. The mechanism of hydrogenation was explored using several different polyamines. It was shown that a two-carbon spacer between amine groups is critical for efficient hydrogenation, as well as the presence of at least two adjacent amines that are not tertiary. The extent of hydrogenation on the fullerenes is a function of reaction temperature. C_{3v} $C_{60}H_{18}$ forms preferentially at approximately 200 °C whereas $C_{60}H_{36}$ species are preferentially formed at approximately 340 °C and above. S_6 $C_{60}H_{24}$ was found to be produced in small quantities whenever fulleranes were produced. Despite attempts to isolate S_6 $C_{60}H_{24}$ by HPLC chromatography, only a few milligrams could be obtained. The material was shown to be particularly insoluble in its purified form making detailed spectroscopic

analysis difficult.

The synthesis of acenes, bisacenes and periacenes was accomplished. Unsubstituted bipentacene was successfully synthesized for the first time and showed improved solubility compared to pentacene. Peripentacenequinone was also synthesized, a stable organic semiconductor that exhibits poor solubility. A new type of organic semiconductor, trithiapentacenone (TTPO), was also synthesized. TTPO exhibits superior thermal and photooxidative stability, and is in fact stable in air at 400 °C. The distribution of charge in TTPO promotes crystallization with a head-to-tail stacking arrangement that promotes parallel displaced columnar stacks. TTPO shows variable temperature transistor behavior with higher mobilities at higher temperatures.

Exploration into the formation of graphene nanoribbons from small molecules (bottom-up synthesis) was explored. By thermal annealing of substituted and unsubstituted pentacenes, large polymeric systems akin to nanoribbons were produced. Using similar methods, a bottom-up synthesis of [60]fullerene was explored and the rapid, efficient synthesis of several precursors including decacyclene was accomplished.

CHAPTER 1

INTRODUCTION

1.1 Fullerenes

1.1.1 History of Fullerenes

Fullerenes were first detected in 1984 by Rohlfing and co-workers when graphite was evaporated using a pulsed laser, producing materials of even carbons units between 2 and 200, with 60 carbon units being the most abundant. At the time, acetylene-like molecules were the suspected product.[1] Conditions were later developed to make clusters of 60 carbon atoms almost exclusively with smaller amounts of 70 carbon clusters.[2] Smalley and co-workers proposed that the carbon clusters were arranged as a closed spherical structure that resembled a soccer ball (Figure 1), which they dubbed "Buckminsterfullerenes" after the famed architect Richard Buckminster Fuller, who was known for the construction of large geodesic structures. The structure consisted of 60 equivalent sp^2-hybridized carbon atoms arranged as a truncated icosahedron with 12 pentagons and 20 hexagons giving the structure icosahedral or I_h symmetry. The structure was confirmed by Taylor and co-workers in 1990 by NMR spectroscopy[3] and by Krätschmer and co-workers by x-ray diffraction.[4] Later, for simplicity, the name was shortened to [60]fullerene where the number in brackets indicates the number of carbon atoms.

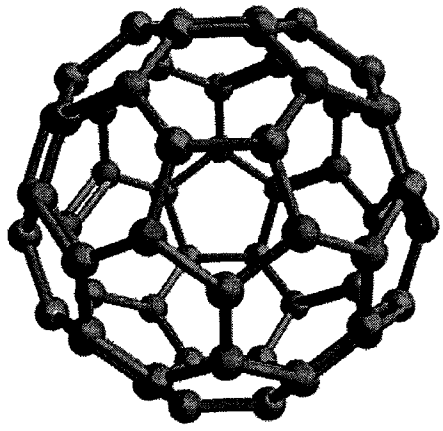

Figure 1: Structure of [60]fullerene

1.1.2 Natural Occurrence of Fullerenes

Shortly after the discovery of fullerenes, a search began to find whether or not natural sources of fullerenes existed. After a number of surveys, several samples of carbonaceous minerals from different parts of the world were discovered to have fullerenes.[5,6] It was theorized that the fullerenes were produced by a cataclysmic event, such as an asteroid strike, or a massive volcanic eruption that occurred near a large carbon source which atomized the carbon and formed the fullerenes.[7] [60]Fullerene and [70]fullerene have been detected in planetary nebula, large gas clouds formed by expansion of the outer shell of a dying star.[8]

1.1.3 Synthesis of Fullerenes

Although fullerenes were discovered in 1985, research into the chemistry of fullerenes was inhibited by their extreme cost and difficult production. It wasn't until the 1990 that Krätschmer, *et al.* found a simple and cheap arc discharge method to produce

abundant [60]fullerenes.[4] Using graphite rods with an arc discharge in a helium atmosphere a large amount carbon soot could be produced, which was enriched in [60]fullerene and contained lesser amounts of [70]fullerene. The two fullerenes can be separated by with column chromatography.

In 2002 Scott, *et al.* developed the only total synthesis of the [60]fullerene, using flash vapor pyrolysis (FPV). [60]Fullerene was synthesized in 12 steps using a chlorinated polycyclic aromatic hydrocarbon as a synthetic intermediate (Scheme 1).[9] While the fullerene was detectable by mass spectrometry, the overall yield of the reaction was well under 1%, making the synthetic path impractical for routine use. Nonetheless the synthesis demonstrated how to achieve bond formation in curved polycyclic aromatic hydrocarbon systems, and represents an important milestone.

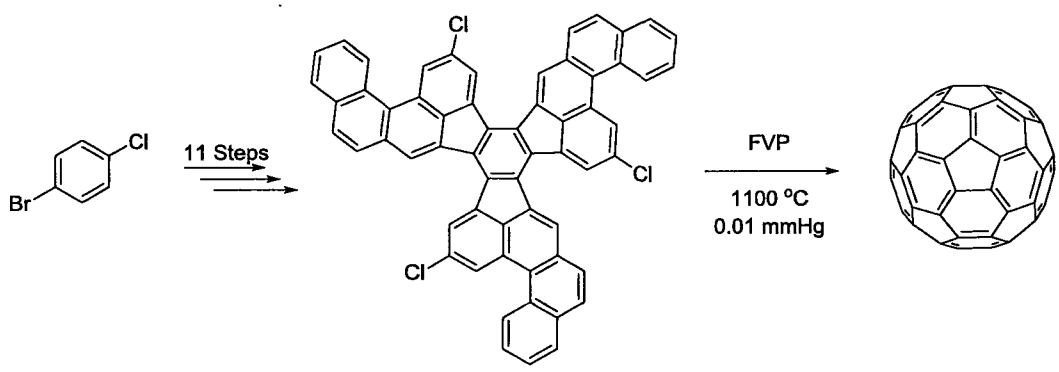

Scheme 1: Total synthesis of [60]fullerene

1.1.4 Hydrogenation of Fullerenes

Once synthetic conditions were established to make bulk quantities of [60]fullerenes, experiments designed to gauge chemical reactivity began. One of the

first of these experiments was hydrogenation using a reductive metal process called the Birch reduction.[10] The reaction led to a mixture of $C_{60}H_{36}$ fullerane isomers. Heating $C_{60}H_{36}$ fulleranes led to the formation of $C_{60}H_{18}$. Later, Taylor and co-workers were able to identify the structure of a commercial source $C_{60}H_{18}$ as having a crown-like structure with C_{3v} symmetry. In the C_{3v} crown structure, all of the hydrogen atoms are attached to one side of the [60]fullerene (Figure 2) Later, three groups all proposed different structures for the $C_{60}H_{36}$ product with D_{3d},[11] C_{3i},[12] and T_h,[13] symmetries respectively. High resolution NMR spectroscopy studies eventually demonstrated that the Birch reduction product consisted of 3 closely related isomers of $C_{60}H_{36}$ with C_1, C_3, and T_h symmetries.[14]

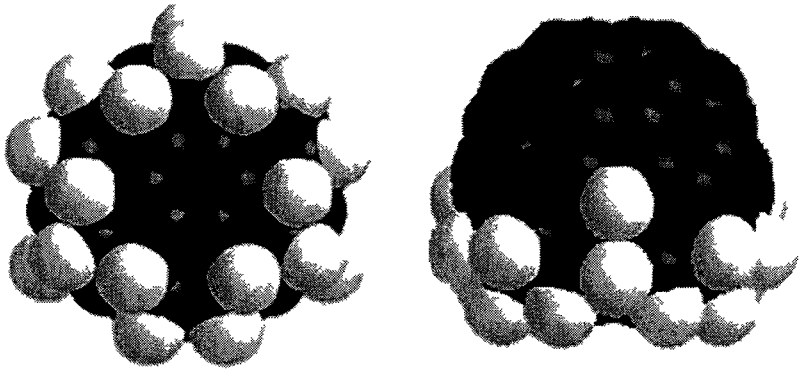

Figure 2· Top and side views of C_{3v} $C_{60}H_{18}$ fullerane with a crown-like structure

Along with $C_{60}H_{18}$ and $C_{60}H_{36}$, many other fulleranes are known, including $C_{60}H_2$, $C_{60}H_4$, $C_{60}H_6$[15] and $C_{60}H_8$.[16] There are numerous methods for forming fulleranes such as zinc-hydrochloric acid reductions,[17] borane reductions,[18] hydrogenation using

hydrogen gas with a transition metal catalyst,[19] and hydrogen transfer reactions.[20]

1.2 Nanotubes

1.2.1 Discovery and Synthesis of Nanotubes

Six years after the discovery of fullerenes, carbon nanotubes were made in 1991 by Sumio Iijima. Carbon nanotubes were synthesized through the arc discharge method similar to that used for that synthesis of fullerenes.[21] These first nanotubes were later called "multi-walled nanotubes" or MWNTs due to their structure consisting of multiple layers of cylindrical tubes. In 1993 Iijima, and Bethune and co-workers independently synthesized nanotubes that contained only a single layer. The synthesis of single-walled nanotubes or SWNTs was accomplished using the same arc discharge method but in the presence of an iron catalyst[23] SWNTs could also be synthesized using a cobalt catalyst (Figure 3).[22,23]

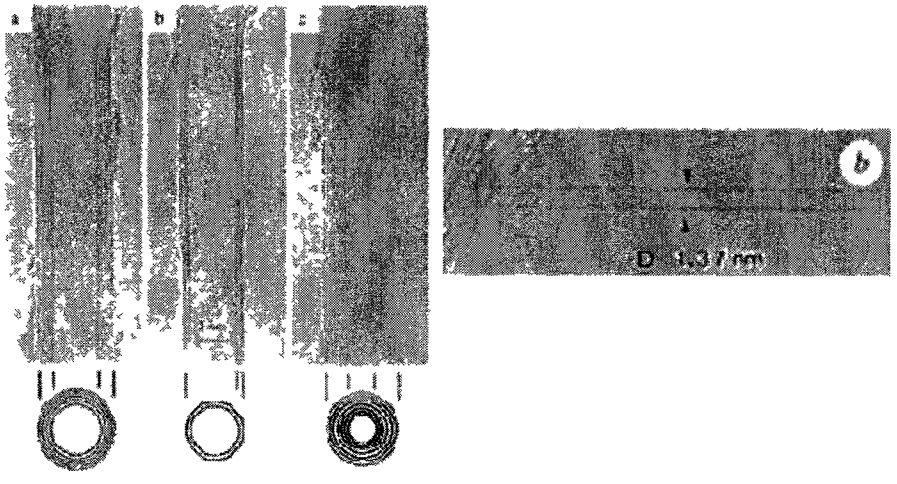

Figure 3: First images of MWNTs[21] (left) and SWNTs[22] (right)

Computational modeling was utilized to investigate the structure and properties of SWNTs. The modeling suggested that there are three types of SWNTs: armchair, zigzag, and chiral (Figure 4). It was also determined that these types of nanotubes would have either conducting (or metallic) properties, in the case of armchair nanotubes, or semiconducting properties, in the case of zigzag or chiral nanotubes.[24-26] These electronic properties were confirmed experimentally six years later by Odom, Wielder and co-workers.[27,28]

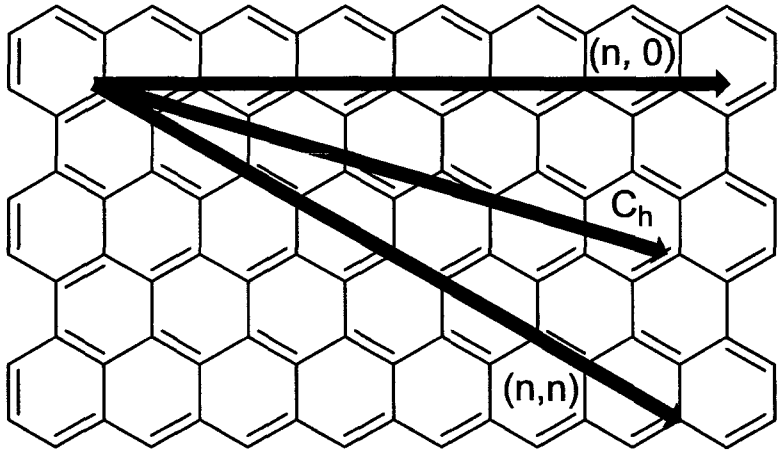

Figure 4: Schematic of a flattened nanotubes surface illustrating zigzag (n,0), armchair (n,n), and chiral (C_h) nanotubes[27]

Band gaps are projected to be between 0.6 eV and 2.0 eV for semiconducting SWNTs,[28] and zero for the conducting nanotubes. In contrast, electron mobilities are expected to be 70 times greater than silicon.[29] For these reasons, there is great interest in

using nanotubes for nanoscale electronics. Along with their superior electronic properties, the tensile strength of an individual nanotubes is on the order of over 100 times that of steel,[30] making them suitable for structural material applications as well.

For both structural and electronic applications, a method to make nanotubes of high quality at low costs is desirable. The method that has been shown to work best for synthesizing both SWNTs and MWNTs is a method called chemical vapor deposition, or CVD. In order to make nanotubes by this method, a stream of a source gas (usually methane or acetylene) is carried though an ultra-high vacuum chamber by an inert gas which is then ionized by a high-frequency radio source to form a plasma. After the dissociation, the material is deposited onto a metal surface (Scheme 2).[31]

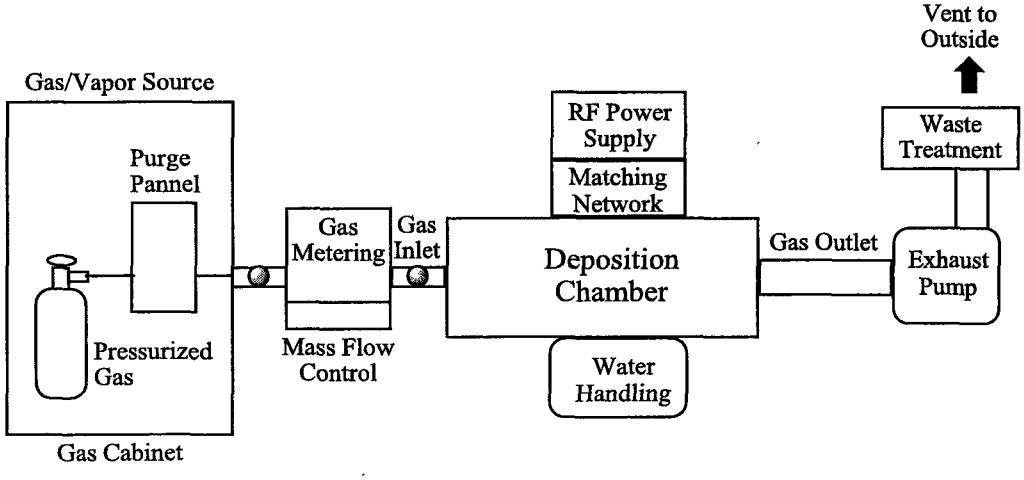

Scheme 2: Generic scheme for a RF CVD process

The CVD method has been shown to be most effective when using a catalyst to promote the growth of the nanotubes. This method can also be used with variety of different transition metals such as gold[32] or cobalt[33] nanoparticles. Using metallic mixtures of catalysts such as Fe-Mo[34,35] or MgO[36] with a feed gas such as methane results in high yields of nanotubes with uniform lengths. These methods have allowed for the price of nanotubes to drop precipitously. Currently, manufacturing plants are able to synthesize upwards of 3000 metric tons of nanotubes per year.[37]

1.2.2 Hydrogenation of Nanotubes

One of the first chemical modifications performed on nanotubes was hydrogenation. In 2001 Pekker and co-workers were able to synthesize hydrogenated single-walled nanotubes (H-SWNTs).[38] To determine the rate of hydrogenation, they performed thermogravimetric analysis (TGA), which measures the rate of mass loss over a temperature gradient. They discovered that hydrogenation of nanotubes is reversible, and that they could achieve a level of hydrogenation of approximately 9%. By attaching the TGA to a mass spectrometer, these researchers found that thermal annealing led to the formation of hydrogen as well as more complex molecules such as methanol and methane. It was believed that disruption of the nanotube surface by forming weaker Csp^3-H carbon bonds allowed for easier fracturing of the carbon-carbon bonds in the nanotube under high-temperature conditions, which in turn released carbon to react with hydrogen and trace oxygen to form hydrocarbons.

In 2002, Khare and co-workers were able to successfully hydrogenate SWNTs

using atomic hydrogen from a glow discharge. A glow discharge is simply a cold plasma (300-1000 K) generated from a gas in the presence of high frequency radio waves or from low wattage microwaves.[39] The plasma was then passed over a sample of nanotubes at low pressure. Through radical reactions, hydrogenation of the nanotubes occurs. The hydrogenation reaction was monitored using infrared spectroscopy with special attention paid to the regions where either C-H stretching or C-C stretching are typically observed (Figure 5).

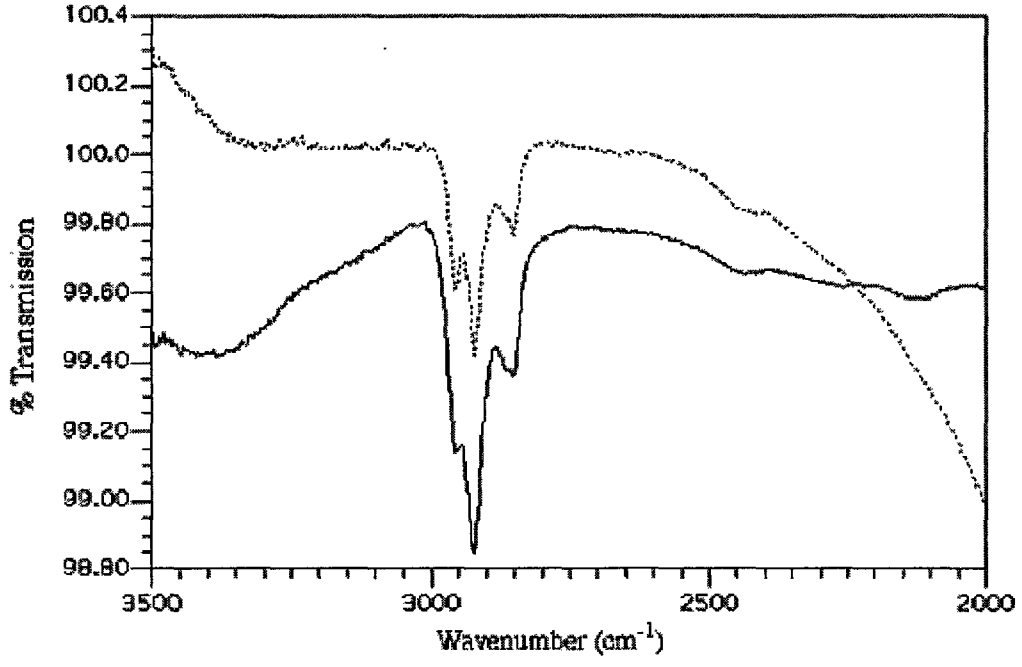

Figure 5: Intensity comparison of hydrogenated SWNTs (solid) and hydrocarbon contamination in SWNT samples (dotted)[40]

Another analytical method that is often used to determine the level of hydrogenation of a nanotube is Raman spectroscopy. A Raman spectrum of a nanotube

includes two important bands: the disordered band (D band) which is a measurement of the amount of defects in the nanotube and the graphitic band (G band) which is a measure of the graphite-like structure within the nanotube. Zhang and co-workers proposed that cutting a nanotube with a hydrogen plasma, led to hydrogenation on the edges of the nanotube, as evidenced by very specific signals in the Raman spectra.[41] The ratios of the D/G band increased indicating an increase in the disorder in the nanotube, consistent with partial hydrogenation and an increase in the Csp^3:Csp^2 ratio. This phenomena was later corroborated by Meletov and co-workers when they performed high-pressure/high-temperature hydrogenation on nanotubes using a nickel-yttrium catalyst.[42] Using Raman spectroscopy, they found that thermal annealing of the hydrogenated nanotube at temperatures over 350 °C led to dehydrogenation with the recovery of pristine nanotubes.

A different method for detecting hydrogenation in a nanotube is to look at the effect that hydrogenation has on the electrical properties of the nanotubes. Kim and co-workers synthesized hydrogenated nanotubes using the same method as Khare and co-workers, and then measured their band gap and current. They discovered that the band gap increased dramatically from 0.8 eV to 4.4 eV after hydrogenation while the current that could be passed through the nanotubes was reduced.[43] While this method indicates a disruption in the π-network of the nanotubes, it should be noted that other methods of analysis are required in order to confirm hydrogenation. Modification of the band gap and current flow could be explained by any other chemical functionalization that disrupts the conjugation of the nanotubes.

1.3 Graphene

1.3.1 Nomenclature and Properties

Related to fullerenes and nanotubes, graphite and graphene comprise another allotrope of carbon. When the term "graphene" is used, it is meant to describe a single sheet of graphite consisting of sp^2-hybridized carbon atoms arranged in a hexagonal fashion. Normally, these individual layers stack upon one another due to π - π sacking interactions to form evenly spaced rows separated by 3.35Å to form graphite (Figure 6). Since single layers of graphite have vastly different electronic[44] and thermal[45] properties than bulk graphite a different term was needed.

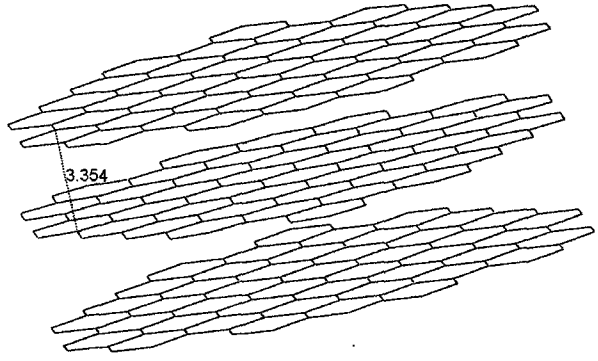

Figure 6: *Graphite's structure*[46] *(measurement in Å)*

The term "graphene" was first coined in 1987 to describe the individual layers of graphite that were formed through the intercalation of metals in graphite.[47] Later in 1998, it was used to describe an individual sheet of graphite that was formed on a silicon

surface through the decomposition of silica carbide.[48] In the present day, graphene is now used to describe a single layer or a few layers of free-standing graphite.

Graphene is of great interest to researches due to its phenomenal properties. Graphene highest tensile strength ever measured,[49] has the highest electron mobility[6] and electron velocity[50,51] ever measured in a conductor, and has thermal conductance on par with that of nanotubes.[52] All of these factors lead to the possibility that graphene could be made into high strength, highly efficient electronic components. Research has already been done to make graphene into components for field-effect transistors,[53] liquid crystal displays,[54] light-emitting diodes,[55] and photovoltaics.[56,57] While none of these devices have yet to be commercialized, graphene has the potential to revolutionize every aspect of modern technology.

1.3.2 Discovery and Synthesis of Graphene

The first recorded synthesis of graphene turned out to be surprisingly simple. Using only adhesive tape and highly-oriented pyrolytic graphite (HOPG), single-sheet graphene was produced through repeated adhesion and peeling.[58] This "Scotch Tape" method allows for inexpensive production of graphene that is experimentally useful and only requires manual labor and some patience. Another mechanical method that can be used to produce graphene is "drawing". Much like writing with a pencil, dragging HOPG across a surface can create single-layer graphene in the absences of other thicker graphene sheets.[59] While both methods can produce graphene, neither is useful on

anything larger than the laboratory scale. Other methods are required to produce graphene on a large scale as will be required for commercial applications.

To obtain bulk graphene, a chemical pathway was derived in which graphite is oxidized and then exfoliated followed by a reduction.[60] The oxidation of graphite had been well established in 1958 by Hummer and Offeman.[61] The "Hummer method" uses a combination of sulfuric acid, potassium permanganate and hydrogen peroxide for oxidation. More recently, other methods of oxidizing graphite using sulfuric and phosphoric acids have been developed and they produce less toxic by-products than the Hummer method.[62] Oxidizing the graphite surface causes a loss in conjugation; this causes the graphite samples to change from the typical metallic color to yellow. Corresponding to the color change, the π - π stacking or van der Waals interactions are greatly reduced, allowing for exfoliation of the corresponding graphite oxide (GO). These GO sheets are easily dispersed in solvents like water, which allows greater processability than that of graphene produced from mechanical methods. The GO then requires a reduction step in order to produce single-sheet graphene. The modifications on the GO surfaces are fairly extensive, with addition of epoxide, carboxylic acid, ketone, and alcohol functional groups (Figure 7), [63] all of which makes reduction to pristine graphene difficult.

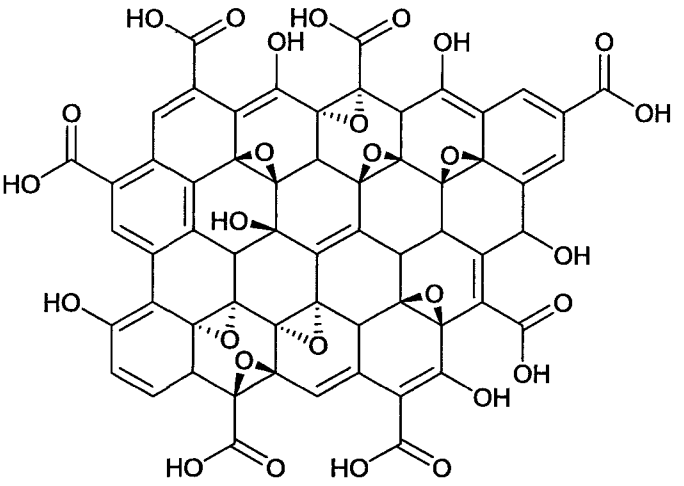

Figure 7: Idealized structure of graphite oxide (GO)

Graphite oxide is itself an insulator[64] and therefore not useful for electronic components. A chemical method is needed to produce single-sheet graphene from GO and a number of reductive methods have been tested. The most commonly used method is a hydrazine reduction that was developed by Stankovich and co-workers.[60] This method reduces the overall oxygen content in GO by approximately a factor of 10, giving the product similar electronic properties to that of graphene sheets produced by less effective methods.[65] However, this reductive method does not produce graphene that has electronic properties that are on par with that of graphene made by mechanical exfoliation.[59] Another difficulty with this reductive method is the use of hydrazine which is a highly toxic material that can also pose an explosion risk. The reduction can be made more effective by using poly(sodium 4-styrenesulfonate)[66] in conjunction with hydrazine which allows for a more highly dispersed product that allows for better processing. This still leaves the problem of hydrazine, however, which is too toxic, dangerous and expensive to be used in industrial settings. A cheaper, safer and more environmentally

friendly method is needed.

Some new methods for the reduction of GO that require less harsh conditions include the use of hydroquinone,[67] sodium borohydride,[68] alkaline solutions,[69] and hydroiodic acid.[70] While all those methods reduce GO, questions remain about their effectiveness. From the limited data available, electronic properties of the sodium borohydride reduced GO material are limited compared to that of pristine graphene.[68] It is also clear from analyses that reduction of GO by either hydroquinone and hydroiodic acid is only partial.[67,70] The alkali reduction is used in conjunction with sonication to remove oxygen from the surfaces. As with the other methods described, it is hard to determine whether or not the quality of the reduced GO is high enough for electronic applications.[69]

Reducing GO sheets is not limited to chemical methods; other potentially scalable methods are also being explored. For example, the use of UV-assisted photocatalytic reduction in the presence of titanium oxide[71] has shown to reduce GO sheets. There have been several examples of using microwave irradiation to exfoliate graphite to GO sheets,[72,73] as well using microwave irradiation to reduce GO sheets to graphene.[74,75]

Currently, there are several methods under study to reduce GO in ways that are not only more environmentally friendly, but are applicable to bulk scale-up.[76,77] One such method involves using hydrothermal reduction of GO sheet in an autoclave. Heating a sample of GO sheet to 180°C in the presence of water for 6 hours reduces the sample to a graphene material with similar properties to that of hydrazine reduced GO, though the electrical properties have not been fully resolved.[78] Another method that is

less toxic has been developed by Choucair and co-workers. A combination of sodium and ethanol in an autoclave followed by sonication produces separate graphene layers.[79] Many of these methods to reduce GO hold promise but the electrical properties of the resulting graphene materials are not fully understood. Moreover, these methods do not make uniform graphene sheets, but rather a large distribution of shapes and sizes.

Recently, a new and interesting approach to reducing GO uses bacteria rather than chemical or thermal methods.[80] The advantage of bacterial reduction is that it is a much "greener" method requiring only heat and feedstock for the bacteria to grow. Using several different subtypes of bacteria from different environments showed that some types of bacteria were able to reduce nearly all of the GO sheets to graphene *via* an enzymatic process.[80] This method could be scaled for industrial manufacturing using common equipment such as fermenters and bio-reactors.

While chemical pathways to graphene are common a number of physical methods have also been studied including evaporation. The surface of a single crystal of silicon carbide can be etched with either hydrogen gas or an oxidant to prepare the surface to make a device. The surface can then be heated to over 1000 °C under a ultrahigh vacuum.[81] This cause desorption of the silicon layer leaving on average two or three layers of pristine graphene. The graphene that is produced in this manner has been shown to be very similar to that of graphene that has been produced by non-oxidative methods such as mechanical exfoliation.[82]

The method that currently has industrial applications is CVD. This deposition method has initially been used to make graphene on a variety of metal surfaces such as

cobalt,[83] copper,[84] nickel,[85] platinum,[86,87] iridium,[88] and ruthenium.[89] However, much of the focus lately has been on the nickel surfaces. Instead of high frequency radio waves, high temperatures (900-1000°C) can dissociate the carbon from the carrier gas and be used for the deposition. By carefully controlling the features of the Ni(111) surface,[90] or by regulating the cooling rate,[91,92] high quality graphene can be made over a large areas. More importantly, using these methods allows for transfer of the graphene onto useable substrates and templates made from an insulator like SiO_2,[91,92] or a polymer like PMMA.[36] This ability to transfer CVD grown graphene onto new substrates allows for the potential of manufacturing devices made from graphene in a controlled and reproducible manner.

1.3.3 Hydrogenation of Graphene to Graphane

While the reductive hydrogenation of graphite[38] and the catalytic hydrogenation of graphite[93,94] have been well known for a number of decades, the hydrogenation of graphene to graphane is a new phenomenon. The term "graphane" refers to the product of hydrogenation of graphene by a chemical method where covalent bonds have been formed between carbon atoms on graphene and hydrogen atoms to make new sp^3 hybridized carbons. This is different from the physisorption of hydrogen on a graphene surface, which does not involve covalent bond formation between the graphene and the hydrogen. Rather, molecular hydrogen adhereds to the surface of the graphene through van der Waals interactions.[95]

The first example of graphene hydrogenation comes from Elias and co-workers,

where graphene was hydrogenated *via* a hydrogen plasma source.[96] After exposing the graphene to the hydrogen plasma, analysis by Raman spectroscopy indicated structural changes to the graphene surface. The electronic properties of the graphane was notably different from that of graphene, the resistance of the graphane was markedly higher than that of graphene due to the loss of conjugation of the graphene from hydrogenation.[96] This effect was also evident in the reduction of the electron mobility on the graphane surface.

Studies have explored not only hydrogenation of graphene but dehydrogenation of graphane. It was shown that the level of hydrogenation on the graphane surface could be controlled by careful thermal annealing. As the sample of graphane was heated, there was a marked decrease in the resistance of the graphane as well as an increase in the electron mobility. Raman spectroscopy indicated that graphane was fully reversed to graphene after heating to 450 °C for 24 hours in an inert atmosphere.[96]

Further plasma-based hydrogenation experiments determined the relationship between the thickness of graphene and the level of hydrogenation in graphane. Work by Luo and co-workers showed that as the numbers of layers of graphene increased, the energy required for hydrogenation decreased.[97] It was theorized that as the layers of graphene increase their energy levels become higher and less uniform. This causes the graphene to hydrogenate more compared to that of a single-sheet graphene where the energy level was lower and uniform. The dehydrogenation of graphane was easier with multi-layered graphane than with single-layer graphane for the same reason.

While plasma-based hydrogenation was the first method to make graphane, other

methods have also been developed. Catalytic hydrogenation has been demonstrated by Schäffel and co-workers.[98] Using metal nanoparticles in the presence of hydrogen gas over a range of temperatures, graphane was prepared. Cobalt nanoparticles effected hydrogenation at 600 °C at 60 mbar of pressure where as nickel and iron nanoparticles require higher temperatures.

Another method to produce graphane combined physisorption with electron irradiation. Samples of graphene with either water or ammonia physisorbed on the surface were irradiated with an electron beam to produce graphane.[99] While this method only allows for localized production, it could be used to produce nanoelectronics devices where the electronic properties, such as resistance, could be modulated within a very specific area. A similar method was developed where graphene was imprinted onto a surface of hydrogen silsesquioxane (empirical formula $HSiO_{1.5}$) [100] and then exposed to an electron beam to dissociate the Si-H bond with hydrogen transfer to the graphene.[101] However; on a single layer of graphene, only 0.03 % of the carbon is hydrogenated and that level decreases by a factor of 15 for experiments conducted on two-layer graphene. The authors propose that this decrease in hydrogenation is caused by the π-π stacking interactions which increases the activation energy required and decrease the reactivity of graphene.[102] As with other methods of hydrogenation, dehydrogenation occurred with simple thermal heating annealing indicating that any method of hydrogenation should be thermally reversible.

1.4 Acenes

1.4.1 Background on Acenes

Acenes are molecules composed of lineally fused benzene rings. They are a part of the polycyclic aromatic hydrocarbon (PAH) family (Figure 8).[103] The term "acene" was derived from anthracene which in turn was named from a combination of "anthrac", Greek for "coal", and "ene" for the conjugated π-system that the molecule contains. After anthracene, acenes adopt the classical Greek prefixes of "tetra", "penta", "hexa" and so forth, to describe the number of rings in the linear system.

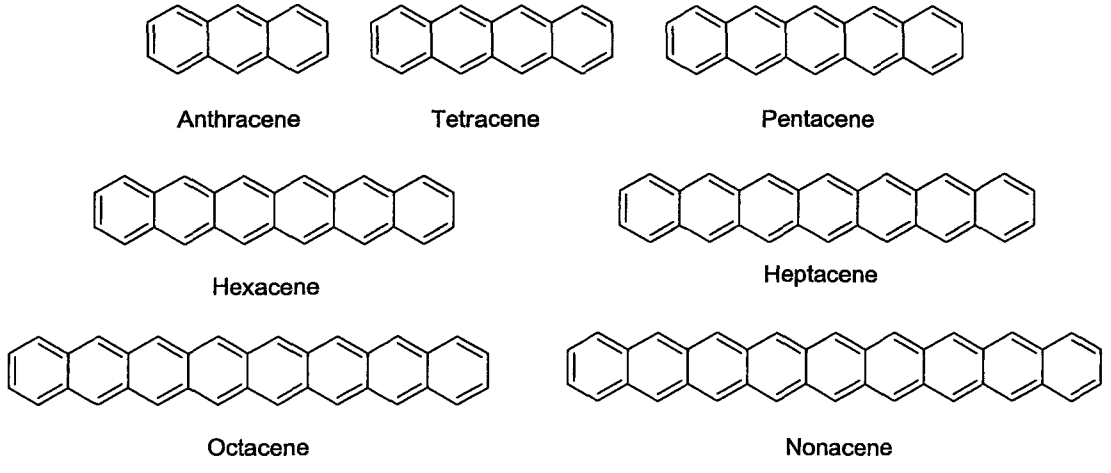

Figure 8: Structures of acenes

The nomenclature of acenes for systems larger than anthracene follows the rule that numbering starts on bottom left carbon and follows clockwise around the acene. The numbering only counts the carbons have hydrogen. If the quaternary carbon is referenced, then it is given the prime of the previous carbon (*i.e.* 6') (Figure 9).

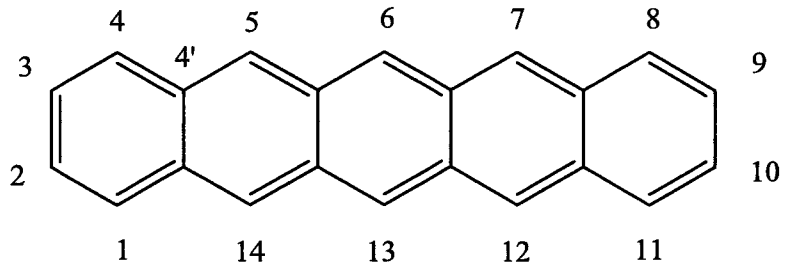

Figure 9: Numbering of Pentacene

As the length of the acene increases so does the extended conjugated π-bond system which allows for a more free flow of π-electrons and a narrowing of the HOMO-LUMO gap. This causes a number of physical changes in the acenes, such as the color which changes from off-white in the case of anthracene to bright orange for tetracene to purple for pentacene and then green for hexacene. The solubility of the acenes also decreases due to increased intermolecular π- π stacking interactions as the molecules become larger. Conversely, the reactivity of the molecules increases with increasing length due to the more conjugated π-system. Whereas anthracene is stable in solution, tetracene is prone to oxidation after a day in solution under ambient light and air. Pentacene oxidizes in within minutes in solution.[104] As noted above, a narrowing of the HOMO-LUMO gap is also observed with increasing length. This gap becomes small enough with tetracene and higher acenes such that the molecules have interesting semiconductor properties. These have been exploited to make field-effect transistors and photovoltaic devices.[105]

1.4.2 Synthesis of Unsubstituted Acenes

While anthracene can be extracted from natural sources, the lager acenes must be synthesized. The first such synthesis was detailed by Clar utilizing a Friedel-Crafts acylation.[106] Later, the synthesis was refined in order to make it more efficient. Thus, reacting α,α,α',α'-tetrabromo-o-xylene with 1,4-napththoquinone in the presence of potassium iodide in refluxing N,N-dimethylformamide generated a 5,12-tetracenequinone via an *in situ* Diels-Alder [4+2] cycloadditon.[107] The 5,12-tetracenequinone can be reduced in a number of different ways to yield the corresponding tetracene. Reductions include lithium aluminum hydride, which leads directly to tetracene, or sodium borohydride which produces the 5,12-tetracenediol, that can be reductively aromatized using $SOCl_3$, or KI/AcOH (Scheme 3).[108]

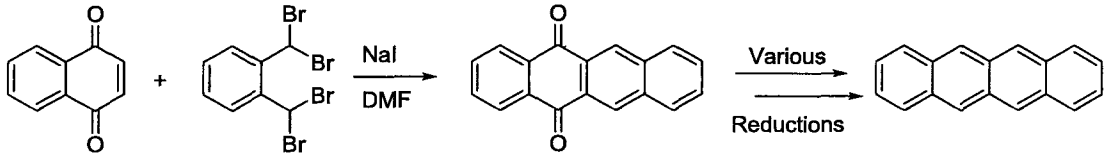

Scheme 3: Tetracene synthesis

The method of Scheme 3 is also useful for the synthesis of pentacene. Variations include the synthesis of pentacene-6,13-dione via aldol condensation[108] or acid-catalyzed condensation.[109] After condensation, a reduction can be performed in the same fashion as for tetracene (Scheme 4).

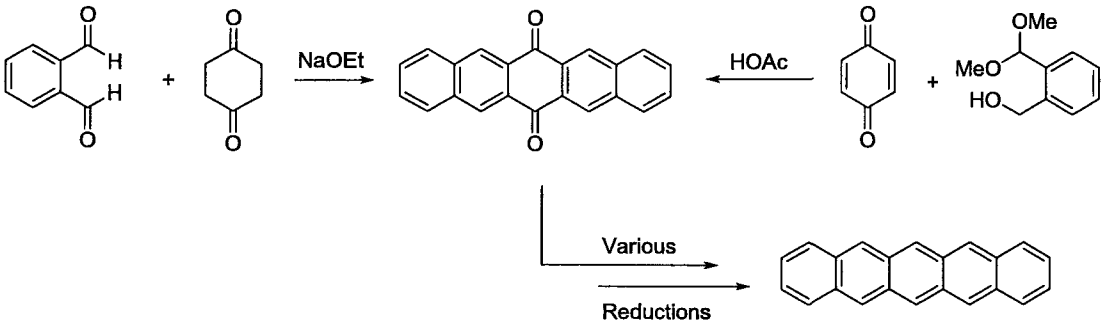

Scheme 4: Pentacene synthesis

As the acenes become larger, their synthesis becomes much more difficult due to increased instability. For hexacene through nonacene, syntheses must be carried out under conditions that completely isolate the compound from oxygen, such as a polymer matrix or argon matrix. The final step in the synthesis of larger acenes is done at extremely low temperatures to keep the molecules from reacting with the matrix itself.[110] Thus, bicyclo[2.2.2]oct-2,3,5,6,7-pentaene was treated with n-butyl lithium and either 1,2-dibromobenzene or 2,3-dibromonaphthalene to give the corresponding reduced bicyclohexacene or bicycloheptacene respectively (Scheme 5). These reduced species were then aromatized using chloranil to give the corresponding bicycloacenes, which were converted to the α-diketones and sealed in a matrix of PMMA. The polymer matrices were then irradiated with light at 395 nm at 30 Kelvin in a solid argon matrix[111] or at room temperature[112] to produce heptacene or hexacene, respectively.

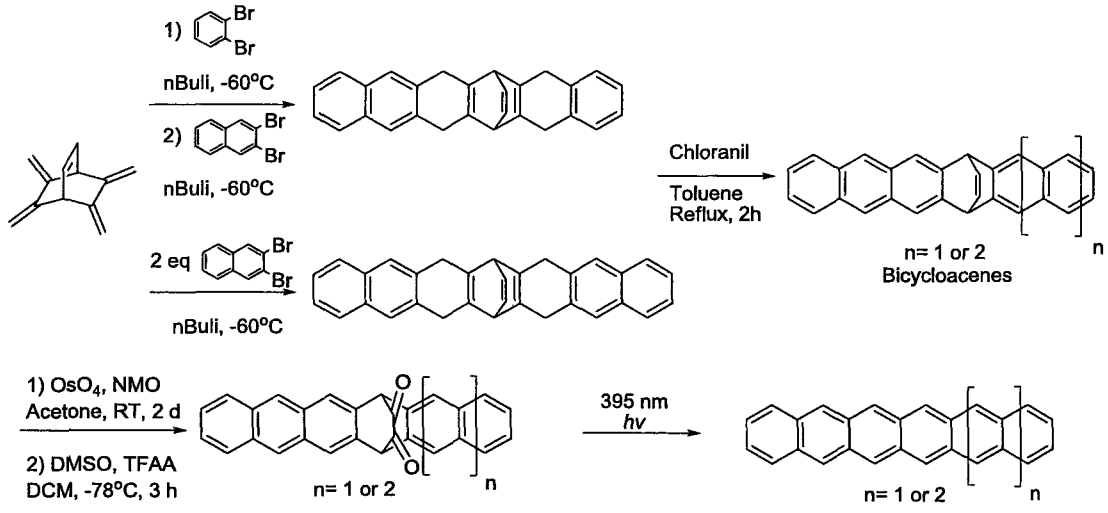

Scheme 5: Synthesis of hexacene and heptacene

For the synthesis of octacene and nonacene, the strategy is similar. Thus, bicyclo[2.2.2]oct-2,3,5,6,7-pentaene is reacted with n-butyl lithium and 1,2-dibromobenzene, results in a common precursor. This precursor can either be reacted with half an equivalent of 1,2,4,6-tetrabromobenzene to give the tricyclononacene precursor or a full equivalent of 1,2,4,6-tetrabromobenzene followed by a bicyclodiene to produce the tricyclooctacene precursor. As before the tricycloacene precursors are aromatized and then oxidized to give the corresponding α-diketone species. These α-diketones are then trapped in a solid argon matrix and subjected to two laser pulses at different wavelengths to remove two equivalents of carbon monoxide producing octacene and nonacene (Scheme 6).[113]

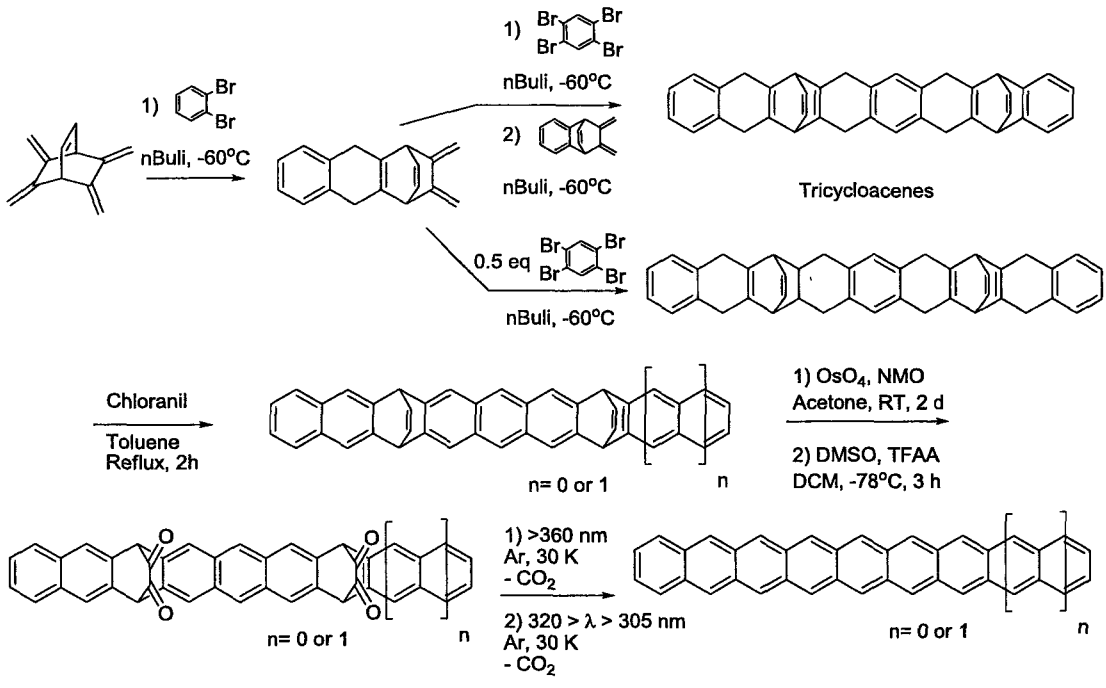

Scheme 6: Synthesis of octacene and nonacene

1.4.3 Synthesis of Substituted Acenes

While bare acenes have interesting properties their use in devices is very limited due to their by their poor solubility and low stability. To overcome these problems functional groups can be added to the acene skeleton. The first functionalized pentacene was produced by Bell and Allen in 1942, where they added the Grignard reagent phenylmagnesium bromide to 6,13-pentacenequinone followed by a potassium iodide and acetic acid reduction of the corresponding diol to produced 6,13-diphenylpentacene (Scheme 7).[114]

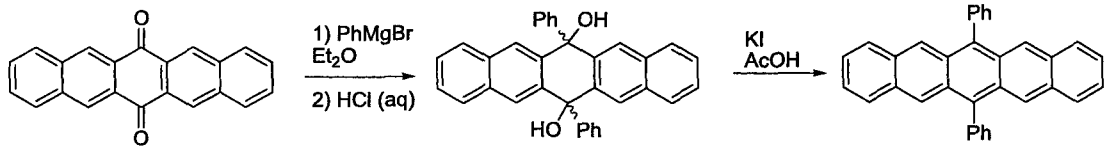

Scheme 7: Synthesis of 6,13-diphenylpentacene

Since this original synthesis of 6,13-diphenylpentacene, a host of substituted pentacenes have been prepared using either Grignard reagent, organolithiums or completely different set of conditions. Functional groups include aryl,[115,116] thiol,[115] and ethynyl groups,[117] all of which lead to some improvement in stability and solubility compared to unsubstituted pentacene. To date, the most popular substitution in the literature for pentacene is the triisopropylsilylethynyl or TIPS group[118]

Alkylthio and arylthio substituents are becoming increasingly popular as they improve solubility while providing superior resistance to photooxidation .[119] A detailed substituent effect study indicated that photooxidative resistance in substituted acenes is influenced by a combination of steric and electronic effects. [119] Several substituted pentacenes and their corresponding half-lives are illustrated in Scheme 8.

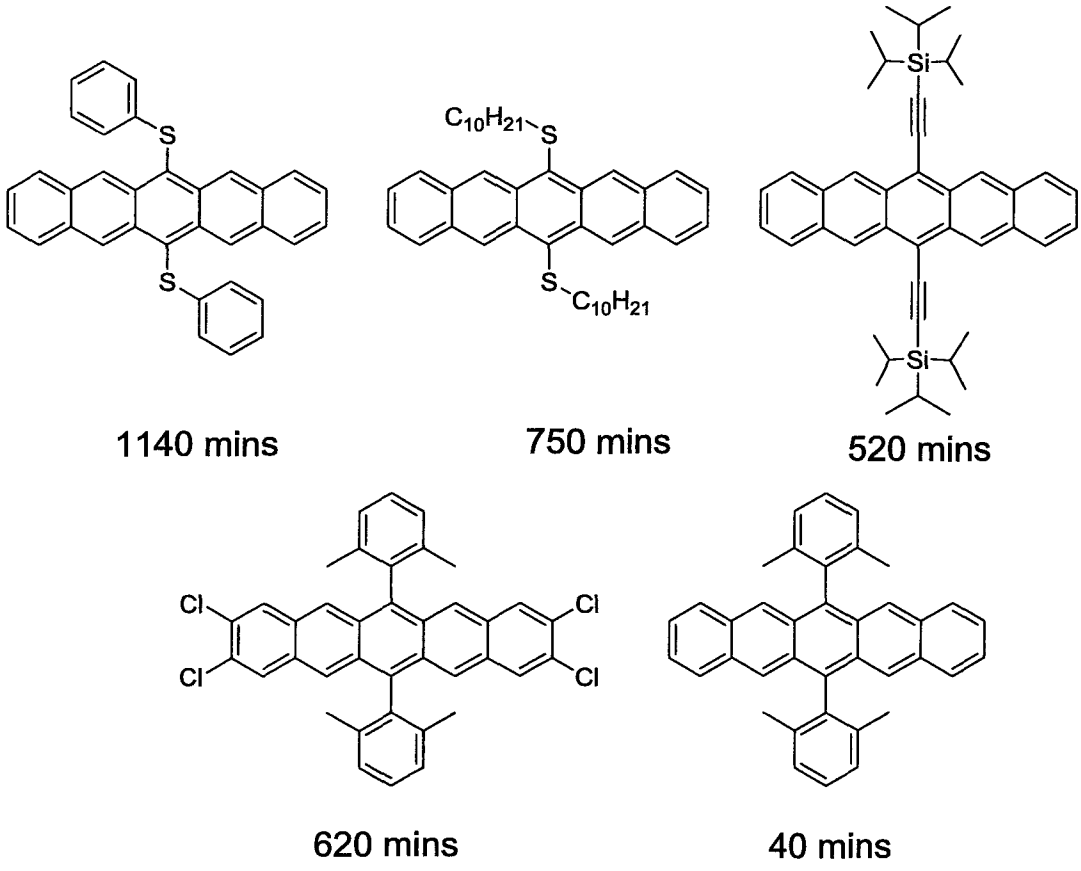

Scheme 8: Substituted pentacenes with solution phase half-lives ($t_{½}$) in minutes. Half-life measurements are based on the rate of oxidation at 25°C in ambient light for solutions of pentacenes in CH_2Cl_2 in solution with an initial concentration of 2×10^{-4} M.[119]

While the TIPS and organothio substituted exerts an electron withdrawing effect on their corresponding pentacenes, the impact of electron withdrawing substituents is dramatically illustrated by comparison of 6,13-bis(2',6'-dimethylbenzene)pentacene and 2,3,9,10-tetrachloro-6,13-bis(2',6'-dimethylbenzene)pentacene. The tetrachloro derivatives has a $t_{1/2}$ value that is an order of magnitude greater, presumably due to a lowering of both the HOMO and LUMO energies leading to a less reactive molecule.

Introducing bulky substituents as illustrated in Scheme 9 consisting of TIPS-hexacene, TIPS-heptacene[120] and their longer-lived derivative that bears additional trifluoromethylphenyl substituents[121] have shown to increase the photooxidative stability of systems as compared to that of unsubstituted hexacene and heptacene.

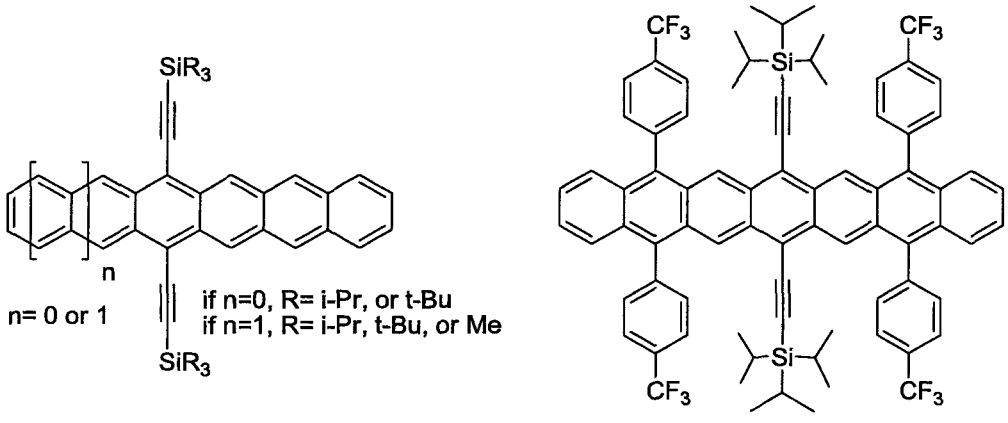

Scheme 9: Examples of TIPS substituted hexacenes and heptacenes

Likewise, alkylthio and arylthio substituted acenes become increasingly resistant to photooxidation upon addition of bulky substituents, as in the molecule depicted in Scheme 10.[122]

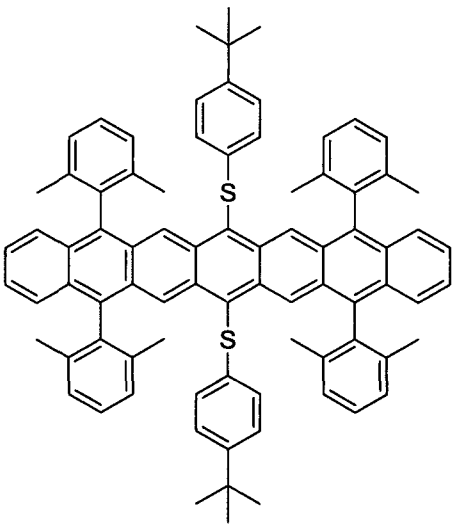

Scheme 10: Example of *tert*-butylphenyl thiol substituted heptacene

This same method was applied to produce the nonacene derivative of Scheme 11 whereby a combination of t-butylphenyl thiol and 2',6'-dimethylphenyl substituents led to a molecule of enhanced stability.[123]

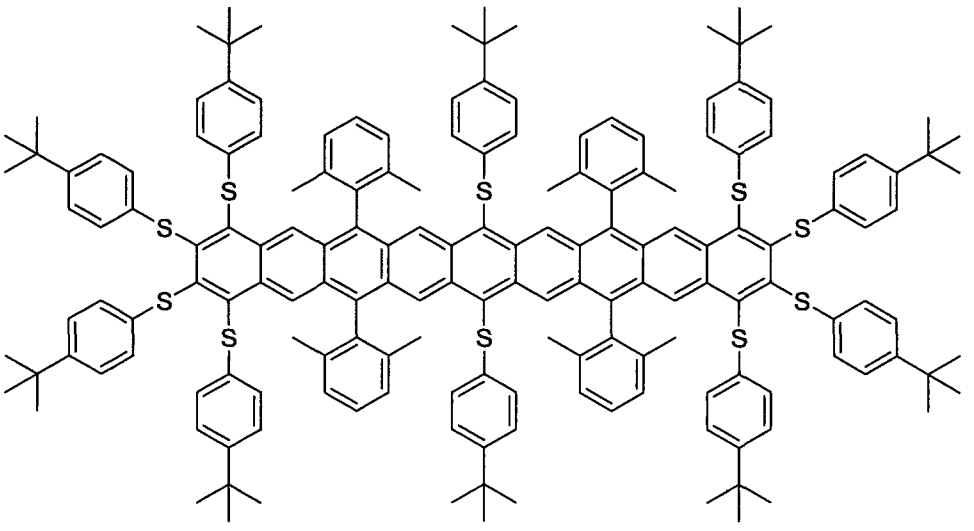

Scheme 11: Structure of first soluble, persistent nonacene

CHAPTER 2

SYNTHESIS OF FULLERANES AND HYDROGENATED SINGLE-WALLED NANOTUBES

2.1 Fulleranes

2.1.1 Background of Polyamine Hydrogenation of [60]Fullerene

The simplest of all functionalized fullerenes, hydrogenated fullerenes or fulleranes were first prepared by Smalley and co-workers using a Birch reduction procedure.[124] In so doing, they demonstrated the reactive nature of [60]fullerene and initiated a decade of chemical investigations that produced many intriguing compounds. Fulleranes themselves have been investigated as potential H-storage materials[125-127] and as potential cause of radio emissions originating from interstellar and circumstellar dusts.[128,129] In addition to the aforementioned Birch reduction, multiple methods exist to hydrogenate fullerenes including zinc/acid reduction,[130,131] borane reduction,[132] transfer hydrogenation,[14,133,134] and catalytic hydrogenation.[19] In these manners, a range of fullerane molecules have been prepared and reported. Most of these methods produce mixtures of fulleranes that are difficult to separate.[135] Recently, we reported[136] the regioselective hydrogenation of [60]fullerene in boiling diethylenetriamine (DETA). This reaction is convenient and scalable and affords C_{3v} $C_{60}H_{18}$ fullerane[137] in excellent yield.

A high temperature, high pressure hydrogenation reaction was also recently employed for the selective synthesis of C_{3v} $C_{60}H_{18}$.[138]

The polyamine hydrogenation of fullerenes is a novel reaction. Prior to the DETA hydrogenation of [60]fullerene,[136] polyamines had not previously been reported as hydrogenation reagents for any substrate. We proposed a polyamine hydrogenation mechanism involving successive electron transfer – protonation cycles as illustrated in Scheme 1. The first two steps of the proposed mechanism are in fact similar to those reported for fullerene hydroamination in the absence of molecular oxygen.[139] Thus, electron transfer from the amine to the fullerene is followed by NH proton transfer from amine radical cation to fullerene radical anion. At or near room temperature, the resulting fullerene-amine radical pair can collapse to form the corresponding hydroamination product.[139] At elevated temperatures in neat polyamine, however, a second electron transfer is competitive with radical combination and this is followed by a second proton transfer to give fullerane product (Scheme 12).

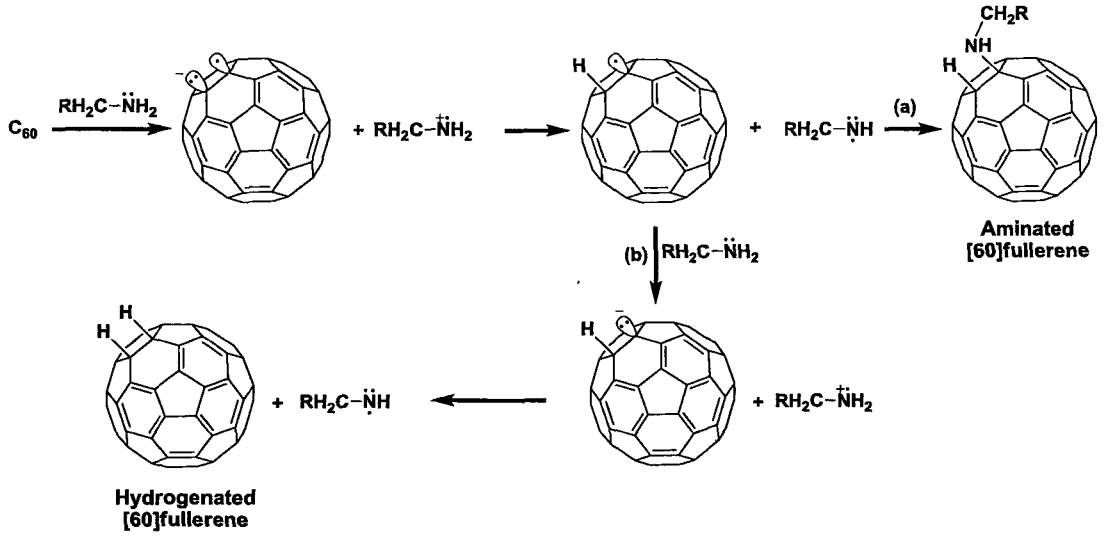

Scheme 12: Partial mechanism proposed for the polyamine hydrogenation of fullerene

The proposed polyamine hydrogenation mechanism involving NH proton transfers is consistent with the results of deuterium labeling studies. Thus, DET-d_5 was prepared by mixing DET with D_2O and then evaporating to remove H_2O/HOD/D_2O. DETA-d_5 was then reacted with [60]fullerene under conditions (reflux, 15 h) that would otherwise produce C_{3v} $C_{60}H_{18}$ in the presence of protio-DET. The resulting product was isolated and characterized as before. LDI mass spectra reveal the product to be $C_{60}D_{15\text{-}18}$ (Scheme 13). The modest rate retardation observed in DET-d_5 suggests that N-H(D) transfer is not rate limiting. ^{1}H NMR spectra show no signals due to hydrogenated fullerene above the noise. We conclude that polyamine hydrogenation of fullerene involves exclusive transfer of N-H rather than C-H hydrogen atoms from polyamine to fullerene in proton transfer steps that are not rate limiting.

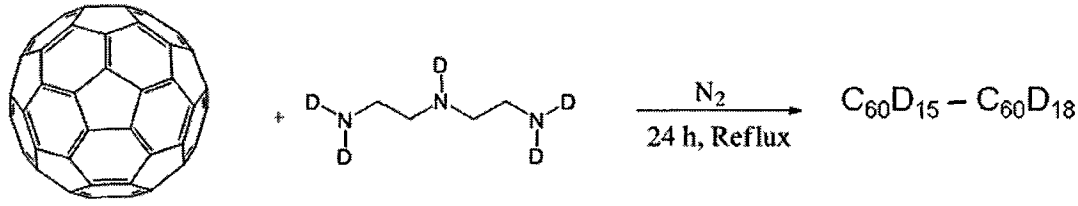

Scheme 13: Deuteration of [60]fullerene

When $C_{60}H_{18}$ was subjected to the polyamine hydrogenation conditions, $C_{60}D_{18}$ was produced indicating that polyamine hydrogenation is a reversible process and that the regioselective nature leads to a single, thermodynamically stable species.

2.1.2 Long Chain Polyamine Hydrogenation of [60]Fullerene and [70]Fullerene

With hydrogenation of fullerenes using DETA well established, it was important to explore whether or not longer chained polyamines would perform the same types of hydrogenation as DETA. A series of large polyamines with higher boiling points but the same repeating aminoethyl unites were studied, including triethylenetetramine (TETA, b.p. 266-267 °C), tetraethylenepentamine (TEPA, b.p. 340 °C), and pentaethylenehexamine (PETA, b.p 380 °C) (Scheme 14).

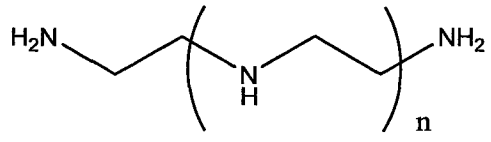

n=2 for TETA, n=3 for TEPA, n=4 for PEHA

Scheme 14: Structure of Polyamines

When these various polyamines were mixed with [60]fullerene and heated to reflux for 24 hours, more than 18 hydrogens added to the cage. Examination by NMR and mass spectroscopy showed hydrogenation occurred more readily with the higher boiling polyamines than did with DETA, with an average level of approximately 24 hydrogens per [60]fullerene cage when TETA was used and approximately 32 hydrogens per [60]fullerene cage when either TEPA or PEHA was used. (Scheme 15)

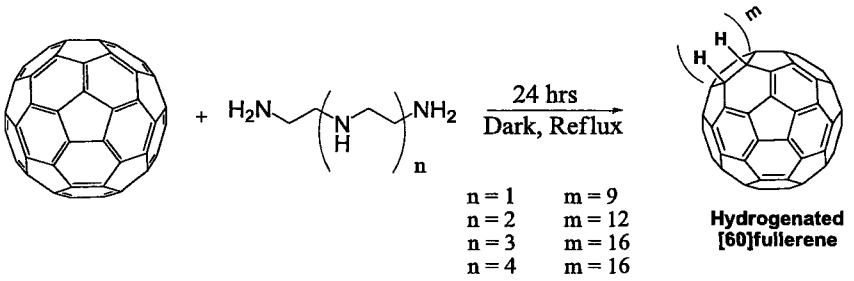

Scheme 15: Hydrogenation of [60]fullerene with polyamines

Similar results were seen when DETA was heated in a sealed high pressure reactor at temperatures above the boiling point. Thus, when a DETA reaction was run at approximately 300 °C the product profile based on ^{1}H-NMR and mass spectroscopy was very similar to that of the hydrogenated [60]fullerene from TETA showing that the level of hydrogenation is a function of reaction temperature, not the molecular weight of the chosen polyamine. This was further confirmed by use of a long chain poly(ethyleneimine) of approximately 80,000 Daltons which gave rise to a similar product as obtained through the use of TETA. The poly(ethyleneimine) chosen was 50% water by weight which reduced its boiling point to approximately 250 °C.

Under comparable reaction conditions (i.e., conventional or microwave heating in the presence of polyamine), [70]fullerene is also hydrogenated in excellent yield. Unlike [60]fullerene, however, the reaction with [70]fullerene is not regioselective at any temperature tested. For example, after 16 hours of conventional heating in DET at 205-206 °C, the resulting hydrogenated [70]fullerene contains 28 hydrogens on average as evidenced by LDI mass spectra. ^{1}H NMR spectra show broad, complex, overlapping signals between 3 and 5 ppm (i.e., "haystack" signals) indicating formation of a complex mixture of [70]fullerane products (Figure 10). After heating for 1 week in DET at 205-206 °C, the resulting mixture of hydrogenated [70]fullerene contains marginally more hydrogen, 31 hydrogens per [70]fullerene on average, but ^{1}H NMR spectra still indicate a complex mixture of [70]fulleranes. Upon reacting [70]fullerene with DET in a sealed stainless steel Swagelok vessel at 300 °C for 15 hours, an average of 27 hydrogens is observed to add to each [70]fullerene cage. In this case, ^{1}H NMR spectra reveal several distinct multiplets between 3 and 5 ppm indicating marginally improved regioselectivity (Figure 10). No attempt was made to isolate individual [70]fullerene compounds.

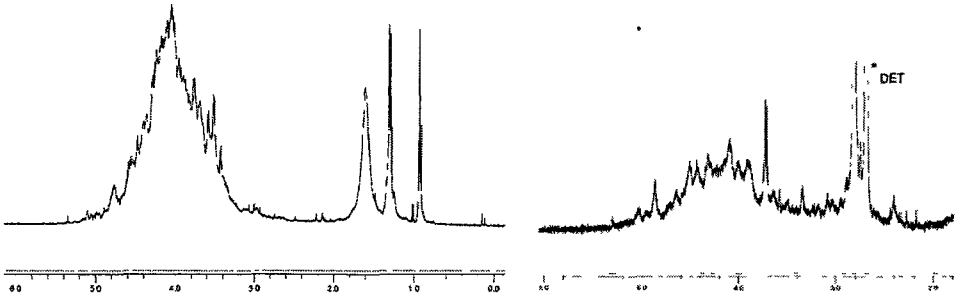

Figure 10: ^{1}H NMR spectra of [70]fullerane ($CDCl_3$, ppm scale) produced after 1 week in boiling DET (left) and 15 h in DET at 300 °C (right).

Although numerous studies of [60]fullerene and [70]fullerene hydrogenation have been reported, there is only one report of an attempted hydrogenation (Zn/HCl) of larger fullerenes ([76]-, [78]- and [84]fullerenes)[12] and no reports concerning the hydrogenation of giant fullerenes. We studied the DET hydrogenation of large and giant fullerenes extracted from SWNT soot (MER Corp.). The fullerenes were extracted using 1-phenylnaphthalene (b.p. 324-5 °C) as solvent. In this manner, fullerenes ranging in size from C_{60} to C_{250} were extracted and detected by LDI mass spectrometry (Figure 11). Following removal of the solvent, the 1-phenylnaphthalene extract was added to boiling DET for 15 h and worked up in the normal manner. LDI mass spectrometry provides clear, convincing evidence for the hydrogenation of large and giant fullerenes (Figure 11). It is possible to quantify the level of hydrogenation for fulleranes as large as [96]fullerane (Table 1) but decreasing signal intensities associated with still larger fulleranes prohibits their quantitative evaluation. Qualitatively, it does appear that all of the fullerenes, including the giant fullerenes, are hydrogenated using polyamines.

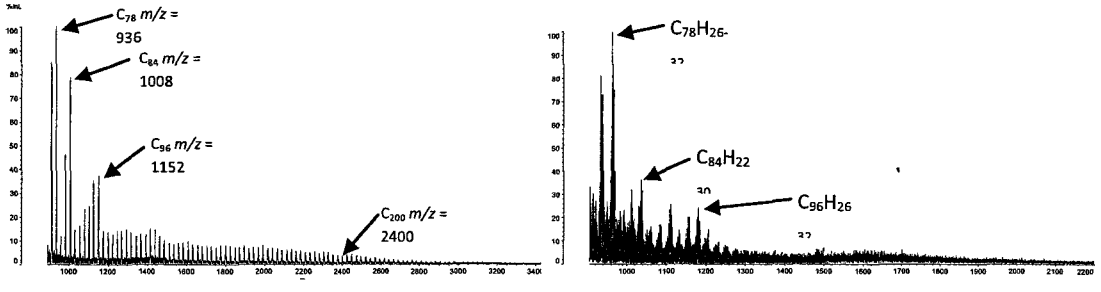

Figure 11: LDI mass spectrum of a 1-phenylnaphthalene extract of Kratschmer-Huffman soot before hydrogenation.

Fullerene	Approx. No. H additions[a]
[76]	21-28
[78]	26-32
[80]	24
[82]	28
[84]	22-30
[86]	28
[88]	28
[90]	30
[92]	28
[94]	30
[96]	26-32

[a]As detected by LDI mass spectrometry; fulleranes with >96 carbon atoms could not be quantitatively assessed due to poor *S/N* ratios in the LDI mass spectrum.

Table 1: Approximate number of additions to large fullerenes during DET hydrogenation of 1-phenylnaphthalene extraction

2.1.3 Transition Metal Catalyzed Polyamine Hydrogenation of [60]Fullerene

The mostly highly hydrogenated [60]fulleranes are produced through a combination of elevated temperatures and added cobalt (Co). Thus, upon reacting [60]fullerene with TEP in the presence of 5 weight % Co for 15 h, [60]fullerane product with an average of 30 hydrogens per cage is produced. Running an otherwise identical reaction in the higher boiling PEH produces [60]fullerane product with an average of 32 hydrogens per cage (Figure 12).

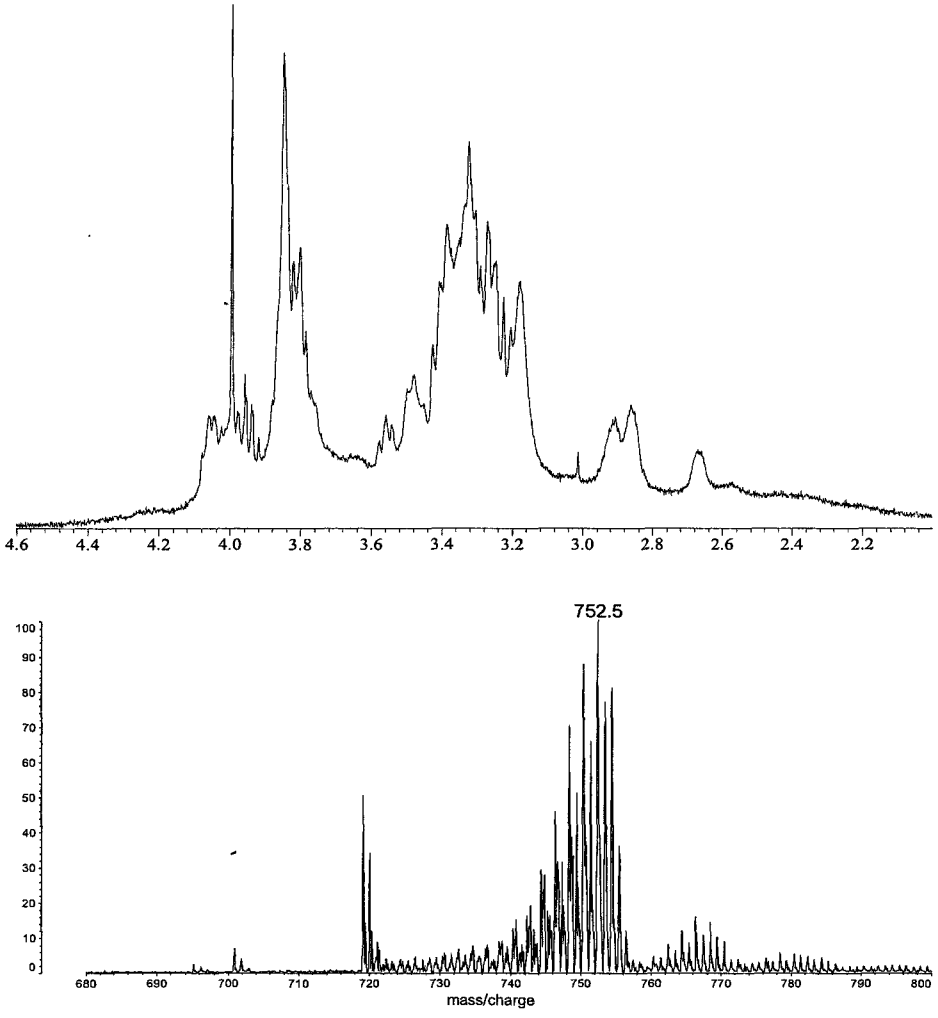

Figure 12: ^{1}H NMR spectrum (top, C_6D_6, ppm scale) and LDI mass spectrum (bottom) of [60]fullerane produced after 15 h in boiling PEH with 5 weight % Co added.

In the initial synthesis of hydrogenated fullerenes there was an attempt to insert the fullerenes into SWNTs in order to make a hydrogenated version of the "nano-peapods"[140] and to investigate their properties. Using commercially available SWNTs and [60]fullerenes and refluxing in DETA for approximately 24 hours resulted in much

higher levels of hydrogenation then would be expected. Analysis by NMR spectroscopy and mass spectrometry showed that the level of hydrogenation was on par with that if TEPA had been used instead of DETA.

Investigations into this phenomenon lead us to consider that the catalyst used in the production of the SWNTs was facilitating hydrogenation. The commercially available nanotubes that we used were synthesized via CVD using cobalt nanoparticles as nucleation sites. Even though the material was purified after synthesis, approximately 2.5% by weight of cobalt remained in the SWNTs. To test this hypothesis, a similar polyamine hydrogenation reaction was performed using off-the-shelf cobalt metal particles that had an average diameter of 20 micrometers. When 5 mole percent of cobalt was used in conjunction with DETA and [60]fullerene, no difference was observed as compared to that of a reaction run without any metal catalyst. The cobalt particles were then subjected to ball milling conditions to reduce the size of their size to approximately 2 micrometers in diameter, thus greatly increasing their surface area. When the milled cobalt metal was used as catalyst in an otherwise normal [60]fullerene/DETA reaction, a noticeable increase in hydrogenation was observed similar to that as hydrogenating [60]fullerene with boiling TETA . Further testing with commercially available cobalt nanoparticles, possessing an average diameter of 50 nanometers, showed similar results to that of the milled cobalt metal.

To continue this study several different transition metals were tested under standard [60]fullerene/DETA hydrogenation conditions (24 h, boiling DETA, dark). All

the metals that were selected had particle sizes comparable to that of the milled cobalt and in each case, the metals were used at 5 mole percent (Scheme 16 and Table 2).

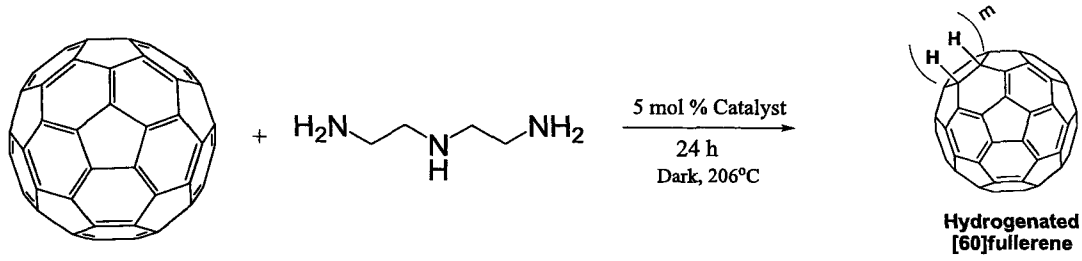

Scheme 16: Hydrogenation of [60]fullerene with DETA in the presence of catalyst

Catalyst	Product
Iron	$C_{60}H_{18}$
Cobalt	$C_{60}H_{18} - C_{60}H_{36}$
Nickel	$C_{60}H_{18}$
Copper	$C_{60}H_{18}$
Rhodium (5% on carbon)	$C_{60}H_{18}$
Ruthenium (5% on carbon)	$C_{60}H_{18}$
Palladium (5% on carbon)	$C_{60}H_{18} - C_{60}H_{36}$
Platinum	$C_{60}H_{18}$
Zinc	$C_{60}H_{18}$

Table 2: Results of hydrogenation in the presence of transition metal catalyst

The metals selected are all known to catalyze standard hydrogenations using hydrogen gas. As described in the table above, only two of these the metals promoted polyamine hydrogenation of [60]fullerene, cobalt and palladium.

2.1.4 Exploration of Mechanism/Unusual Amines for Hydrogenation

To further understand the polyamine hydrogenation mechanism experiments were conducted to see if the hydrogenation is limited to oligo and poly(ethylenediamine) species or if any polyamine, regardless of structure, is sufficient. In addition to amines structure, temperature is also important. In the case of DETA and other poly(ethylenediamine) based polyamines, hydrogenation only occurs at elevated temperatures. If a poly(ethylenediamine) based reaction is attempted at, or near at room temperature, then only hydroamination dominates.[139]

A series of polyamines was selected in order to see if the carbon spacer between the amino groups is critical factor in polyamine hydrogenation. These polyamines include dipropylenetriamine, dihexylenetriamine and hexylenediamine. Decylamine, with a boiling point similar to that of DETA, was also tested. All of these reactions were run under conditions (dark, N_2, 210 °C) that simulate DETA hydrogenation in an open vessel. Under these conditions, each polyamine gave primarily hydroamination product with only a small amount of hydrogenated fullerene detected by mass spectroscopy (Scheme 17).

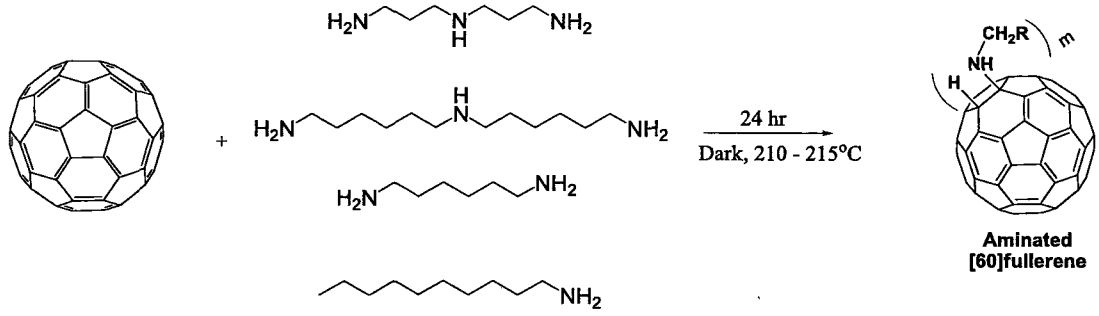

Scheme 17: Amination of fullerenes from polyamines and decylamine

Although a small amount of hydrogenation was detectable by mass spectroscopy, NMR spectroscopy was consistent with hydroamination. Based on the ^{1}H-NMR spectra collected (Figure 13), it is clear that the amination is occurring in a reasonably symmetric fashion. This is unusual for a hydroamination reaction. Low molecular weight aliphatic amines are known to add in a less selective manner.[141] Mass spectra indicate multiple additions of the polyamines. Further study is warranted. For the purpose of this study, it is evident that a two-carbon spacer may be critical for the hydrogenation of fullerenes.

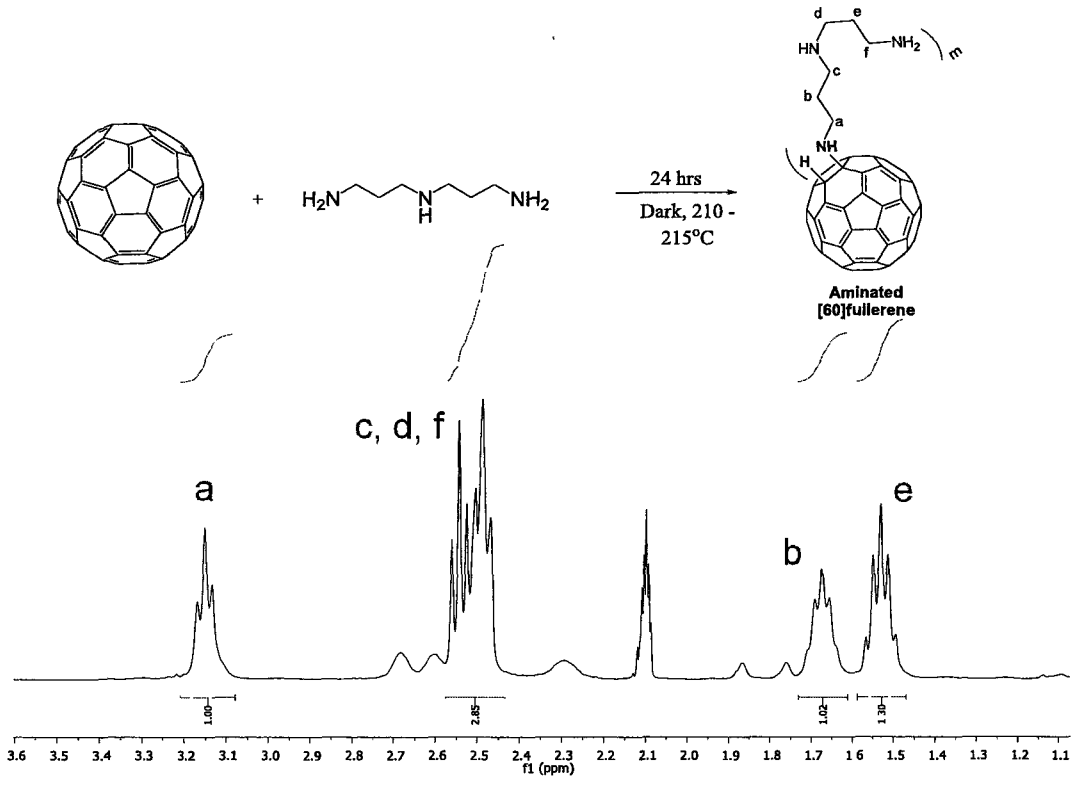

Figure 13: ^{1}H NMR of the amination of [60]fullerenes from dipropylenetriamine

Having established that a two-carbon spacer in the polyamine supports hydrogenation, we next sought to understand the substitution requirements on each nitrogen. Thus, we studied a series of different substituted polyamines (Table 3), all of which possess two carbon spaces between adjacent nitrogen atoms. All of the reactions were run at the boiling point of the polyamine in the presence of [60]fullerene for 24 hours, under nitrogen and in the dark. Although the temperature varied from reaction to reaction, in general the boiling points of the substituted amines were close to that of DETA (207 °C) making comparison reasonable. The results (Table 3) are clear. If all nitrogen atoms are tertiary, as in the N,N,N′,N′,N″-pentamethyl diethylenetriamine, then

there is no hydrogenation observed. In fact, no reaction is observed. This is consistent with the results of previous research in the Miller group when deuterated DETA (i.e. DETA-d^5 in which all hydrogen atoms on nitrogen were replaced with deuterium) gave rise to $C_{60}D_{15\text{-}18}$ product.[142]

Amine	Reaction Temperature (°C)	Result
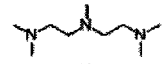	208	No Reaction
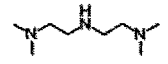	198	Predominantly Hydroamination
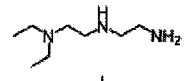	223	Hydrogenation and Hydroamination
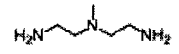	217	Hydrogenation only
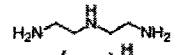	207	Hydrogenation only
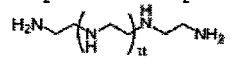	266-380	Hydrogenation only

Table 3: Reactions between [60]fullerene and substituted polyamines

Thus, the hydrogen atoms on the nitrogen are responsible for hydrogenation. Polyamines with all nitrogen atoms tertiary have no N-H hydrogens to donate. The data in Table 3 also suggests that hydrogenation is facilitated by terminal primary amino groups. Therefore, those polyamines were not as effective at hydrogenation. Conversely, substitution at the interior nitrogen, already secondary nitrogen in DETA, seems less important.

To further understand the mechanism for hydrogenation, cyclic amines were also examined. While the cyclic amines chosen (Table 4) have lower boiling points than DETA, they can be heated to over 200 °C degrees in a closed vessel. The cyclic amines

were reacted with [60]fullerene at reflux temperature or higher, in the dark and under nitrogen to simulate DETA hydrogenation conditions.

Amine	Reaction Temperature	Time	Result
	138	24 h	No reaction
	129	24 h	No reaction
	146	24 h	Slight Hydrogenation
	210 (Microwave)	30 min	Hydrogenation only
	210 (Sealed vessel)	24 h	Hydrogenation only
	106	24 h	Slight Hydrogenation
	210 (Microwave)	30 min	Slight Hydrogenation

Table 4: Reactions between [60]fullerene and cyclic amines or cyclic polyamines

In the case of morpholine and N-methylpiperizine there was no sign of hydrogenation at the boiling temperature of the respective amines. Piperazine, however, did show a small amount of hydrogenation product with an average of 8 hydrogens per [60]fullerene, as evidenced by mass spectrometry. When the temperature was increased to that of the boiling point of DETA by either using a sealed pressurized vessel, with conventional or microwave heating, the level of hydrogenation was the same as with DETA. That is, $C_{60}H_{18}$ was produced. These results indicate that secondary diamines with two carbon spacers are sufficient for fullerene hydrogenation. By contrast, piperidine only produces a small amount of hydrogenated fullerene with approximately 6

hydrogens per [60]fullerene, even when it is heated to 210 °C. Piperidine and morpholine are both known to form amination products when the reactions are performed at room temperature.[141] Thus, it appears that a diamine with both nitrogen atoms primary or secondary and with a two-carbon spacer between the nitrogen atoms is a minimum requirement for efficient hydrogenation. A mechanism involving concerted electron transfer and proton donation can be considered as in Scheme 18.

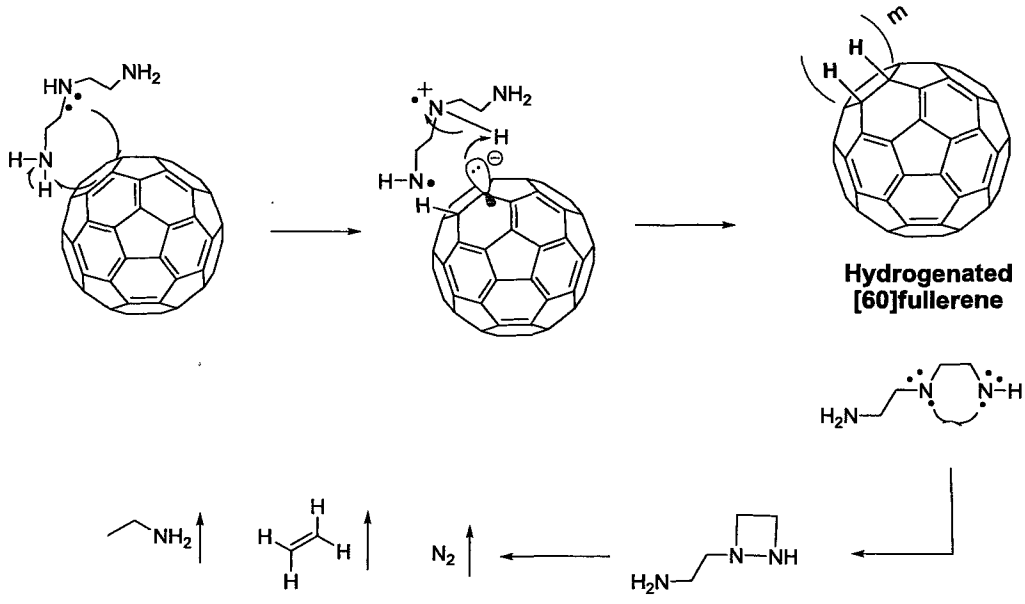

Scheme 18: Proposed hydrogen transfer mechanism for polyamine hydrogenation of [60]fullerene

In this mechanism a lone pair of the nitrogen, from either a primary, secondary or tertiary amine donates an electron to the [60]fullerene to generate a fullerene radical anion that immediately abstracts a proton from an adjacent primary or secondary nitrogen atom. The two-carbon space allows for a seven-membered transition state to form which may be energetically favorable. The mechanism is preliminary and still requires detailed

study, both experimentally and computationally. Ethyleamine has been detected by IR spectroscopy as an off gas of the reaction.

2.1.5 Proposed Synthesis of S_6-$C_{60}H_{24}$

When a polyamine hydrogenation of [60]fullerene was performed using a catalytic amount of cobalt nanoparticles and an excess of DETA a mixture of white and yellow fullerene products were seen. Upon ^{1}H-NMR analysis it was clear that the compounds formed were considerably more hydrogenated than the $C_{60}H_{18}$, the normal product of DETA reactions. By mass spectrometry, over 30 hydrogens had added to the surface of the fullerene, indicating the possible formation of $C_{60}H_{36}$ However, the main product appeared to have approximately 24 hydrogens added. Interestingly, the ^{1}H-NMR spectrum indicated the presence of a singlet at 4.42 ppm in $CDCl_3$, which appeared to be the only signal associated with the main product. We immediately began to consider structures in which all hydrogens are equivalent. Once the number of hydrogens reaches 24, there are very few species with sufficient symmetry that a lone singlet should be observed in the ^{1}H-NMR spectrum. An example is S_6- $C_{60}H_{24}$ in Figure 14.

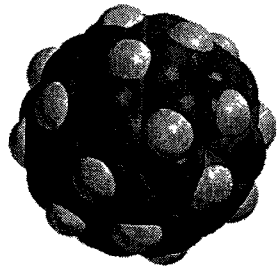

Figure 14: Proposed structure of S_6-$C_{60}H_{24}$

We soon observed that a reaction between [60]fullerene and boiling TETA (b.p 266-267 °C) gave a much higher concentration of what is believed to be the S_6-$C_{60}H_{24}$, as evidenced by ^{1}H-NMR spectroscopy (Figure 15).

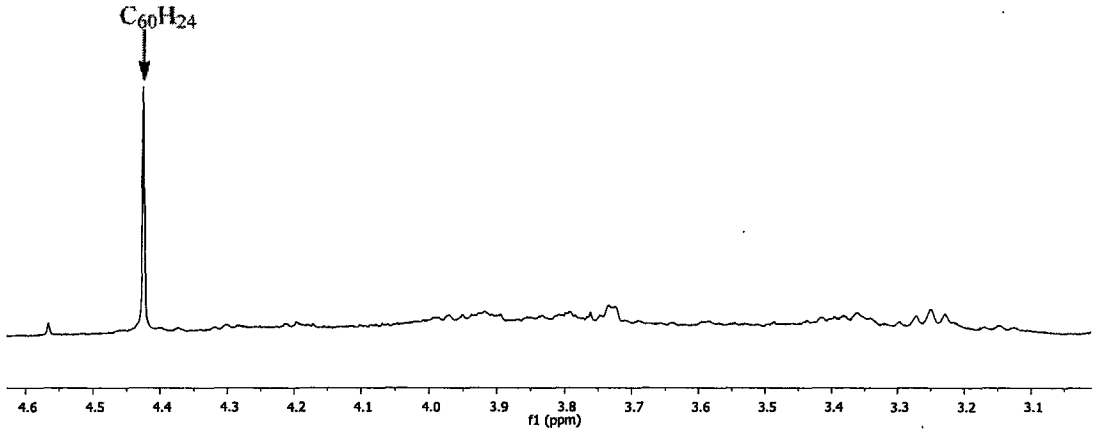

Figure 15: ^{1}H-NMR spectra of the products from the [60]fullerenes/TETA reaction

^{13}C-NMR and 2D NMR experiments (gHSQC and gHMBC) were performed. The spectra indicated that S_6-$C_{60}H_{24}$ was formed in the presence of a fair amount of other hydrogenated fullerenes. Based on the ^{13}C-NMR spectra (Figure 16), gHSQC and gHMBC spectra (see supplemental data for cross-correlation spectra) two hydrogenated [60]fullerenes were identified , S_6-$C_{60}H_{24}$ and T_d- $C_{60}H_{36}$.[14]

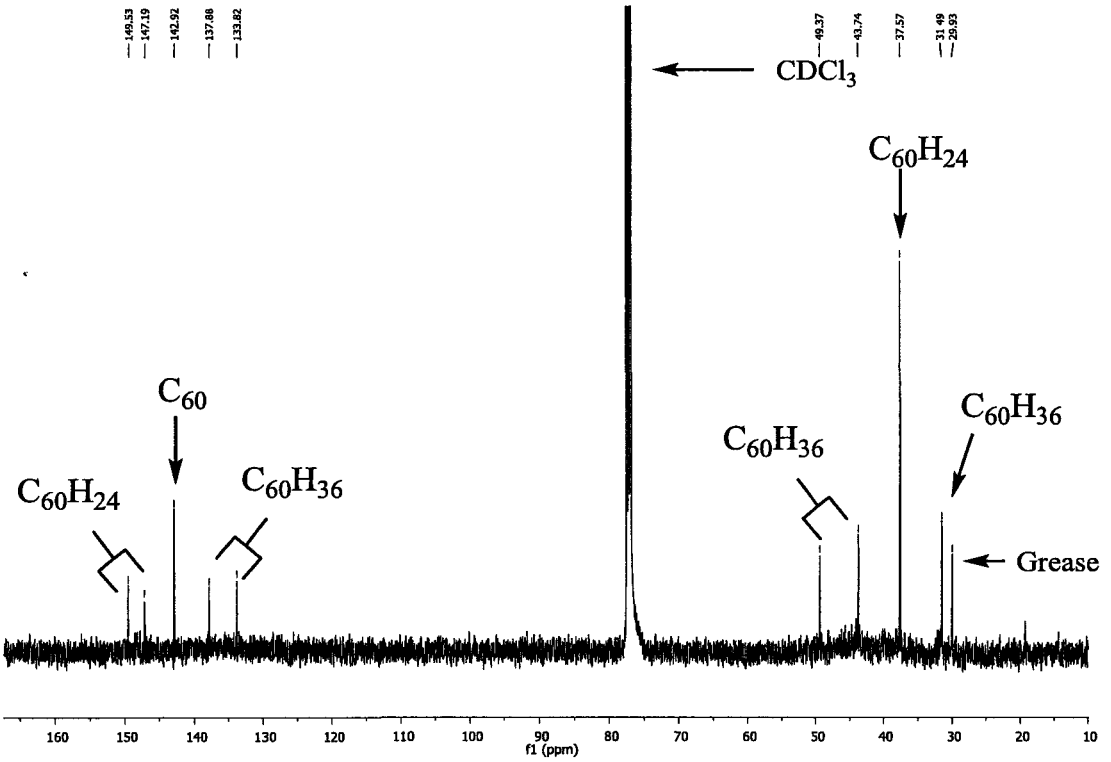

Figure 16: ^{13}C-NMR spectra of the products from the [60]fullerenes/TETA reaction

We attempted to isolate the S_6-$C_{60}H_{24}$ by HPLC using a Buckyclutcher HPLC column and a 224 nm detector. The hydrogenated fullerenes were prepared by refluxing [60]fullerenes in TEPA for 18 hours in the dark under nitrogen. After washing with water to remove any remaining amine, the hydrogenated fullerene mixture was dissolved in dichloromethane and then injected into the HPLC using 250 microliter aliquots. The HPLC separation was performed with a 50/50 mixture of hexanes and dichloromethane over the first 4 minutes, then increasing to 100% dichloromethane over the next 11 minutes, holding for 5 minutes followed by reducing to 50% dichloromethane and finally holding at a 50/50 mixture of hexanes and dichloromethane for 10 minutes. This

complex gradient method enabled a separation of the mixture of hydrogenated fullerenes (Figure 17). Identification of the $C_{60}H_{18}$ and $C_{60}H_{36}$ fractions were achieved by subjecting purified compound to identical HPLC conditions and measuring the retention times.

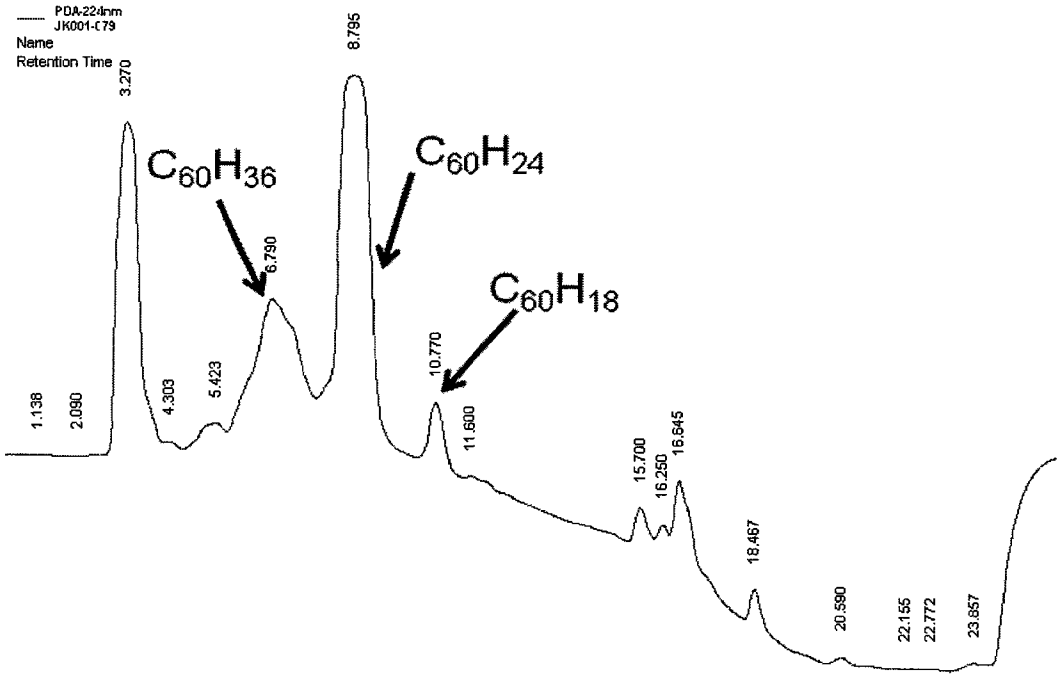

Figure 17: HPLC profile for the separation of the products from the [60]fullerenes/TEPA reaction

While the HPLC separation of S_6-$C_{60}H_{24}$ was successful there are problems with this method. Due to the solubility restrictions and column load considerations, we could only inject 250 microliters per run. Over 100 runs would be required to isolate 1 milligram of S_6-$C_{60}H_{24}$ material. Because the solubility of the pure S_6-$C_{60}H_{24}$ is so low, ^{1}H-NMR spectra never indicated a satisfactory signal-to-noise ratio. It is interesting that

the solubility of S_6-$C_{60}H_{24}$ appears to be greater in the presence of hydrogenated fullerene impurities than in its pure form, however this property complications characterization.

In summary, polyamines have been shown to be effective reagents for the hydrogenation of fullerenes and the method is amenable to scale-up. The mechanism of hydrogenation has been explored using several different polyamines including those with different sized carbon spacers between amine functional groups. It was shown that a two-carbon spacer between amine groups is critical for efficient hydrogenation. It was also shown that the presence of at least two amines that are not tertiary leads to effective hydrogenation. The extent of hydrogenation on the fullerenes is a function of reaction temperature. C_{3v} $C_{60}H_{18}$ forms preferentially at approximately 200 °C whereas $C_{60}H_{36}$ species are preferentially formed at approximately 340 °C and above. While either C_{3v} $C_{60}H_{18}$ or $C_{60}H_{36}$ species dominate at essentially all reaction temperatures, S_6 $C_{60}H_{24}$ was found to be produced in small quantities whenever fulleranes were produced. Despite attempts to isolate S_6 $C_{60}H_{24}$ by HPLC chromatography, only a few milligrams could be obtained. The material was shown to be particularly insoluble in its purified form making detailed spectroscopic analysis difficult.

2.2 Hydrogenated Nanotubes

2.2.1 Hydrogenation and Characterization of SWNTs

With the hydrogenation of fullerenes by polyamines well established, we sought to hydrogenate SWNTs using a similar method.. Unmodified SWNTs exist in bundled structures

held together by a combination of van der Waals and very weak non-covalent interactions.[143,144] While bundled SWNTs have useful properties, the most synthetically useful nanotubes have been isolated into individual tubes to be used in an array of electronic devices.[144] Current techniques to disperse SWNTs include use physical agitation by ultrasound (or sonication) in conjunction with surfactants or polymers. However this method is known to damage the surface of the SWNTs and to cut the length of the SWNTs, especially with long sonication times.[145,146] Another problem with using sonication to disperse SWNTs is that it can cause chemical reactions between SWNTs and dispersing solvents like ortho-dichlorobenzene.[147]

Surfactant used to disperse the SWNT work by coating the surface of the nanotubes which helps break up π-π stacking interactions between tubes. The surfactants have limitations since they do not completely coat the SWNTs or penetrate into the insides of the larger nanotube bundles limiting their ability to disperse high concentrations of SWNTs. Another method that has shown promise in making individual SWNTs is chemical modification. One of first methods used to disperse nanotubes was by oxidizing the surface of the SWNTs using a combination of sulfuric acid, nitric acid, and in some cases hydrogen peroxide.[148,149] This method has been shown to greatly increase the dispersibility of nanotubes in aqueous or polar solvents. One problem with the oxidation method is that many structural changes in the SWNTs can occur such as opening of the end-caps of the nanotubes, opening the nanotubes along their long axis, shortening the length of the nanotubes and causing the addition carboxylic acid, ketone, or alcohol functional groups on the surface of the nanotubes. All of these issues can

cause a dramatic reduction in the electronic properties of the SWNTs and make them less desirable for use in electronics.[150]

Other chemical functionalizations can also increase dispersion of the SWNTs but without significant structural damage. Some of these methods include addition of azomethine ylides,[151] or aryl diazoniums,[152] or by fluorination.[153,154] These methods debundle the SWNTs by chemically modifying the sidewalls of the nanotubes. By converting the sp^2 carbons to sp^3 the conjugation of the sidewalls on the nanotubes and π-π stacking between tubes interactions are greatly reduced. This causes greater dispersion of the nanotubes and allows them to be manipulated in a variety of solvents. Much like oxidation, however this functionalization leads to a decrease in the electronic properties of the nanotubes, which possibly makes them unsuitable for some devices.

To conduct the polyamine hydrogenation of SWNTs, we used PEHA (b.p. 380 °C) which is the highest boiling polyamine amongst the set of commercially available low molecular weight polyamines. Since the reactivity of the SWNTs is much lower than that of the fullerenes, the reaction must be performed at high temperatures. We utilized a sealed high-pressure stainless steel vessel and heated to approximately 500 °C for 24 hours. This reaction is catalyzed by cobalt nanoparticles. If the cobalt is not already present in the SWNTs, then cobalt nanoparticles can be added. Cobalt is used as catalyst for CVD growth of the SWNTs so it often present in commercial samples. We utilized SWNTs that were prepared using a cobalt catalyst and had a purity of ~90 %. After the reaction was completed, care was taken during cool down and opening of the vessel as a large quantity of amine gas is produced under these conditions. Hydrogenated SWNTs

(or H-SWNTs) can be cleaned of polyamine by washing in solvents such as water or ethanol in conjunction with a centrifuge in order to separate the treated nanotubes from the polyamines. The H-SWNTs are then dried by vacuum and characterized by several different techniques.

Characterization of H-SWNTs takes several different forms. One of the easiest methods is to suspend 1 milligram of H-SWNTs in 5 milliliters of methanol followed by 1 minute of sonication. As compared to as-purchased SWNTs, the H-SWNTs stay suspended for a much longer time. Whereas as-prepared SWNTs precipitated from solution within minutes, H-SWNTs stay partially dispersed for days (Figure 18).

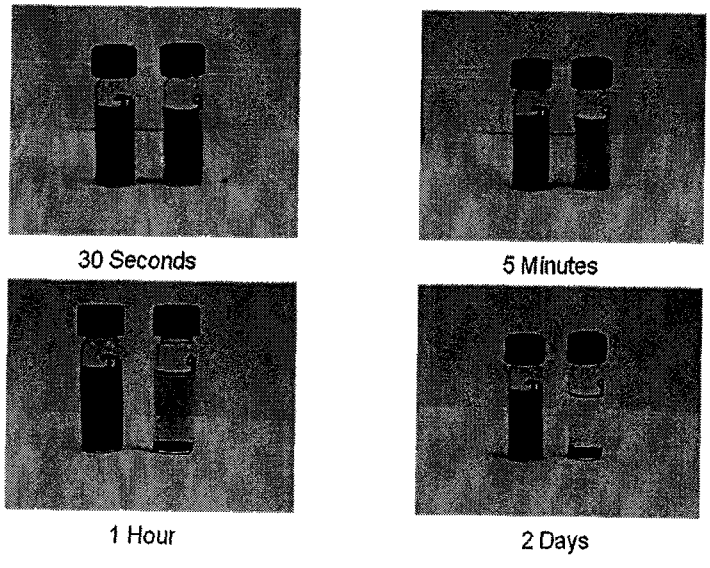

Figure 18: Comparison between H-SWNTs (left) and as purchased SWNTs (right) suspended in methanol

Another method to characterize H-SWNTs is transmission electron microscopy (TEM). TEM detects crude structural changes in the SWNTs, as one would expect upon

converting sp^2 carbons to sp^3. Following polyamine treatments, high resolution TEM indicates a highly corrugated nature to the sidewalls of the tubes. Moreover, the TEM also indicates debundling of the nanotubes, indicative of a reduction in π-π stacking interactions. This debundling can be clearly seen when compared to that of the untreated nanotubes (Figure 19).

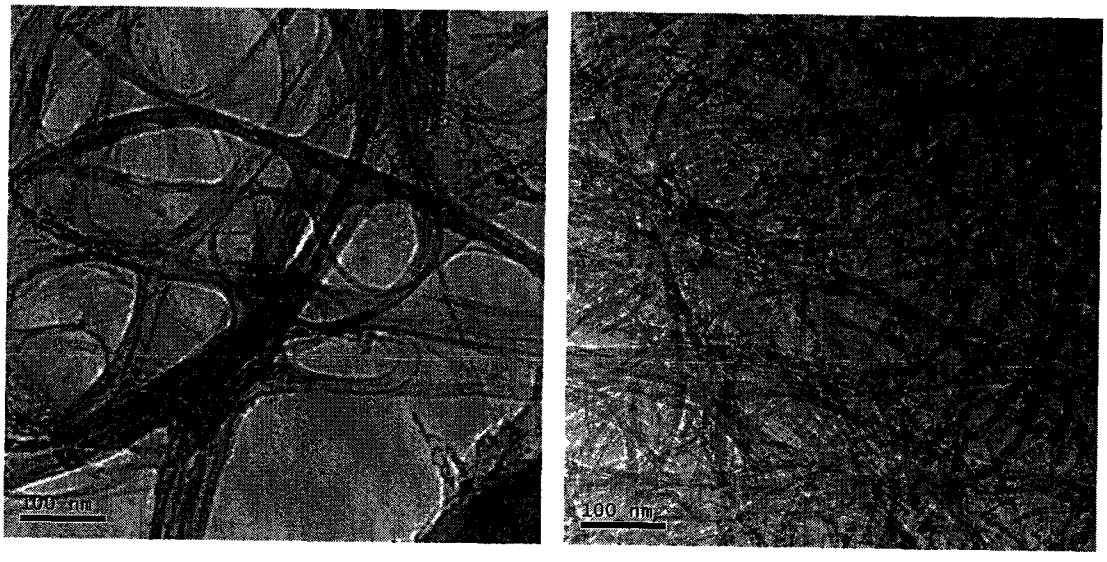

Figure 19: TEM of nanotubes before hydrogenation (left) and after hydrogenation (right) (at 25000x)

To further confirm that hydrogenation has occurred, the polyamine treated SWNTs were thermally annealed to remove hydrogen and return the nanotubes to their pre-treated state. Using a thermogravimetric analyzer (TGA) for thermal annealing, an 8% weight loss was observed for a sample heated under N_2 from room temperature to 800 °C. Pekker and co-workers reported qualitatively similar TGA data for SWNTs hydrogenated using a dissolving metal reduction,[155] but they observed less than 5%

weight loss up to 900°C, indicating overall lower levels of hydrogenation. In Pekker's work, the effluent gases were analyzed by a mass spectrometer revealing the release of several molecules including hydrogen, methane, and methanol. By comparing the results of the polyamine hydrogenation to Pekker's study, it was deduced that the C:H ratio of the H-SWNTs was 10:1. After thermal annealing of our H-SWNTs to 800 °C, a sample was analyzed by TEM. The resulting images are identical to those of as-produced SWNTs, which show a similar propensity to bundle (Figure 20). Thus, we conclude that polyamine hydrogenation is thermally reversible.

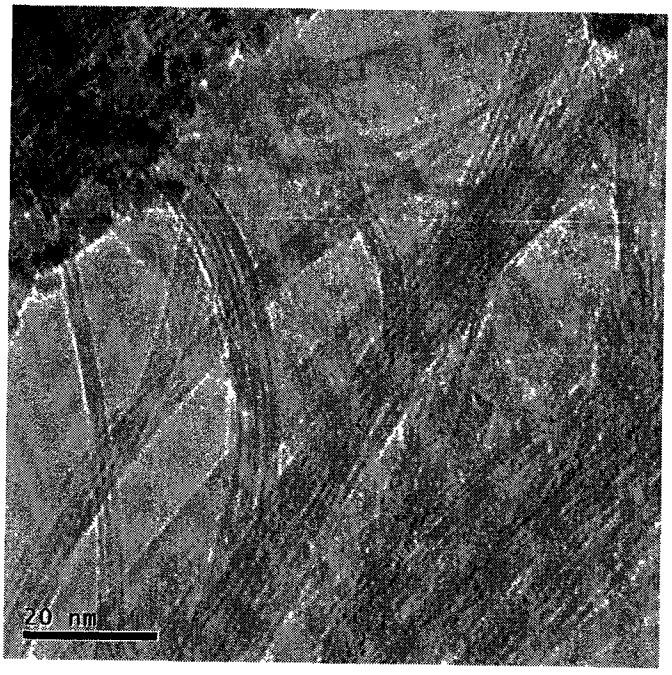

Figure 20: TEM of SWNTs after thermal annealing in which bundling is clearly seen (at 160000x)

Raman spectroscopy or Fourier transform infrared spectroscopy (FT-IR) can also be used to determine if there is modification on the surface of the nanotubes. The Raman characterization of the H-SWNTs is consistent with the formation of functionalized

SWNTs, in which sp^2 carbons are converted to sp^3 carbons. As seen in the Raman spectra (Figure 21), the D band, indicative of sp^3 carbon formation along the sidewalls of the SWNT and centered at approximately 1300 cm^{-1} , grows relative to the graphitic G-band, centered at approximately 1580 cm^{-1}, following polyaminehydrogenation.

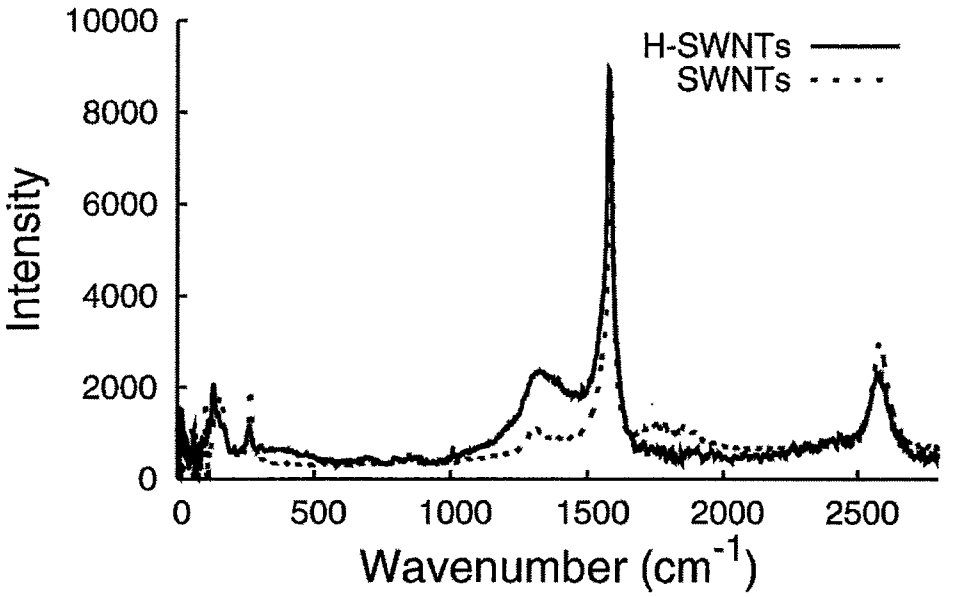

Figure 21: Raman spectra of SWNTs and H-SWNTs

FT-IR characterization of SWNTs is much more problematic and infrequently utilized. The absorbance of nanotubes is extremely high making use of direct measurement with Attenuated Total Reflectance or ATR very difficult. A method that does work involves making a mull with a fluorinated hydrocarbon known commercially as Fluorolube. Fluorolube mulls were prepared by mixing H-SWNTs and Fluorolube oil using a mortar and pestle. The resulting mull was placed between two NaCl plates and the plates pressed together prior to recording the first FT-IR spectrum. Using an iterative process, the film between the NaCl plates was systematically thinned by removing mull

from the plates and re-recording until IR spectra of suitable quality were obtained. It was important that the amount of Fluorolube was kept to a minimum because there is a very small amount of hydrocarbon in the Fluorolube which if sufficiently concentrated, can complicate detection of C-H bands stretching from the H-SWNTs (Figure 22).

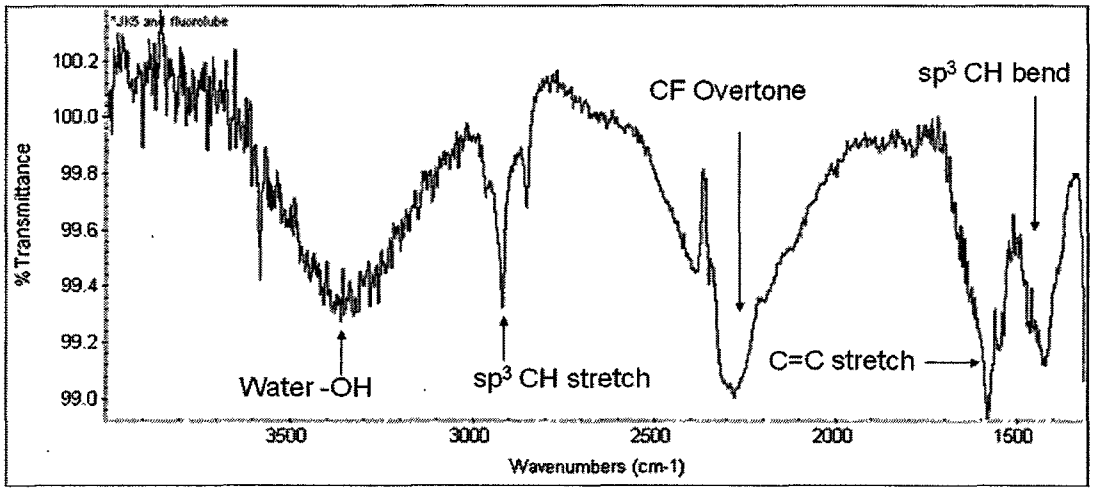

Figure 22: IR spectra of H-SWNTs in Fluorolube mull

The FT-IR spectra reveal C(sp^3)-H stretching vibrations at 2962 cm^{-1}, 2918 cm^{-1}, and 2849 cm^{-1} as shown in Figure 22. Additional IR bands include a relatively intense band at 1580 cm^{-1} corresponding to C=C double bond stretching vibrations. These experimental values for C(sp^3)-H stretching vibrations are in close agreement with those recorded for SWNTs hydrogenated using a H-plasma[40] at 2955 cm^{-1}, 2924cm^{-1}, and 2854 cm^{-1}.

A combination of characterization methods provides compelling evidence that polyamines effectively hydrogenates SWNTs. This method of hydrogenation has

advantages over other methods. Other chemical functionalization and other hydrogenation protocols (e.g H-plasma) are not scalable. We envision utilizing polyamine produces H-SWNTs in applications where dispersion of large quantities of SWNTs in a matrix or on a substrate is required for electronic (as opposed to mechanical) applications. Thus, following the hydrogenation, the H-SWNTs are dispersed in the matrix of choice or patterned on a substrate of choice and then thermally annealed to produce pristine SWNTs.

CHAPTER 3

SYNTHESIS OF GRAPHANE

3.1 Graphane

3.1.1 Exfoliation of Graphene from HOPG using high boiling Hydrocarbon Solvents

Since the discovery of graphene in 2004, much work has focused on uncovering a method for bulk scale production. Current methods are either too inefficient or too expensive for the large scale production of low cost, high quality graphene. One approach that has been extensively studied involves the chemical exfoliation through oxidation in order to form graphene oxide (GO). Subsequent reduction of GO produces a graphene material with diminished electrical properties compared to pristine graphene. To combat this problem, a simpler method that could be used is thermal exfoliation though high temperature reactions that do not chemically modify graphene. One way to perform these reactions is by contacting graphite with high boiling aromatic or non-aromatic solvents. Thus, we heated solvent to high temperatures in a high pressure reactor in the presence of either graphite or highly oriented pyrolytic graphite (HOPG). The high temperature conditions can conceivably exfoliate graphene via solvent intercalation or through high energy collisions with the graphite surface and effectively disrupt π-π interactions between adjacent layers. With the introduction of aromatic compounds such as

naphthalene or chrysene, it is also possible that solvent-graphite π-π stacking interactions could facilitate exfoliation, akin to a molecular "Scotch Tape" effect.

Reactions were performed by taking a 1 mm disk of commercially available HOPG and placing it in a stainless-steel high pressure reactor in the presence of a large excess (greater than 2 grams) of either naphthalene, adamantane or chrysene. The vessel was sealed and then heated to 500 °C for 24 hours (Scheme 19).

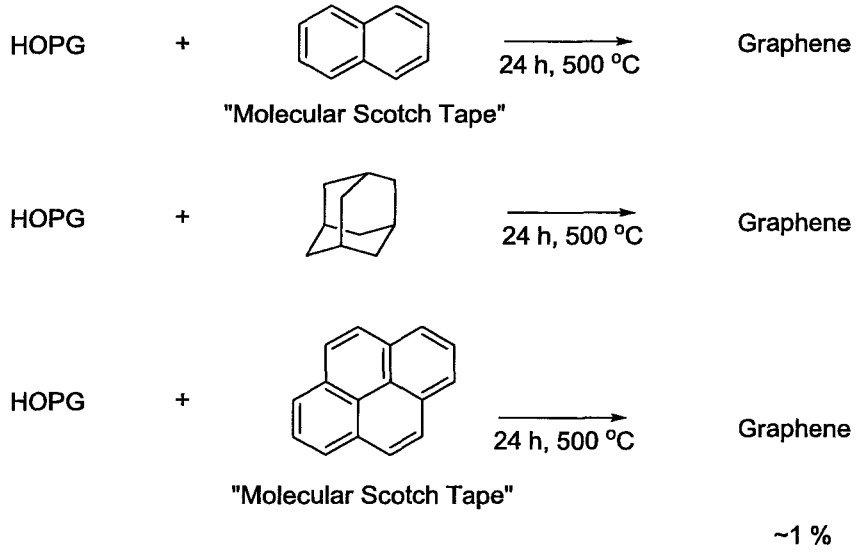

Scheme 19: Synthesis of graphene from high temperature hydrocarbon reaction

After each reaction was completed, the corresponding sample was washed three times with chloroform to remove solvent, allowing for the graphitic materials to settle for 30 minutes between each wash. The graphitic product was then imaged by TEM using a 200 mesh lacey carbon grid. Analysis of the TEM images showed that exfoliation of the HOPG had occurred and that single-layered and few-layer graphene was produced during

these reactions (Figure 23). However, the yield of graphene product was low, about 1% based on gravimetric analysis of the HOPG disk before and after the reaction.

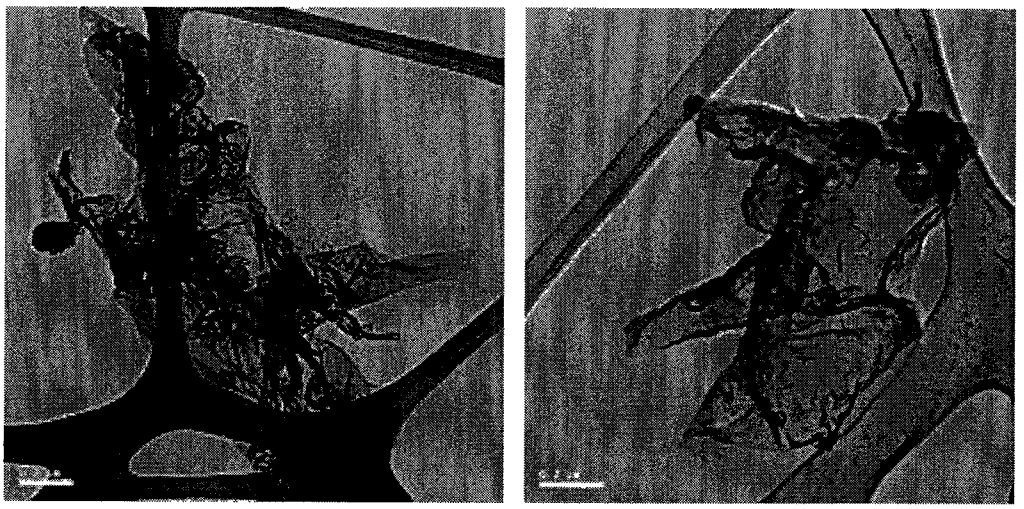

Figure 23: Examples of graphene from exfoliation with naphthalene (let) and adamantane (right) (scale of bar is 200 nm)

As seen in the TEM images of Figure 23, graphene sheets produced in this manner are typically on the order of a few square micrometers with distorted shapes. This is not unexpected as graphene tends to bundle and fold in on itself when it is free standing. Few-layer and multi-layer graphene is much more flat in appearance due to the van der Waals interactions between the graphene layers. For example the graphene nanoribbons of Figure 24 are believed to be a few layers thick, as evidenced by their relatively flat appearance. They are not, however, tens of layers thick as they appear transparent in the TEM images.

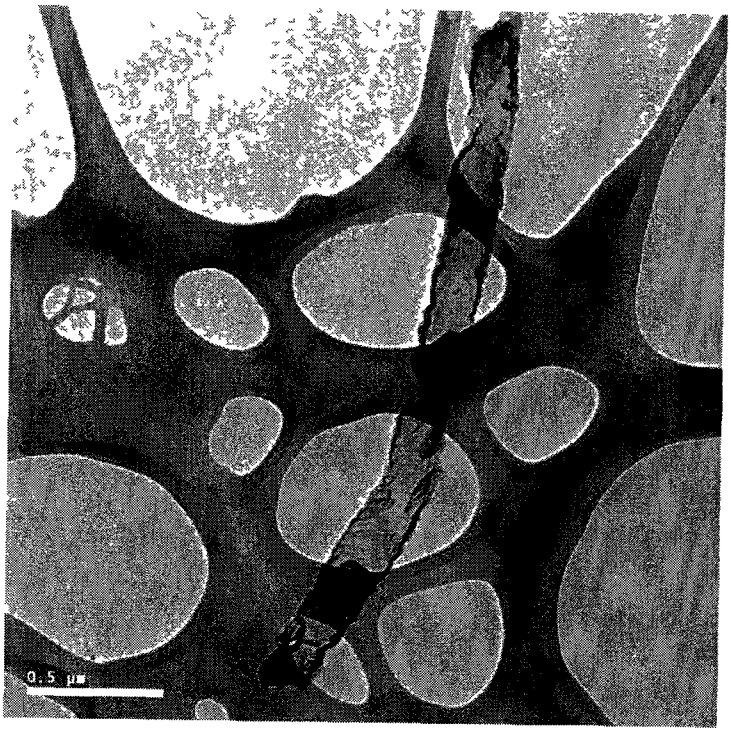

Figure 24 Examples of a multi-layer graphene nanoribbon produced from exfoliation by adamantane (scale of bar is 500 nm)

While successful in synthesizing low yields of graphene, high boiling solvents do not allow for formation of relatively large graphene sheets. Based on a survey of TEM samples that were produced using high boiling solvents, the corresponding graphene can range in area from a few hundred square nanometers to several tens of square micrometers, with the largest population at the lower end of the range. The method could be used to prepare small numbers of test devices like field-effect transistors by "harvesting" graphene onto silicon, but it is likely not useful in a commercial setting due to the low yields and the non-uniform nature of the graphene sheets produced.

3.1.2 Hydrogenation and Exfoliation of bulk Graphite and HOPG and Synthesis of Graphane

Since graphene was first isolated, there have been several investigations concerning its hydrogenation. Methods that have been reported often use a plasma source[96] or e-beam lithography[101] to etch the surface of graphene with hydrogen. While these methods work well in a research laboratory setting, they cannot be scaled readily. As discussed in chapter 2 of this thesis, polyamines effectively hydrogenate fullerenes[136,142,156] and single-walled nanotubes,[157] and we reasoned they may also hydrogenate graphene to produce graphane. We also considered that hydrogenation may facilitate exfoliation such that bulk graphite and HOPG could be used as graphane precursors. In this way, polyamine hydrogenation of graphite and HOPG represent an alternative method to graphene oxide production. Exfoliation of graphite using a reductive method has a number of advantages over the current method of exfoliation by oxidation. One of the disadvantages to an oxidative exfoliation is the need to reduce graphene oxide (GO) back to a graphene-like state using hydrazine as reductant,[60] or thermal annealing.[158] Neither method is successful in reducing the GO back to graphene. The partially reduced graphene oxide material does not possess the desired electrical properties of pristine graphene.[64]

Conversely, it has been shown that when pristine graphene is hydrogenated and then thermally annealed back to graphene the original electronic properties are recovered.[96] By using a reductive exfoliation method followed by a thermal

annealing step, graphene can be prepared with properties identical to that of unmodified graphene.

To hydrogenate graphene pentaethylenehexamine (PEHA) was selected as polyamine due to its high boiling point (~380 °C). With both high temperatures and polyamine hydrogenation conditions, it was thought that exfoliation could occur via two routes: though high energy solvent-induced shearing, and through hydrogenation of the graphite surface the π-π stacking interactions, much like the debundling of the SWNTs after hydrogenation. Attempts to produce graphane were made using PEHA in conjunction with both bulk graphite and HOPG.

Bulk graphite is inexpensive and processes that use it are, in principle, readily scaled. In order to make the bulk graphite more reactive, it was milled into smaller particles sizes using a vibrational ball mill. The advantage of using ball milling is two-fold: reduces the overall size of the graphite particles and causes fracturing on the surfaced of the graphite, both of which may lead to greater reactivity and for more effective exfoliation (Figure 25).

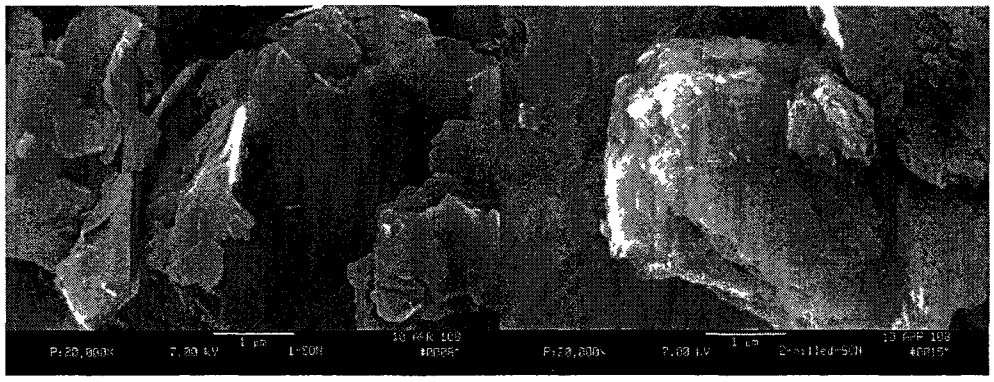

Figure 25: SEM images of bulk graphite before (left) and after (right) ball milling (scale of bar is 1 micrometer)

Ball milling graphite does, however lead to some unexpected products including a variety of nano-onions (spherical and square, filled and empty) and multi-walled nanotubes (Figure 26). These materials are believed to form because of a combination of mechanical stresses on the graphite sheets as well as the heat associated with the milling process.[144]

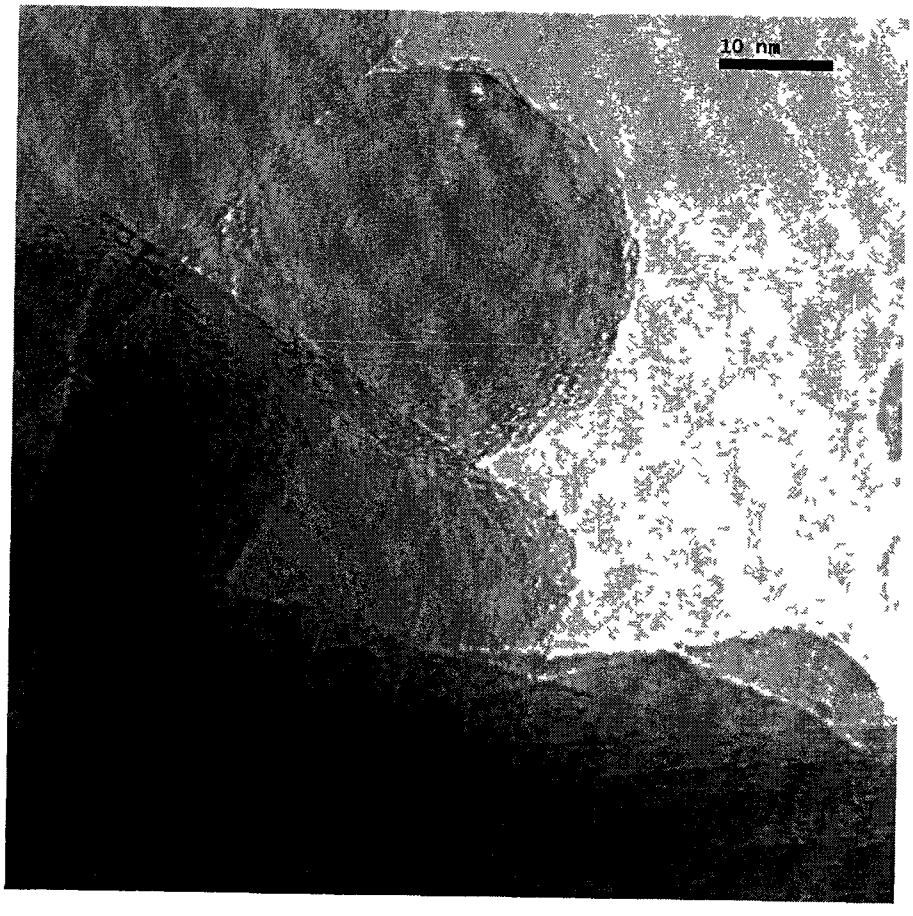

Figure 26 HRTEM images of nano-onions and MWNT formed from vibrational ball milling

Ball milled samples of graphite were reacted with PEHA in a round bottom flask (380°C) under nitrogen for 36 hours. After heating was completed, the solid

was cleaned with denatured ethanol three times using a centrifuge to compact the solid between each rinse. After the amine was sufficiently removed, the ethanol was then removed by rotary evaporation. To take TEM images, a 1 mg sample was suspended in ~80 mL of denatured ethanol and sonicated for a few seconds. The dispersion was then placed on a 200 mesh lacey silicon grid and the solvent was evaporated. (Figure 27)

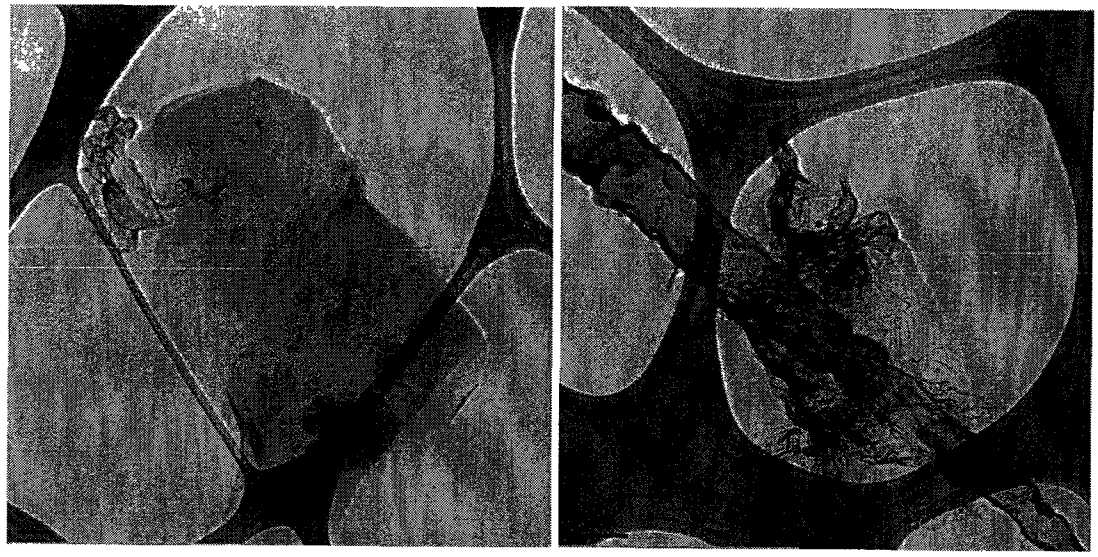

Figure 27: TEM images of bulk graphite after milling and hydrogenation containing multi-layered graphane and single sheet-graphane (left) and single-sheet graphane and graphane nanoribbons (right) (scale of bar is 200 nanometers)

Based on the images of figure 27, it is clear that single and multi-sheet graphane was successfully exfoliated from the bulk graphite. Much like the exfoliation from

high boiling hydrocarbon solvents, the graphene sheets produced by reaction in PEHA has areas ranging from several hundred square nanometers to hundreds of square micrometers. The larger sheets were better imaged using SEM than TEM due to their size (Figure 28). As before, the shapes and sizes of sheets were not uniform. Polyamine reactions were also completed at 500 °C using high pressure reactors, but the TEM results did not indicate any noticeable difference from those reactions completed at 380 °C.

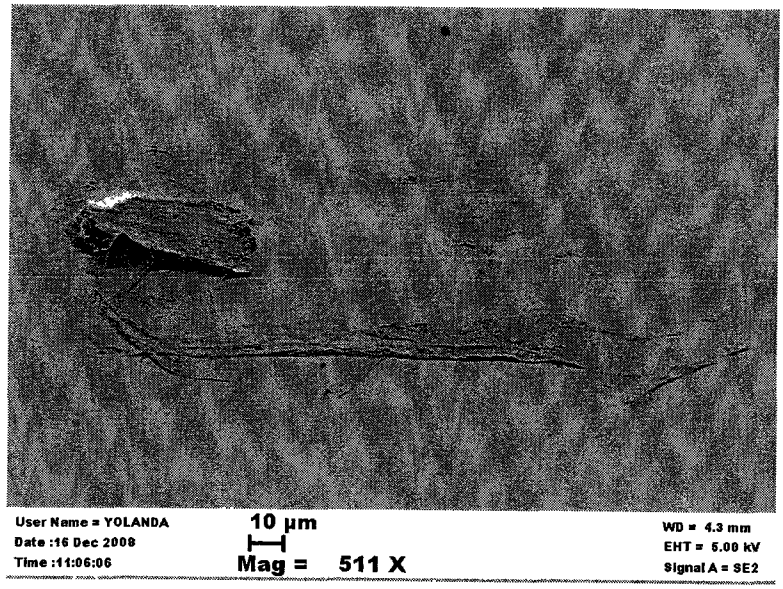

Figure 28: SEM image of graphane made from bulk graphite (Image taken by Dr. Yolanda Echegoyen)

While exfoliation of graphene was successful, the formation of other nano-structured carbon forms as by-products was a complication. For this reason HOPG was also utilized as raw material in boiling PEHA. Using HOPG has the added benefit that it allows for facile quantification of product yields via simple

measuring of the HOPG before and after reaction.

For exfoliation of HOPG, a 1 mm HOPG disk was placed in a stainless steel high pressure reactor with 1mL of PEHA and heated to 500°C for 24 hours. After cooling, the vessel was opened in a vented fume hood, in order to safely release gases that form. The sample was then washed with ethanol three times allowing for the graphitic materials to settle for 30 minutes between each rinse. The single layer and few layer graphene products were imaged by TEM (Figure 2) in the same manner as the exfoliated graphite. The corresponding sheets were also analyzed by Raman spectroscopy in order to monitor hydrogenation (See section 3.1.3 below).

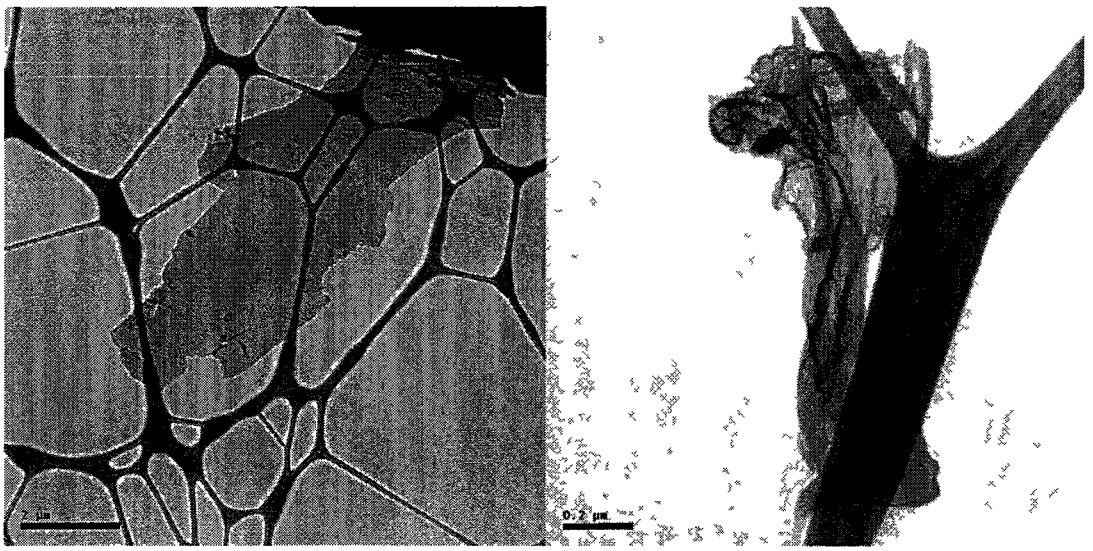

Figure 29 TEM images of HOPG after hydrogenation and exfoliation containing multi-layered graphane (left, scale of bar is 2 micrometers) and single sheet-graphane (right) (scale of bar is 200 nanometers)

Graphite sheets produced in this manner were of a similar size as that produced by polyamine treatment of bulk graphite. Based on mass loss of the HOPG disk after reaction the amount of graphite exfoliated was less than 1%.

3.1.3 Characterization of Graphane

In the past, plasma induced hydrogenation of graphene to graphane in a small localized area was confirmed by Raman spectroscopy.[96] Thus, we sought to use confocal Raman spectroscopy to ascertain if our polyamine treated graphite produced either graphene or graphane. In order to obtain accurate Raman spectra, a TEM grid that had already been imaged was scanned by the confocal microscope to produce multiple Raman spectra. For comparison to pristine graphene, Dr. Bogdan Diaconescu used the "Scotch Tape" method[58] and to mechanically exfoliate graphene and analyzed this sample by Raman spectroscopy (Figure 30).

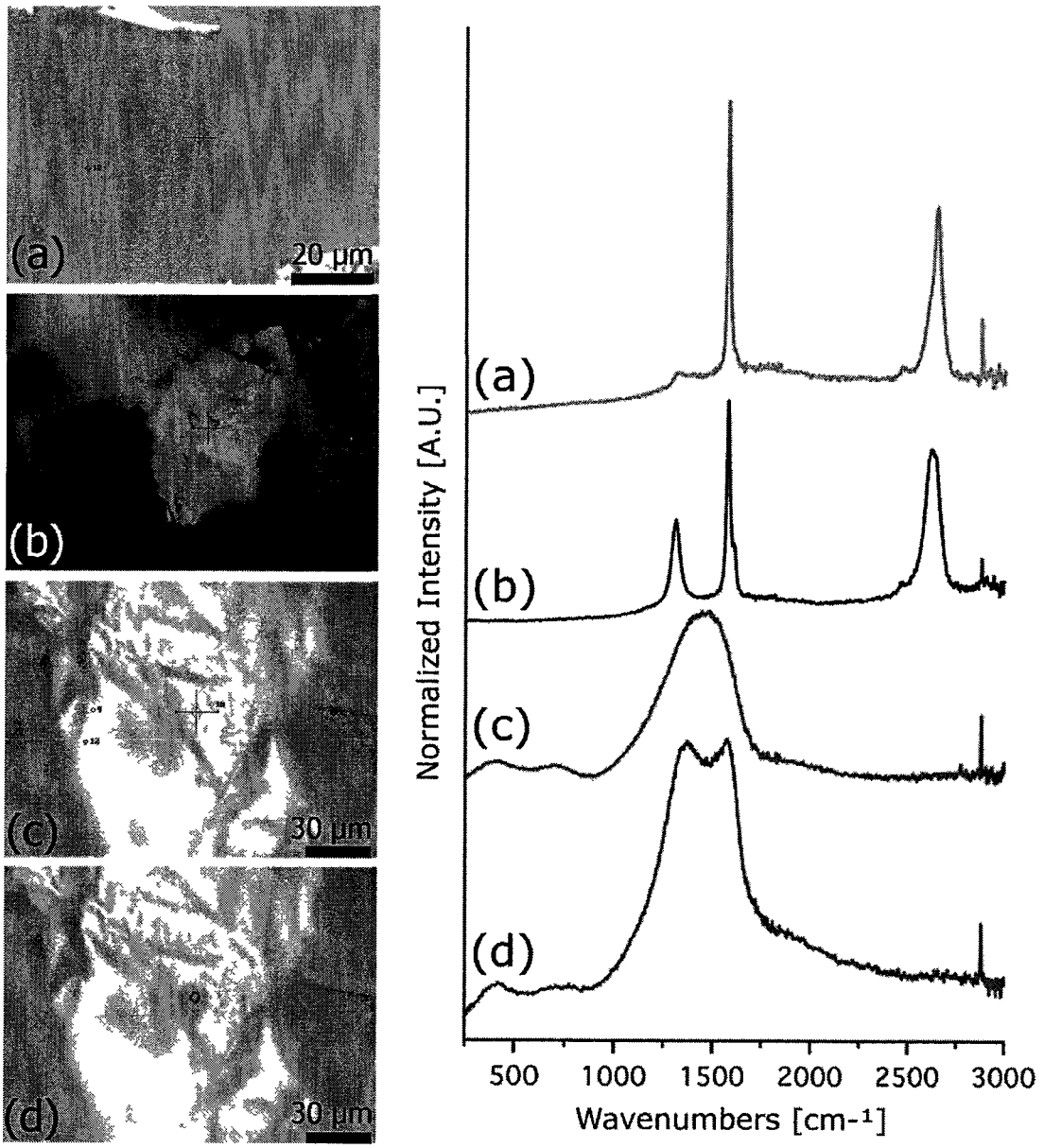

Figure 30 Microscope images and Raman spectra of (**a**) Graphene prepared by mechanical exfoliation ("Scotch Tape" method) of HOPG (**b**) Few-layer graphane from polyamine treated HOPG (**c**) Large particles of hydrogenated graphite from HOPG (**d**) Laser annealed hydrogenated graphite (Figures constructed by Dr Bogdan Diaconescu)

As illustrated in Figure 30, a clear difference exists between pristine graphene (Figure 30a) and samples prepared from polyamine treated graphite (Figure 30b). In particular, the polyamine treated samples shows a significant D-band signal at approximately 1350 cm^{-1} consistent with functionalization. An interesting observation is that functionalization also occurred on the bulk graphite flakes. The Raman spectra of the bulk hydrogenated graphite show a large band at about 1500 cm^{-1}, which is an overlap of the G and D bands and is comparable to literature values.[159] Furthermore, when the bulk hydrogenated graphite is subjected to laser annealing, a small splitting is observed between the two overlapping G and D bands. This also matches literature observations and is believed to be caused by partial dehydrogenation of the sample back to graphite. Thus, the Raman data supports hydrogenation of both graphene and bulk graphite by polyamines.

Disorder bands in the Raman spectra are associated with the conversion of sp^2 hybridized carbon atoms to sp^3. The D and 2D bands are the most pronounced in graphane as compared to that of graphene as highlighted in Figure 31.

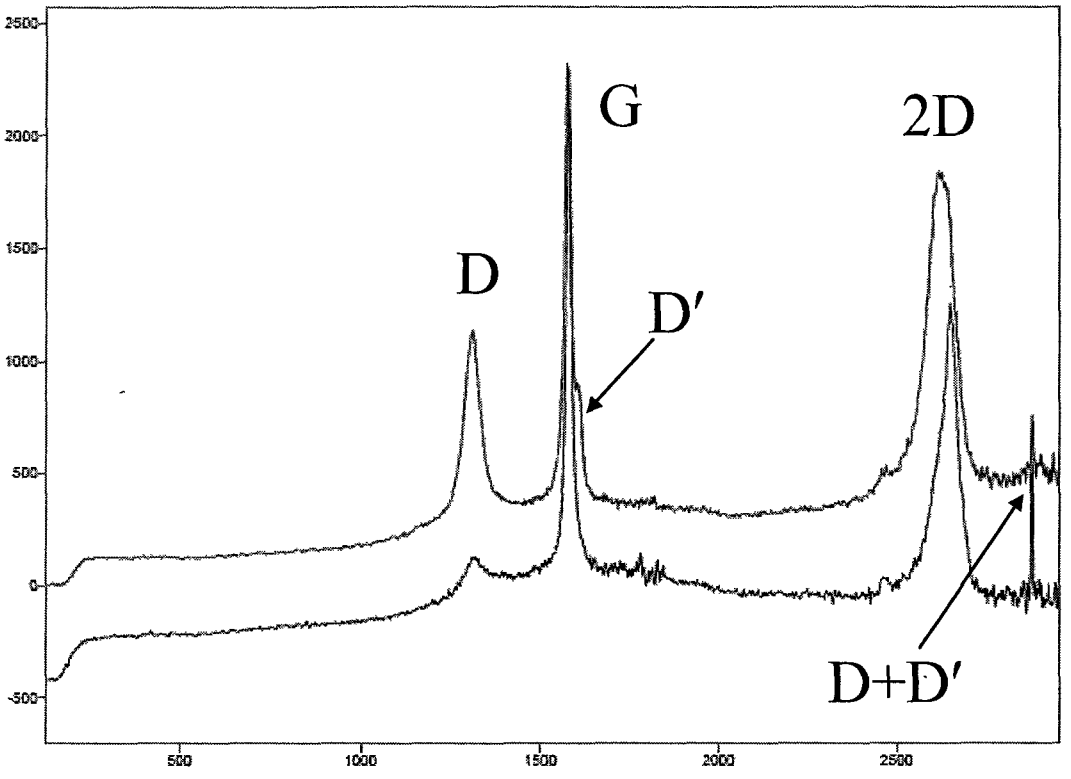

Figure 31: Comparison of Raman spectra of graphene (blue) and graphane (red)

In collaboration with the Pohl group at the University of New Hampshire, graphene also was prepared by CVD on a Ru(0001) surface and then subjected to polyamine hydrogenation. In this case, the method of hydrogenation was slightly different, PEHA was used but at a much lower temperature (200 °C) and treatment stopped after 1 hour. The PEHA was removed by vacuum and the resulting sample was analyzed by various techniques.

Raman spectroscopy was initially attempted. However, since the graphene sample was only single layer on Ru(0001), no useable spectrum was obtained. Scanning tunneling microscopy (STM) was also utilized to compare graphene before and after

treatment with polyamine. The STM images show a great deal of distortion of the graphene surface, consistent with the conversion of sp^2 carbons to the longer and tetrahedral sp^3 type. Another imaging method that compared graphene to graphene was low energy electron diffraction or LEED. This method showed the standard diffraction pattern from graphene had been disrupted with the loss of the hexagonal Moiré pattern and a second diffuse band appearing at 30° intervals between the more prominent bands. This result suggests poor interaction between the ruthenium surface and carbon which is caused when the sp^2 hybridized carbons of graphene are converted to sp^3. Lastly Auger electron spectroscopy (AES) showed no difference between the graphitic sample before and after polyamine treatment (Figure 32) since AES cannot detect hydrogen but does detect other atoms like carbon, nitrogen, oxygen, sulfur, *etc.* The only explanation that fits the observations is that the conversion of sp^2 hybridized carbon to sp^3 carbon (Raman, STM, and LEED) is accompanied by C—H bond formation. That is, polyamine treatment converts graphene to graphane without complicating side reactions like amination. With these analyses, there is certainty that partially hydrogenated graphene has been successfully synthesized.

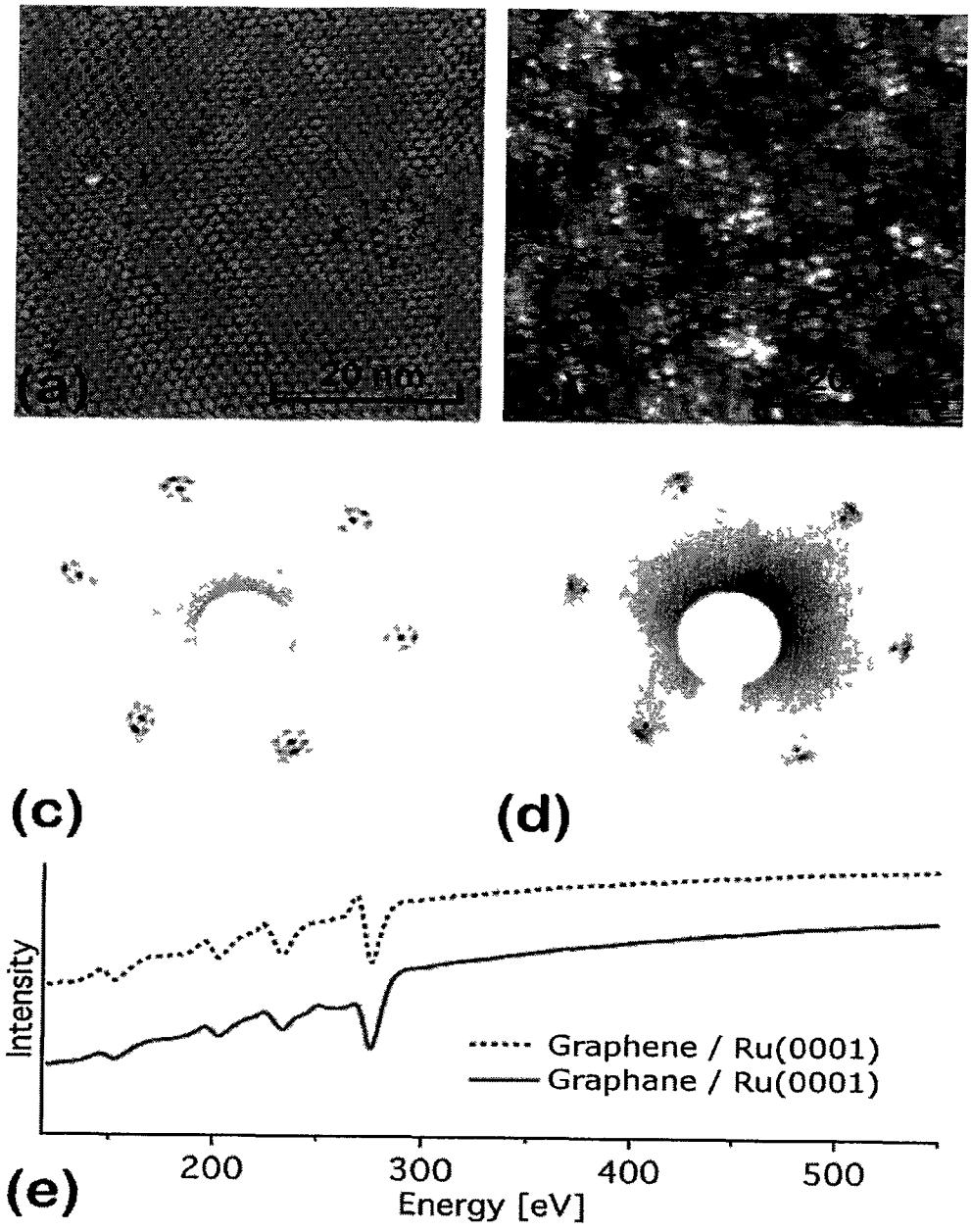

Figure 32: Hydrogenation of single layer graphene on Ru(0001) (a) STM image of single layer graphene on Ru(0001), (b) STM image of the same sample after polyamine hydrogenation, (c) LEED diffraction pattern of the sample corresponding to image (a), (d) LEED diffraction pattern of the sample corresponding to image (b), (e) AES spectra for the samples in (a) and (b) (Figures constructed by Dr Bogdan Diaconescu)

CHAPTER 4

SYNTHESIS OF BISACENES, PERIACENES AND THIAACENES

4.1 Bisacenes and Periacenes

4.1.1 Background

There is only a small selection of biacenes, bisacenes, and fused bisacenes that have been synthesized. Biacenes are dimers of acenes containing a single bond between the two ring systems. Bisacenes are dimers of acenes containing a double bond between the two ring systems. Fused bisacenes are biacenes or bisacenes that have additional carbon-carbon bonds between the two ring system. Most of these compounds are anthracene derivatives and only recently has work been done to make perianthracene derivatives.[160-163] The first example of bipentacene was demonstrated by Zhang and co-workers in which a TIPS substituted bipentacene was synthesized from the corresponding bispentacenequinone by an addition reaction followed by reductive aromatization (Scheme 20).[164]

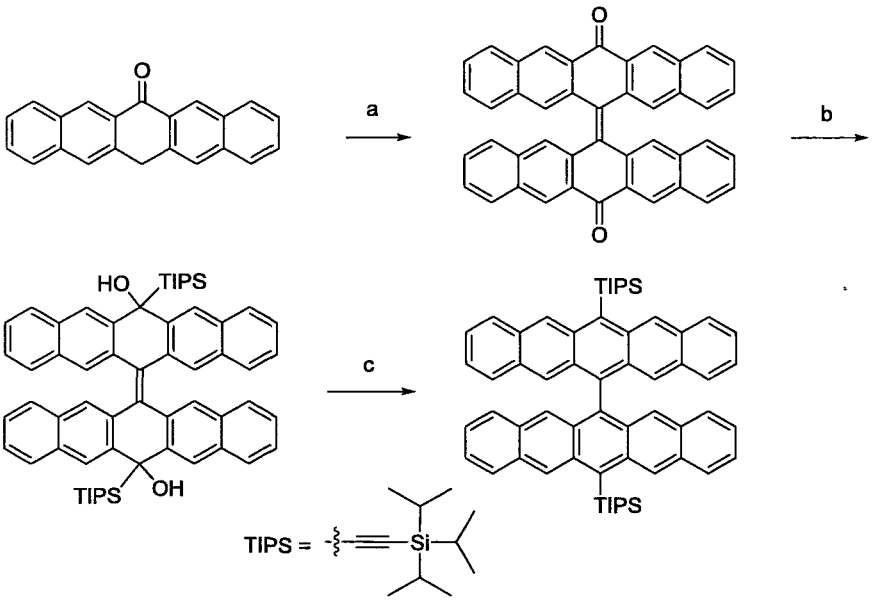

Scheme 20: Synthesis of TIPS-Bipentacene. Reagents and Conditions: a) Pyridine, piperidine, pyridine N-oxide, $FeSO_4$, 83 %; b) TIPS Anhydride, nBuLi, THF, 40 %; c) NaH_2PO_2 , NaI, CH_3COOH, 74 %.

TIPS-bipentacene has approximately the same electronic properties as TIPS-pentacene (HOMO-LUMO gap, electron mobility, etc.), but greater solubility and stability. The stability of TIPS-pentacene in ambient light at room temperature is about 3 times longer than TIPS-pentacene. This potentially opens a new area of organic semiconductor chemistry where analogs of known pentacene compounds could be made to have much greater stability than their parent compounds.

The Zhang group also attempted to make a fused bipentacene compound known as a peripentacene. Thus, bispentacenequinone was subjected to light in an oxidative cyclization/fusion to form a peripentacenequinone reaction that formed the partly fused bispentacenequinone. Full cyclization was not achieved because the intermediate material was too insoluble and precipitated out of solution as soon as it was formed. The

material was then subjected to Grignard conditions leading to the 1,4-Michael addition of aryl grounds, exactly as with 6,13-pentacenequinone. (Scheme 21).[165]

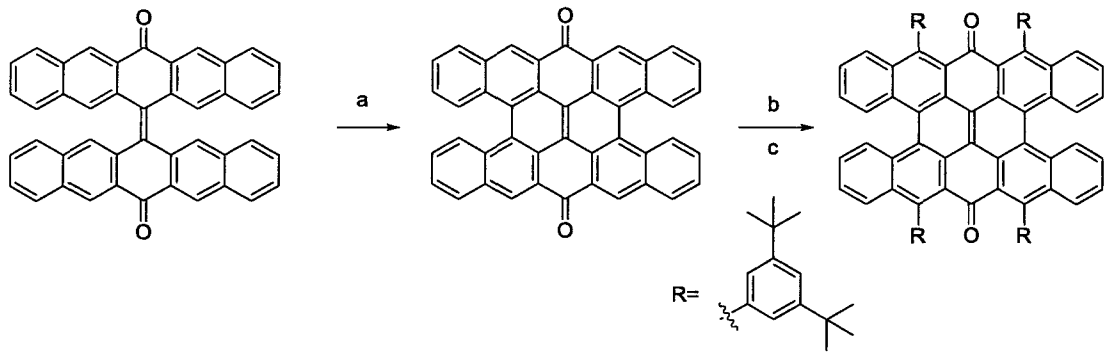

Scheme 21: Synthesis of fused bispentacenequinone. Reagents and Conditions: a) I_2, Benzene, *hv*, propylene oxide, 59 %; b) 3,5-di-tert-butylphenylmagnesium bromide, THF, 50 %; c) 3,5-di-tert-butylphenylmagnesium bromide, THF, 36%

While Zhang and co-workers have made progress in this field, there is considerably more work to do in order to realize partially fused bispentacenes and peripentacenes. If formed, these systems could provide interesting new thin-film materials for electronic applications.

4.1.2 Synthesis of Unsubstituted Bipentacene

We endeavored to make unsubstituted bipentacene using a path analogous to that described by Zhang and co-workers[164,165] as illustrated in Scheme 22.

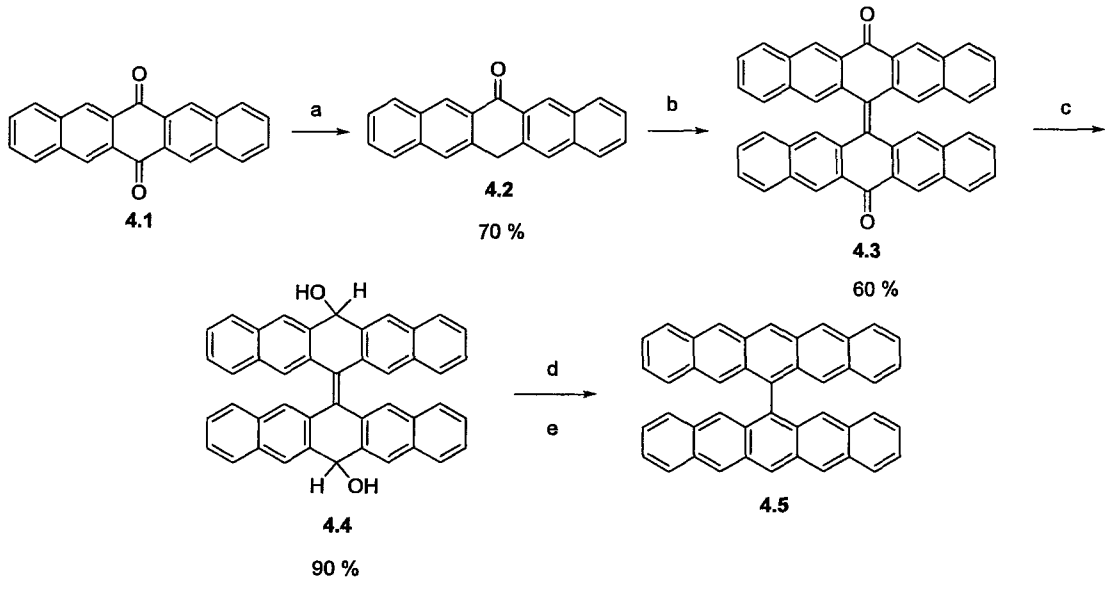

Scheme 22: Synthesis of bipentacene. Reagents and Conditions: a) HI/HOAc, Reflux, 5 h, 70 %; b) DCM, DBU, 5 min, RT, I_2, 24 h, RT, 60 % c) $NaBH_4$, THF, 24 h, RT, 90 %; d) $SnCl_2$, 10% HCl, $CHCl_3$ extraction, 80 %; e) Se^0, TCB, Reflux, 30 min.

Starting from 6,13-pentacenequinone (**4.1**), a reduction was performed using a 1:1 ratio of hydriodic acid (55-58%, unstabilized) and glacial acetic acid. The reaction mixture contains 20 mL of HI/HOAc per 100 mg of **4.1**, and was refluxed for precisely 5 hours in order to obtain the maximum yield of **4.2** with minor amounts of **4.1** and 6,13-dihydropentacene (**5.8**). After washing with aqueous $NaHSO_3$ and filtering, the material was dissolved in chloroform and extracted with water to remove any sulfate impurities. In this was **4.2** was produced with on average 70 % yields. Using a method modified from Donavan, *et al*[166], **4.2** was then dissolved in dry dichloromethane and purged with nitrogen, 1,8-Diazabicyclo[5.4.0]undec-7-ene (DBU) was added and stirred at room temperature for 5 minutes to generate an enolate anion. Crystals of resublimed iodine

were then added to the reaction and stirred for 24 hours to produce **4.3**. The dichloromethane was removed under reduced pressure and the sample was washed with acetone to reveal a bright yellow solid obtained in 50 % yield. The purity of **4.3** is typically 70-90 % with **4.1** as the major impurity. Quinone **4.1** forms upon oxidation of **4.2**. Careful purging with nitrogen gas will minimize its formation. A crystal structure of **4.3** was obtained through the slow evaporation of a saturated solution in chloroform (Figure 33).

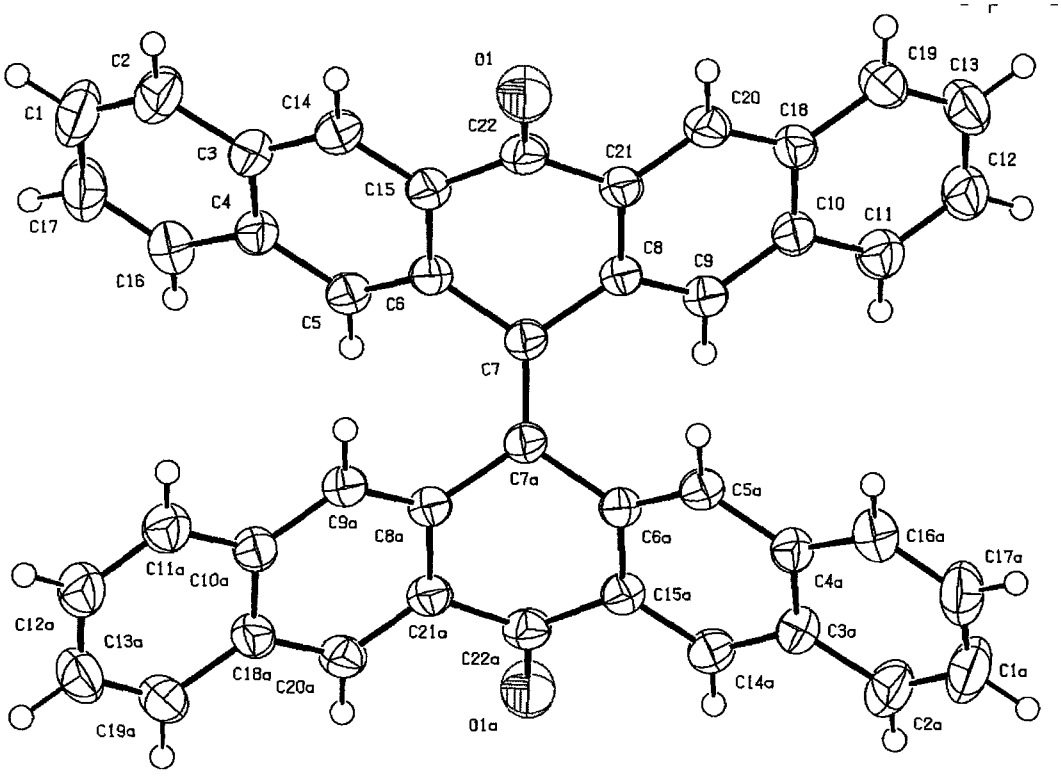

Figure 33: X-Ray crystal structure of compound **4.3**

Dione **4.3** was then reduced to diol **4.4** by reacting it with $NaBH_4$ in THF at room temperature for 24 hours. Along with impurity **4.1**, a small amount of 6,13-pentacenediol

was observed. This impurity can be eliminated by aromatizing to pentacene using $SnCl_2$ and 10% HCl and then extracting the unreacted **4.4** with chloroform. The isolated **4.4** was then be dissolved in 1,2,4-trichlorobenzene and reacted with selenium to produce **4.5**. The sample could then be dissolved in solvents such as chloroform or benzene for analysis by UV-Vis spectrometry (Figure 34). The extreme instability of the **4.5** makes NMR analysis difficult.

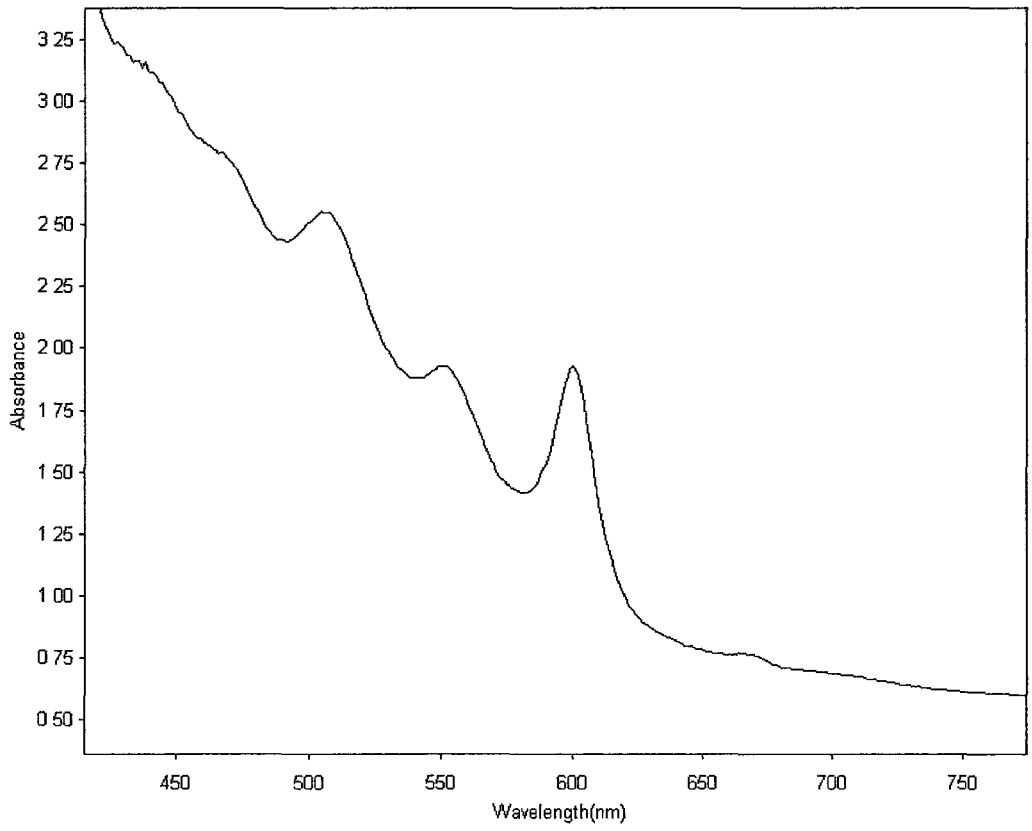

Figure 34: UV/Vis spectrum of compound **4.5**

With the λ_{onset} of bipentacene **4.5** at approximately 600 nm in chloroform, the optical HOMO-LUMO gap is calculated to be 2.16 eV, approximately 0.05 eV lower

than unsubstituted pentacene. It is not surprising that the optical HOMO-LUMO gap of bipentacene **4.5** is similar to that of pentacene itself. TIPS-pentacene and TIPS-bipentacene have almost the same optical HOMO-LUMO gap.[164]

This phenomenon results from the non-planar conformation that bipentacene **4.5** and TIPS-bipentacene must adopt. Since the two π-systems of bipentacene are nearly orthogonal to each other there is increasing steric bulk in the system. Due to this effect, its stability in solution in ambient light at room temperature is approximately 15 minutes approximately twice that of pentacene based on UV/Vis degradation studies.

Analysis by mass spectrometry shows that the oxidized bipentacene **4.5** produces di-endoperoxide species like **4.6** of Figure 35. Formation of endoperoxides of pentacene and pentacene derivates are well known so it is not surprising that a di-endoperoxide of **4.5** should form.

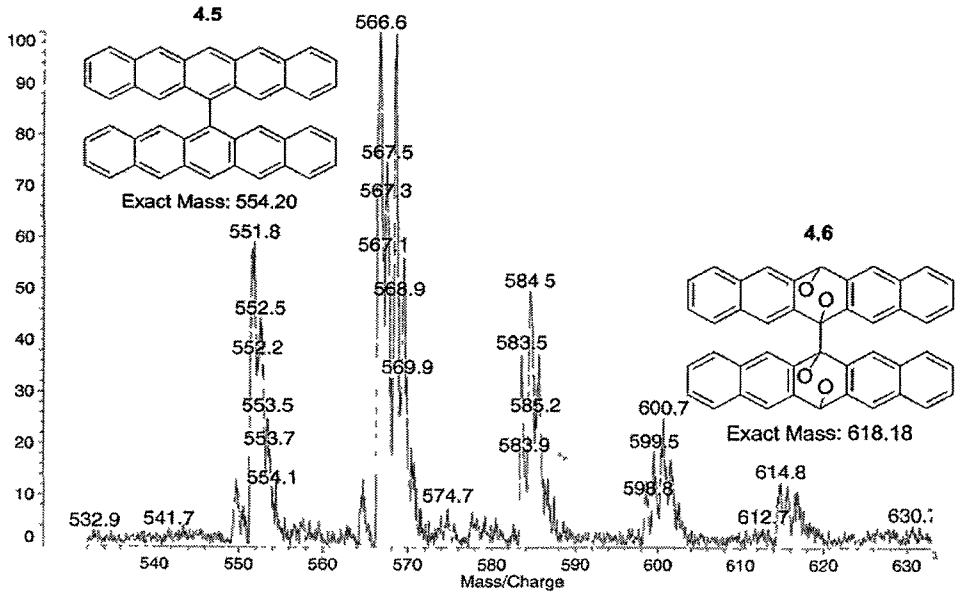

Figure 35: Mass spectrum of bipentacene and its di-endoperoxide derivative

With the successful synthesis of TIPS-bipentacene and bipentacene **4.5**, it seems reasonable that a host of similar compounds could be made. While bipentacene itself is not particularly useful, due to its poor stability in light and air, an array of derivatives including stabilized bipentacene and larger conjugated systems represent reasonable targets for future work.

4.1.3 Synthesis of Peripentacenequinone

Using a similar method to producing the bipentacene, peripentacene could potentially be produced in only four steps from bispentacenequinone **4.3** (Scheme 23).

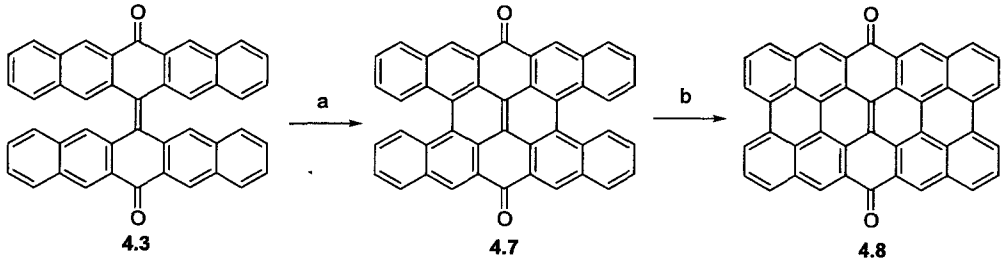

Scheme 23: Synthesis of Peripentacenequinone. Reagents and Conditions : a) NBS, Benzene, *hυ*, 2 h; b) 380°C, 2 h

The synthesis of the partly fused bisquinone species **4.7** was made in 80 % yield using a modified method of Zhang, *et al.* where NBS was used as a radical initiator as well as a hydrogen scavenger. This allowed to reaction to go to completion after only 2 hours of exposure to a 350W lamp, whereas Zhang's previous synthesis required 48 hours with a 450W lamp. We then subjected partially fused bispentacenequinone **4.7** to high temperatures to complete the oxidative cyclization to the corresponding

peripentacenequinone **4.8**. Originally, Scholl conditions were utilized to form **4.8** but the yields were low at approximately 5 %. By using heat in a solid state reaction to promote the cyclization, the yields improved to 80 %. Peripentacenequinone could potentially be reduced to make the corresponding diol **4.9** which could then be made into the trithiaperipentacenone **4.15** (See Section 4.2.4).

Characterization of **4.8** is difficult due to the inherent insolubility of the product. Due to its large size and flat planar π-system the solubility of **4.8** in chlorinated aromatic solvents is approximately $1x10^{-4}$ M. While this makes identification by NMR problematic, it does allow for product characterization by mass spectrometry as seen in Figure 36 and UV/Vis spectroscopy, where it shows a λ_{max} of 525 nm. This represents a red-shift of approximately 100 nm as compared to 6,13-pentacenequinone (Figure 37)

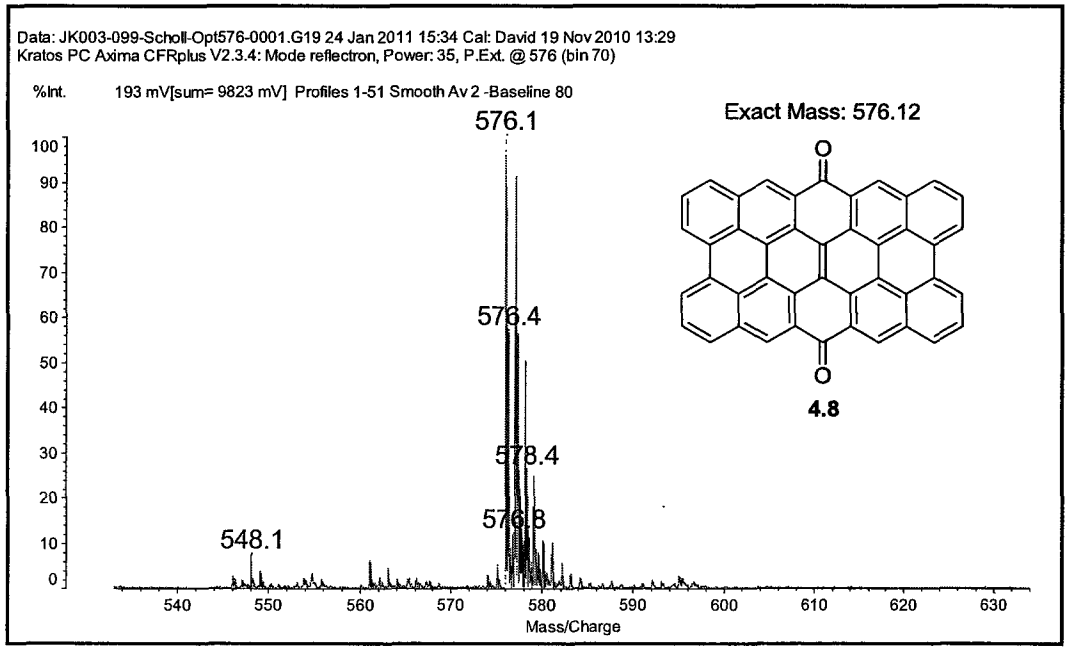

Figure 36: Mass spectrometry of compound **4.8**

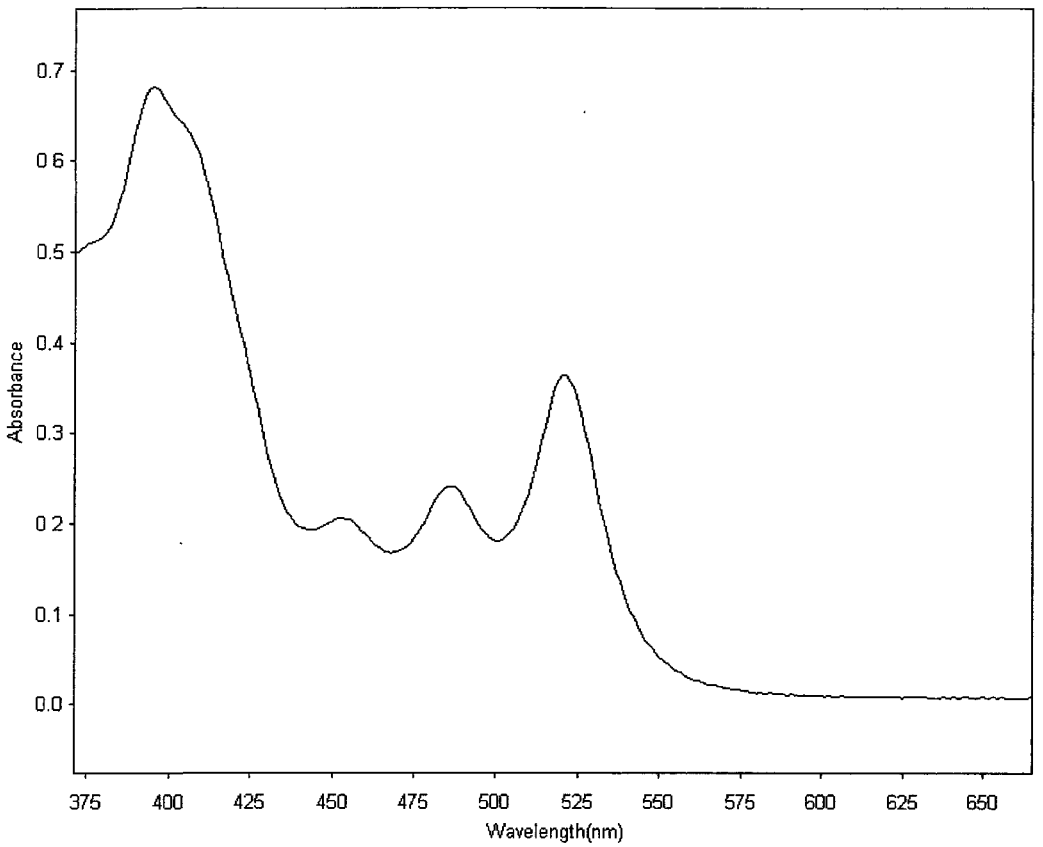

Figure 37: UV/Vis spectrum of compound **4.8**

A partially fused bipentacene was also produced from the partially fused bisquinone **4.3**. Following reduction with $NaBH_4$ to the corresponding diol **4.10** was produced. This diol, while having poor solubility, is shown to be a very bright emitter of a blue/white light when irradiated with UV light, and may have some potential in OLED lighting. The diol can be reductively aromatized to the partially fused bipentacene species **4.11** (Scheme 24) using $SnCl_2$/HCl.

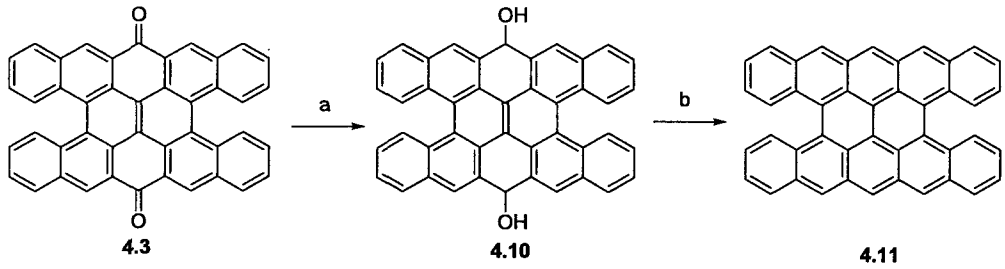

Scheme 24: Synthesis of Fused Bipentacene, Reagents and Conditions a) $NaBH_4$, THF, 24 h, RT; b) $SnCl_2$, 10% HCl, 10 min

The solubility of **4.11** is very poor making analysis difficult. While mass spectrometry indicated formation of the product the UV/Vis spectrum for **4.11** showed only a λ_{max} of 575 which is much lower than expected. This UV/Vis spectrum from a large aromatic system such as this should include a λ_{max} of approximately 1050 nm based on DFT calculations. The calculations also show that **4.11** is an open-shell singlet which means that it is highly reactive and very prone to oxidation. Thus, **4.11** is oxidizing as soon as it is formed. In the future, a derivative may show enhanced stability if appropriate substituents are chosen, as described next.

4.1.4 Proposed Synthesis of Substituted Bipentacenes

Using principles learned in the synthesis of bipentacenes **4.5** and peripentacenequinone **4.8** along with the syntheses of stabilized acenes, the synthesis of substituted bipentacenes should be achievable. By starting from small substituted molecules and slowly building to substituted pentacenequinones, substituted bipentacenes should be synthesized in only four additional steps.

In an initial attempt Scheme 25, the diol **4.4** was treated with ZnI_2 and decanethiol to produce the organothiol substituted species **4.12**. Several attempts were made to aromatize this material to the bis(6,6'-decathio)bipentacene, however none of the aromatization conditions were successful. It is hypothesized that the bend in the carbonyl carbons on bispentacenequinone **4.3**, as seen the in crystal structure in Figure 33, forces the corresponding diol **4.4** into a *trans* configuration. This is supported by the ^{1}H-NMR spectrum showing one diastereomer (See appendix pages S78 and S79). Since the substitution step to form the organothiol substituted species proceeds through a S_N2 mechanism the *trans* configuration is maintained. It is though the *trans* configuration makes the subsequent aromatization difficult since standard chloranil conditions are more reactive for the *cis* isomer, however this has not yet been confirmed.

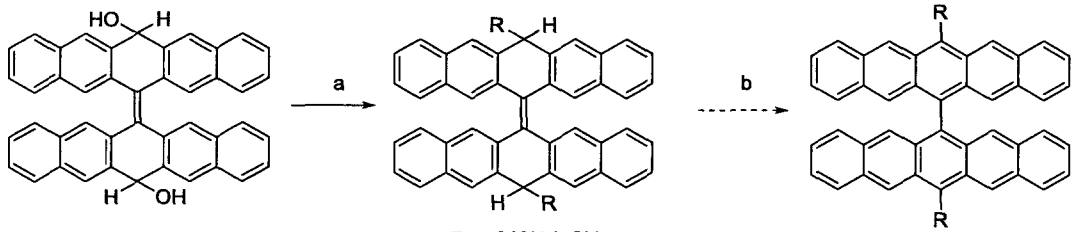

Scheme 25: Attempted synthesis of a 6,6'-substituted bipentacene. Reagents and Conditions: a) ZnI_2, DCM, R^2-SH; b) Chloranil, DCM, Reflux, 48 h

Since the initial synthesis was not successful, a new route is suggested (Scheme 26). It is thought that a di-substituted orthoxylene starting material could be brominated to produce a tetrabromo-o-xylene derivative and then be cyclized with benzoquinone

under standard o-xylene forming conditions. After partial reduction to the substituted pentacenone (step c of Scheme 26), a DBU mediated homocoupling would produce either the dipentacenone or the substituted bispentacenequinone depending upon the conditions used and choice of substituents. Addition to the 6,6'-position could be achieved with either a Grignard or lithium reagent for the case of the bispentacenequinone. The dipentacenone could be reduced to a diol followed by standard S_N2 substitution chemistry to produce the reduced organiothiol substituted species. The final material can then be produced via aromatization using either $SnCl_2$ in the case of the substituted bispentacenediol or chloranil for the substituted dihydrobispentacene species.

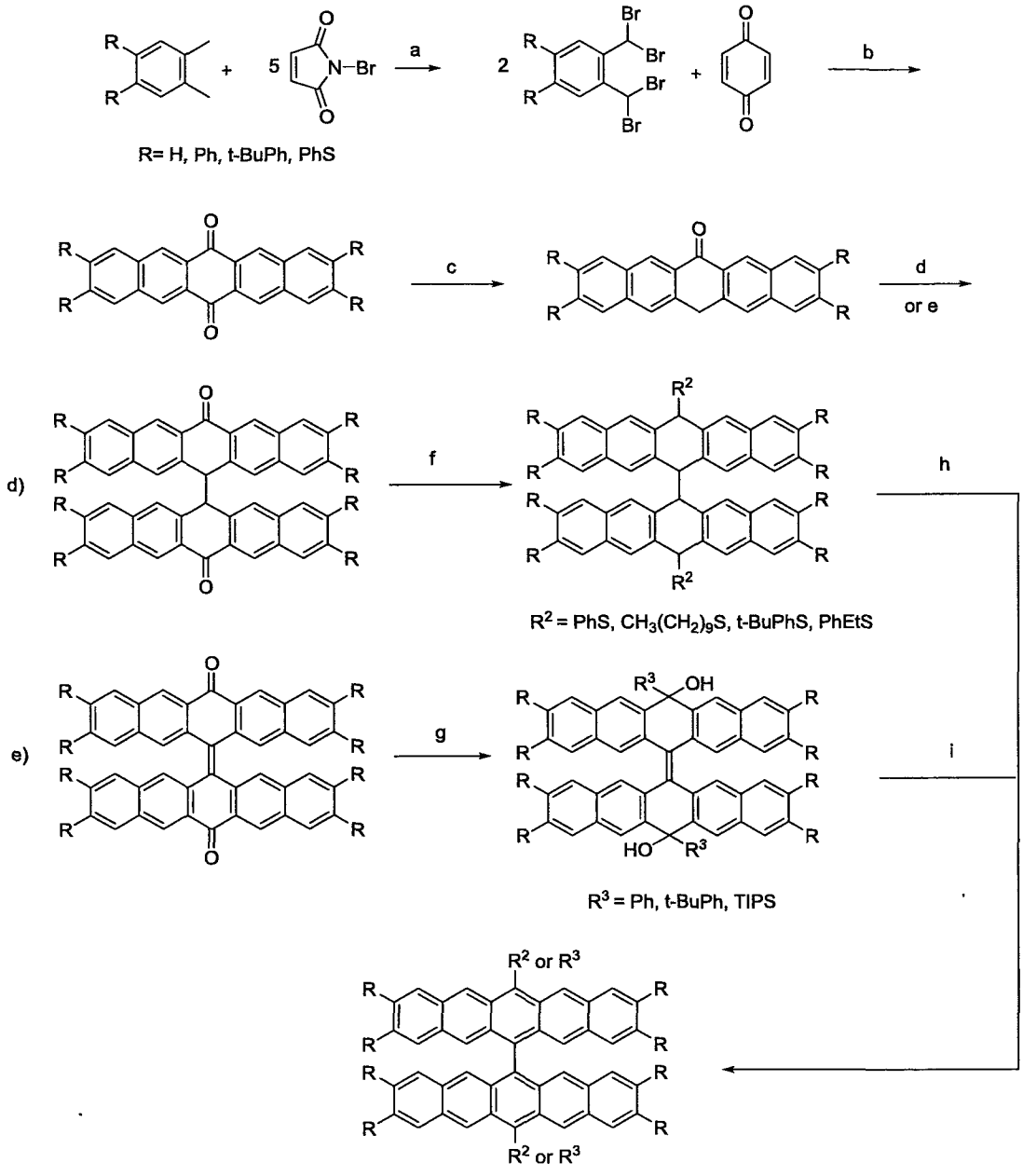

Scheme 26: Proposed synthesis of substituted bisacenes, Reagents and Conditions: a) AIBN, $CHCl_3$, Reflux, *hv*, 8 h; b) KI, DMF, Reflux, 18 h; c) HI/HOAc, Reflux, 5 hours; d) DCM, 6 eq DBU, 5 min, 3 eq I_2, 24 h, RT; e) DCM, 6 eq DBU, 5 min, 1 eq I_2, 24 h, RT; f) 1) $NaBH_4$, THF, RT 24 h 2) ZnI_2, DCM, R^2-SH; g) R^3-MgBr, or R^3-Li, THF, -78°C; h) Chloranil, DCM, Reflux, 48 h; i) $SnCl_2$, 10% HCl, 10 min

4.1.5 Proposed Synthesis of Substituted Peripentacenes

Using a similar synthetic pathway, it is proposed that a substituted, soluble peripentacene could also be made (Scheme 27). Starting with the coupling of a substituted tetrabromo-o-xylene and 1,4-anthracenequinone, unsymmetrical pentacenequinones can be produced. These quinones can be reduced to the corresponding pentacenones and then coupled to make a substituted bispentacenequinone. With the bulky substituents a "head-to-tail" arrangement should be produced exclusively due to the steric requirement of the substituents. A photochemical oxidative aromatization followed by heating should produce the corresponding substituted, soluble peripentacenequinone provided the substituents survive the high temperature cyclization reaction. The molecule could then be further substituted in the 6,6'-position to help increase the photooxidative resistance and the solubility of the final product. With the peripentacene precursor formed, it should only take a simple dehydrogenative or reductive aromatization or deoxygenation to produce the final peripentacene product, depending upon which substituents were used in the 6,6'-position. The precursors should all be stable in light and air; only the final product is expected to require being kept as a solid and in the dark due to its potential to be reactive.

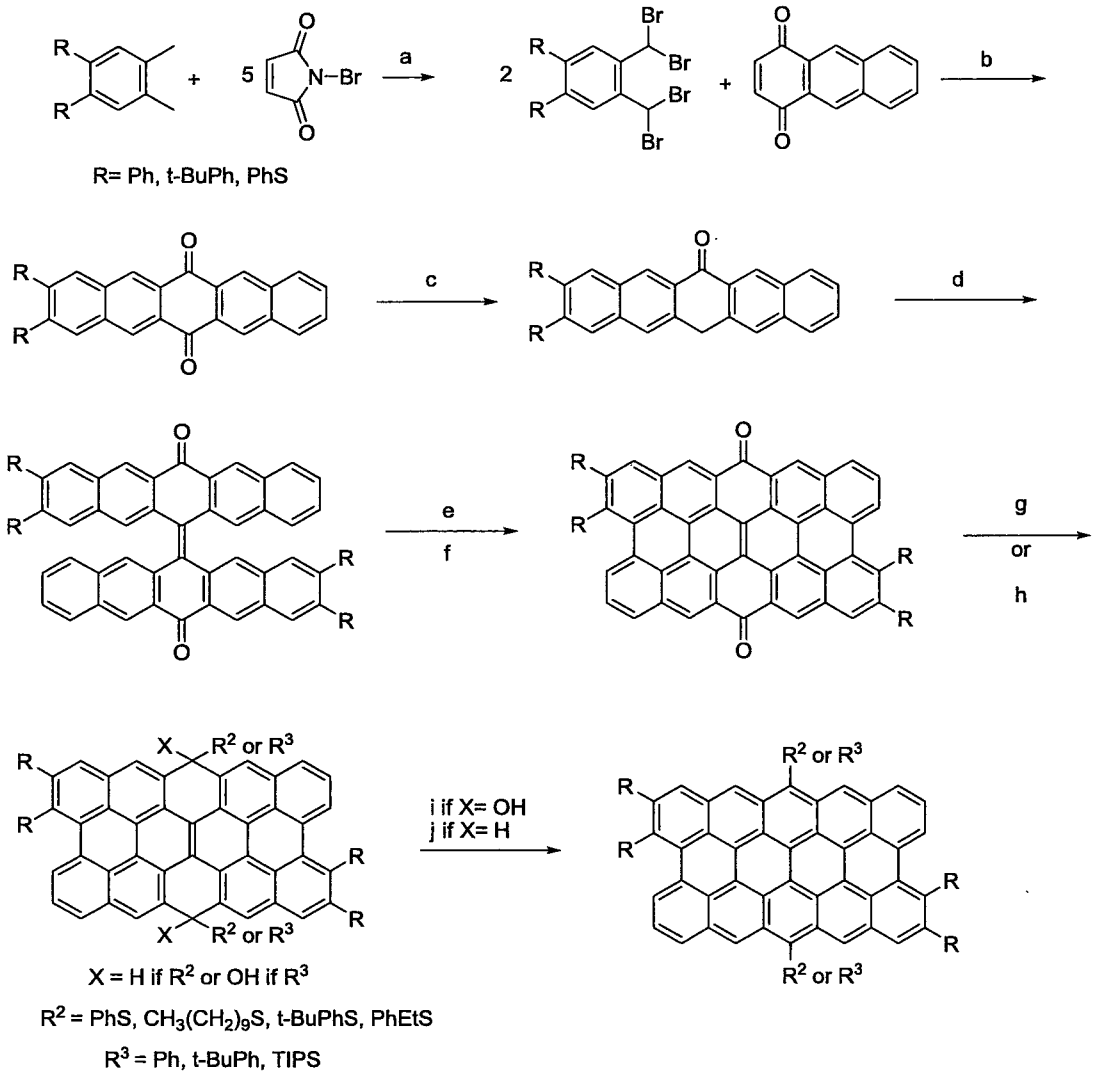

Scheme 27: Proposed synthesis substituted periacenes, Reagents and Conditions: a) AIBN, $CHCl_3$, Reflux, *hv*, 8 h; b) KI, DMF, Reflux, 18 h, c) Hi/HOAc, Reflux, 1d; d) 1) DBU, DCM 5min, 2) I_2, 24 h, RT, e) NBS, Benzene, *hv*, 2 h; f) 380°C, 2 h; g) ZnI_2, DCM, R^2-SH; h) R^3-MgBr, or R^3-Li, THF, -78°C; i) Chloanil, DCM, Reflux, 48 h; j) $SnCl_2$, 10% HCl, 10 min

4.2 Trithiaacenes and Hexathiaacenes

4.2.1 Background of Hexathiapentacene (HTP)

In 1939 Charles Marschalk synthesized hexathiapentacene (HTP) from both pentacene and 6,13-dihydropentacene by refluxing one or the other in trichlorobenzene in the presence of elemental sulfur (Scheme 28).[167] This compound became the first compound in the series of what are now known as "thiaacenes". Hexathiapentacene was largely abandoned for almost 40 years until they were analyzed for their electronic properties and was shown to robust organic semi-conductors.[168] Again, the molecule resided in obscurity for another 30 years until Wudl and co-workers explored its utility in thin-film electronics. HTP thin films showed transistor behavior with an extremely high on:off ratio of greater than $1x10^6$, high enough to be viable for practical use.[169]

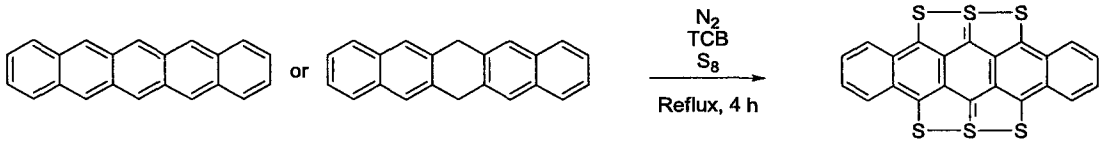

Scheme 28: Synthesis of hexathiapentacene (HTP)

HTP has a very interesting arrangement of three sulfur atoms to from three sulfur bridge on either side of the pentacene. The carbon-sulfur-sulfur-carbon dihedral angle is virtually 0 °. The resonance form that is drawn in the Scheme 29 above is a simplification of the true structure. For practical reasons, the middle carbon-sulfur bond is drawn as a double bond, but is more likely to be zwitterionic in nature than a true double bond. The molecule can be drawn in several resonance forms as illustrated in Scheme 28. There is some debate about which resonance form is the most meaningful.

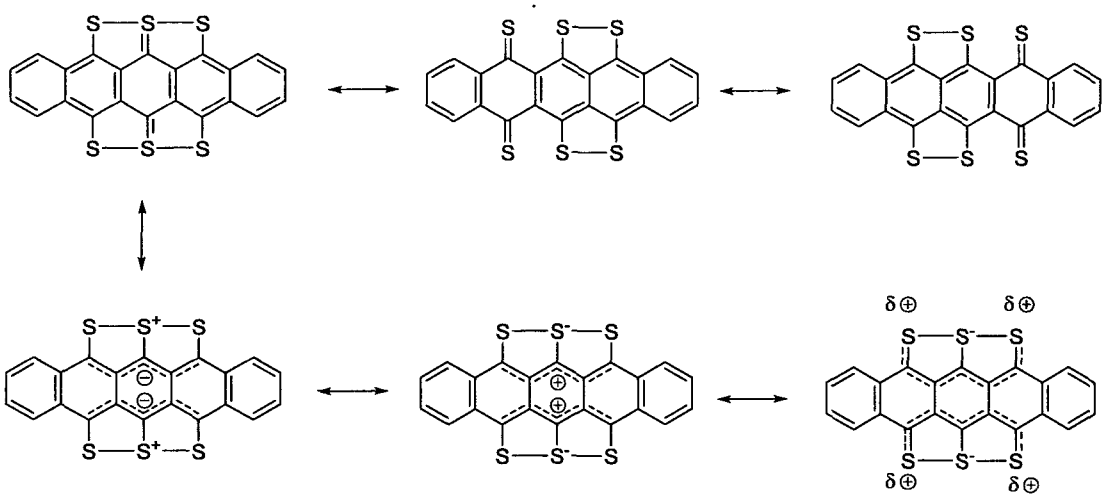

Scheme 29: Resonance forms of hexathiapentacene (HTP)

4.2.2 Synthesis and Characterization of Trithiapentacenone (TTPO)

Using reaction conditions that were outlined by Goodings and co-workers[168] on systems other than that of pentacene, a new class of compounds was explored. Starting material pentacenone (**4.2**) or 6,13-pentacenediol, both of which are produced from quinone **4.1,** were dissolved in either N,N-dimethylfomamide (DMF) or 1,2,4-trichlorobenzene (TCB) and elemental sulfur was added. The reaction was then refluxed under nitrogen for either 4 hours in the case of TCB solvent or 24 hours in the case of the DMF solvent (Scheme 30).

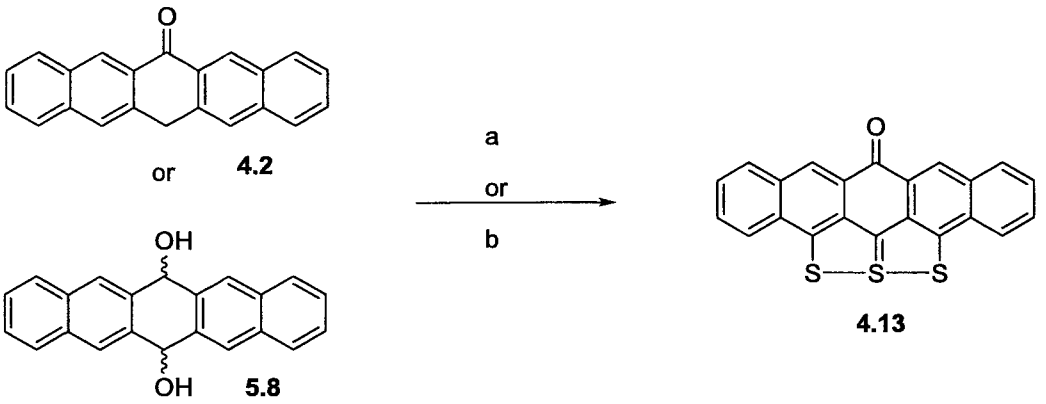

Scheme 30: Synthesis of Trithaipentacenone (TTPO). Reagents and Conditions: a) N_2, DMF, S_8, Reflux 24 h; b) N_2, TCB, S_8, Reflux, 4 h

The material **4.13** can be isolated simply by precipitation from the solvent with either water in the case of the reaction in DMF, or methanol when TCB is used. A navy blue solid is produced which is a vibrant blue color in a range of solvents such as tetrahydrofuran, chloroform, or methylene chloride. TTPO molecule **4.13** was confirmed by mass spectrometry and NMR spectroscopy, though the solubility of the molecule is very low so collecting a reasonable NMR spectrum required a large number of scans. The low solubility of **4.13** combined with its deep color suggests that the molecule has high molar absorptivity, but this has yet to be measured. Based on the UV/Vis spectra, the optical HOMO-LUMO gap of the TTPO is approximately 1.95 eV, which is somewhat smaller than that of pentacene at 2.21 eV.[170]

TTPO **4.13** shows very high photooxidative resistance. When it is exposed to ambient light and air for several days, there is little to no oxidation back to pentacenequinone. Only under the extreme condition of using a 500W lamp while stirring a solution of TTPO in air does oxidation occur over multiple hours. When crystalline, the

compound is very robust and can be heated to 388-392°C in air before melting. TTPO thermally evaporates to produce high quality thin films which potentially can be used to make thin-film electronic devices. When TTPO is saturated in chloroform with slow evaporation of solvent, x-ray quality crystals are formed (Figure 38).

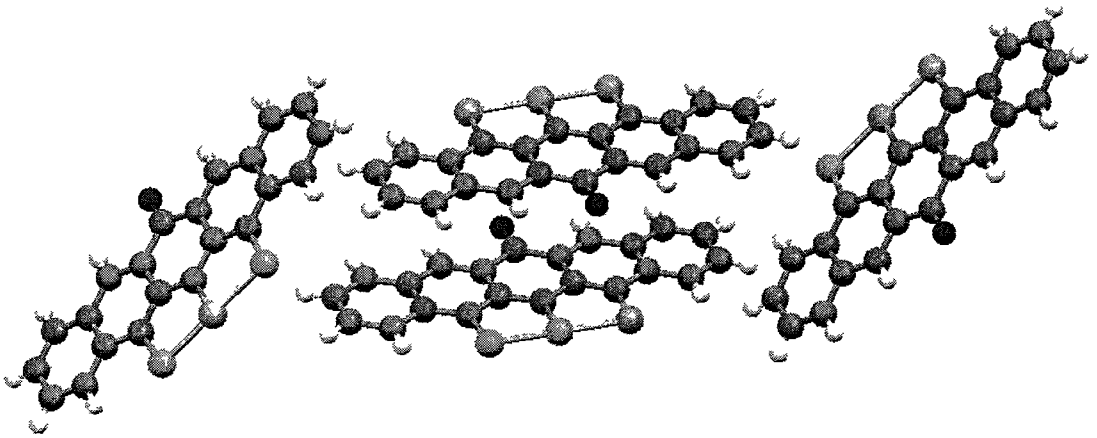

Figure 38: Unit cell for the crystal structure of trithaipentacenone (TTPO)

Based upon the crystal structure there are numerous intermolecular interactions at play that help stabilize the crystals. These include CH-π stacking interaction, π-π stacking interactions and H-bonding interactions. The π-π stacking interactions are quite interesting because of the "head-to-tail" arrangements of adjacent TTPO molecules in each columnar or "1D" stacks. These stacks (Figure 39) are considered ideal for electron and hole mobility through thin films. Consequently, crystalline thin-films of TTPO may prove to be useful in field-effect transistors, photovoltaics, and light-emitting devices.

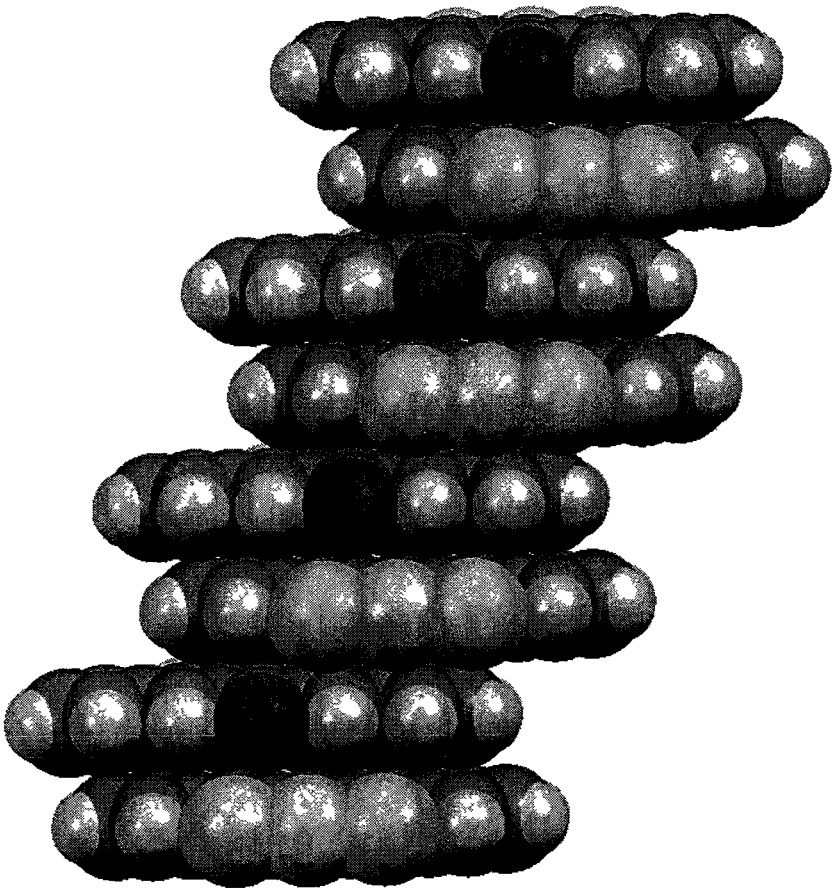

Figure 39: Head-to-Tail arrangement of TTPO and columnar stacking as observed in the x-ray crystal structure Red = Oxygen, Yellow = Sulfur, Grey = Carbon, White = Hydrogen.

To understand the head-to-tail arrangement of TTPO molecules in each stack, DFT calculations were performed to identify the charge density distribution within each molecule using natural bond orbital (NBO) population analysis. These calculations indicate that there are alternating positive and negative charges throughout the molecule allowing for alignment of opposite charges during head-to-tail, columnar stacking (Figure 40). Thus carbons 5, 6, and 7 all show significant positive character while carbons 12,

13, and 14 on the opposite side of the acene show significant negative character. In order to maximize intermolecular interactions between adjacent columnar stacks (e.g. O-H, S-S and C-H$^{\cdots}$ π interactions), the molecules in each stack are parallel displaced with respect to each other resulting in "tilted" columnar stacks. Or, in other words, the axis that defines the center of mass of each column is not perpendicular to the 2D plane defined by the atoms in any TTPO molecule. The net effect of the multitude of intermolecular interactions at play in the TTPO crystal structure helps its tendency to crystallize from many solvents including benzene, chloroform and toluene.

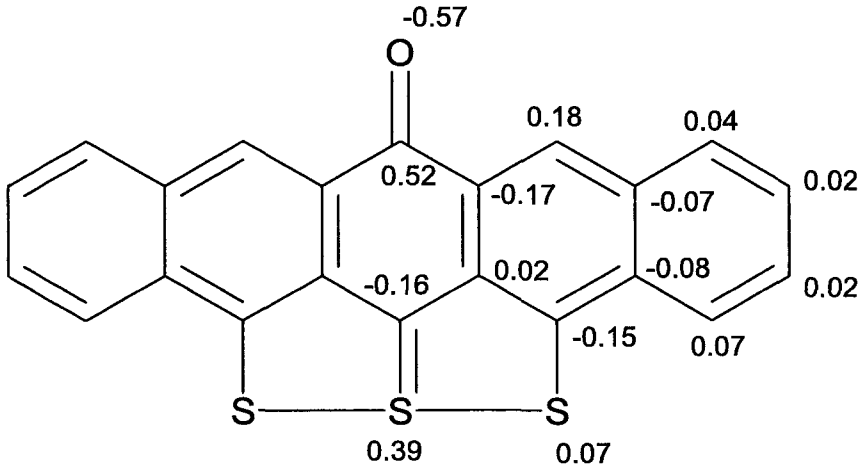

Figure 40: DFT NBO population analysis of TTPO at B3LYP/6-311+G(d,p) (Calculations performed by Dr. Jennifer Hodgson)

In fact the tendency of TTPO to crystallize is not limited to pure samples of TTPO. When TTPO is made from 6,13-pentacenediol in 1,2,4-trichlorobenzene, there is often a significant amount of 6,13-pentacenequione that is formed as by-product in the reaction. TTPO often crystallizes from the impure mother liquor after filtration of the solids. After washing the solids with acetone light green crystals (rather than purple) typically form in

the altered mother liquor. Although a crystal structure has yet to be determined, NMR analysis of the isolated green crystals indicates a 1:1 ratio of TTPO to pentacenequinone. After washing with methanol, the altered mother liquor yields dark green crystals that contain a 2:1 ratio of TTPO to pentacenequinone as determined by NMR spectrum. As with the 1:1 co-crystal the structure has yet to be determined. With this strong tendency to crystallize it is possible that co-crystals with other organic-semiconductors can be readily prepared thereby making novel thin-film materials that have finely tuned band gaps depending on the ratios of the compounds in co-crystals.

In addition to possessing superior thermal stabilities and photo-oxidative resistances, TTPO and its derivatives are soluble in a variety of organic solvents and therefore represent excellent candidates for organic thin-film electronic devices prepared using low cost, roll-to-roll manufacturing techniques. Because of its superior thermal stability, organic thin-film electronic devices of TTPO and its derivatives may also be prepared using techniques like thermal evaporation (Figure 41). An organic thin-film transistor (OTFT) prepared from TTPO showed a field effect mobility of 1.27×10^{-6} cm^2 V^{-1} s^{-1} at 75 °C and 8.05×10^{-6} cm^2 V^{-1} s^{-1} at 100 °C (see Figure 42 for drain-source current versus drain-source voltage behavior as a function of gate voltage). Given the enhanced thermal stability and photo-oxidative resistance of TTPO and its derivatives, these compounds represent a superior class for organic thin-film electronic devices including devices to be utilized at high temperatures like, for example, sensors and controls, transistors, organic photovoltaics and organic light emitting devices.

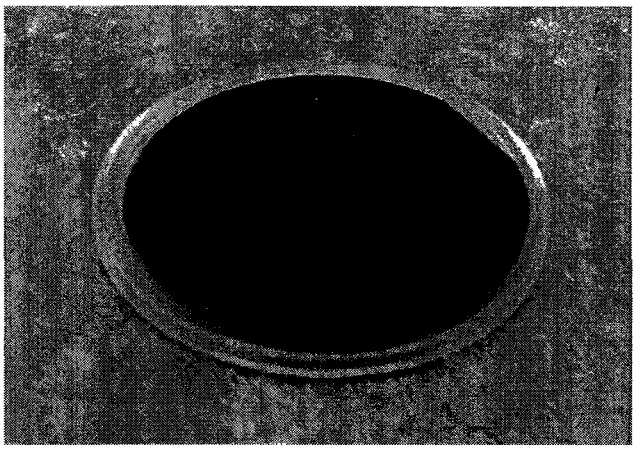

Figure 41: Thermal evaporation of **4.13** onto a SiO_2 wafer

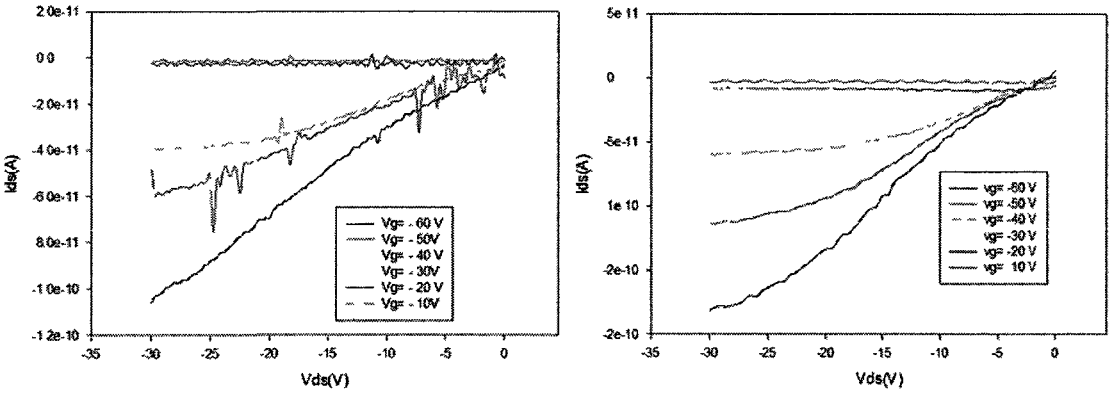

Figure 42: Drain-source current versus drain-source voltage behavior as a function of gate voltage

4.2.3 Proposed Synthesis of Substituted TTPO derivatives

Using the chemistry that has been detailed, it is possible to combine several different synthetic pathways to form soluble derivatives of TTPO as well as large acene systems. Starting from a di-substituted or tetra-substituted o-xylene and subjecting it to bromination conditions, the corresponding tetrabromo-species can be formed (Scheme 31). Cyclization with benzoquinone will allow for the formation of the corresponding

substituted quinone which can be reduced to the diol and then subjected to the sulfur addition chemistry to produce the TTPO derivative. The diol could also be aromatized to the substituted pentacene which could then be reacted with sulfur to produce the substituted hexathiapentacene.

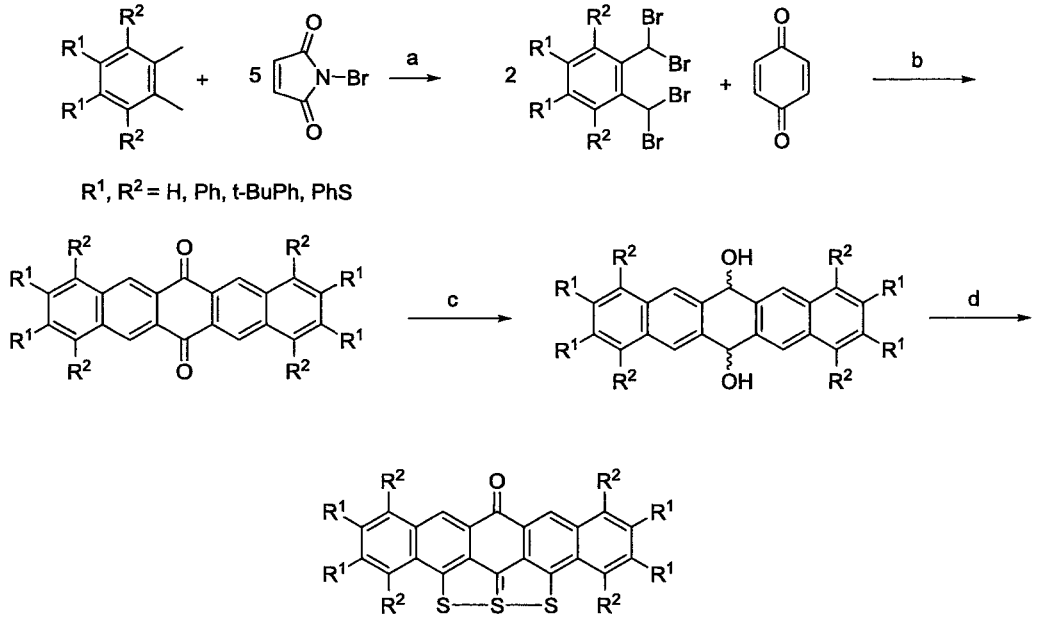

Scheme 31: Proposed synthesis of substituted TTPO. Reagents and Conditions: a) AIBN, $CHCl_3$, Reflux, *hv*, 8 h; b) KI, DMF, Reflux, 18 h, 24 h, RT; c) $NaBH_4$, THF, RT 24 h; d) S_8, TCB, Reflux 4h

4.2.4 Progress Towards the Synthesis of Fused Bistrithiapentacenones and Trithiaperipentacenone

By combining the sulfur addition chemistry of the TTPO with schemes to synthesize fused bispentacene or peripentacene, large thia-substituted bisacenes could possibly be produced (Scheme 32). Preliminary calculations suggest that these species

will exist as closed-shell species in their ground states, unlike peripentacene and related species. Starting from **4.3**, conversion to partially fused species **4.7** and fully fused **4.8** has already been discussed. Reduction of either species should lead to a diol that can be reacted with sulfur to produce both partially fused (**4.14**) and fully fused (**4.15**) trithiabispentacenone species. Both of these compounds have been subjected to DFT calculations and are predicted to be closed shelled species with HOMO-LUMO gaps in the range of 1.8 to 2 eV. (See appendix pages S96-S98 for results of thiaacene calculations)

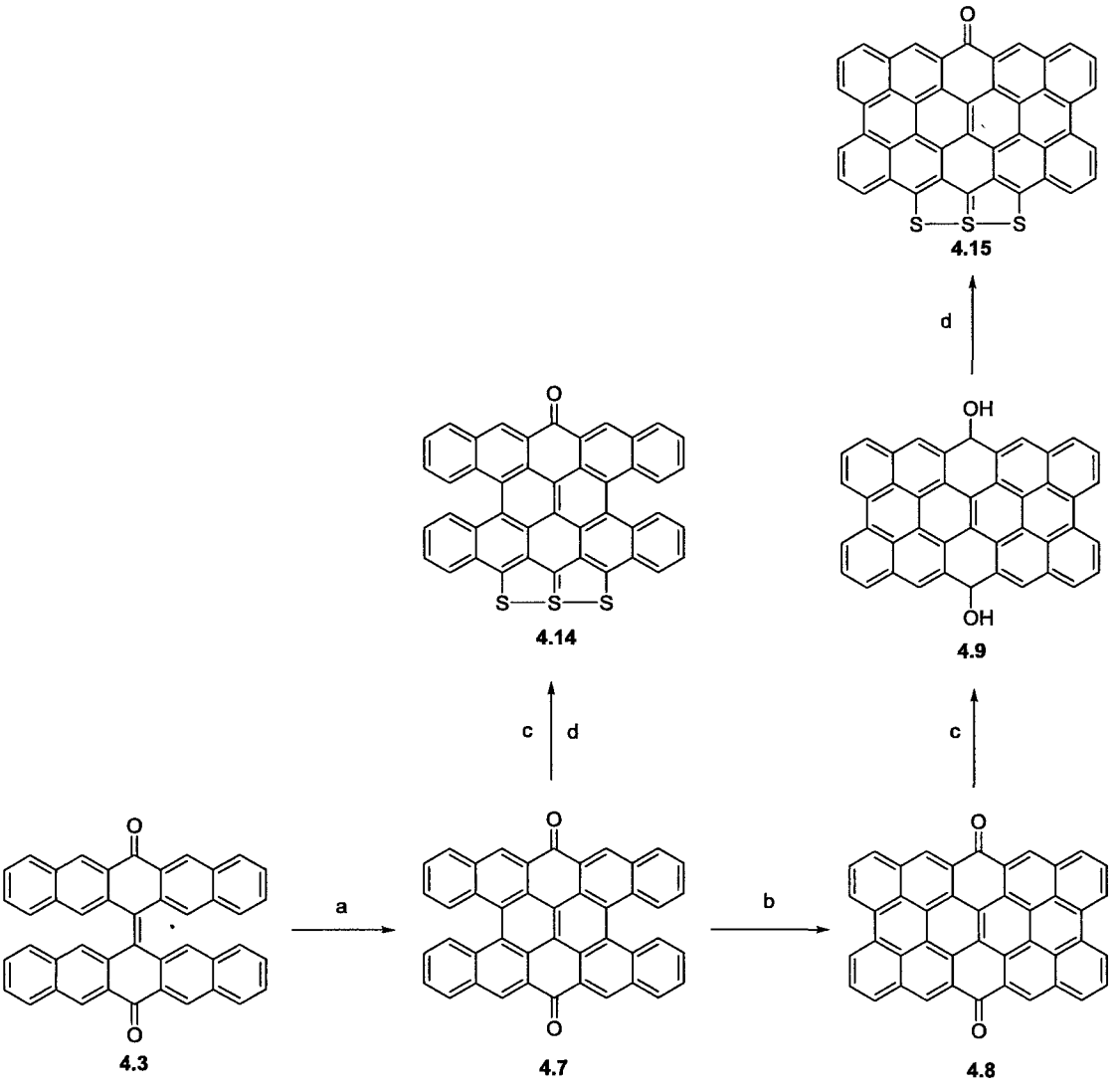

Scheme 32. Synthesis of Fused Trithiabispentacenone and Trithiaperipentacenone. Reagents and Conditions: a) NBS, benzene, *hv* ,2 h; b) 380°C, 2h; c) $NaBH_4$, THF, 24 h, RT; d) S_8, TCB, Reflux, 6h

As previously discussed, **4.7** was prepared from **4.3**. Reduction of **4.7** to the corresponding diol using $NaBH_4$ was followed by reaction with sulfur to potentially produce the partially fused trithiabispentacenone **4.14**. Characterization of **4.14** has been

difficult due to its extremely low solubility. While a vibrant emerald green color when dissolved in chloroform suggests the desired molecule, the overall solubility is too low to study its structure by NMR spectroscopy. Numerous side products are observed by mass spectrometry. Difficulties have also been encountered in the preparation of **4.15**. Since the solubility of peripentacenequinone **4.8** is extremely low in every common organic solvent, reduction using $NaBH_4$ is difficult. Characterization of the corresponding peripentacenediol is also hampered a by lack of solubility. Reaction of the ill-defined diol with elemental sulfur does not appear to lead to **4.15**. In the future, the reduction of **4.8** will be run at elevated temperatures where the peripentacenequinone may show greater solubility.

CHAPTER 5

TOWARDS THE RATIONAL SYNTHESIS OF FULLERENES AND NANORIBBONS FROM HYDROGENATED POLYAROMATIC HYDROCARBONS

5.1 Synthesis of Fullerenes

5.1.1 Towards Synthesis of [60]Fullerene

The most common synthesis of [60]fullerene, [70]fullerene and larger fullerenes involves the use of electric arc discharge to produce a fullerene enriched soot which then has to be extracted using an appropriate solvent followed by column chromatography and in some cases sublimation. While effective, this method has several drawbacks: (1) it is an energy intensive process; (2) it does not allow for selective isotopic labeling; (3) the large fullerenes are prepared in very low concentrations using electric arc discharge; and (4) isolating many of the larger fullerenes free of other fullerenes is very difficult. To overcome these problems, selective syntheses of individual fullerene compounds are needed. Thus far, the only selective chemical synthesis of a fullerene compound was achieved by Scott and co-workers using flash vacuum pyrolysis (FVP) at 1100 °C in the final step of a multi-step synthesis. FVP was needed to fragment carbon-chlorine bonds in the final step in order to initiate radical reactions that were needed to "stitch up" the

[60]fullerene product. Using this method, the overall yield of [60]fullerene was less than 1 %[9] (Scheme 33).

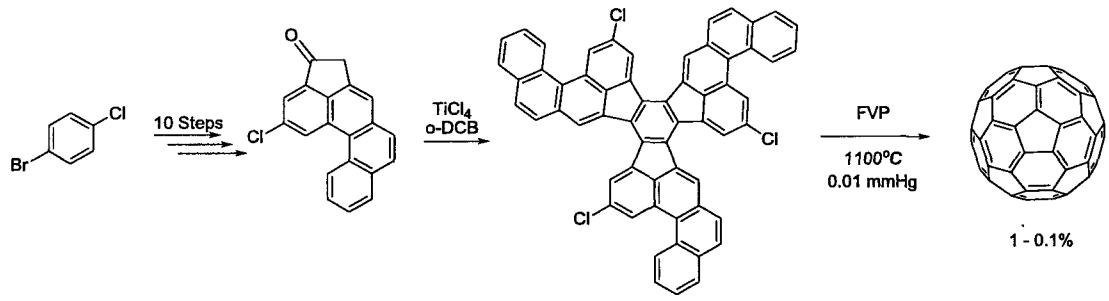

Scheme 33: Scott's total synthesis of [60]fullerene

New selective syntheses of fullerenes are needed that allow formation of several different fullerene structures in good yield. The new methods would ideally involve synthetic steps that can be run under milder conditions. Here, a method is proposed that has some similarities to the Scott synthesis, but with no FVP required for the final "stitching". Like the Scott synthesis, the method proposed here builds large polycyclic aromatic hydrocarbons from smaller aromatic systems. Our method of construction takes advantage of the ease with which relatively stable radicals can from partially hydrogenated aromatic systems. For example, we found that when two equivalents of acenaphthylene is heated to its boiling point (approximately 280°C) in the presence of one equivalent acenaphthene in a sealed vessel, decacyclene forms spontaneously in good yield (~50 % crude) plus three equivalents of acenaphthene (Scheme 34).

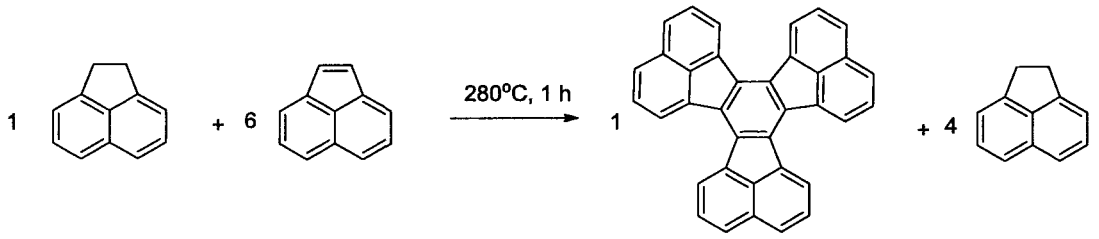

Scheme 34: Our novel synthesis of decacyclene

It is believed that the formation of the decacyclene is initiated by the thermally induced cleavage of a C-H bond on acenaphthene to generate a resonance delocalized organic free radical species that initiates a cyclotrimerization with two equivalents of acenaphthalene (Scheme 35). The initial cyclotrimerization product is itself a resonance delocalized free radical which can eliminate five successive hydrogen atoms to generate a fully aromatized decacyclene plus two equivalents of acenaphthene and a new acenaphthenyl radical which is then available to initiate another round of cyclotrimerization (Scheme 35).

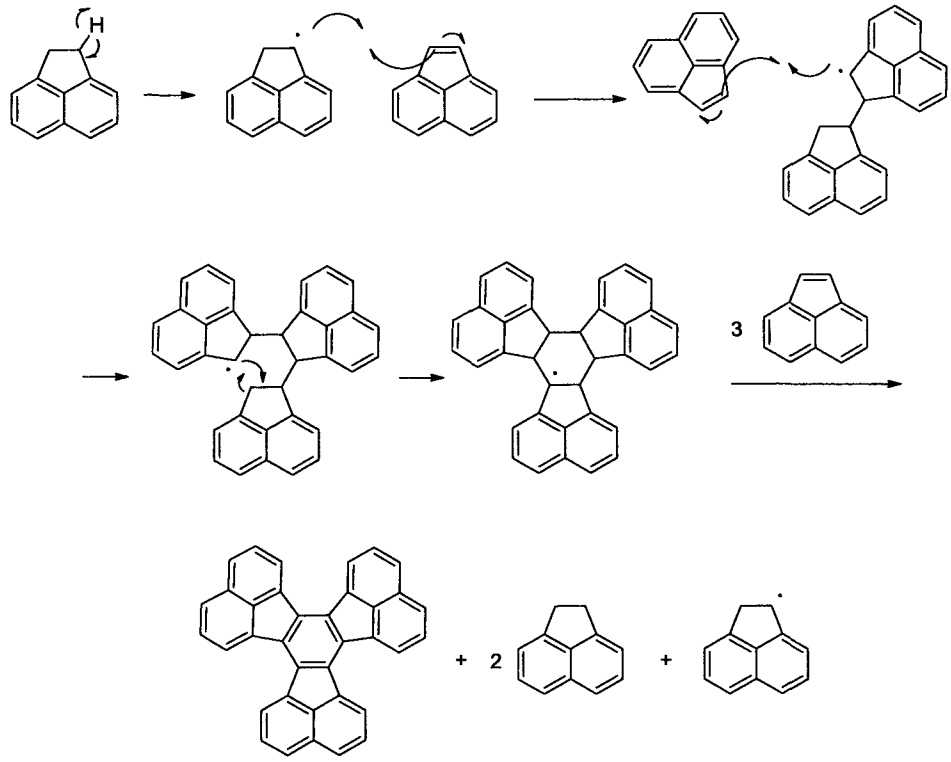

Scheme 35: Proposed mechanism for decacyclene synthesis using acenaphthylene in the presence of acenaphthene

This facile synthesis of decacyclene from smaller aromatic molecules potentially allows for new synthetic pathways to fullerene compounds utilizing small, partially hydrogenated PAHs as free radical precursors, much as Scott utilized halogenated species as free radical precursors under FVP conditions. The main difference is that our method does not require FVP and has the possibility of being highly efficient. The partially hydrogenated PAHs would be reacted with the appropriate fully aromatized species to initiate cyclotrimerizations leading to fullerene precursors that could be "stitched-up" to form the corresponding fullerenes. Scheme 36 illustrates a proposed synthesis of

[60]fullerene using this approach. The steps shown in bold face have yet to be performed.

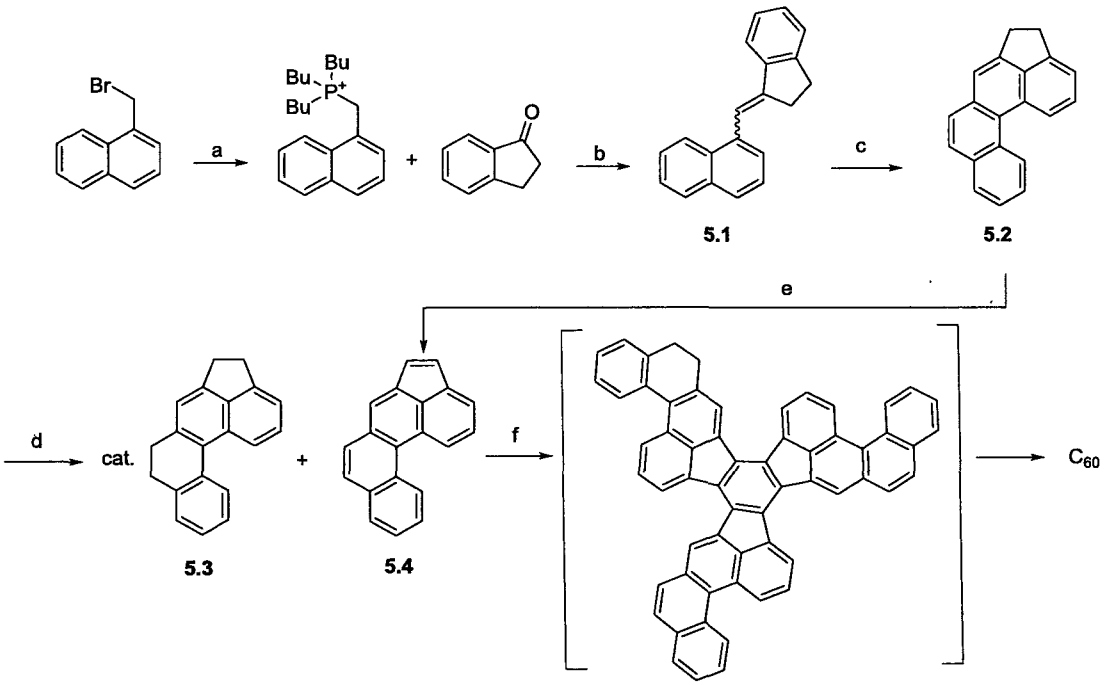

Scheme 36: Proposed synthesis of [60]fullerene using a partially hydrogenated PAH compound as free radical initiator. Reagents and Conditions: a) p-xylene, PBu_3, reflux, 3 h; b) nBuLi, THF, -78°C, 1 h; c) I_2, benzene, propylene oxide, *hv*, 8 h; **d) H_2, Pd/C, Benzene, Reflux, 24 h; e) DDQ, Benzene, reflux 2 h; f) 350°C, 1 h (steps shown in bold face have yet to be performed)**

Starting from 1-(bromomethyl)naphthalene, the corresponding phosphonium salt is generated with tributylphosphine in high yield. The phosphonium salt is then used to perform a Wittig reaction on 1-indole to form compound **5.1**. Compound **5.1** is then photochemically cyclized to compound **5.2**. Compound **5.2** must then be reduced though hydrogenation to yield **5.3** and also dehydrogenated to the fully aromatic **5.4**. Upon

heating these two compounds, **5.3** and **5.4**, at or near their melting points (~ 350 °C), a cyclotrimerization should be initiated leading to a decacyclene-like intermediate that should spontaneously assembly into [60]fullerene.

5.2 Synthesis of graphene nanoribbons

5.2.1 Initial Discovery

During our attempts to hydrogenate [60]fullerene to higher levels than could be achieved using polyamine reagents, we considered transfer hydrogenation chemistries in which [60]fullerene is heated in the presence of such materials as 9,10-dihydroanthracene. Hydrogenating [60]fullerene with 9,10-dihydroanthracene at the boiling point of the partially hydrogenated PAH (~320 °C) results in the synthesis of $C_{60}H_{36}$ species, but never more highly hydrogenated fullerene species. We therefore sought to perform similar transfer hydrogenation reactions using higher molecular weight partially hydrogenated PAH compounds with higher boiling points. Our first target was 5,12-dihydrotetracene due to its expected ease of synthesis (Scheme 37) and its relatively high boiling point (~ 420 °C).

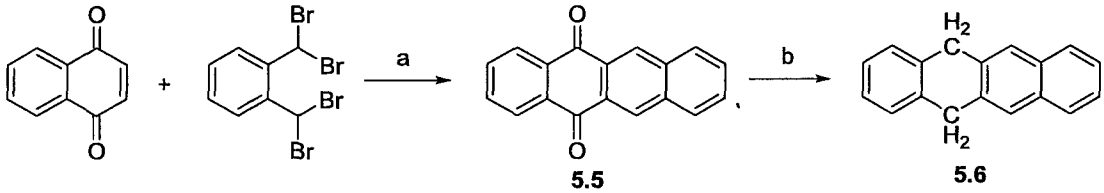

5.5 **5.6**

Scheme 37: Synthesis of 5,12-dihydrotetracene. Reagents and Conditions: a) KI, DMF, reflux 18 h; b) HI/HOAc, Reflux 24 h

Thus, 5,12-tetracenequinone, **5.5**, was synthesized in 50-60% yield by condensation of 1,4-napthlenequinone and α,α,α',α'-tetrabromo-*o*-xylene, in the presence of potassium iodide. After water filtration and drying, **5.5** was dissolved in a 1:1 mixture of hydroiodic acid (55-58%, unstabilized) and glacial acetic acid and heated to boiling for approximately 16 hours.[171] The corresponding 5,12-dihydrotetracene, **5.6**, was filtered and isolated in 70% yield.

Compound **5.6** was then mixed in a 65:1 ratio with [60]fullerene and heated to its boiling point for 3 hours in a sealed, thick-walled tube. After completion of the reaction, there was a mixture of black, yellow and orange solids. The orange and yellow solids were soluble in several solvents and were identified by ^{1}H-NMR spectroscopy as a mixture of **5.5**, **5.6**, tetracene, and traces of hydrogenated [60]fullerene. A separate material was detected by mass spectrometry that appeared to include dimers, trimers and larger oligomers of tetracene (Figure 43).

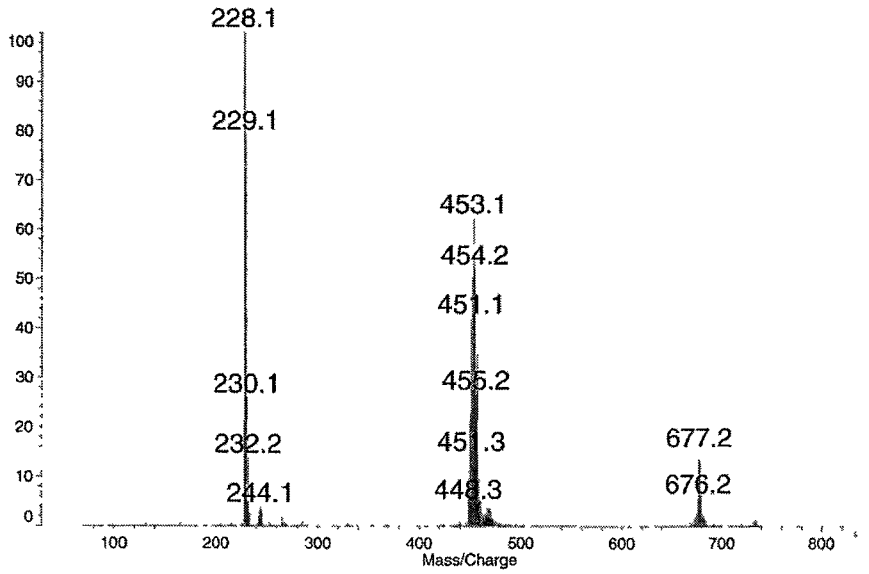

Figure 43: Mass spectrometry of [60]fullerene/**5.6** reaction product

A review of work published by Roberson and co-workers indicated that upon heating pentacene in the presence of dihydropentacene, spontaneous formation of peripentacene was observed.[172] Based upon this literature, we surmised that an analogous reaction had occurred in our reaction between **5.6** and [60]fullerene producing a peritetracene species. That is, it appears that **5.6** does undergo a transfer hydrogenation with [60]fullerene to produce partially hydrogenated fullerene and tetracene. The tetracene then reacts with another equivalent of **5.6** to form a peritetracene. This process can then repeat, allowing for the growth of larger oligoperitetracene molecules, as observed by mass spectrometry (Figure 43). These oligoperitetracene species represent graphene nanoribbons with exceedingly small widths. Mass spectrometry analysis of the black insoluble material formed in the reaction confirms this hypothesis. Larger oligoperitetracene nanoribbons were formed along with the smaller peritetracenes (Figure 44).

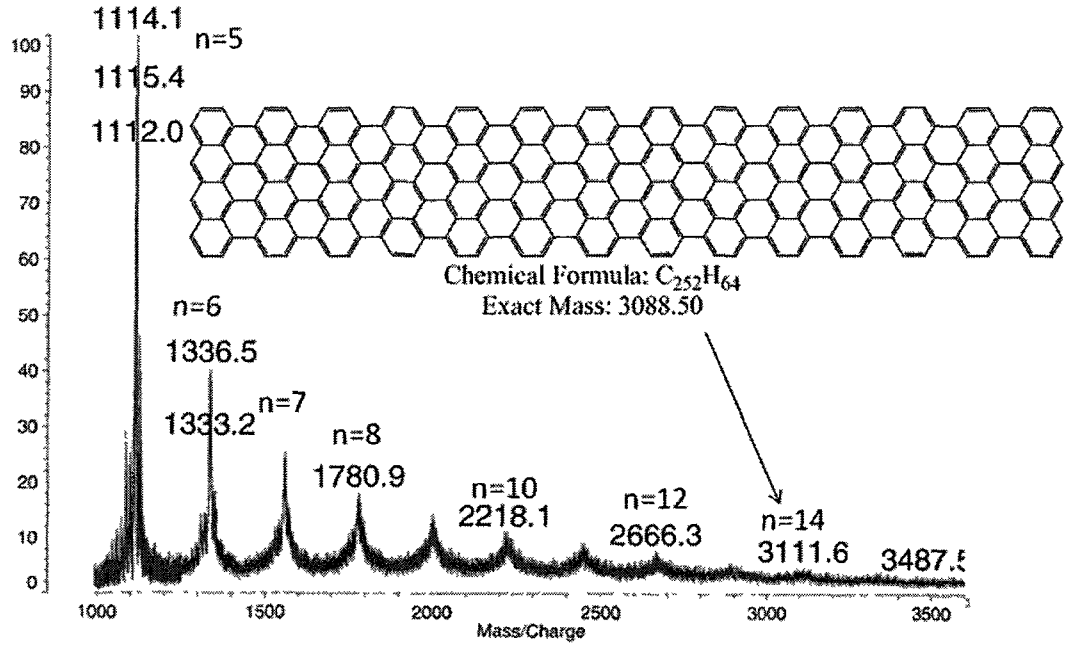

Figure 44: Laser desorption ionization mass spectrum of oligoperitetracenes or nanoribbons formed in the reaction between [60]fullerene and **5.6**. The 'n' indicates the number of tetracene repeat units in the nanoribbon.

It should be noted that the nanoribbon signals in the mass spectrum appear as "hay stacks" indicative of a range of compounds with very similar masses. Moreover, the average mass of each "hay stack" is larger than expected. As seen in Figure 44, the mass of the 14 repeat unit nanoribbon detected by mass spectrometry is approximately 23 atomic mass units higher expected. This is believed to be caused by incomplete carbon-carbon bond formation within the nanoribbon and by the formation of partially reduced (hydrogenated) nanoribbon either by incomplete aromatization (dehydrogenation) of the growing oligomer or by hydrogen transfer from **5.6**. Rapid oxidation of the nanoribbons could also partially account for the larger than expected mass.

In an attempt to simplify the reaction conditions and to see if [60]fullerene was required for initiating nanoribbon formation, several test reactions were conducted with a mixture of **5.6** and commercially available tetracene. Using various ratios of **5.6** to tetracene from 1:1 to 1:20 and heating to 360 °C for 1 hour in a sealed vessel containing a glass wool plug in order to suppress sublimation, similar results were observed to those of the reaction between [60]fullerene and **5.6**. Analysis by mass spectrometry confirmed the formation of similar tetracene nanoribbons (Scheme 38). Thus, [60]fullerene is not required for the formation of the nanoribbons and only a catalytic quantity of 5,12-dihydrotetracene is needed to initiate reaction.

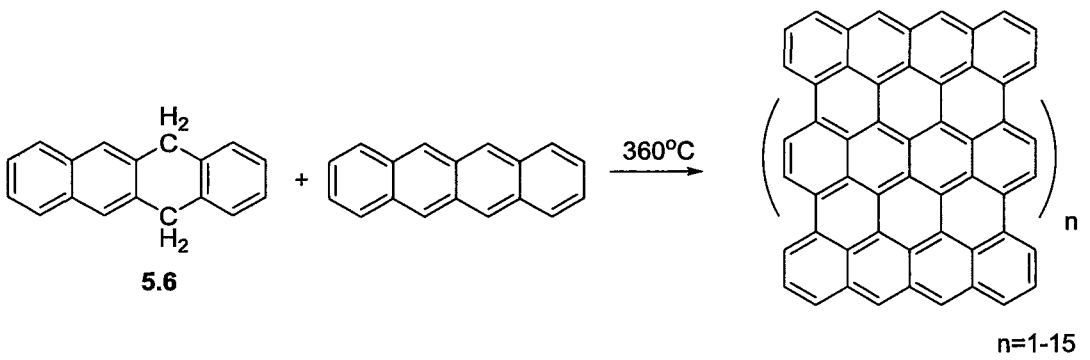

Scheme 38: Synthesis of tetracene nanoribbons from tetracene and 5,12-dihydrotetracene

5.2.2 Oligoperipentacenes as Graphene Nanoribbons

Along with the synthesis of tetracene nanoribbons, attempts to synthesize the corresponding pentacene nanoribbons were also made. Using a similar approach as described above, pentacene and 6,13-dihydropentacene were produced (Scheme 39).

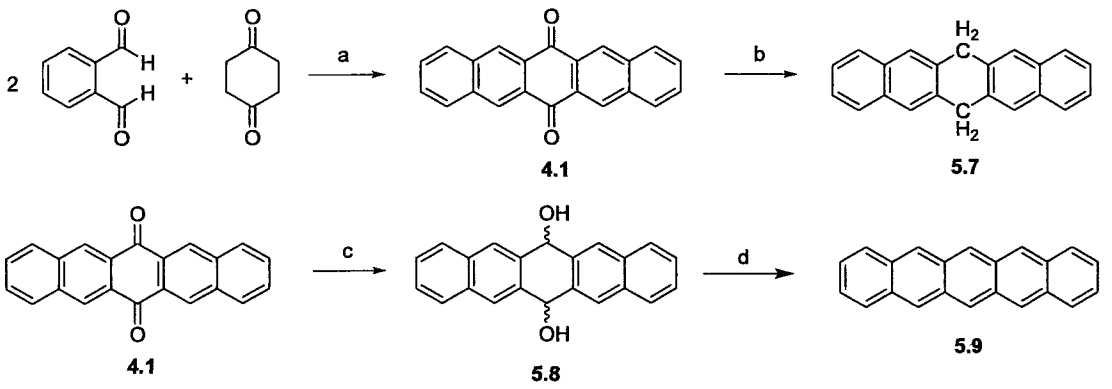

Scheme 39: Synthesis of 6,13-dihydropentacene and pentacene. Reagents and Conditions: a) 5% NaOEt, EtOH, RT, 24h, b) HI/HOAc, Reflux 3 d, c) THF, $NaBH_4$, RT, 24 h, d) $SnCl_2$, 10% HCl, RT, 10 min

Thus, stirring 1,4-cyclohexanedione in a sodium ethoxide solution for 10 minutes to generate the corresponding enolate followed by the addition of *o*-phthalaldehyde led to formation of 6,13-pentacenequinone (**4.1**) in 70-80% yield. Compound **4.1** is then either reduced with a boiling 1:1 mixture of hydroiodic acid (55-58%, unstabilized) and glacial acetic acid for 3 days to produce 6,13-dihydropentacene (**5.7**) in greater than 90% yield, or it is reduced to 6,13-pentacenediol (**5.8**) using sodium borohydride in THF. Diol **5.8** can then be aromatized to the corresponding pentacene (**5.9**) in 95% yield by stirring in a solution of tin(II) chloride in 10% HCl.

Using the same conditions as with the tetracene analogs, **5.7** and **5.9** were mixed in various ratios from 1:1 to 1:20, sealed in a high pressure reaction vessel and heated to approximately 360 °C (Scheme 40). The boiling points of these materials are much higher than 360 °C. However, reactions run at higher temperatures are complicated by sublimation of reactants which greatly reduces the overall yield. Employing a glass wool plug to reduce the effects of the sublimation is of minimal value here.

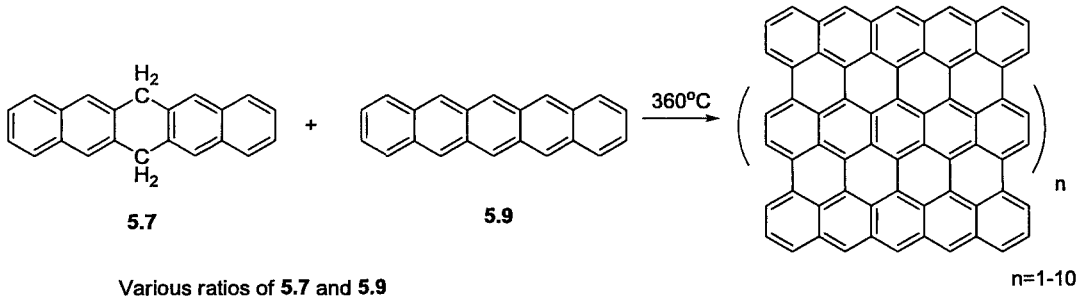

Scheme 40: Synthesis of pentacene nanoribbons from pentacene and 6,13-dihydropentacene

Analysis of the soluble materials by ^{1}H NMR spectroscopy shows a large amount of **5.7** and some **4.1** which is expected given the relative ease with which pentacene oxidizes. It is no surprise that oligoperipentacenes were not observed in the soluble fraction given their expected insolubility. Analysis of the insoluble material by mass spectrometry reveals a mixture of **5.7**, **5.9**, peripentacene and oligoperipentacenes (i.e., pentacene nanoribbons, Figure 45). The pentacene nanoribbons produced in this fashion are not as long as the tetracene nanoribbons, averaging only about 7 repeat units with a maximum detected at 10. This is approximately 5 repeat units shorter than was observed for the tetracene analogs.

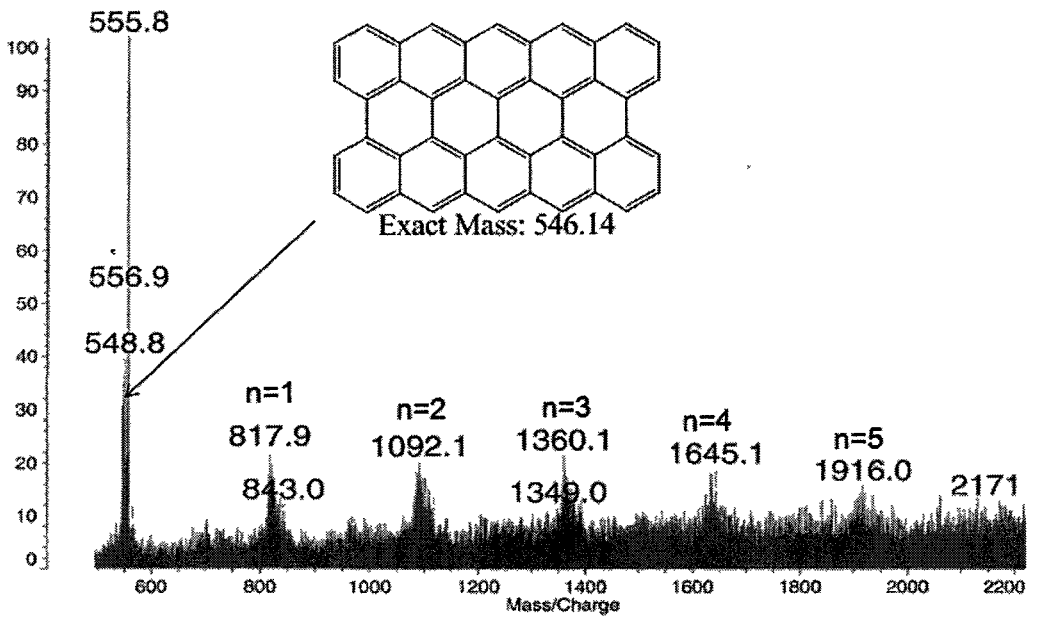

Figure 45: Mass spectrometry of pentacene nanoribbons from the reaction between **5.8** and **5.10**. The 'n' indicates the number of pentacene repeat units in the growing nanoribbon.

As previously noted for tetracene nanoribbons, the mass spectrometry signals associated with the pentacene nanoribbons are broadened packets of signals with average masses that are slightly higher than expected. This may be due to incomplete C-C bond formation in the growing nanoribbons, incomplete aromatization (dehydrogenation), hydrogen transfer from **5.7** or rapid oxidation.

Several attempts were made to make more uniform nanoribbons. Samples of the pentacene nanoribbons were mixed with a large excess of palladium metal on barium sulfate in toluene and heated to reflux for 24 hours in an attempt to force dehydrogenation. This proved to be unsuccessful either because of the low temperatures involved in the dehydrogenation or the insolubility of the pentacene nanoribbons. A

sample of the insoluble pentacene nanoribbons was also sealed in a high pressure vessel and heated to approximately 450 °C for 1 hour in an effort to induce thermal dehydrogenation. Mass spectrometry analysis of the crude product showed no noticeable difference from the starting material.

Recently, work published by Cai and co-workers detailed the formation of anthracene based nanoribbons of various lengths. Brominated bisanthracene was deposited onto either a Au(111) or a Ag(111) surface and then heated up to 400°C.[173] While the overall yield of nanoribbons produced in this fashion was less than 1%, the work represents an interesting method to produce nanoribbons. We deposited **5.7** onto cobalt nanoparticles (average radius 20 nm) by dissolving **5.7** in chloroform, adding the nanoparticles with mixing, and evaporating the solvent. Cobalt was selected because the metal is a well known hydrogen transfer catalyst and it can be removed later by dissolution into fairly benign solvents such as an aqueous hydrochloric acid, or other mild acid. The nanoparticles were selected because their small size allows for higher surface areas than bulk metals. The sample of deposited material was then sealed in a high pressure vessel and heated to 400 °C for 1 hour to facilitate nanoribbon formation. The coated nanoparticles were then dissolved in an aqueous solution of 10% HCl and a black material was collected and analyzed by TEM and mass spectrometry. TEM and mass spectrometry revealed no signs of nanoribbon formation. Instead, only amorphous carbon formed. In the future, alternative methods to form nanoribbons will be conducted by depositing **5.7** onto either gold or silver surfaces by CVD and then thermally annealing the samples, akin to the method of Cai and co-wokers.[173]

5.2.3 Attempted Synthesis of Soluble Nanoribbons

While the synthesis of unsubstituted nanoribbon is synthetically interesting, there is an inherent drawback in their lack of solubility. Insolubility complicates the use of nanoribbons in device applications since the materials cannot be easily and controllably deposited onto a surface. Therefore, a method is needed to make the nanoribbons soluble so that they could potentially be solution processable. A simple solution is to add bulky aromatic substituents to one end of the acene precursors. The substituents should only be placed on one side of the molecule so as not to interfere with nanoribbon formation. That is, bulky substituents at both ends of the acene monomer would raise the energy of periacene formation to such an extent that it would not form. However, with substituents at one end only, periacene formation is favorable provided the growing nanoribbon arranges in a head-to-tail fashion (Figure 46). Substituents should also reduce π-π stacking interactions between nanoribbons, thereby improving solubility. Also by carefully selecting what substituents are used, the electronic properties could potentially be tuned to fit a wide range of applications.

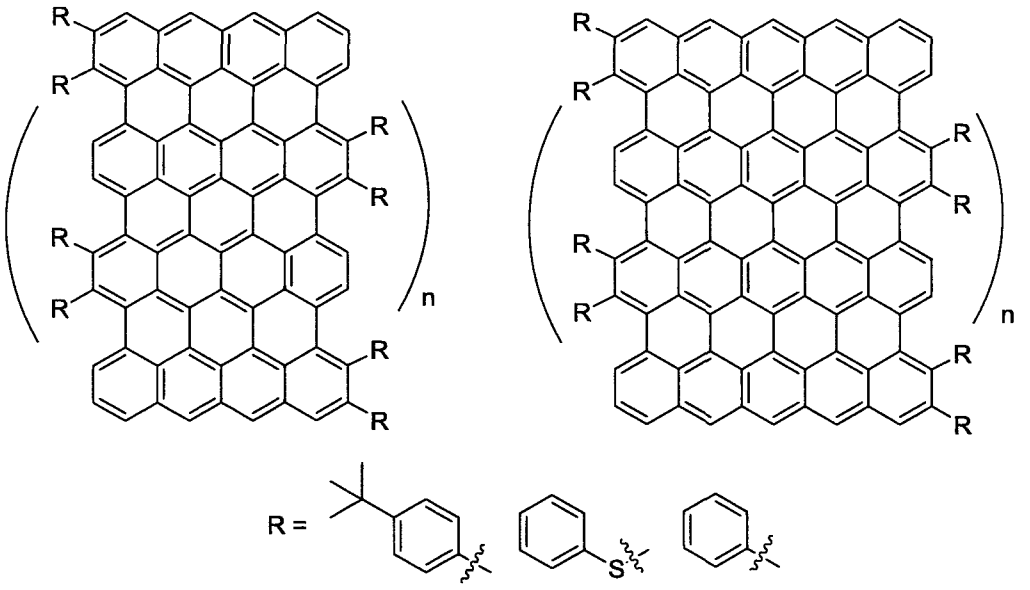

Figure 46: Examples of 'head-to-tail' substituted tetracene and pentacene nanoribbons

The synthesis of soluble nanoribbons begins with small molecules that can act as precursors to an acene monomer (Scheme 41).

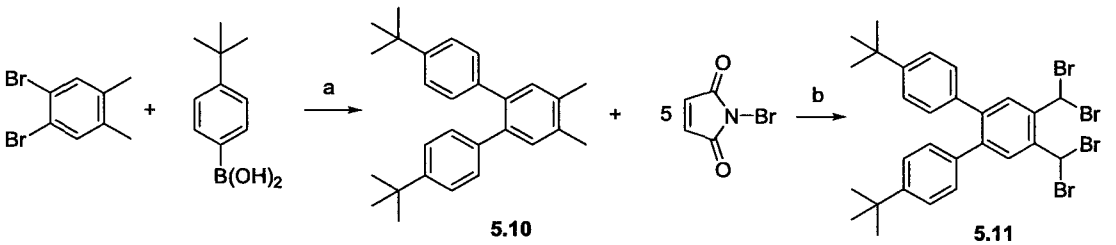

Scheme 41: Synthesis of a small molecule precursor to a soluble acene. Reagents and Conditions: a) $Pd(PPh_3)_4$, 1M Na_2CO_3, Toluene, Reflux 5 d, b) AIBN, $CHCl_3$, Reflux, *hv*, 8 h.

Starting with 1,2-dibromo-4,5-dimethylbenzene and 4-*t*-butylphenylboronic acid, a Heck coupling was performed using palladium(triphenylphosphine)tetrakis in a mixture of base and toluene. After a quick silica filtration, a yellow solution was collected and

crystallized by evaporation of the solvents overnight to obtain **5.10** in 65% yield. The large clear crystals were then dissolved in chloroform and 5 equivalents of NBS was added. The mixture was heated to reflux while shining a 500W lamp on the flask for 8 hours. After the reaction was completed, **5.11** was precipitated by evaporation of the chloroform solvent and acetone titration. After drying, pure **5.11** was used to make soluble, substituted tetracene and pentacene quinones, **5.12** and **5.13**, according to Scheme 42.

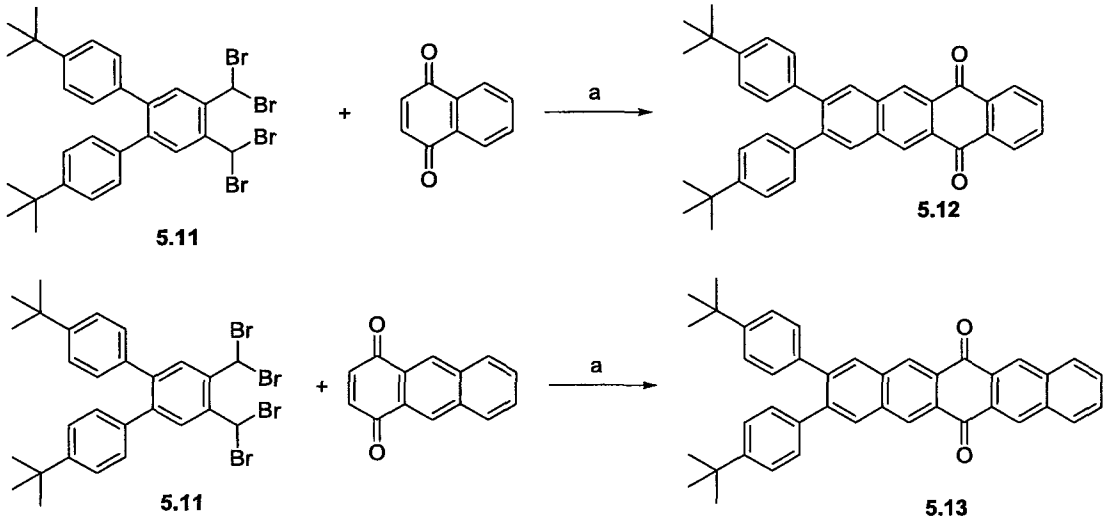

Scheme 42: Synthesis of soluble acenequinones. Reagents and Conditions: a) KI, DMF, Reflux, 18 h

Thus, **5.11** was mixed with 1,4-naphthlenequinone in the presence of potassium iodide in DMF. The solution was heated to boiling for 18 hours to produce **5.12** in 51% yield. The same starting material was also used to make soluble pentacene quinone **5.13** in 70%

yield. Compounds **5.12** and **5.13** were then taken onto the corresponding acenes and dihydroacenes using standard procedures, as elaborated in Scheme 43.

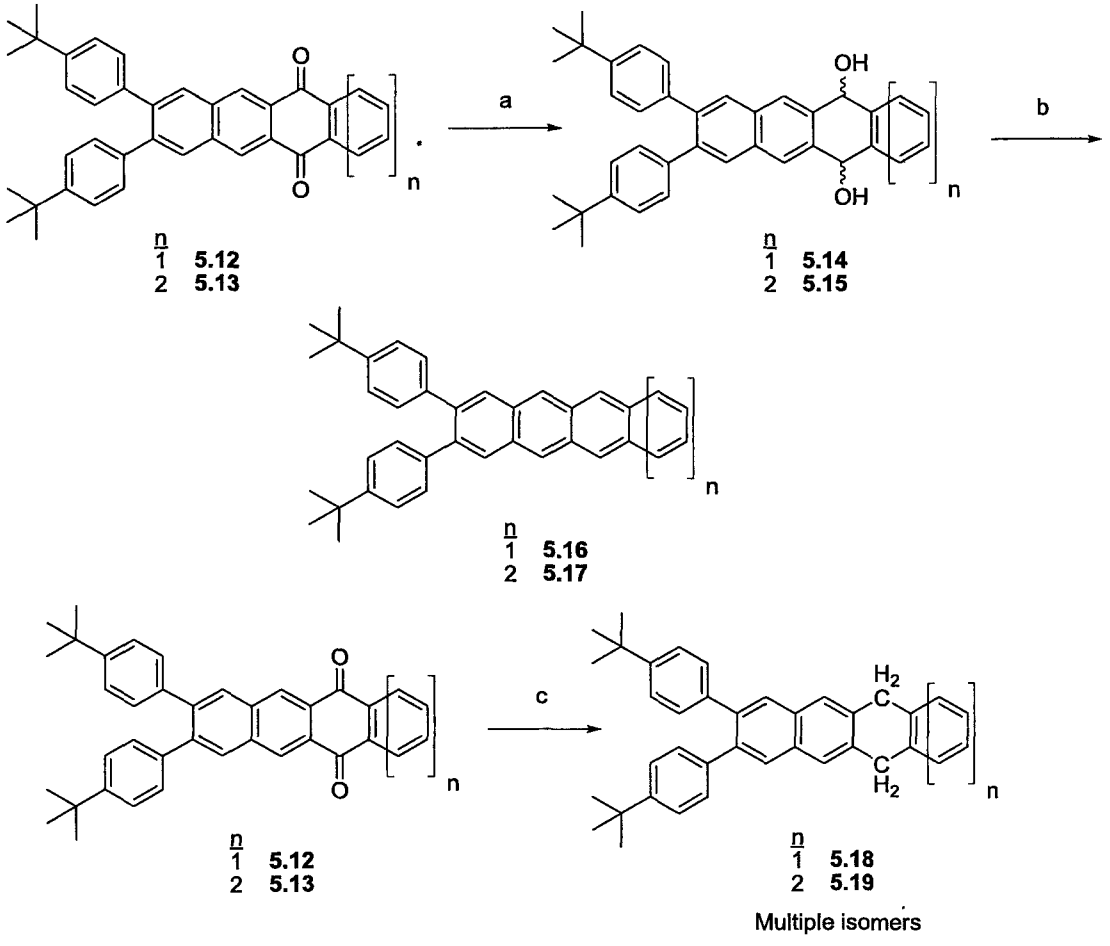

Scheme 43: Synthesis of soluble acenes and dihydroacenes. Reagents and Conditions: a) THF, $NaBH_4$, RT, 24 h, b) $SnCl_2$, 10% HCl, RT, 10 min, c) HI/HOAc, Reflux 21 d

Thus, **5.12** and **5.13** were separately reduced to the corresponding diols in 95% yield (**5.14** and **5.15** respectively) and then aromatized to either the substituted tetracene **5.16**

in 95% yield or substituted pentacene **5.17** in low yield. A problem arose in the latter synthesis of pentacene **5.17**. This pentacene either rapidly oxidized to the corresponding endoperoxide or dimerized,[174] or both. Both reactions are potentially reversibly at elevated temperatures so we opted to push the compromised **5.17** forward as starting material for pentacene nanoribbon.

Another issue arose during the reduction of the substituted acenequinones **5.12** and **5.13** to the corresponding dihydroacenes. With unsubstituted acenequinones, the HI-AcOH reduction would normally take 1 to 3 days to complete. However, with **5.12** and **5.13**, the reaction required 21 days to complete. The dihydroacene compounds prepared, **5.18** and **5.19**, were each isolated as a mixture of dihydro isomers that could not be resolved by column chromatography. However, we did not anticipate that this would hinder the formation of acene nanoribbons.

With the synthesis of substituted acenes and/or acene precursors and dihydroacene species, several attempts were made to synthesize soluble pentacene nanoribbons (Scheme 44).

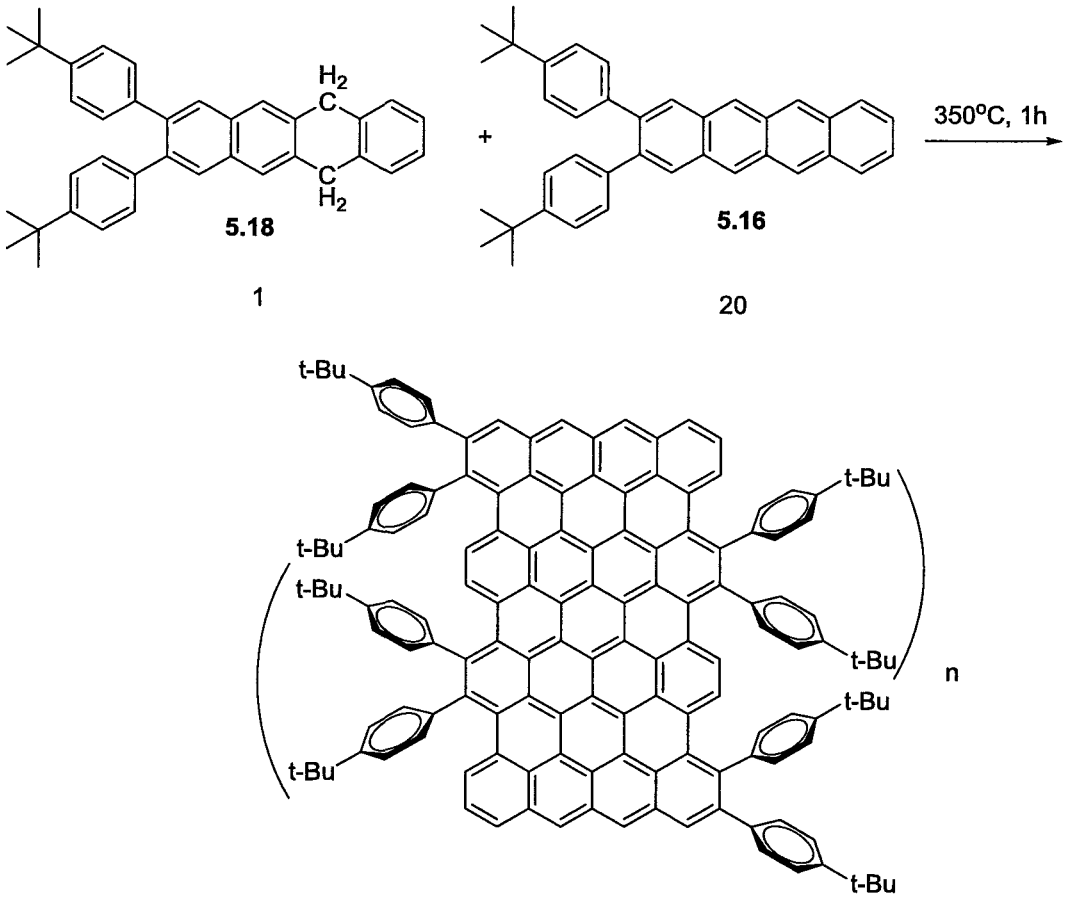

Scheme 44: Synthesis of soluble tetracene nanoribbons

A 20:1 mixture of **5.16** and **5.18** was placed in a sealed high pressure tube and heated to approximately 350 °C for 1 hour. After the reaction mixture was cooled, the material was fully dissolved in $CDCl_3$ to produce a brown solution that showed yellow fluorescence. The solution was analyzed by ^{1}H-NMR spectroscopy revealing the presence of **5.18** mainly with very little **5.16** despite its large excess at the beginning of the reaction. The sample was also analyzed by mass spectrometry to indicate that some

nanoribbon potentially formed with up to 6 repeat units (Figure 47). The signal-to-noise ratio is quite low, however, suggesting a low yield.

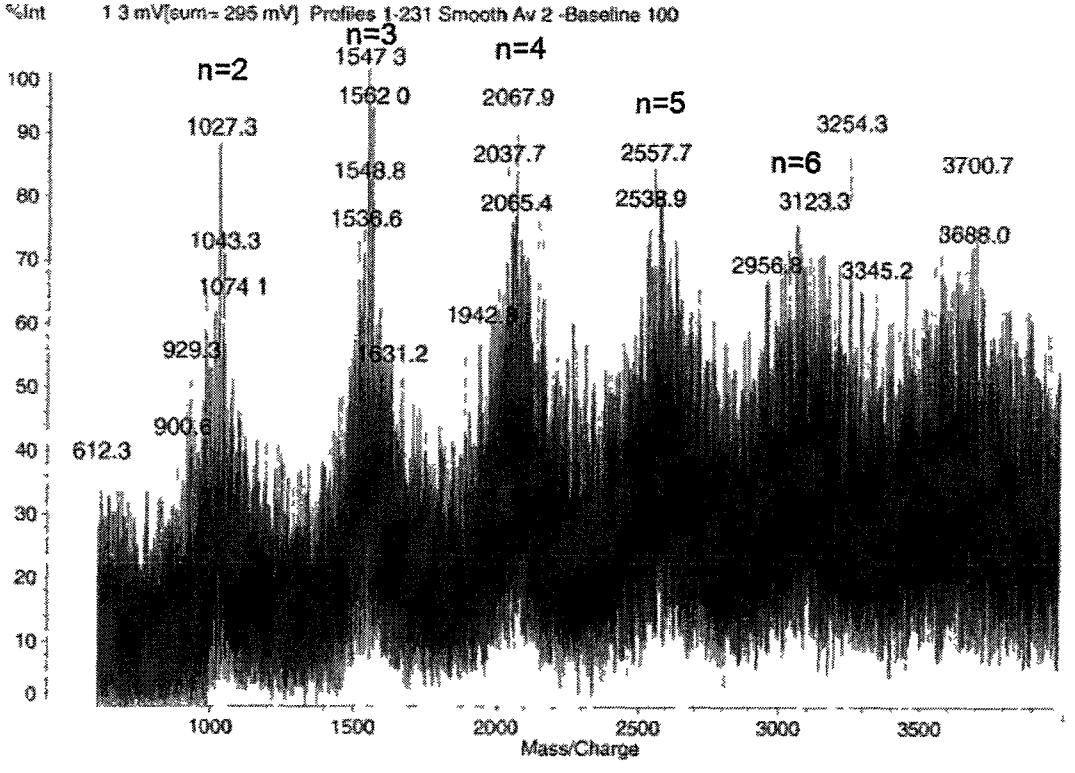

Figure 47: Mass spectrum of soluble tetracene nanoribbons in the reaction between **5.16** and **5.18**. The 'n' indicates the number of tetracene repeat units in the nanoribbon

Using similar conditions, soluble pentacene nanoribbons were synthesized using a 20:1 mixture of **5.17** and **5.19** and the same conditions as described above for the tetracene derivative. After the reaction was cooled, the crude product was fully dissolved in $CDCl_3$ to produce a brown solution that showed light blue fluorescence. Analysis by ^{1}H-NMR spectroscopy indicated the presence of **5.19** mainly with very **5.17**, much like

the tetracene reaction. The sample was also analyzed by mass spectrometry. Once again, some evidence for nanoribbon formation exists with up to 6 repeat units (Figure 48) but the signal-to-noise ratio is very low suggesting poor yield.

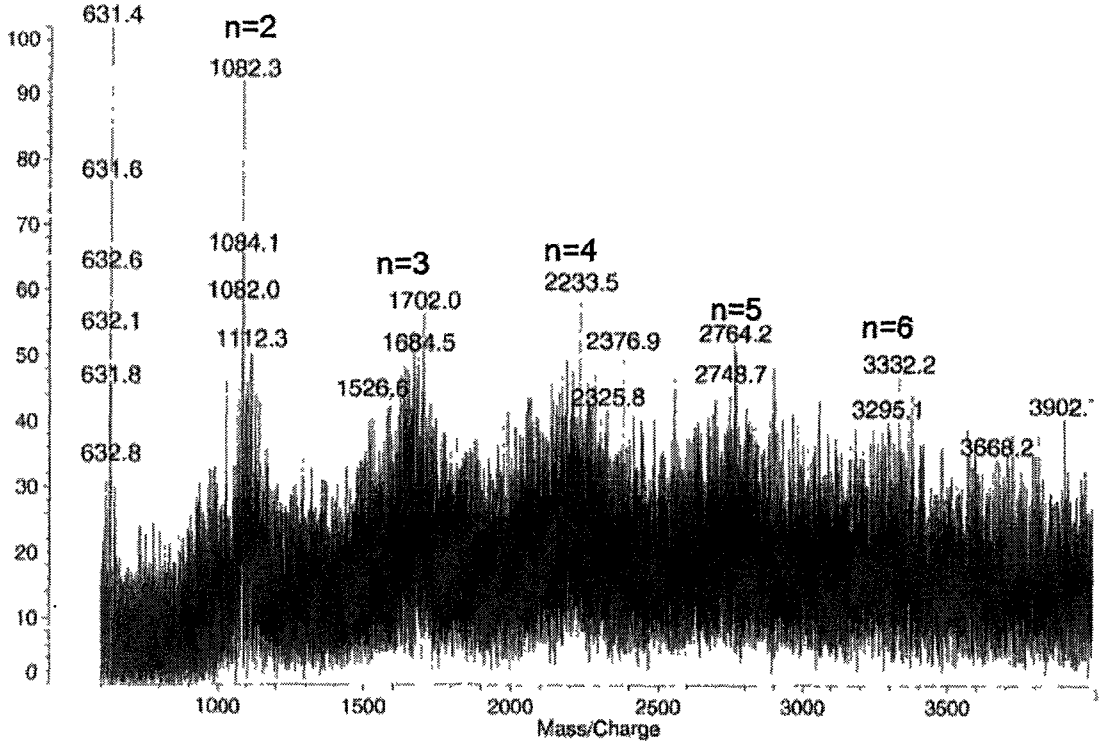

Figure 48: Mass spectrum of soluble pentacene nanoribbons in the reaction between **5.17** and **5.19**. The 'n' indicates the number of pentacene repeat units in the nanoribbon

As before, the mass spectrometry signals were broad suggesting to incomplete C-C bond formation in the growing nanoribbons, incomplete aromatization (dehydrogenation), hydrogen transfer from **5.7** or rapid oxidation. An attempt was made to dehydrogenate the crude products by dissolving them in toluene and then adding an equal mass of 5% palladium on carbon. After refluxing overnight, the reactions were

filtered on Celite to remove the catalyst and the solvent was removed by rotary evaporation. Analysis by mass spectrometry showed few if any changes. In the future the reaction will be performed at high temperatures for longer durations.

CHAPTER 6

CONCLUSIONS

Research has been completed on a variety of polycyclic aromatic hydrocarbon (PAH) structures including fullerenes, single walled nanotubes (SWNTs), graphene, acenes, periacenes, 5,6,7-trithiapentacen-13-one (TTPO, **4.13**) and acene derived nanoribbons. A common thread through much of the research has been the formation and use of partially hydrogenated PAH compounds. Thus, polyamine hydrogenations of fullerenes to produce fulleranes, of SWNTs to produced hydrogenated SWNTs (H-SWNTs), and of graphite to produce graphane have all been demonstrated. Moreover, a rational synthesis of fullerenes has been proposed based upon an observed condensation reaction between acenaphthalene and its partially hydrogenated derivative, acenapthene, to produce decacylene in good yield. Acene derived nanoribbons were produced by heating either partially hydrogenated tetracene or pentacene in the solid state.

Another thread that relates much of the work is the use of high temperature reaction conditions (e.g., > 200 °C) to produce thermodynamically favored structures. Thus, a new, robust fullerane, S_6 $C_{60}H_{24}$, has been prepared by heating [60]fullerene in either diethylenetriamine in the presence of catalytic cobalt or in neat triethylenetetramine at 205 or 266 °C, respectively. Likewise, H-SWNTs and graphane have been prepared by heating either SWNTs or graphene in pentaethylenehexamine at 380 °C. Peripentacenequinone (**4.8**) was produced in 80% yield by heating solid state,

partially fused bispentacenequinone (**4.7**) to 380-450 °C. TTPO is produced in good yield by heating pentacene-6,13-diol with elemental sulfur in boiling trichlorobenzene at 214 °C. Finally, acene derived nanoribbons were produced by heating either 5,12-dihydrotetracene or 6,13-dihydropentacene to 360 °C.

For the polyamine hydrogenation of fullerenes, the level of hydrogenation can be made to vary as a function of temperature and choice of catalyst. It was also determined that polyamines bearing a two-carbon spacer between adjacent amino groups are most efficient in promoting hydrogenation. Polyamine hydrogenated H-SWNTs show less bundling behavior as compared to pristine SWNTs due to reduced π - π stacking interactions along the long axes of the tubes. Polyamine hydrogenated graphene or graphane was successfully produced from CVD grown graphene, bulk graphite and highly ordered pyrolitic graphite (HOPG). Scanning electron microscope (SEM), transmission electron microscope (TEM), and scanning tunneling microscope (STM) images of graphene reveal a structure that readily folds upon itself and one that is distorted relative to graphene itself due to the formation of sp^3 hybridized carbon atoms. The synthesis of H-SWNTs and graphane could have important implications in device applications since the hydrogenated structures disperse well in a number of solvents and matrices, and the hydrogen can be removed through thermal annealing to leave pristine SWNTs and graphene, respectively.

The synthesis of several organic semiconductor compounds was completed including the first synthesis of unsubstituted bipentacene, prepared using a novel selenium based deoxygenation reaction. The first synthesis of peripentacenequinone was

also demonstrated. Likewise, TTPO is a new molecule and its synthesis opens the door to a variety of structurally similar structures in which trithia bridges and ketone functions are appended to opposite sides of an acene. TTPO is an extraordinarily robust acene derivative that can be heated to temperatures in excess of 400 °C without decomposition. It shows variable temperature transistor behavior that implies thermistor applications. The columnar stacking of TTPO in its crystalline thin films should promote charge carrier separation and could lead to more efficient devices such as organic photovoltaics.

The synthesis of acene derived nanoribbons and fullerenes from partially hydrogenated PAHs shown great promise for further work. If the nanoribbons can be made to be uniform and soluble, they will have a large number of applications in thin-film organic electronics. Likewise, the rational synthesis of [60]fullerene from a partially hydrogenated PAH is a potentially high yielding, highly selective reaction that could revolutionize the production of fullerenes and endohedral fullerene complexes.

CHAPTER 7

EXPERIMENTAL SECTION

7.1 General Method

NMR Spectra

^{1}H-NMR: Spectra were collected on either a Varian Mercury Plus 400 FT-NMR or a Varian INOVA 500-FT-NMR spectrometer at 399.4491 MHz or 499.7733 MHz, respectively. Data analyses were performed using MestReNova software package, Version 6.0.2-5475.

^{13}C-NMR: Spectra were collected on either a Varian Mercury Plus 400 FT-NMR or a Varian INOVA 500-FT-NMR spectrometer at 100.5169 MHz or 125.6680 MHz, respectively. Data analyses were performed using MestReNova software package, Version 6.0.2-5475.

Mass Spectra

Mass spectrometery was performed using a Shimadzu Group, Kratos Analytical Division, Axima-CFR LDI-TOF laser desorption, time-of-flight mass spectrometer. Data analysis was performed with the Kompact software package, Version 2.3.4.

Raman Spectroscopy

Raman spectra were obtained using a RamanRxn1 Microprobe analyzer (Confocal Raman Microscope, Kaiser Optical Systems)

FT-IR Spectroscopy

IR spectra were obtained using a Thermo-Nicolet 6700 FT-IR spectrometer

Transmission Electron Microscopy

TEM images were recorded using a Zeiss/LEO 922 Omega Transmission Electron Microscope with accelerating voltages of 120 kV and 200 kV

Chromatography

Silica Gel, 230-400 mesh was purchased from Natland International Corporation for use in column chromatography or plug chromatography. Thin layer chromatography plates and preparative chromatography plates were purchased from Analtech, Inc.

7.2 Solvents

All solvents were used as purchased unless otherwise noted in experimental

Acetic Acid was obtained from EMD Chemicals

Acetone was obtained from Pharm-eco Laboratories (Johnson Mathey)

Benzene was obtained from EMD Chemicals

2-Butantol was obtained from EMD Chemicals

Chloroform was obtained from EMD Chemicals

Deuterated NMR solvents were obtained from Cambridge Isotope Company

Dichlormethane was obtained from EMD Chemicals

1,4-Dioxane was obtained from Sigma-Aldrich

N,N'-dimethylformamide was obtained from EMD Chemicals

Ethanol (absolute or denatured) was obtained from Pharm-eco Laboratories (Johnson Mathey)

Hexanes were obtained from EMD Chemicals

Hydrochloric Acid; was obtained from EMD Chemicals

Methanol was obtained from EMD Chemicals

Nitromethane was obtained from Sigma-Aldrich

Tetrahydrofuran was obtained from EMD Chemicals

Toluene was obtained from EMD Chemicals

7.3 Reagents

All reagents were used as purchased unless otherwise noted in experimental

1,4-Anthracenequinone was obtained from an in-house source

1,4-Benzoquinone was obtained from Sigma-Aldrich

Bis(hexamethylene)triamine was obtained from Sigma-Aldrich

Bis(3-aminopropyl)amine was obtained from Sigma-Aldrich

N-Bromosuccinimide was obtained from Sigma-Aldrich

2M n-Butyl Lithium in cyclohexane was obtained from Sigma-Aldrich

t-Butylphenylboronic acid was obtained from TCI America

Decylamine was obtained from Sigma-Aldrich

1,8-Diazabicyclo[5.4.0]undec-7-ene was obtained from TCI America

1,6-Diaminohexane was obtained from Sigma-Aldrich

1,2-Dibromo-4,5-dimethyl-bezene was obtained from an in-house source

Diethylenetriamine was obtained from Sigma-Aldrich

N,N-Diethyldiethylenetriamine was obtained from Sigma-Aldrich

[60]Fullerene was obtained from M.E.R. Corp.

[70]Fullerene was obtained from M.E.R. Corp

Graphite was obtained from Sigma-Aldrich

Highly ordered pyrolytic graphite (HOPG) was obtained from Ted Pella, Inc

Hydriodic acid (55-58%, unstabilized) was obtained from Alfa Aesar

Iodine was obtained from Sigma-Aldrich

Iron(III) tribromide was obtained from Sigma-Aldrich

1-Indaneone was obtained from Sigma-Aldrich

Potassium iodide was obtained from EM Science

Sodium Bisulfite was obtained from EM Science

Morpholine was obtained from Sigma-Aldrich

N-Methyl-2,2'-diaminodiethylamine was obtained from TCI America

N-Methylpiperzine was obtained from Sigma-Aldrich

1,4-Napthalenequinone was obtained from TCI America

Palladium tetrakis(triphenylphosphine) ($Pd(PPh_3)_4$) was obtained from TCI America

Pentaethylenehexamine was obtained from Sigma-Aldrich

Piperdine was obtained from Alfa Aesar

Piperzine was obtained from Sigma-Aldrich

N,N,N',N",N"-Pentamethyldiethylenetriamine was obtained from Sigma-Aldrich

Propylene oxide was obtained from Sigma-Aldrich

Single-Walled Nanotubes (SWNTs) were obtained from Cheap Tubes, Inc.

Sodium bohorhydride was obtained from Sigma-Aldrich

Sodium Carbonate was obtained from EM Science

Sulfur, resublimed was obtained from Sigma-Aldrich

α,α,α′,α′-Tetrabromomorthoxylene was obtained from TCI America

N,N,N',N'-Tetraethyldiethylenetriamine was obtained from Sigma-Aldrich

Tetraethylenepentamine was obtained from Sigma-Aldrich

Tin(II) chloride was obtained from Sigma-Aldrich

Tributyl(2-naphthalenylmethyl) phosphonium bromide was obtained in house

Triethylenetetramine was obtained from Sigma-Aldrich

Reaction Workup

Unless otherwise noted, all solvents were removed by use of the Büchi Rotavapor R-205 rotary evaporator equipped with a Büchi V-500 vacuum pump.

7.4 Synthesis

7.4.1 General Hydrogenation Synthesis:

General procedure for reaction of [60]fullerene, [70]fullerene, SWNTs or graphite with oligo(ethyleneamine) at refluxing temperature: Nanostructured carbon (0.100 g) was added to the oligo(ethyleneamine) (3 mL) and heated to the boiling temperature of the polyamine for 3 days. The hydrogenated nanostructured carbon that was produced was precipitated and washed with methanol or ethanol and concentrated by centrifuge (5000 rpm, 15 min) three times, and then dried under vacuum. Yields averaged 50-70% regardless of amine used. Spectral characterization of the reaction between [60]fullerene and diethylenetriamine is detailed on page S2 of the appendix; spectral characterization of the reaction between [60]fullerene and triethylenetetramine is detailed on page S8 of the appendix; spectral characterization of the reaction between [60]fullerene and tetraethylenepentamine is detailed on pages S10-S13 of the appendix; spectral characterization of the reaction between [60]fullerene and pentaethylenehexamine is detailed on page S15 of the appendix; spectral characterization of the reaction between pentaethylenehexamine and graphite is detailed on pages S45-S50 of the appendix.

General procedure for reaction of [60]fullerene, [70]fullerene, SWNTs or graphite with oligo(ethyleneamine) at refluxing temperature with catalyst: Nanostructured carbon (0.100 g) was added to the oligo(ethyleneamine) (3 mL), catalyst (5 mol %) and

then heated to the boiling point of the polyamine for 3 days. The hydrogenated nanostructured carbon produced was precipitated and washed with methanol or ethanol and concentrated by centrifuge (5000 rpm, 15 min) three times and then dried under vacuum. Yields averaged 50-70% regardless of amine used. Spectral characterization of the reaction between [60]fullerene and diethylenetriamine is detailed on pages S3-S4 of the appendix; spectral characterization of the reaction between [60]fullerene and triethylenetetramine is detailed on page S9 of the appendix; spectral characterization of the reaction between [60]fullerene and tetraethylenepentamine is detailed on page S14 of the appendix; spectral characterization of the reaction between [60]fullerene and pentaethylenehexamine is detailed on pages S16 of the appendix; spectral characterization of the reaction between [70]fullerene and pentaethylenehexamine is detailed on pages S17 of the appendix.

General procedure for reaction of [70]fullerene, SWNTs or graphite with oligo(ethyleneamine) at elevated temperature: Nanostructured carbon (0.100 g) was added to the oligo(ethyleneamine) (1 mL) and sealed in a high pressure vessel consisting of 1 inch male and female Swagelok brand pipe fittings using a vice and wrench. The vessel was then heated to 500 °C for 24 hours. The vessel was then cooled in a large beaker of water and opened carefully in a fume hood. CAUTION: Amine gas is produced in the reaction. If inhaled, it can cause nausea, dizziness, and fainting. The hydrogenated nanostructured carbon that was produced was precipitated and washed with methanol or ethanol and concentrated by centrifuge (5000 rpm, 15 min) three times and

then dried under vacuum. Yields averaged 50% regardless of amine used. Spectral characterization of the reaction between [70]fullerene and pentaethylenehexamine is detailed on page S19 of the appendix; TEM images of H-SWNTs are illustrated on pages S35-S44 of the appendix; TEM images of hydrogenated graphite are illustrated on pages S45-S50 of the appendix; TEM images of hydrogenated HOPG and pentaethylenehexamine are illustrated on pages S51-S56 of the appendix.

General procedure for reaction of [60]fullerene, SWNTs or graphite with oligo(ethyleneamine) at elevated temperature with catalyst: Nanostructured carbon (0.100 g) was added to the oligo(ethyleneamine) (1 mL), catalyst (5 mol %) was added and the mixture was sealed in a high pressure vessel consisting of 1 inch male and female Swagelok brand pipe fittings. The vessel was then heated to 500 °C for 24 hours. The vessel was then cooled in a large beaker of water and opened carefully in a fume hood. CAUTION: Amine gas is produced in the reaction. If inhaled, it can cause nausea, dizziness, and fainting. The hydrogenated nanostructured carbon that was produced was precipitated and washed with methanol or ethanol and concentrated by centrifuge (5000 rpm, 15 min) three times and then dried under vacuum. Yields averaged 50% regardless of amine used. Spectral characterization of the reaction between [60]fullerene and diethylenetriamine is detailed on pages S5-S7 of the appendix; TEM images of the reaction between SWNTs and pentaethylenehexamine are illustrated on pages S35-S44 of the appendix.

7.4.2 General Exfoliation Reaction: Exfoliation of graphite or HOPG with high boiling polyaromatic solvents: Graphite (0.100 g) or 1 HOPG disk was added to a high boiling polyaromatic solvent (2 g) and sealed in a high pressure vessel consisting of 1 inch male and female Swagelok brand pipe fittings. The vessel was then heated to 500 °C for 24 hours. The vessel was then cooled in a large beaker of water and opened carefully in a fume hood. The exfoliated graphite produced was washed with chloroform and concentrated by centrifuge (5000 rpm, 15 min) three times and then dried under vacuum. Characterization was performed using TEM and is detailed on pages S57-S68 of the appendix.

7.4.3 Test reactions of [60]Fullerene with Various Amines:

Reaction of [60]fullerene with bis(3-aminopropyl)amine: [60]Fullerene (0.100 g, 0.138 mmol) was dissolved in 10 mL of bis(3-aminopropyl)amine (81 mmol) and heated to 210 °C in a temperature controlled oil bath and stirred under nitrogen for 24 hours. The crude product was then precipitated from solution with water, filtered through a Büchner funnel, and washed with water to produce a yellow solid, amount and yield not obtained. Spectra characterizations are detailed on pages S26-S27 of the appendix.

Reaction of [60]fullerene with bis(hexamethylene)triamine: [60]Fullerene (0.100 g, 0.138 mmol) was mixed with bis(hexamethylene)triamine (9.750 g, 45.269 mmol), heated to 210 °C in a temperature controlled oil bath with stirring under nitrogen for 24

hours. The crude product was then precipitated from solution with water, filtered through a Büchner funnel, and washed with water to produce a yellow solid, amount and yield not obtained. Spectra characterizations are detailed on page S28 of the appendix.

Reaction of [60]fullerene with hexylenediamine: [60]Fullerene (0.250 g, 0.347 mmol) was mixed with 1,6-diaminohexane (10 g, 86 mmol) and heated to 210 °C in a temperature controlled oil bath with stirring under nitrogen for 24 hours. The crude product was then precipitated from solution with water, filtered through a Büchner funnel, and washed with water to produce a insoluble brown solid, amount and yield not obtained. Spectra characterizations are detailed on page S29 of the appendix.

Reaction of [60]fullerene with decylamine: [60]Fullerene (0.100 g, 0.138 mmol) was dissolved in 5 mL of decylamine (40 mmol) and heated to 210 °C in a temperature controlled oil bath with stirring under nitrogen for 24 hours. The crude product was then precipitated from solution with water, filtered through a Büchner funnel, and washed with water to produce a red/brown solid, amount and yield not obtained. Spectra characterizations are detailed on page S30 of the appendix.

Reaction of [60]fullerene with piperidine: [60]Fullerene (0.100 g, 0.138 mmol) was dissolved in 5 mL of piperidine (68 mmol) and heated to reflux (106 °C) with stirring under nitrogen for 24 hours. The crude product was then precipitated from solution with water, filtered through a Büchner funnel, and washed with water to produce a brown

solid, amount and yield not obtained. Spectra characterizations are detailed on pages S31-S32 of the appendix.

Reaction of [60]fullerene with piperazine at reflux: [60]Fullerene (0.100 g, 0.138 mmol) was mixed with piperazine (5 g, 58 mmol) and heated to 156 °C for 24 hours with stirring in a sealed high pressure vessel after purging with nitrogen. The crude product was then precipitated from solution with water, filtered through a Büchner funnel, and washed with water to produce a solid, amount and yield not obtained. Spectra characterizations are detailed on page S33 of the appendix.

Reaction of [60]fullerene with piperazine in microwave: [60]Fullerene (0.100 g, 0.138 mmol) was mixed with piperazine (3.000g, 34.827 mmol) and heated to 225 °C in a sealed high pressure vessel in a microwave reactor (CEM Corp, Discovery model) after purging with nitrogen for 30 minutes. The crude product was then precipitated from solution with water, filtered through a Büchner funnel, and washed with water to produce an orange/yellow solid, amount and yield not obtained. Spectra characterizations are detailed on page S34 of the appendix.

Reaction of [60]fullerene with N,N,N',N'',N''-pentamethyldiethylenetriamine: [60]Fullerene (0.200 g, 0.278 mol) was dissolved in N,N,N',N'',N''-pentamethyldiethylenetriamine (5 mL, 35 mmol) and heated to reflux (208 °C) for 24 hours. The crude product was then precipitated from solution with methanol, filtered

through a Büchner funnel and washed with methanol to produce a black solid which was identified as unreacted [60]fullerene, amount and yield not obtained.

Reaction of [60]fullerene with N,N-diethyldiethylenetriamine: [60]Fullerene (0.106 g, 0.148 mmol) was dissolved in N,N-diethyldiethylenetriamine (2.5 mL, 18.1 mmol) and heated to reflux (223 °C) for 24 hours. The crude product was then precipitated from solution with methanol, filtered through a Büchner funnel and washed with methanol to produce a yellow/orange solid, amount and yield not obtained. Spectra characterizations are detailed on pages S20-S21 of the appendix.

Reaction of [60]fullerene with N-methyldiethylenetriamine: [60]Fullerene (0.102 g, 0.142 mol) was dissolved in N-methyldiethylenetriamine (7.5 mL, 72.3 mmol) and heated to reflux (217 °C) for 24 hours. The crude product was then precipitated from solution with methanol, filtered through a Büchner funnel and washed with methanol to produce a yellow/orange solid, amount and yield not obtained. Spectra characterizations are detailed on pages S22-S23 of the appendix.

Reaction of [60]fullerene with N,N,N',N'-tetraethyldiethylenetriamine: [60]Fullerene (0.120 g, 0.167 mol) was dissolved in N,N,N',N'-tetraethyldiethylenetriamine (4 mL, 22 mmol) and heated to reflux (198 °C) for 24 hours. The crude product was then precipitated from solution with methanol, filtered through a Büchner funnel and washed

with methanol to produce a yellow/orange solid, amount and yield not obtained. Spectra characterizations are detailed on pages S24-S25 of the appendix.

7.4.4 Small Molecule Organic Synthesis

6,13-Pentacenequinone (4.1): α,α,α′,α′-Tetrabromomorthoxylene (6.748 g, 16.085 mmol) and 1,4-benzoquinone (0.865 g, 7.993 mmol) were combined with potassium iodide (11.032 g, 0.066 mol) in dimethylforamide and heated to 153 °C under nitrogen gas for 18 hours. After cooling, the product was precipitated from solution with water, filtered through a Büchner funnel and washed with 2-butanol. After drying, the product produced was a bright yellow powder (0.650 g, 26% yield). ^{1}H-NMR (400 MHz, $CDCl_3$) δ (ppm): 7.72 (m, 4H), 8.14 (m, 4H), 8.96 (s, 4H) ^{13}C-NMR (100 MHz, $CDCl_3$) δ (ppm): 129.5, 129.8, 130.1, 130.6, 135.3, 183.0.[145]

6(13H)-Pentacenone (4.2): Compound **4.1** (0.500 g, 1.621 mmol) was dissolved in 50 mL of hydriodic acid (55-58 %, unstabilized) and 50 mL of glacial acetic acid and then heated to reflux under nitrogen for precisely 5 hours. The reaction was cooled and the crude product was precipitated from solution using copious amounts of water, and then washed with 10 mL of saturated $NaHSO_4$ to quench any remaining hydriodic acid. The material was then filtered through a Büchner funnel, water washed and dried resulting in a brown/yellow powder (0.360 g, 75% yield, 90-95% pure). ^{1}H NMR (500 MHz, $CDCl_3$) δ (ppm): 9.00 (s, 1H), 8.11 (d, J = 8.2 Hz, 1H), 7.99 (s, 1H), 7.93 (d, J = 8.3 Hz, 1H),

7.65 (m, 1H), 7.61 – 7.54 (m, 1H), 4.74 (s, 1H). ^{13}C NMR (126 MHz, $CDCl_3$) δ (ppm): 185.41, 135.62, 135.60, 131.94, 130.38, 129.94, 129.40, 128.65, 127.13, 126.76, 126.15, 32.58. Spectra are detailed on pages S69-S70 of the appendix.

13-(13-oxo-6(13H)-pentacenylidene)-6(13H)-Pentacenone (4.3): Compound **4.2** (0.200 g, 0.684 mmol) was dissolved in 5 mL dichloromethane after purging with nitrogen for 20 minutes followed by the addition of 1,8-Diazabicyclo[5.4.0]undec-7-ene (DBU: 0.60 mL, 3.87 mmol) and stirred for 5 minutes. Molecular iodine was added (0.355g, 1.399 mmol) and the solution stirred for 24 hours under nitrogen. The solvent was removed by rotary evaporation and the product precipitated with acetone and filtered through a Büchner funnel. The resulting material was then washed with acetone to produce a bright yellow powder (0.120g, 60% yield, 80% pure). ^{1}H NMR (400 MHz, $CDCl_3$) δ (ppm): 8.76 (s, 1H), 7.99 (d, J = 8.2 Hz, 1H), 7.56 (s, 1H), 7.46 (ddd, J = 8.1, 6.8, 1.1 Hz, 1H), 7.30 (ddd, J = 8.1, 6.8, 1.1 Hz, 1H), 7.11 (d, J = 8.2 Hz, 1H). ^{13}C NMR (101 MHz, $CDCl_3$) δ (ppm): 187.84, 133.94, 133.66, 133.01, 132.45, 132.04, 129.37, 128.53, 128.34, 127.91, 127.16. MS (LDI) calcd. m/z = 584.1, found m/z= 584.2 Spectra are detailed on pages S71-S77 of the appendix.

6,13-dihydro-13-(13-hydroxy-6(13H)-pentacenylidene)-6-Pentacenol (4.4): Unpurified Compound **4.3** (0.100g, 0.171 mmol) was dissolved in anhydrous tetrahydrofuran and sodium borohydride (0.100 g, 2.643 mmol) was added and stirred for 24 hours under nitrogen. The solvent was removed with rotary evaporation. The crude product was precipitated with water and filtered through a Büchner funnel, suspended in

5 mL 10% aqueous HCl solution with tin(II) chloride (0.200 g, 1.054 mmol), and stirred for 10 minutes to convert trace 6,13-pentacenediol to pentacene. The sample was then washed with water and filtered through a Büchner funnel, followed by extraction with chloroform to produce a white/yellow solid (0.025 g, 25% yield). ^{1}H NMR (500 MHz, $CDCl_3$)) δ (ppm): 8.27 (s, 2H), 7.81 (d, J = 12.5 Hz, 2H), 7.58 (s, 2H), 7.32 (m, 2H), 7.23 (d, J = 8.1 Hz, 2H), 7.19 – 7.13 (m, 2H), 6.50 (d, J = 7.8 Hz, 1H), 4.34 (d, J = 7.7 Hz, 1H). Spectra are detailed on pages S78-S79 of the appendix.

6,6'-Bipentacene (4.5): Compound **4.4** (0.025g, 0.042 mmol) was added to a solution of 2 mL of 1,2,4-tricholorobenzene and selenium metal (0.300 g, 3.799 mmol) that had been heated to a boil and stirred in the dark for 1 hour to produce a dark blue/purple solution. A small sample was then extracted, diluted with chloroform and analyzed by UV/Vis spectroscopy and mass spectrometry. A yield could not be obtained due to the instability of **4.5**. MS (LDI) calcd. m/z = 554.2, found m/z= 554.5. Spectrum is illustrated on page S80 of the appendix.

Dinaphtho[1,2,3-gh:1',2',3'-tu]pyranthrene-10,21-dione (4.7): Compound **4.4** (0.120 g, 0.020 mmol) was dissolved in 60 mL dry benzene with 5 mL of propylene oxide and resublimed iodine (0.196 g, 0.772 mmol). The vessel was then exposed to a 500W lamp and stirred for 24 hours. The material was then filtered through a Büchner funnel and washed with acetone and benzene to produce a bright yellow solid that was fluorescent bright green under UV irradiation (0.109 g, 90% yield). ^{1}H NMR (400 MHz, $CDCl_3$) δ 9.41 (s, 1H), 8.34 (dd, J = 11.4, 8.6 Hz, 2H), 7.68 (t, J = 7.0 Hz, 1H), 7.48 (t, J = 7.0 Hz,

1H). MS (LDI) calcd. *m/z* = 580.2, found *m/z*= 580.1 Spectra are detailed on pages S81-S83 of the appendix.

Peripentacenequinone (4.8): Compound **4.7** (0.100 g, 0.172 mmol) was placed in a 50 mL thick walled vessel and heated to approximately 400 °C in the presence of ambient air for 2 hours. The material was then washed with chloroform to produce a dark red/black material (0.080 g, 80% yield) UV/Vis analysis was performed with 1,2,4-trichlorobenzen at 200°C. MS (LDI) *m/z* = 576.2, found *m/z*= 576.11. Spectra are detailed on pages S84-S85 of the appendix.

10,21-Dihydro-dinaphtho[1,2,3-gh:1',2',3'-tu]pyranthrene-10,21-diol (4.10): Compound **4.7** (0.010 g, 0.017 mmol) was dissolved in anhydrous tetrahydrofurnan and sodium borohydride (0.200 g, 5.287 mmol) was added and stirred for 24 hours under nitrogen. The solvent was removed with rotary evaporation and the product was precipitated with water and filtered through a Büchner funnel to produce a white/yellow solid. The material was a mixture of isomers that was not separated. The material was fluorescent bright blue/white under UV irradiation (0.034g, 57% yield). MS (LDI) calcd. *m/z* = 584.1, found *m/z*= 584.9. Spectrum is illustrated on page S86 of the appendix.

Naphtho[2,1,8,7-fghi:3,4,5,6-f'g'h'i']dipentacene (7CI,8CI,9CI) (4.11): Compound **4.10** (0.005 g, 8.560×10^{-6} mol) was mixed with 5 mL of 10% aqueous HCl solution and tin(II) chloride (0.100 g, 0.527 mmol) and stirred in the dark for 10 minutes to produce a dark brown material which was filtered through a Büchner funnel and dried in the dark

(0.002 g, 40% yield). MS (LDI) calcd. *m/z* = 850.1, found *m/z*= 849.9. Spectrum is illustrated on page S87 of the appendix.

6,13-Dihydro-13-(6-decathio-13(6H)-pentacenylidene)-6-pentacenedecathiol (4.12): Compound **4.4** (0.024 g, 0.043 mmol) was dissolved in 20 mL of dichloromethane to which decanethiol (0.150 g, 0.860 mmol) was added followed by zinc(II) iodide (0.195 g, 0.611 mmol) with stirring under nitrogen at room temperature for 24 hours. The solvent was removed by rotary evaporation and purified using silica column chromatography with 1:1 hexanes/dichloromethane as eluant to produce a yellow oil (0.012 g, 33% yield). ^{1}H NMR (400 MHz, $CDCl_3$) δ (ppm): δ 7.90 (s, 2H), 7.79 (d, *J* = 8.2 Hz, 2H), 7.67 (s, 2H), 7.36 (t, *J* = 7.4 Hz, 2H) 7.23 (d, *J* = 7.6 Hz, 2H), 7.18 (t, *J* = 7.6 Hz 2H), 5.51 (s, 1H), 2.89 (t, *J* = 7.4 Hz, 2H), 1.85 (quin, *J*=4.7 Hz, 2H), 1.57 (s, 2H), 1.52 (quin, *J*=4.7 Hz, 2H), 1.34-1.22 (m, 6H), 0.88-0.83 (m, 7H). ^{13}C NMR (101 MHz, $CDCl_3$) δ (ppm): 137.33, 135.92, 132.19, 132.12, 131.65, 128.82, 128.35, 127.39, 126.25, 125.83, 125.74, 77.56, 77.24, 76.92, 51.02, 33.53, 32.11, 29.99, 29.94, 29.82, 29.80, 29.63, 29.54, 22.89, 14.34. Spectra are detailed on pages S88-S89 of the appendix.

Trithiapentacenone (4.13): 6,13-pentacenediol (0.100 g, 0.342 mmol) and elemental sulfur (0.020g, 0.554 mmol) were dissolved in 5 mL of N,N-dimethylformamide and heated to 153 °C under nitrogen gas for 24 hours. The reaction was then cooled to room temperature and the crude product precipitated from solution with water and filtered through a Büchner funnel. Following washing with copious amount of acetone and chloroform to remove any unreacted 6,13-pentacenediol, a deep blue solid or a purple

crystalline material with a metallic luster was produced (0.070 g, 57% yield). ^{1}H NMR (500 MHz, $CDCl_3$) δ (ppm): 8.95 (s, 1H), 8.79 – 8.73 (m, 1H), 8.26 – 8.20 (m, 1H), 7.91 – 7.83 (m, 2H). MS (LDI) calcd. *m/z* = 386.0, found *m/z*= 385.3. Spectra are detailed on pages S90-S95 of the appendix.

2-(2,3-dihydro-1H-inden-1-ylidenemethyl)naphthalene (5.1): Tributyl(2-naphthalenylmethyl) phosphonium bromide (1.350 g, 3.188 mmol) was added to a 2-neck flask and stirred with 40 mL of still dried THF on molecular sieves. The solution was cooled to -78 °C and flushed with nitrogen. A volume of 3.50 mL of 2M *n*-BuLi in cyclohexane was added and stirred for 5 minutes. Next, 1-indanone (0.422 g, 3.193 mmol) was added and stirred for 5 minutes. The reaction was then heated to 66 °C and refluxed for 18 hours. The reaction was then quenched with 10% HCl and extracted with chloroform. The solution was passed through a plug of silica using 3:1 hexanes:chloroform as eluant to produce a colorless solution which became a white solid upon evaporation of solvents (0.233 g, 28% yield). ^{1}H NMR (400 MHz, $CDCl_3$) δ (ppm) 7.91 (s, 1H), 7.87 – 7.79 (m, 2H), 7.65 m, 2H), 7.50 – 7.39 (m, 2H), 7.34 – 7.28 (m, 1H), 7.28 – 7.22 (m, 2H), 7.11 (t, *J* = 2.5 Hz, 1H), 3.23 (m, 1H), 3.14 (m, 1H). ^{13}C NMR (101 MHz, $CDCl_3$) δ (ppm): 146.12, 144.89, 142.84, 136.06, 133.84, 132.24, 128.47, 128.19, 128.04, 127.79, 127.26, 126.89, 126.36, 125.85, 125.54, 120.47, 119.31, 31.13, 31.07. Spectra are detailed on pages S99-S100 of the appendix.

8,9-Dihydro-benz[l]acephenanthrylene (5.2): Compound **5.1** (0.145 g, 0.566 mmol) was dissolved in 10 mL benzene and added to 400 mL of hexanes in a quartz round bottom flask. Then 10 mL of propylene oxide and iodine (0.210 g, 0.827 mmol) was added and the system was purged with nitrogen for 15 minutes. The vessel was then placed in a 3 kW Rayonet UV-reactor and irradiated with 254 nm light for 3 hours. The solution was then quenched with saturated $NaHSO_4$ solution and the organic solvent was extracted and reduced to a brown oil. The oil was passed through a plug of silica using hexanes as eluant to produce a colorless solution which became a white solid upon evaporation of solvents (0.085 g, 60% yield). ^{1}H NMR (400 MHz, $CDCl_3$) δ (ppm): 9.28 (d, J = 8.6 Hz, 1H), 8.92 (d, J = 8.5 Hz, 1H), 8.01 (d, J = 8.1, 1H), 7.86 (m, 2H), 7.77 – 7.56 (m, 4H), 7.49 (d, J = 6.9 Hz, 1H), 3.60 – 3.45 (m, 4H). ^{13}C NMR (126 MHz, $CDCl_3$) δ (ppm): 145.90, 144.67, 142.64, 135.86, 133.65, 132.05, 128.62, 128.26, 127.98, 127.84, 127.58, 127.05, 126.68, 126.15, 125.64, 125.32, 123.50, 120.26, 119.12, 30.93, 30.87. Spectra are detailed on pages S101-S102 of the appendix.

5,12-Tetracenequinone (5.5): α,α,α′,α′-Tetrabromomorthoxylene (3.378 g, 8.009 mmol) was added to a mixture of 1,4-napthalenequinone (1.273 g, 8.049 mmol) and potassium iodide (5.516 g, 33.229 mmol) in 50 mL of dimethylformamide and heated to 153 °C for 24 hours under a nitrogen atmosphere. Crude product was precipitated from solution with deionized water and filtered through a Büchner funnel and washed with 2-butanone to produce a yellow powder (1.261 g, 65%). ^{1}H NMR (400 MHz, $CDCl_3$) δ (ppm): 8.87 (s, 1H), 8.45 – 8.37 (m, 1H), 8.18 – 8.07 (m, 1H), 7.88 – 7.80 (m, 1H), 7.74 – 7.67 (m,

1H). ^{13}C NMR (126 MHz, $CDCl_3$) δ (ppm): 183.02, 135.22, 134.54, 134.18, 130.16, 129.82, 129.60, 129.50, 127.53. Spectra are detailed on pages S103-S106 of the appendix.[146]

5,12-Dihydrotetrtacene (5.6): Compound **5.5** (2.249 g, 8.708 mmol) was added to 100 mL of glacial acetic acid and 50 mL of hydriodic acid (55-58%, unstabilized) and refluxed for 5 days. Crude product was precipitated from solution with saturated $NaHSO_4$ solution and filtered through a Büchner funnel to give a dark brown solid. The solid was extracted with diethyl ether and isolated as an orange crystalline solid after evaporation of solvent (1.548 g, 77% yield). ^1H NMR (500 MHz, $CDCl_3$) δ (ppm): 7.81 – 7.76 (m, 1H), 7.75 (s, 1H), 7.43 – 7.38 (m, 1H), 7.36 – 7.31 (m, 1H), 7.23 – 7.19 (m, 1H), 4.09 (s, 2H). ^{13}C NMR (126 MHz, $CDCl_3$) δ (ppm): 137.10, 135.73, 132.44, 127.24, 126.27, 125.29, 125.19, 36.83.[171] Spectra are detailed on pages S107-S109 of the appendix.

6,13-Dihydropentacene (5.7): Compound **4.1** (0.550 g, 1.783 mmol) was added to 50 mL of glacial acetic acid and 50 mL of hydriodic acid (55-58%, unstabilized) and then heated to reflux for 5 days. Crude product was precipitated from solution using saturated $NaHSO_4$ and filtered through a Büchner funnel to give a brown/yellow solid. The solid was extracted with chloroform and isolated as a yellow solid after evaporation of solvent (0.375 g, 75% yield). ^1H NMR (400 MHz, $CDCl_3$) δ (ppm): 7.80 (m, 1H), 7.42 (m, 1H),

4.25 (s, 1H). ^{13}C NMR (126 MHz, $CDCl_3$) δ (ppm): 135.88, 132.48, 127.24, 125.36, 125.13, 37.38.[171] Spectra are illustrated on pages S110-S111 of the appendix.

6,13-Pentacenediol (5.8): Compound **4.1** (0.100 g, 0.324 mmol) was added to 5 mL of dry tetrahydrofuran to which sodium borohydride (0.100 g, 2.643 mmol) was added and stirred at room temperature for 18 hours under nitrogen. The solvent was removed by rotary evaporation and the product was precipitated from solution using water and then filtered through a Büchner funnel and dried to produce a white powder (0.095 g, 95% yield) as a mix of *cis* and *trans* isomers. ^1H NMR (300 MHz, $CDCl_3$): δ (ppm): 8.1 (s, 1H), 7.9 (m , 1H) , 7.5 (m 1H), 6.6 (d, J = 6.2Hz, 1H), 6.1 (d, J = 6.2Hz, 1H) 6.0 (d, J = 6.2Hz, 1H), 5.8(d, J = 6.2Hz, 1H); ^{13}C NMR (75 MHz, $CDCl_3$) δ (ppm): 136.9, 133.0, 127.9, 126.4, 125.0, 60.4. [108]

Pentacene (5.9): Compound **5.8** (0.100, 0.320 mmol) was mixed in 5 mL of 10% aqueous HCl solution and tin(II) chloride (0.300 g, 1.582 mmol) and stirred in the dark for 10 minutes to produce a dark purple solid which was filtered through a Büchner funnel, washed with water, and then dried in the dark (0.080 g, 90% yield). MS (LDI) calcd. m/z = 278.4, found m/z= 278.8.[147]

1,2-di-*tert*-butylphenyl-4,5-dimethylbenzene (5.10): 1,2-Dibromo-4,5-dimethylbezene (2.160 g, 8.183 mmol) was added to *t*-butylphenylboronic acid (4.320 g, 24.642 mmol) in a solution of 50 mL toluene and 50 mL 1 M Na_2CO_3. To the solution was added

$Pd(PPh_3)_4$ (0.090 g, 0.077 mmol) and the reaction was heated to reflux for 3 days. The mixture was then extracted with ethyl acetate and the solvent was removed to produce a yellow oil which was passed through a silica plug column using hexanes as eluent. Following evaporation of solvent, a yellow oil was obtained which was allowed to sit for several days to produce colorless crystals (1.510 g, 50% yield). ^{1}H NMR (500 MHz, $CDCl_3$) δ (ppm): 7.20 (m, 3H), 7.08 – 7.01 (m, 2H), 2.33 (s, 3H), 1.30 (s, 9H). ^{13}C NMR (126 MHz, $CDCl_3$) δ (ppm): 148.94, 138.57, 137.99, 135.47, 131.94, 129.45, 124.57, 34.39, 31.37, 19.38. Spectra are detailed on pages S112-S113 of the appendix.

1,2-di-*t*-butylphenyl-α,α,α′,α′-tetrabromo-4,5-dimethlybenzene (5.11): Compound **5.10** (2.170 g, 5.855 mmol) was added to N-bromosuccinimide (14.174 g, 79.678 mmol) and AIBN (0.210 g, 1.279 mmol) in 100 mL of dry chloroform and irradiated with a 500 W lamp for 8 hours under nitrogen. As the reaction cooled, succinimide precipitated from solution and was filtered using a Büchner funnel. The solvent was removed using rotary evaporation. The product was precipitated from solution using methanol and filtered to produce a white/orange solid (2.755 g, 69% yield). ^{1}H NMR (400 MHz, $CDCl_3$) δ (ppm): 7.69 (s, 1H), 7.29 – 7.23 (m, 2H), 7.18 (s, 1H), 7.10 – 7.04 (m, 2H), 1.30 (m, 9H). ^{13}C NMR (101 MHz, $CDCl_3$) δ (ppm): 150.64, 136.67, 129.47, 125.21, 36.59, 34.74, 31.51. Spectra are detailed on pages S114-S115 of the appendix.

2,3-di-*t*-butylphenyl-5,12-tetracenequinone (5.12): Compound **5.11** (1.372 g, 1.998 mmol) was added to a mixture of 1,4-napthalenequinone (0.476 g, 2.972 mmol) and

potassium iodide (1.680 g, 10.120 mmol) in 50 mL of N,N-dimethylformamide and heated to 153 °C for 24 hours under a nitrogen atmosphere. Crude product was precipitated from solution using deionized water, filtered through a Büchner funnel, and washed with acetone to produce a yellow solid (0.570 g, 51% yield). ^{1}H NMR (500 MHz, $CDCl_3$) δ (ppm): 8.92 (s, 1H), 8.48 – 8.44 (m, 2H), 8.17 (s, 2H), 7.90 – 7.85 (m, 2H), 7.36 – 7.32 (m, 2H), 7.23 – 7.18 (m, 2H), 1.37 (s, 9H). ^{13}C NMR (126 MHz, $CDCl_3$) δ (ppm): 183.04, 150.33, 143.15, 137.39, 134.62, 134.40, 134.14, 131.31, 129.94, 129.48, 129.39, 127.52, 124.94, 34.54, 31.33. Spectra are detailed on pages S116-S117 of the appendix.

2,3-di-*t*-butylphenyl-6,13-pentacenequinone (5.13): Compound **5.11** (1.372 g, 1.998 mmol) was added to a mixture of 1,4-anthracenequinone (0.632 g, 3.036 mmol) and potassium iodide (1.680 g, 10.120 mmol) in 50 mL of N,N-dimethylformamide and heated to 153 °C for 24 hours under a nitrogen atmosphere. Crude product was precipitated from solution using deionized water, filtered through a Büchner funnel, and washed with acetone to produce a yellow solid (0.810 g, 70% yield). ^{1}H NMR (500 MHz, $CDCl_3$) δ (ppm): 9.00 (s, 1H), 8.18 (m, 2H), 7.75 (m, 1H), 7.34 (m, 2H), 7.21 (m, 2H), 1.37 (s, 9H). ^{13}C NMR (126 MHz, $CDCl_3$) δ (ppm): 183.02, 150.32, 143.15, 137.42, 135.31, 134.50, 131.27, 130.74, 130.15, 129.78, 129.59, 129.50, 124.93, 34.55, 31.34. Spectra are detailed on pages S118-S119 of the appendix.

2,3-di-*t*-butylphenyl-5,12-dihydro-5,12-tetracenediol (5.14): Compound **5.12** (0.270 g, 0.516 mmol) was added to 5 mL of dry tetrahydrofuran to which sodium borohydride (0.400 g, 10.573 mmol) was added and stirred at room temperature for 24 hours under nitrogen. The solvent was removed by rotary evaporation. The product was precipitated with water, filtered through a Büchner funnel, and dried to produce a yellow/orange solid (0.180 g, 67% yield) as a mix of *cis* and *trans* isomers. ^{1}H NMR (400 MHz, $CDCl_3$) δ (ppm): 8.11 (s, 1H), 8.02 (s, 1H), 7.89 (s, 1H), 7.80 (s, 1H), 7.71 (m, 1H), 7.63 (1, 1H), 7.45 – 7.36 (m, 2H), 7.28 – 7.22 (m, 7H), 7.17 – 7.11 (m, 4H), 6.02 (d, J = 6.0 Hz, 1H), 5.70 (d, J = 6.4 Hz, 1H), 1.31 (s, 9H). ^{13}C NMR δ (ppm): (126 MHz, $CDCl_3$) δ 149.54, 139.91, 139.51, 139.03, 138.38, 138.31, 137.24, 137.08, 132.23, 132.13, 129.60, 129.25, 128.51, 128.20, 127.22, 126.18, 126.05, 124.99, 124.69, 71.67, 70.40, 34.46, 31.37. Spectra are detailed on pages S120-S121 of the appendix.

2,3-di-*t*-butylphenyl-6,13-dihydro-6,13-pentacenediol (5.15): Compound **5.13** (0.205 g, 0.358 mmol) was added to 10 mL of dry tetrahydrofuran to which sodium borohydride (0.400 g, 10.573 mmol) was added and stirred at room temperature for 24 hours under nitrogen. The solvent was removed by rotary evaporation. The product was precipitated from solution using water, filtered through a Büchner funnel, and dried to produce a yellow/orange solid (0.160 g, 78% yield) as a mix of *cis* and *trans* isomers. ^{1}H NMR (400 MHz, $CDCl_3$) δ (ppm): 8.13 (s, 1H), 8.12 (s, 1H), 8.07 (s, 1H), 8.06 (s, 1H), 7.90 (m, 4H), 7.52 (s, 3H), 7.25 (m, 4H), 7.13 (m, 4H), 6.22 ((d, J = 6.1 Hz, 1H), 5.89 (d, J = 6.1 Hz, 2H), 1.31 (s, 9H). ^{13}C NMR (126 MHz, $CDCl_3$) δ (ppm): 149.75, 140.18, 139.97,

138.72, 138.58, 138.50, 137.23, 137.14, 133.36, 133.19, 132.55, 132.39, 129.80, 129.47, 129.43, 128.17, 128.11, 127.46, 126.83, 126.60, 126.35, 125.21, 124.89, 124.84, 124.79, 72.50, 71.20, 34.66, 31.57. Spectra are detailed on pages S122-S123 of the appendix.

2,3-di-*t*-butylphenyltetracene (5.16): Compound **5.14** (0.180 g, 0.342 mmol) was mixed in 2 mL of 10% aqueous HCl and the resulting solution was added to 25 mL of 1,4-dioxane and tin(II) chloride (0.300 g, 1.582 mmol). The mixture was stirred in the dark for 30 minutes under nitrogen to produce a bright orange solid that was filtered through a Büchner funnel and dried in the dark (0.085 g, 50% yield). ^{1}H NMR (400 MHz, $CDCl_3$) δ (ppm): 8.67 (s, 1H), 8.65 (s, 1H), 8.04 (s, 1H), 8.00 (m, 1H), 7.39 (m, 1H), 7.31 – 7.26 (m, 2H), 7.22 – 7.16 (m, 2H). 1.37 (s, 9H). ^{13}C NMR (126 MHz, $CDCl_3$) δ (ppm): 149.54, 139.06, 138.46, 131.56, 130.99, 130.59, 129.47, 129.23, 128.33, 126.34, 126.05, 125.15, 124.65, 77.28, 77.02, 76.77, 34.49, 31.39. Spectra are detailed on pages S124-S125 of the appendix.

2,3-di-*t*-butylphenylpentacene (5.17): Compound **5.15** (0.160 g, 0.277 mmol) was mixed in 2 mL of 10% aqueous HCl and the resulting solution was added to 25 mL of 1,4-dioxane and tin(II) chloride (0.400 g, 2.110 mmol). The mixture was stirred in the dark for 30 minutes under nitrogen to produce a purple solid which rapidly photooxidized to a brown solid that was filtered through a Büchner funnel and dried in the dark (0.125 g, 83% yield, photooxidation product). MS (LDI) calcd. m/z = 542.3, found m/z= 541.1. Spectrum is detailed on page S126 of the appendix.

2,3-di-*t*-butylphenyl-5,12-dihydrotetracene (5.18): Compound **5.14** (0.225 g, 0.430 mmol) was added to 50 mL of glacial acetic acid and 225 mL of hydriodic acid (55-58%, unstabilized) and then heated to reflux for 21 days under nitrogen. The material was precipitated from solution using saturated $NaHSO_4$ and filtered through a Büchner funnel to give a black/brown solid as a mixture of isomers (0.183 g, 92% yield). ^1H NMR (400 MHz, $CDCl_3$) δ 7.80 (m, 1H), 7.40 (m, 1H), 7.28 – 7.04 (m, 5H), 4.17 (s, 1H), 4.12 (s, 1H), 1.33 (s, 1H), 1.31 (s, 2H), 1.30 (s, 2H). Spectrum is illustrated on page S127 of the appendix.

2,3-di-*t*-butylphenyl-6,13-dihydropentacene (5.19): Compound **5.14** (0.360 g, 0.628 mmol) was added to 50 mL of glacial acetic acid and 100 mL of hydriodic acid (55-58%, unstabilized) and then heated to reflux for 21 days under nitrogen. The material was precipitated from solution using saturated $NaHSO_4$ and filtered through a Büchner funnel to give a black/brown solid as a mixture of starting material, product isomers and over-reduced species (0.085 g, 16% yield). ^1H NMR (400 MHz, $CDCl_3$) δ 8.15 – 7.75 (m, 1H), 7.36 – 6.97 (m, 4H), 4.26 (s, 1H), 4.00 – 3.86 (m, 1H), 2.31 (s, 9H), 2.27 (s, 6H), 2.25 (m, Hz, 1H). Spectrum is illustrated on page S128 of the appendix.

REFERENCES

(1) Rohlfing, E. A.; Cox, D. M.; Kaldor, A. *J. Chem. Phys.* **1984**, *81*, 3322.

(2) Kroto, H. W.; Heath, J. R.; O'Brien, S. C.; Curl, R. F.; Smalley, R. E. *Nature* **1985**, *318*, 162.

(3) Taylor, R.; Hare, J. P.; Abdul-Sada, A. A. K.; Kroto, H. W. *J. Chem. Soc., Chem. Commun.* **1990**, 1423.

(4) Kratschmer, W.; Lamb, L. D.; Fostiropoulos, K.; Huffman, D. R. *Nature* **1990**, *347*, 354.

(5) Parthasarathy, G.; Srinivasan, R.; Vairamani, M.; Ravikumar, K.; Kunwar, A. C. *Geochim. Cosmochim. Acta* **1998**, *62*, 3541.

(6) Mossman, D.; Eigendorf, G.; Tokaryk, D.; Gauthier-Lafaye, F.; Guckert, K. D.; Melezhik, V.; Farrow, C. E. G. *Geology* **2003**, *31*, 255.

(7) Buseck, P. R. *Earth Planet. Sci. Lett.* **2002**, *203*, 781.

(8) Cami, J.; Bernard-Salas, J.; Peeters, E.; Malek, S. E. *Science* **2010**, *329*, 1180.

(9) Scott, L. T.; Boorum, M. M.; McMahon, B. J.; Hagen, S.; Mack, J.; Blank, J.; Wegner, H.; de Meijere, A. *Science* **2002**, *295*, 1500.

(10) Haufler, R. E.; Conceicao, J.; Chibante, L. P. F.; Chai, Y.; Byrne, N. E.; Flanagan, S.; Haley, M. M.; O'Brien, S. C.; Pan, C.; et al. *J. Phys. Chem.* **1990**, *94*, 8634.

(11) Hall, L. E.; McKenzie, D. R.; Attalla, M. I.; Vassallo, A. M.; Davis, R. L.; Dunlop, J. B.; Cockayne, D. J. H. *J. Phys. Chem.* **1993**, *97*, 5741.

(12) Attalla, M. I.; Vassallo, A. M.; Tattam, B. N.; Hanna, J. V. *J. Phys. Chem.* **1993**, *97*, 6329.

(13) Dunlap, B. I.; Brenner, D. W.; Mintmire, J. W.; Mowrey, R. C.; White, C. T. *J. Phys. Chem.* **1991**, *95*, 5763.

(14) Gakh, A. A.; Romanovich, A. Y.; Bax, A. *J. Am. Chem. Soc.* **2003**, *125*, 7902.

(15) Bergosh, R. G.; Meier, M. S.; Spielmann, H. P.; Wang, G.-W.; Weedon, B. R. *Proc. - Electrochem. Soc.* **1997**, *97-14*, 240.

(16) Billups, W. E.; Luo, W.; Gonzalez, A.; Arguello, D.; Alemany, L. B.; Marriott, T.; Saunders, M.; Jiménez-Vázquez, H. A.; Khong, A. *Tetrahedron Lett.* **1997**, *38*, 171.

(17) Avent, A. G.; Birkett, P. R.; Darwish, A. D.; Kroto, H. W.; Taylor, R.; Walton, D. R. M. *Mol. Cryst. Liq. Cryst. Sci. Technol., Sect. C* **1996**, *7*, 33.

(18) Henderson, C. C.; Cahill, P. A. *Science* **1993**, *259*, 1885.

(19) Drelinkiewicz, A.; Byszewski, P.; Bielanski, A. *React. Kinet. Catal. Lett.* **1996**, *59*, 19.

(20) Rüchardt, C.; Gerst, M.; Ebenhoch, J.; Beckhaus, H. D.; Campbell, E. E. B.; Tellgmann, R.; Schwarz, H.; Weiske, T.; Pitter, S. *Angew. Chem.* **1993**, *105*, 609.

(21) Iijima, S. *Nature* **1991**, *354*, 56.

(22) Iijima, S.; Ichihashi, T. *Nature* **1993**, *363*, 603.

(23) Bethune, D. S.; Klang, C. H.; de Vries, M. S.; Gorman, G.; Savoy, R.; Vazquez, J.; Beyers, R. *Nature* **1993**, *363*, 605.

(24) Dresselhaus, M. S.; Dresselhaus, G.; Saito, R. *Phys. Rev. B: Condens. Matter Mater. Phys.* **1992**, *45*, 6234.

(25) Mintmire, J. W.; Dunlap, B. I.; White, C. T. *Phys. Rev. Lett.* **1992**, *68*, 631.

(26) Hamada, N.; Sawada, S.-i.; Oshiyama, A. *Phys. Rev. Lett.* **1992**, *68*, 1579.

(27) Odom, T. W.; Huang, J.-L.; Kim, P.; Lieber, C. M. *Nature* **1998**, *391*, 62.

(28) Wilder, J. W. G.; Venema, L. C.; Rinzler, A. G.; Smalley, R. E.; Dekker, C. *Nature* **1998**, *391*, 59.

(29) Dürkop, T.; Getty, S. A.; Cobas, E.; Fuhrer, M. S. *Nano Lett.* **2003**, *4*, 35.

(30) Chang, C.-C.; Hsu, I. K.; Aykol, M.; Hung, W.-H.; Chen, C.-C.; Cronin, S. B. *ACS Nano* **2010**, ASAP.

(31) Dobkin, D. M.; Zuraw, M. K. *Principles of Chemical Vapor Deposition*, 2003.

(32) Bhaviripudi, S.; Mile, E.; Steiner, S. A.; Zare, A. T.; Dresselhaus, M. S.; Belcher, A. M.; Kong, J. *J. Am. Chem. Soc.* **2007**, *129*, 1516.

(33) Chatterjee, A. K.; Sharon, M.; Banerjee, R.; Neumann-Spallart, M. *Electrochim. Acta* **2003**, *48*, 3439.

(34) Li, Y.; Liu, J.; Wang, Y.; Wang, Z. L. *Chem. Mater.* **2001**, *13*, 1008.

(35) Cassell, A. M.; Raymakers, J. A.; Kong, J.; Dai, H. *J. Phys. Chem. B* **1999**, *103*, 6484.

(36) Qingwen, L.; Hao, Y.; Yan, C.; Jin, Z.; Zhongfan, L. *J. Mater. Chem.* **2002**, *12*, 1179.

(37) Thayer, A. M. In *Chem. Eng. News.* 2007; Vol. 85, p 29.

(38) Pekker, S.; Salvetat, J. P.; Jakab, E.; Bonard, J. M.; Forro, L. *J. Phys. Chem. B* **2001**, *105*, 7938.

(39) Khare, B. N.; Meyyappan, M.; Kralj, J.; Wilhite, P.; Sisay, M.; Imanaka, H.; Koehne, J.; Baushchlicher, J. C. W. *Appl. Phys. Lett.* **2002**, *81*, 5237.

(40) Khare, B. N.; Meyyappan, M.; Cassell, A. M.; Nguyen, C. V.; Han, J. *Nano Lett.* **2001**, *2*, 73.

(41) Zhang, G.; Qi, P.; Wang, X.; Lu, Y.; Mann, D.; Li, X.; Dai, H. *J. Am. Chem. Soc.* **2006**, *128*, 6026.

(42) Meletov, K. P.; Maksimov, A. A.; Tartakovskii, I. I.; Bashkin, I. O.; Shestakov, V. V.; Krestinin, A. V.; Shulga, Y. M.; Andrikopoulos, K. S.; Arvanitidis, J.; Christofilos, D.; Kourouklis, G. A. *Chem. Phys. Lett.* **2007**, *433*, 335.

(43) Kim, K. S.; Bae, D. J.; Kim, J. R.; Park, K. A.; Lim, S. C.; Kim, J. J.; Choi, W. B.; Park, C. Y.; Lee, Y. H. *Adv. Mater.* **2002**, *14*, 1818.

(44) Kopelevich, Y.; Esquinazi, P. *Adv. Mater.* **2007**, *19*, 4559.

(45) Balandin, A. A.; Ghosh, S.; Bao, W.; Calizo, I.; Teweldebrhan, D.; Miao, F.; Lau, C. N. *Nano Lett.* **2008**, *8*, 902.

(46) Trucano, P.; Chen, R. *Nature* **1975**, *258*, 136.

(47) Mouras; S; Hamm; A; Djurado; D; Cousseins; J, C. *Synthesis of first stage graphite intercalation compounds with fluorides*; Paris, 1987; Vol. 24.

(48) Forbeaux, I.; Themlin, J. M.; Debever, J. M. *Phys. Rev. B: Condens. Matter Mater. Phys.* **1998**, *58*, 16396.

(49) Lee, C.; Wei, X.; Kysar, J. W.; Hone, J. *Science* **2008**, *321*, 385.

(50) Chen, J.-H.; Jang, C.; Xiao, S.; Ishigami, M.; Fuhrer, M. S. *Nat Nano* **2008**, *3*, 206.

(51) Akturk, A.; Goldsman, N. *J. Appl. Phys.* **2008**, *103*, 053702.

(52) Mingo, N.; Broido, D. A. *Phys. Rev. Lett.* **2005**, *95*, 096105.

(53) Lin, Y.-M.; Dimitrakopoulos, C.; Jenkins, K. A.; Farmer, D. B.; Chiu, H.-Y.; Grill, A.; Avouris, P. *Science* **2010**, *327*, 662.

(54) Blake, P.; Brimicombe, P. D.; Nair, R. R.; Booth, T. J.; Jiang, D.; Schedin, F.; Ponomarenko, L. A.; Morozov, S. V.; Gleeson, H. F.; Hill, E. W.; Geim, A. K.; Novoselov, K. S. *Nano Lett.* **2008**, *8*, 1704.

(55) Wu, J.; Agrawal, M.; Becerril, H. c. A.; Bao, Z.; Liu, Z.; Chen, Y.; Peumans, P. *ACS Nano* **2009**, *4*, 43.

(56) Yin, Z.; Sun, S.; Salim, T.; Wu, S.; Huang, X.; He, Q.; Lam, Y. M.; Zhang, H. *ACS Nano*, ASAP.

(57) Liu, Z.; Liu, Q.; Huang, Y.; Ma, Y.; Yin, S.; Zhang, X.; Sun, W.; Chen, Y. *Adv. Mater.* **2008**, *20*, 3924.

(58) Novoselov, K. S.; Geim, A. K.; Morozov, S. V.; Jiang, D.; Zhang, Y.; Dubonos, S. V.; Grigorieva, I. V.; Firsov, A. A. *Science* **2004**, *306*, 666.

(59) Novoselov, K. S.; Jiang, D.; Schedin, F.; Booth, T. J.; Khotkevich, V. V.; Morozov, S. V.; Geim, A. K. *Proc. Natl. Acad. Sci. U. S. A.* **2005**, *102*, 10451.

(60) Stankovich, S.; Dikin, D. A.; Piner, R. D.; Kohlhaas, K. A.; Kleinhammes, A.; Jia, Y.; Wu, Y.; Nguyen, S. T.; Ruoff, R. S. *Carbon* **2007**, *45*, 1558.

(61) Hummers, W. S.; Offeman, R. E. *J. Am. Chem. Soc.* **1958**, *80*, 1339.

(62) Marcano, D. C.; Kosynkin, D. V.; Berlin, J. M.; Sinitskii, A.; Sun, Z.; Slesarev, A.; Alemany, L. B.; Lu, W.; Tour, J. M. *ACS Nano*, *4*, 4806.

(63) Hamilton, C. E., Rice University 2009.

(64) Gómez-Navarro, C.; Weitz, R. T.; Bittner, A. M.; Scolari, M.; Mews, A.; Burghard, M.; Kern, K. *Nano Lett.* **2007**, *7*, 3499.

(65) Subrahmanyam, K. S.; Vivekchand, S. R. C.; Govindaraj, A.; Rao, C. N. R. *J. Mater. Chem.* **2008**, *18*, 1517.

(66) Stankovich, S.; Piner, R. D.; Chen, X.; Wu, N.; Nguyen, S. T.; Ruoff, R. S. *J. Mater. Chem.* **2006**, *16*, 155.

(67) Wang, G.; Yang, J.; Park, J.; Gou, X.; Wang, B.; Liu, H.; Yao, J. *J. Phys. Chem C.* **2008**, *112*, 8192.

(68) Si, Y.; Samulski, E. T. *Nano Lett.* **2008**, *8*, 1679.

(69) Fan, X.; Peng, W.; Li, Y.; Li, X.; Wang, S.; Zhang, G.; Zhang, F. *Adv. Mater.* **2008**, *20*, 4490.

(70) Pei, S.; Zhao, J.; Du, J.; Ren, W.; Cheng, H.-M. *Carbon, In Press, Corrected Proof.*

(71) Williams, G.; Seger, B.; Kamat, P. V. *ACS Nano* **2008**, *2*, 1487.

(72) McAllister, M. J.; Li, J.-L.; Adamson, D. H.; Schniepp, H. C.; Abdala, A. A.; Liu, J.; Herrera-Alonso, M.; Milius, D. L.; Car, R.; Prud'homme, R. K.; Aksay, I. A. *Chem. Mater.* **2007**, *19*, 4396.

(73) Tryba, B.; Morawski, A. W.; Inagaki, M. *Carbon* **2005**, *43*, 2417.

(74) Chen, W.; Yan, L.; Bangal, P. R. *Carbon*, *48*, 1146.

(75) Sridhar, V.; Jeon, J.-H.; Oh, I.-K. *Carbon*, *48*, 2953.

(76) Wei, Z.; Wang, D.; Kim, S.; Kim, S.-Y.; Hu, Y.; Yakes, M. K.; Laracuente, A. R.; Dai, Z.; Marder, S. R.; Berger, C.; King, W. P.; de Heer, W. A.; Sheehan, P. E.; Riedo, E. *Science*, *328*, 1373.

(77) Wang, H.; Robinson, J. T.; Li, X.; Dai, H. *J. Am. Chem. Soc.* **2009**, *131*, 9910.

(78) Zhou, Y.; Bao, Q.; Tang, L. A. L.; Zhong, Y.; Loh, K. P. *Chem. Mater.* **2009**, *21*, 2950.

(79) Choucair, M.; Thordarson, P.; Stride, J. A. *Nat Nano* **2009**, *4*, 30.

(80) Salas, E. C.; Sun, Z.; Lu[illegible]ttge, A.; Tour, J. M. *ACS Nano*, *4*, 4852.

(81) Berger, C.; Song, Z.; Li, T.; Li, X.; Ogbazghi, A. Y.; Feng, R.; Dai, Z.; Marchenkov, A. N.; Conrad, E. H.; First, P. N.; de Heer, W. A. *J. Phys. Chem. B* **2004**, *108*, 19912.

(82) Berger, C.; Song, Z.; Li, X.; Wu, X.; Brown, N.; Naud, C.; Mayou, D.; Li, T.; Hass, J.; Marchenkov, A. N.; Conrad, E. H.; First, P. N.; de Heer, W. A. *Science* **2006**, *312*, 1191.

(83) Vaari, J.; Lahtinen, J.; Hautojärvi, P. *Catal. Lett.* **1997**, *44*, 43.

(84) Gao, L.; Guest, J. R.; Guisinger, N. P. *Nano Lett.* **2010**, *10*, 3512.

(85) Gamo, Y.; Nagashima, A.; Wakabayashi, M.; Terai, M.; Oshima, C. *Surf. Sci.* **1997**, *374*, 61.

(86) Ueta, H.; Saida, M.; Nakai, C.; Yamada, Y.; Sasaki, M.; Yamamoto, S. *Surf. Sci.* **2004**, *560*, 183.

(87) Starr, D. E.; Pazhetnov, E. M.; Stadnichenko, A. I.; Boronin, A. I.; Shaikhutdinov, S. K. *Surf. Sci.* **2006**, *600*, 2688.

(88) Coraux, J.; N'Diaye, A. T.; Busse, C.; Michely, T. *Nano Lett.* **2008**, *8*, 565.

(89) aacute; zquez de Parga, A. L.; Calleja, F.; Borca, B.; Passeggi, M. C. G.; Hinarejos, J. J.; Guinea, F.; Miranda, R. *Phys. Rev. Lett.* **2008**, *100*, 056807.

(90) Obraztsov, A. N.; Obraztsova, E. A.; Tyurnina, A. V.; Zolotukhin, A. A. *Carbon* **2007**, *45*, 2017.

(91) Yu, Q.; Lian, J.; Siriponglert, S.; Li, H.; Chen, Y. P.; Pei, S.-S. *Appl. Phys. Lett.* **2008**, *93*, 113103.

(92) Reina, A.; Jia, X.; Ho, J.; Nezich, D.; Son, H.; Bulovic, V.; Dresselhaus, M. S.; Kong, J. *Nano Lett.* **2008**, *9*, 30.

(93) Keep, C. W.; Terry, S.; Wells, M. *J. Catal.* **1980**, *66*, 451.

(94) Baker, R. T. K.; Sherwood, R. D.; Dumesic, J. A. *J. Catal.* **1980**, *66*, 56.

(95) Qu, D. *Chem.–Eur. J.* **2008**, *14*, 1040.

(96) Elias, D. C.; Nair, R. R.; Mohiuddin, T. M. G.; Morozov, S. V.; Blake, P.; Halsall, M. P.; Ferrari, A. C.; Boukhvalov, D. W.; Katsnelson, M. I.; Geim, A. K.; Novoselov, K. S. *Science* **2009**, *323*, 610.

(97) Luo, Z.; Yu, T.; Kim, K.-j.; Ni, Z.; You, Y.; Lim, S.; Shen, Z.; Wang, S.; Lin, J. *ACS Nano* **2009**, *3*, 1781.

(98) Schäffel, F.; Warner, J. H.; Bachmatiuk, A.; Rellinghaus, B.; Büchner, B.; Schultz, L.; Rümmeli, M. H. *Phys. Status Solidi B* **2009**, *246*, 2540.

(99) Jones, J. D.; Mahajan, K. K.; Williams, W. H.; Ecton, P. A.; Mo, Y.; Perez, J. M. *Carbon* **2010**, *48*, 2335.

(100) Li, G.; Wang, L.; Ni, H.; Pittman, C. U. *J. Inorg. Organomet. Polym.* **2001**, *11*, 123.

(101) Ryu, S.; Han, M. Y.; Maultzsch, J.; Heinz, T. F.; Kim, P.; Steigerwald, M. L.; Brus, L. E. *Nano Lett.* **2008**, *8*, 4597.

(102) Xu, S. C.; Irle, S.; Musaev, D. G.; Lin, M. C. *J. Phys. Chem C.* **2006**, *111*, 1355.

(103) Harvey, R. G. *Polycyclic aromatic hydrocarbons: chemistry and carcinogenicity*; New York, 1991.

(104) Sparfel, D.; Gobert, F.; Rigaudy, J. *Tetrahedron* **1980**, *36*, 2225.

(105) Anthony, J. *Angew. Chem., Int. Ed.* **2008**, *47*, 452.

(106) Clar, E. *Polycyclic Hydrocarbons*; London, 1964; Vol. 1 & 2.

(107) Cava, M. P.; Deana, A. A.; Muth, K. *J. Am. Chem. Soc.* **1959**, *81*, 6458.

(108) Vets, N.; Smet, M.; Dehaen, W. *Tetrahedron Lett.* **2004**, *45*, 7287.

(109) Bruckner, V.; Karczag, A.; Körmendy, K.; Meszaros, M.; Tomasz, J. *Tetrahedron Lett.* **1960**, *1*, 5.

(110) Mondal, R.; Adhikari, R. M.; Shah, B. K.; Neckers, D. C. *Org. Lett.* **2007**, *9*, 2505.

(111) Mondal, R.; Tönshoff, C.; Khon, D.; Neckers, D. C.; Bettinger, H. F. *J. Am. Chem. Soc.* **2009**, *131*, 14281.

(112) Mondal, R.; Shah, B. K.; Neckers, D. C. *J. Am. Chem. Soc.* **2006**, *128*, 9612.

(113) Tönshoff, C.; Bettinger, H. *Angew. Chem., Int. Ed.* **2010**, *49*, 4125.

(114) Allen, C. F. H.; Bell, A. *J. Am. Chem. Soc.* **1942**, *64*, 1253.

(115) Wolak, M. A.; Jang, B.-B.; Palilis, L. C.; Kafafi, Z. H. *J. Phys. Chem. B* **2004**, *108*, 5492.

(116) Vets, N.; Smet, M.; Dehaen, W. *Synlett* **2005**, *2005*, 217.

(117) Anthony, J. E.; Eaton, D. L.; Parkin, S. R. *Org. Lett.* **2001**, *4*, 15.

(118) Anthony, J. E.; Brooks, J. S.; Eaton, D. L.; Parkin, S. R. *J. Am. Chem. Soc.* **2001**, *123*, 9482.

(119) Kaur, I.; Jia, W.; Kopreski, R. P.; Selvarasah, S.; Dokmeci, M. R.; Pramanik, C.; McGruer, N. E.; Miller, G. P. *J. Am. Chem. Soc.* **2008**, *130*, 16274.

(120) Payne, M. M.; Parkin, S. R.; Anthony, J. E. *J. Am. Chem. Soc.* **2005**, *127*, 8028.

(121) Qu, H.; Chi, C. *Org. Lett.* **2010**, *12*, 3360.

(122) Kaur, I.; Stein, N. N.; Kopreski, R. P.; Miller, G. P. *J. Am. Chem. Soc.* **2009**, *131*, 3424.

(123) Kaur, I.; Jazdzyk, M.; Stein, N. N.; Prusevich, P.; Miller, G. P. *J. Am. Chem. Soc.* **2010**, *132*, 1261.

(124) Haufler, R. E.; Conceicao, J.; Chibante, L. P. F.; Chai, Y.; Byrne, N. E.; Flanagan, S.; Haley, M. M.; O'Brien, S. C.; Pan, C.; et, a. *J. Phys. Chem.* **1990**, *94*, 8634.

(125) Peera, A. A.; Alemany, L. B.; Billups, W. E. *Appl. Phys. A: Mater. Sci. Process.* **2004**, *78*, 995.

(126) Kamat, P. *Electrochem. Soc. Interface* **2006**, *15*, 45.

(127) Kornilov, M. Y.; Ljubchuk, T. V.; Isaev, S. D.; Panasyuk, H.; Chernogorenko, V. B.; Shchur, D. V. *Mol. Cryst. Liq. Cryst. Sci. Technol., Sect. C* **2000**, *13*, 285.

(128) Iglesias-Groth, S. *Mon. Not. R. Astron. Soc.* **2006**, *368*, 1925.

(129) Cataldo, F. *Fullerenes, Nanotubes, Carbon Nanostruct.* **2003**, *11*, 295.

(130) Meier, M. S.; Corbin, P. S.; Vance, V. K.; Clayton, M.; Mollman, M.; Poplawska, M. *Tetrahedron Lett.* **1994**, *35*, 5789.

(131) Darwish, A. D.; Abdul-Sada, A. K.; Langley, G. J.; Kroto, H. W.; Taylor, R.; Walton, D. R. M. *Synth. Met.* **1996**, *77*, 303.

(132) Henderson, C. C.; Cahill, P. A. *Science* **1993**, *259*, 1885.

(133) Ruechard, C.; Gerst, M.; Ebenhoch, J.; Beckhaus, H. D.; Campbell, E. E. B.; Tellgmann, R.; Schwarz, H.; Weiske, T.; Pitter, S. *Angew. Chem.* **1993**, *105*, 609.

(134) Gerst, M.; Beckhaus, H.-D.; Rüchardt, C.; Campbell, E. E. B.; Tellgmann, R. *Tetrahedron Lett.* **1993**, *34*, 7729.

(135) Nossal, J.; Saini, Rajesh K.; Alemany, Lawrence B.; Meier, M.; Billups, W. E. *Eur. J. Org. Chem.* **2001**, *2001*, 4167.

(136) Briggs, J. B.; Montgomery, M.; Silva, L. L.; Miller, G. P. *Org. Lett.* **2005**, *7*, 5553.

(137) Darwish, A. D.; Avent, A. G.; Taylor, R.; Walton, D. R. M. J. Chem. Soc., *Perkin Trans. 2* **1996**, 2051.

(138) Wgberg, T.; Johnels, D.; Peera, A.; Hedenstroem, M.; Schulga, Y. M.; Tsybin, Y. O.; Purcell, J. M.; Marshall, A. G.; Noreus, D.; Sato, T.; Talyzin, A. V. *Org. Lett.* **2005**, *7*, 5557.

(139) Miller, G. P. *C. R. Chim.* **2006**, *9*, 952.

(140) Okazaki, T.; Shinohara, H.; Rotkin, S.; Subramoney, S. *Applied Physics of Carbon Nanotubes*; Berlin 2005, 133.

(141) Wudl, F.; Hirsch, A.; Khemani, K. C.; Suzuki, T.; Allemand, P. M.; Koch, A.; Eckert, H.; Srdanov, G.; Webb, H. M. *Fullerenes*; 1992; 481, 161.

(142) Kintigh, J.; Briggs, J. B.; Letourneau, K.; Miller, G. P. *J. Mater. Chem.* **2007**, *17*, 4647.

(143) Thess, A. *Science* **1996**, *273*, 483.

(144) Francke, M.; Hermann, H.; Wenzel, R.; Seifert, G.; Wetzig, K. *Carbon* **2005**, *43*, 1204.

(145) Sawada, T.; Nakayama, S.; Kawai-Nakamura, A.; Sue, K.; Iwamura, H.; Hiaki, T. *Green Chem.* **2009**, *11*, 1675.

(146) Smith, J. G.; Dibble, P. W. *J. Org. Chem.* **1983**, *48*, 5361.

(147) Young, D.; Douglas, K. M.; Eiceman, G. A.; Lake, D. A.; Johnston, M. V. *Anal. Chim. Acta* **2002**, *453*, 231.

(148) Kuznetsova, A.; Popova, I.; Yates, J. T.; Bronikowski, M. J.; Huffman, C. B.; Liu, J.; Smalley, R. E.; Hwu, H. H.; Chen, J. G. *J. Am. Chem. Soc.* **2001**, *123*, 10699.

(149) Wang, Y.; Iqbal, Z.; Mitra, S. *J. Am. Chem. Soc.* **2005**, *128*, 95.

(150) Jhi, S.-H.; Louie, S. G.; Cohen, M. L. *Phys. Rev. Lett.* **2000**, *85*, 1710.

(151) Georgakilas, V.; Voulgaris, D.; Vázquez, E.; Prato, M.; Guldi, D. M.; Kukovecz, A.; Kuzmany, H. *J. Am. Chem. Soc.* **2002**, *124*, 14318.

(152) Stephenson, J. J.; Hudson, J. L.; Leonard, A. D.; Price, B. K.; Tour, J. M. *Chem. Mater.* **2007**, *19*, 3491.

(153) Mickelson, E. T.; Huffman, C. B.; Rinzler, A. G.; Smalley, R. E.; Hauge, R. H.; Margrave, J. L. *Chem. Phys. Lett.* **1998**, *296*, 188.

(154) Khabashesku, V. N.; Billups, W. E.; Margrave, J. L. *Acc. Chem. Res.* **2002**, *35*, 1087.

(155) Borondics, F.; Bokor, M.; Matus, P.; Tompa, K.; Pekker, S.; Jakab, E. *Fullerene Sci. Techn.* **2005**, *13*, 375.

(156) Briggs, J.; Miller, G. P. *ECS Trans.* **2007**, *6*, 21.

(157) Miller, G. P.; Kintigh, J.; Kim, E.; Weck, P. F.; Berber, S.; Tomanek, D. *J. Am. Chem. Soc.* **2008**, *130*, 2296.

(158) Jung, I.; Dikin, D. A.; Piner, R. D.; Ruoff, R. S. *Nano Lett.* **2008**, *8*, 4283.

(159) Ferrari, A. C.; Robertson, J. *Phys. Rev. B: Condens. Matter Mater. Phys.* **2001**, *64*, 075414.

(160) Fort, E. H.; Donovan, P. M.; Scott, L. T. *J. Am. Chem. Soc.* **2009**, *131*, 16006.

(161) Fort, E. H.; Scott, L. T. *Angew. Chem., Int. Ed.* **2010**, *49*, 6626.

(162) Li, J.; Zhang, K.; Zhang, X.; Huang, K.-W.; Chi, C.; Wu, J. *J. Org. Chem.* **2010**, *75*, 856.

(163) Zhang, K.; Huang, K.-W.; Li, J.; Luo, J.; Chi, C.; Wu, J. *Org. Lett.* **2009**, *11*, 4854.

(164) Zhang, X.; Jiang, X.; Luo, J.; Chi, C.; Chen, H.; Wu, J. *Chem.–Eur. J.* **2010**, *16*, 464.

(165) Zhang, X.; Li, J.; Qu, H.; Chi, C.; Wu, J. *Org. Lett.* **2010**, *12*, 3946.

(166) Donovan, P. M.; Scott, L. T. *Polycyclic Aromat. Compd.* **2008**, *28*, 128

(167) Marschalk, C. *Bull. Soc. Chim. Fr.* **1939**, *6*, 1122.

(168) Goodings, E. P.; Mitchard, D. A.; Owen, G. *J. Chem. Soc.,* Perkin Trans. 1 **1972**, 1310.

(169) Briseno, A. L.; Miao, Q.; Ling, M.-M.; Reese, C.; Meng, H.; Bao, Z.; Wudl, F. *J. Am. Chem. Soc.* **2006**, *128*, 15576.

(170) Park, J. H.; Kang, C. H.; Kim, Y. J.; Lee, Y. S.; Choi, J. S. *Mater. Sci. Eng., C* **2004**, *24*, 27.

(171) Athans, A. J.; Briggs, J. B.; Jia, W.; Miller, G. P. *J. Mater. Chem.* **2007**, *17*, 2636.

(172) Roberson, L. B.; Kowalik, J.; Tolbert, L. M.; Kloc, C.; Zeis, R.; Chi, X.; Fleming, R.; Wilkins, C. *J. Am. Chem. Soc.* **2005**, *127*, 3069.

(173) Cai, J.; Ruffieux, P.; Jaafar, R.; Bieri, M.; Braun, T.; Blankenburg, S.; Muoth, M.; Seitsonen, A. P.; Saleh, M.; Feng, X.; Mullen, K.; Fasel, R. *Nature* **2010**, *466*, 470.

(174) Wang, Y.-M.; Fu, N.-Y.; Chan, S.-H.; Lee, H.-K.; Wong, H. N. C. *Tetrahedron* **2007**, *63*, 8586.

APPENDIX

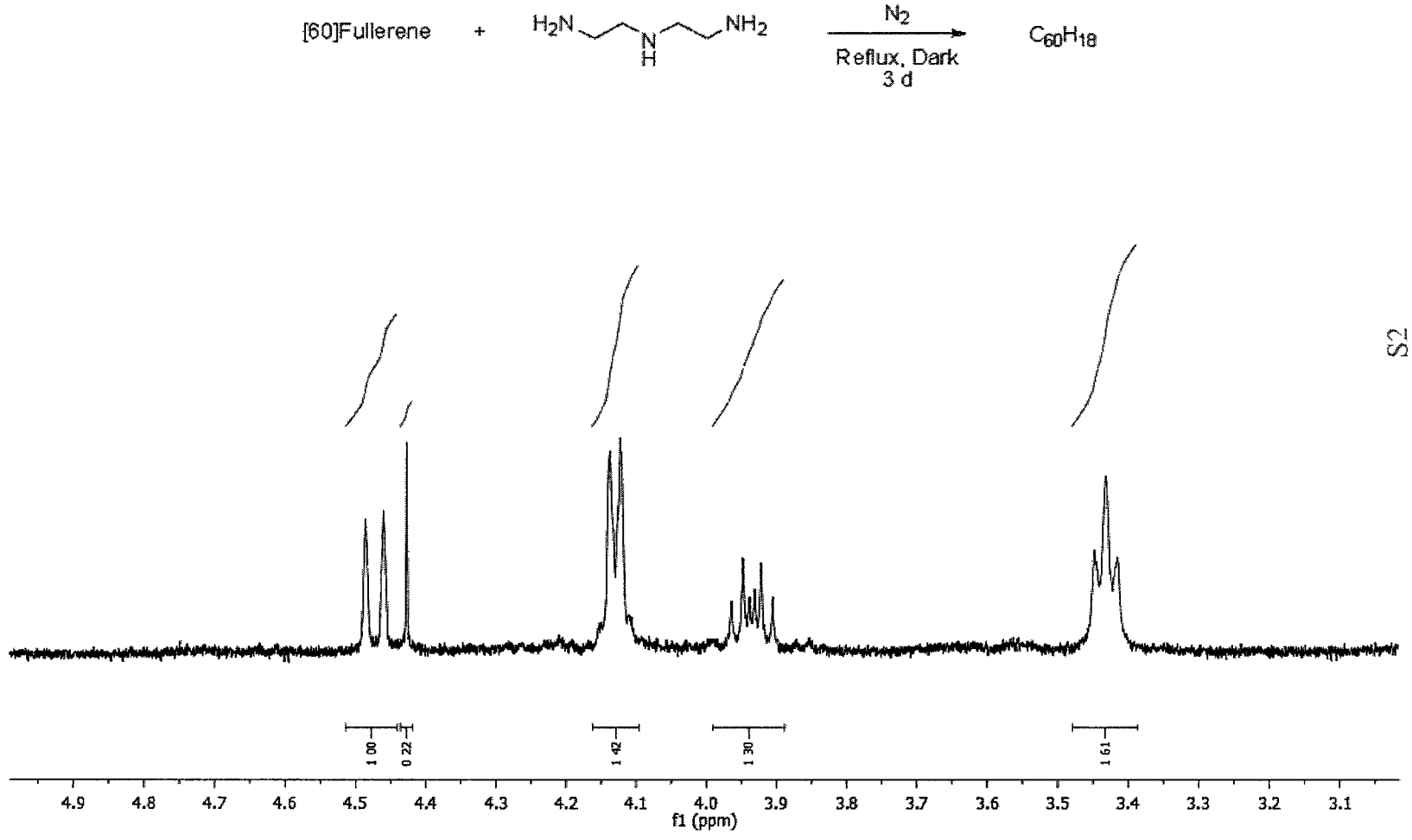
[60]Fullerene
+
H_2N
NH_2
N
H
N_2
Reflux, Dark
3 d
$C_{60}H_{18}$
^{1}H-NMR
1.00
0.22
1.42
1.30
1.61
4.9
4.8
4.7
4.6
4.5
4.4
4.3
4.2
4.1
4.0
3.9
3.8
3.7
3.6
3.5
3.4
3.3
3.2
3.1
f1 (ppm)

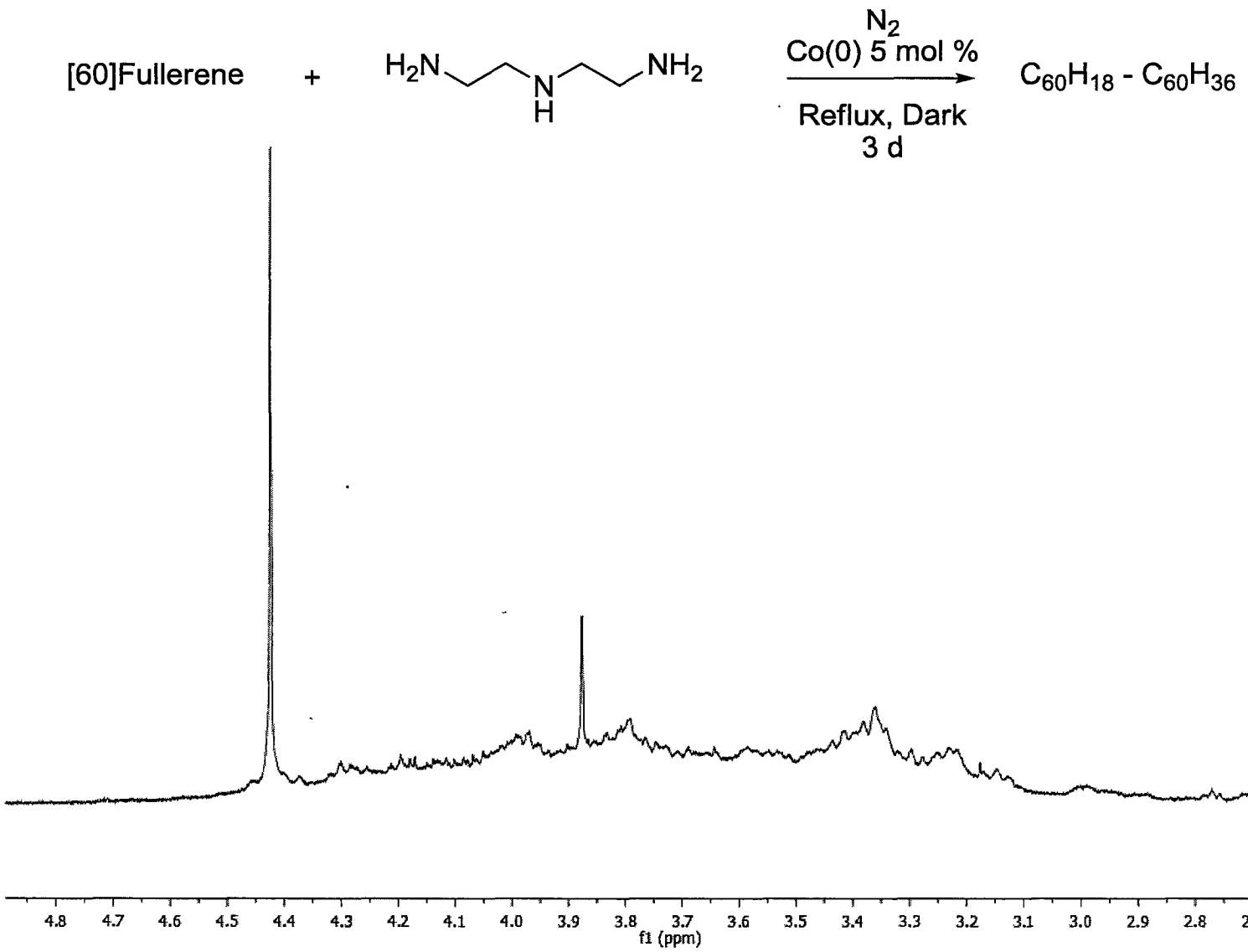
[60]Fullerene
+
H2N
N
H
NH2
N2
Co(0) 5 mol %
Reflux, Dark
3 d
C60H18 - C60H36
1H-NMR
4.8
4.7
4.6
4.5
4.4
4.3
4.2
4.1
4.0
3.9
3.8
3.7
3.6
3.5
3.4
3.3
3.2
3.1
3.0
2.9
2.8
2.7
2.6
f1 (ppm)

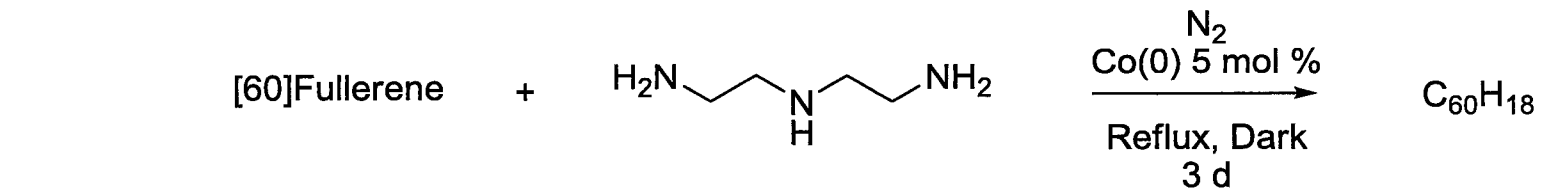
[60]Fullerene
+
H2N
N
H
NH2
N2
Co(0) 5 mol %
Reflux, Dark
3 d
C60H18

Mass Spec

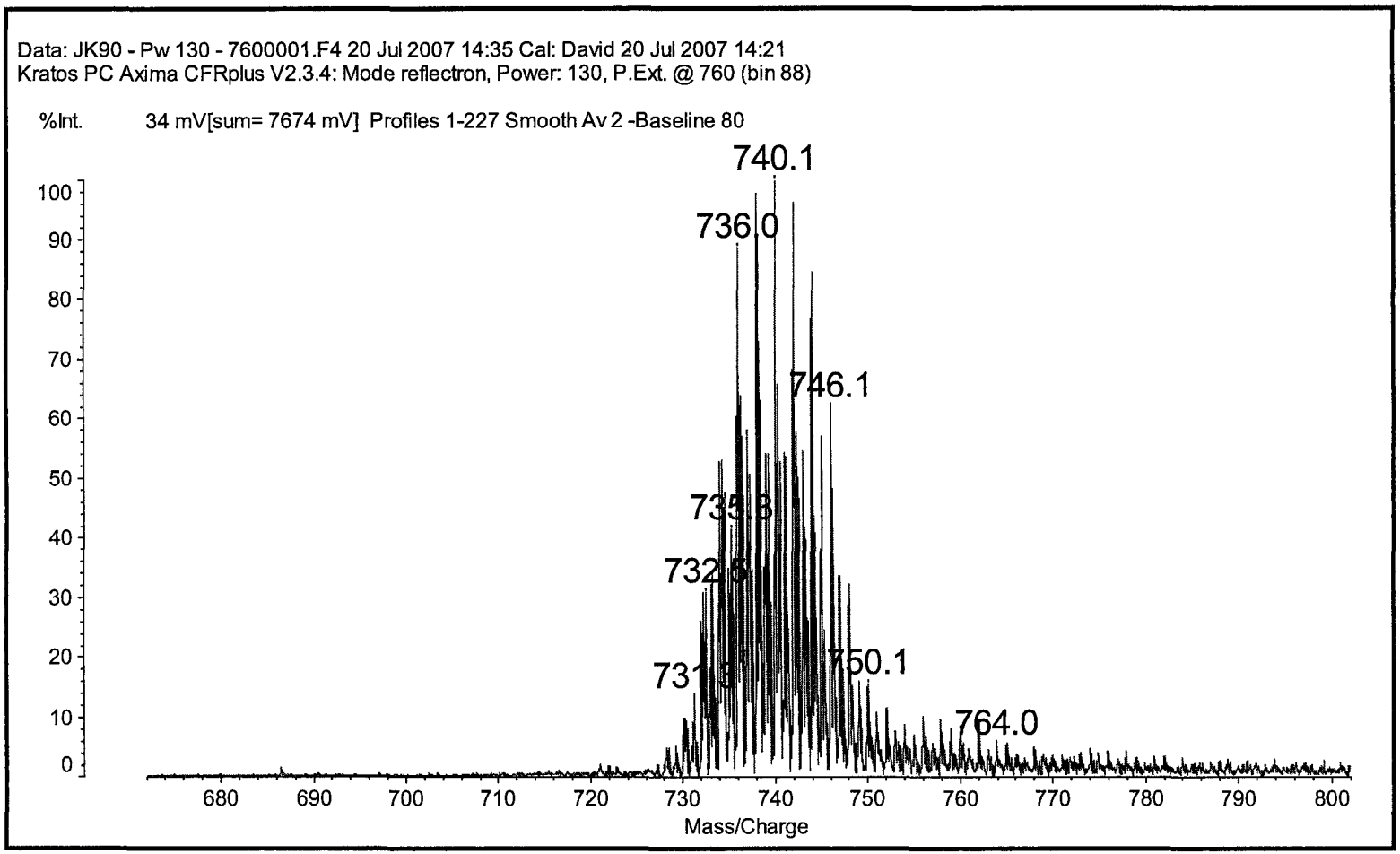
Data: JK90 - Pw 130 - 7600001.F4 20 Jul 2007 14:35 Cal: David 20 Jul 2007 14:21
Kratos PC Axima CFRplus V2.3.4: Mode reflectron, Power: 130, P.Ext. @ 760 (bin 88)
%Int.
34 mV[sum= 7674 mV] Profiles 1-227 Smooth Av 2 -Baseline 80
740.1
736.0
746.1
735.8
732.6
731.3
750.1
764.0
100
90
80
70
60
50
40
30
20
10
0
680
690
700
710
720
730
740
750
760
770
780
790
800
Mass/Charge

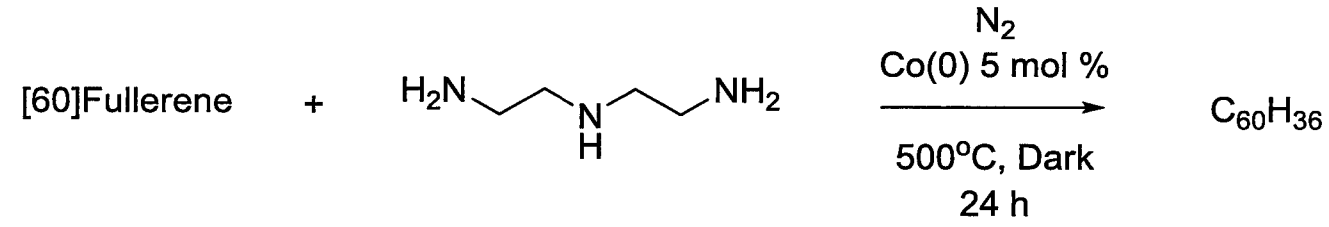
[60]Fullerene
+
H2N
N
H
NH2
N2
Co(0) 5 mol %
500°C, Dark
24 h
C60H36

^{1}H-NMR

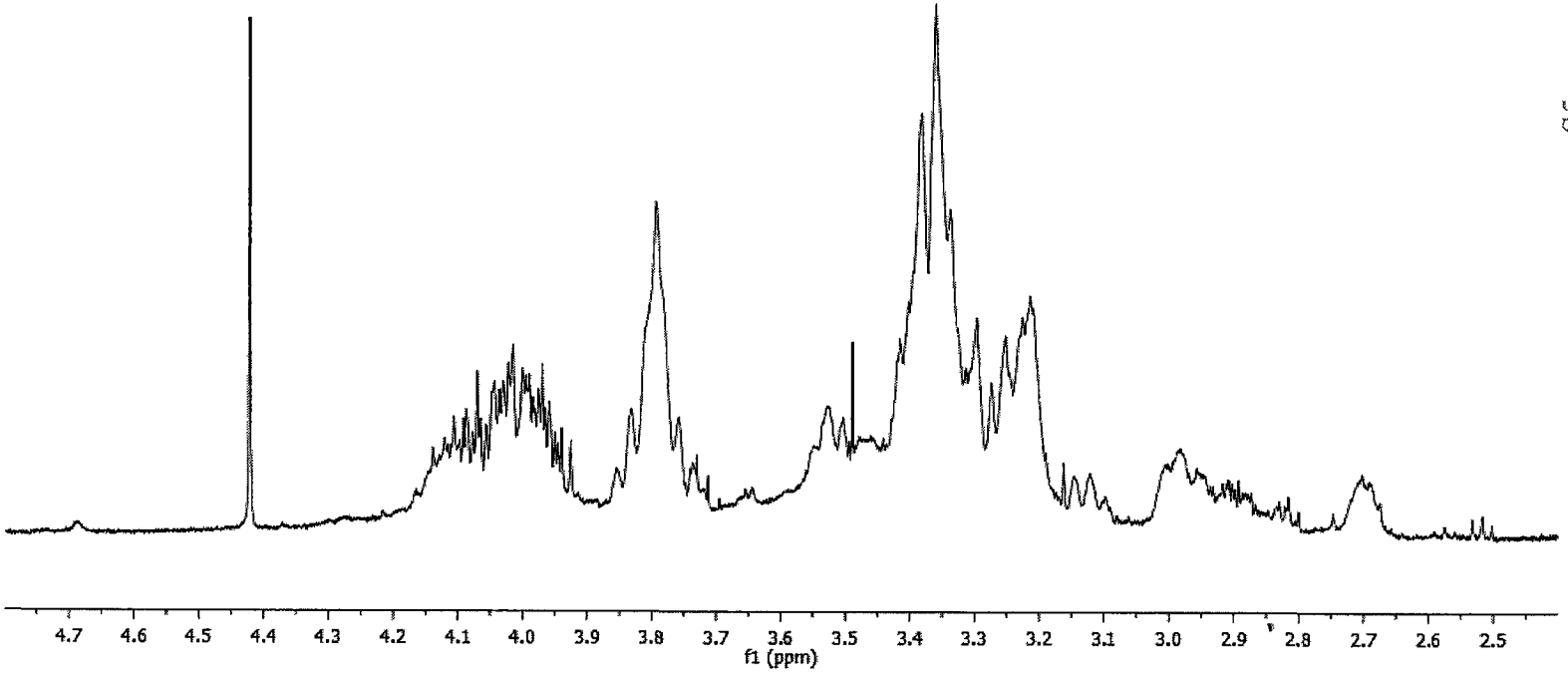
4.7
4.6
4.5
4.4
4.3
4.2
4.1
4.0
3.9
3.8
3.7
3.6
3.5
3.4
3.3
3.2
3.1
3.0
2.9
2.8
2.7
2.6
2.5
f1 (ppm)

^{13}C-NMR

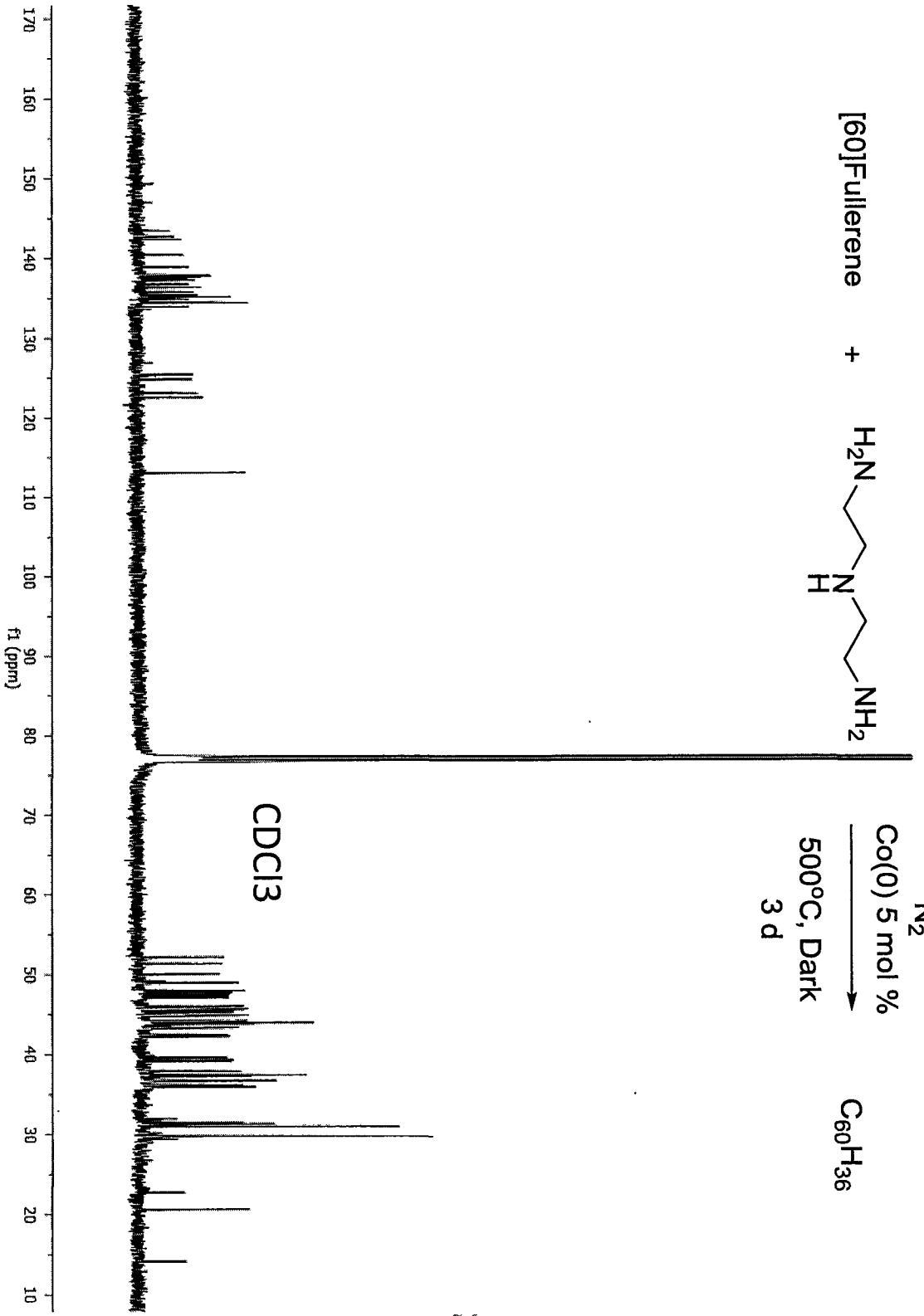
[60]Fullerene
+
H2N
N
H
NH2
N2
Co(0) 5 mol %
500°C, Dark
3 d
C60H36
CDCl3
f1 (ppm)

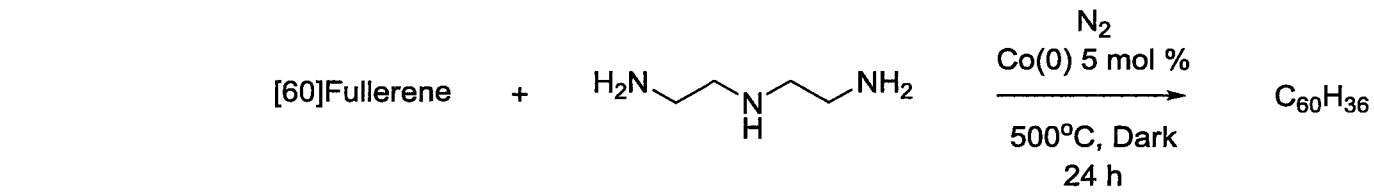
[60]Fullerene
+
H_2N
N
H
NH_2
N_2
Co(0) 5 mol %
500°C, Dark
24 h
$C_{60}H_{36}$

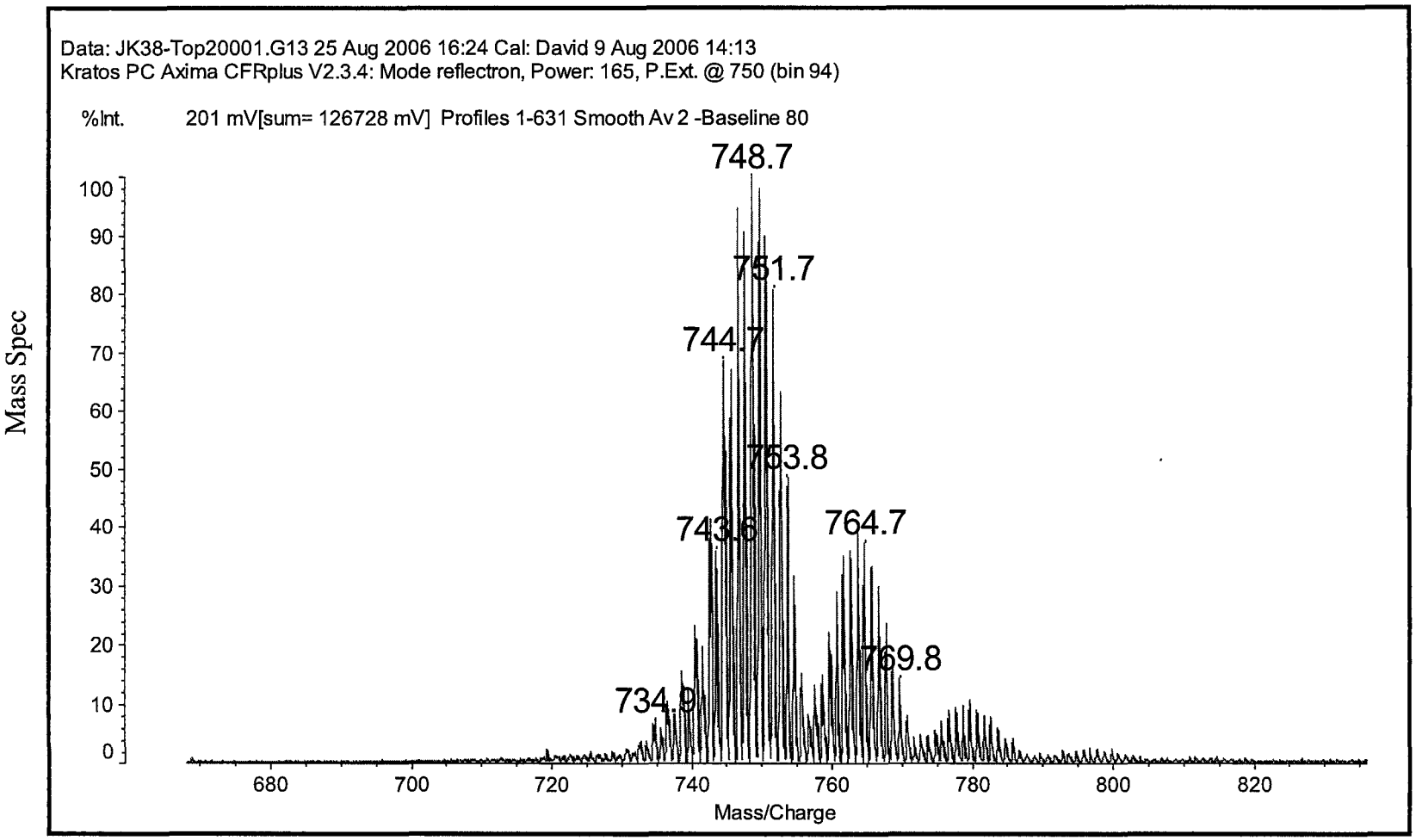
Data: JK38-Top20001.G13 25 Aug 2006 16:24 Cal: David 9 Aug 2006 14:13
Kratos PC Axima CFRplus V2.3.4: Mode reflectron, Power: 165, P.Ext. @ 750 (bin 94)
%Int.
201 mV[sum= 126728 mV] Profiles 1-631 Smooth Av 2 -Baseline 80
748.7
751.7
744.7
753.8
743.6
764.7
769.8
734.9
100
90
80
70
60
50
40
30
20
10
0
680
700
720
740
760
780
800
820
Mass/Charge
Mass Spec

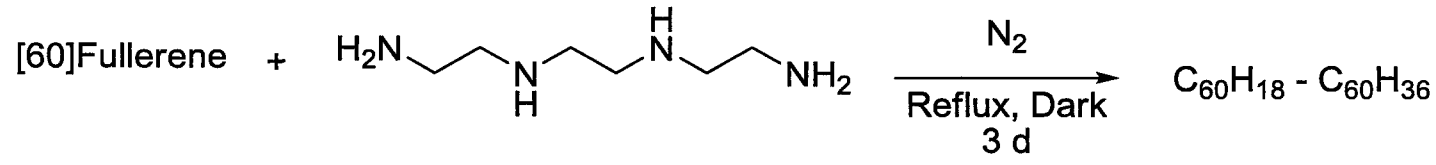
[60]Fullerene
+
H_2N
N
H
H
N
NH_2
N_2
Reflux, Dark
3 d
$C_{60}H_{18}$ - $C_{60}H_{36}$

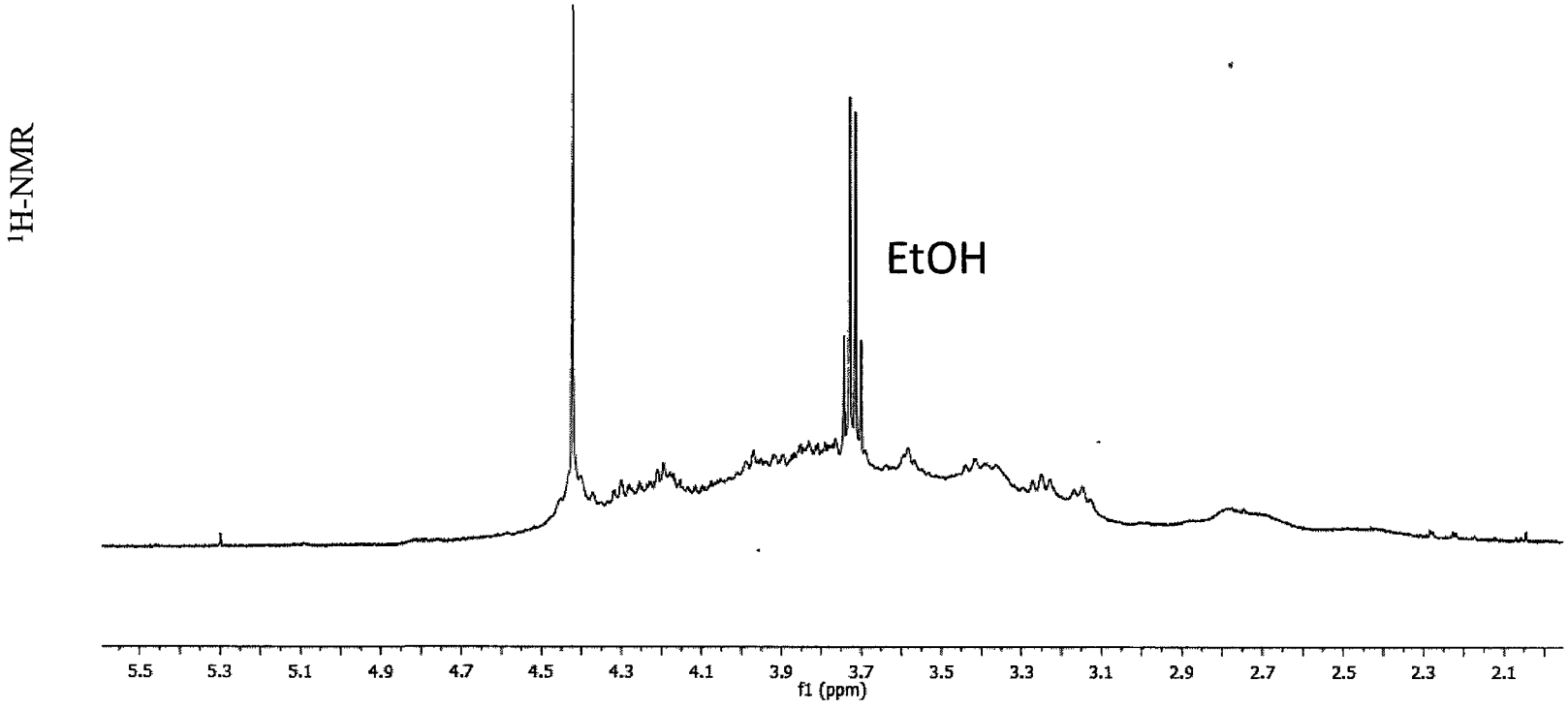
^{1}H-NMR
EtOH
5.5
5.3
5.1
4.9
4.7
4.5
4.3
4.1
3.9
3.7
3.5
3.3
3.1
2.9
2.7
2.5
2.3
2.1
f1 (ppm)

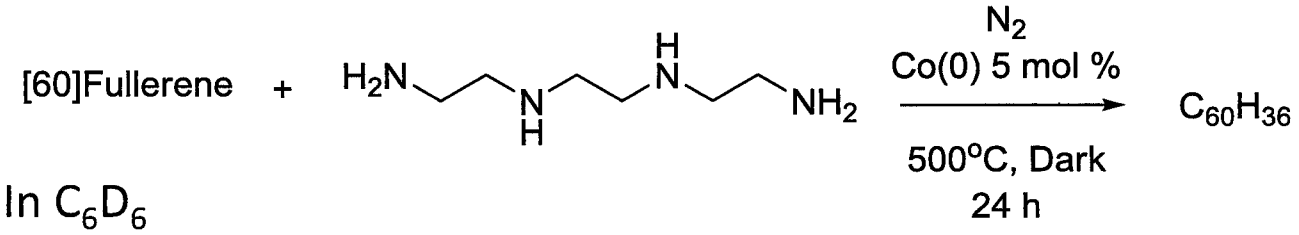
[60]Fullerene
+
H_2N
N
H
H
N
NH_2
N_2
Co(0) 5 mol %
500°C, Dark
24 h
$C_{60}H_{36}$

In C_6D_6

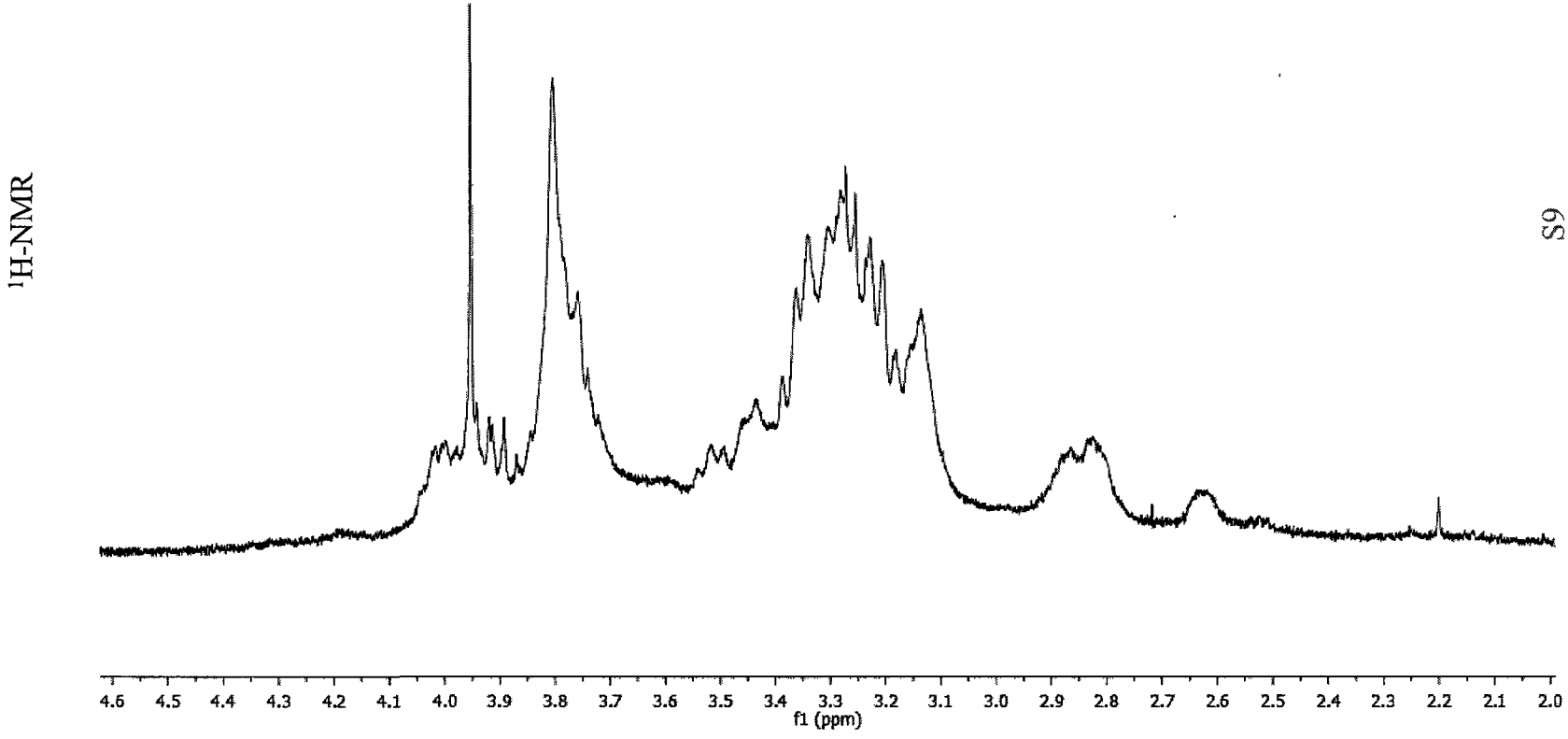
^{1}H-NMR
4.6 4.5 4.4 4.3 4.2 4.1 4.0 3.9 3.8 3.7 3.6 3.5 3.4 3.3 3.2 3.1 3.0 2.9 2.8 2.7 2.6 2.5 2.4 2.3 2.2 2.1 2.0
f1 (ppm)

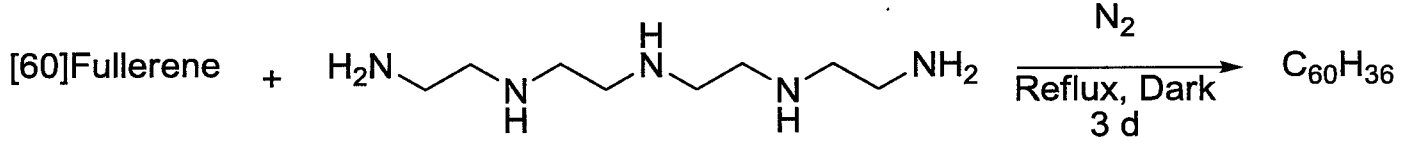
[60]Fullerene
+
H_2N
H
N
N
H
N
H
NH_2
N_2
Reflux, Dark
3 d
$C_{60}H_{36}$

^{1}H-NMR

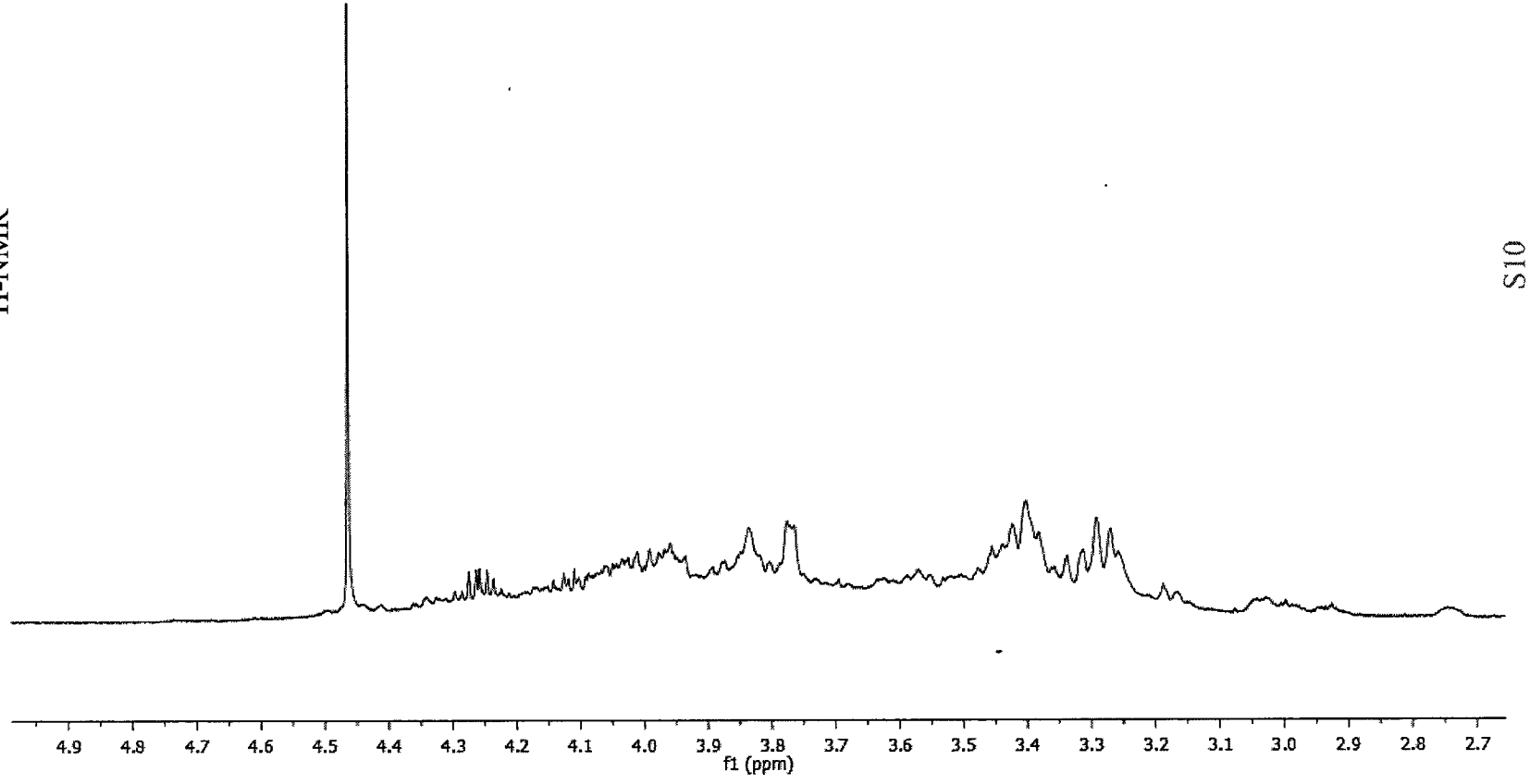
4.9
4.8
4.7
4.6
4.5
4.4
4.3
4.2
4.1
4.0
3.9
3.8
3.7
3.6
3.5
3.4
3.3
3.2
3.1
3.0
2.9
2.8
2.7
f1 (ppm)

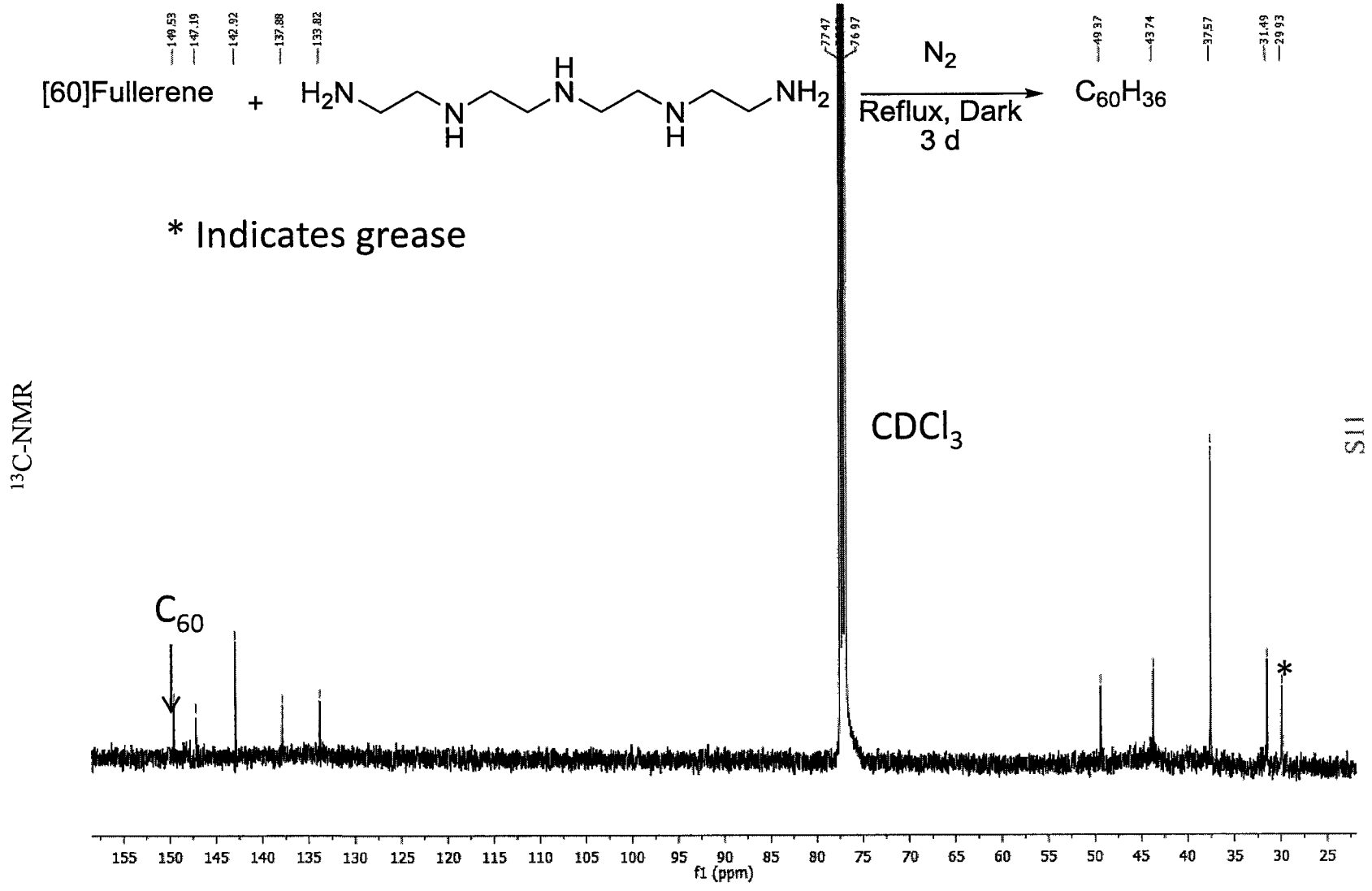
149.53
147.19
142.92
137.88
133.82
77.47
76.97
49.37
43.74
37.57
31.49
29.93
[60]Fullerene + H2N NH NH NH2
N2
Reflux, Dark
3 d
C60H36
* Indicates grease
13C-NMR
CDCl3
C60
*
155 150 145 140 135 130 125 120 115 110 105 100 95 90 85 80 75 70 65 60 55 50 45 40 35 30 25
f1 (ppm)

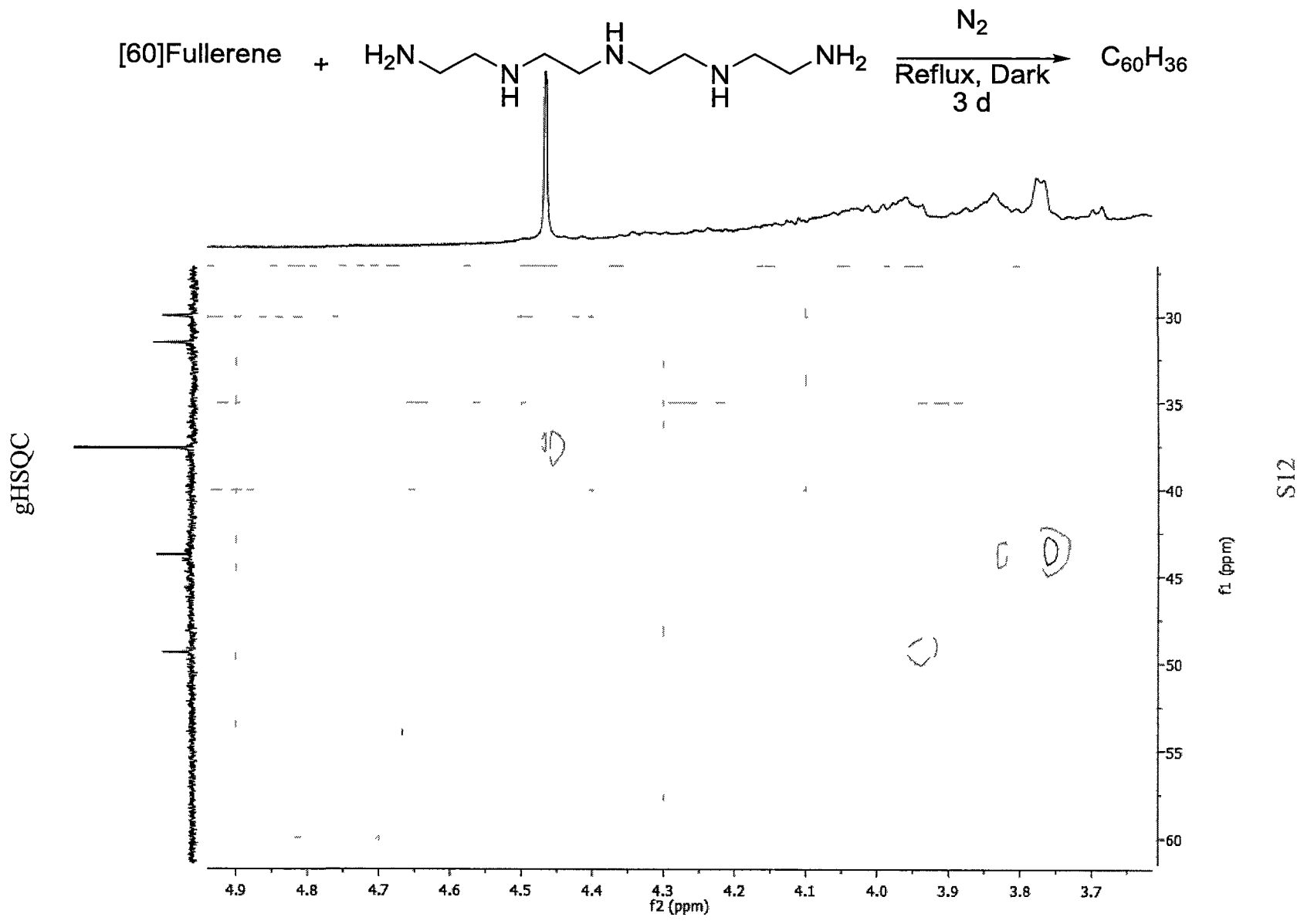
[60]Fullerene
+
H_2N
NH
NH
NH_2
N_2
Reflux, Dark
3 d
$C_{60}H_{36}$
gHSQC
f2 (ppm)
f1 (ppm)

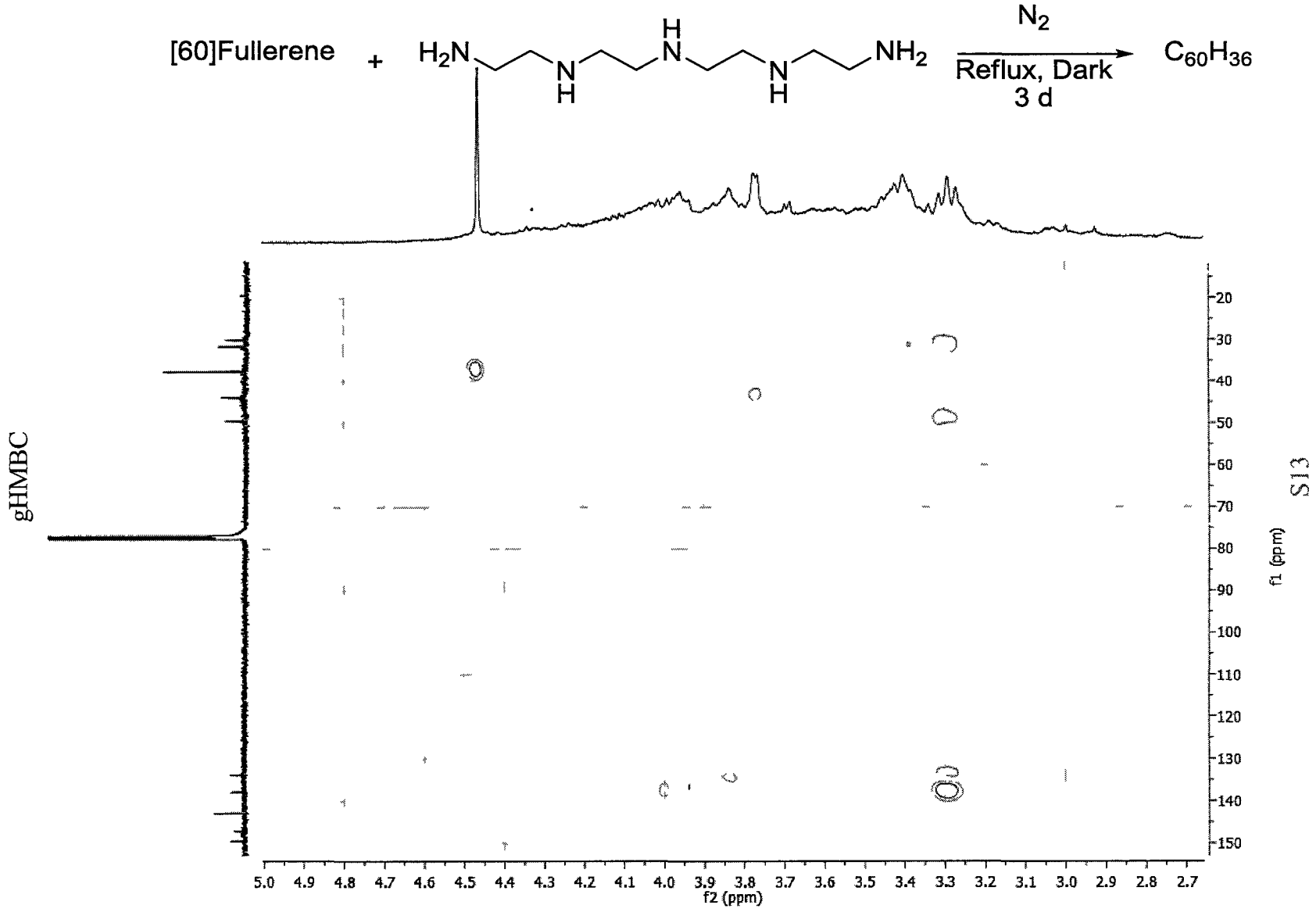
[60]Fullerene
+
H_2N
NH
NH
NH_2
N_2
Reflux, Dark
3 d
$C_{60}H_{36}$
gHMBC
f2 (ppm)
f1 (ppm)

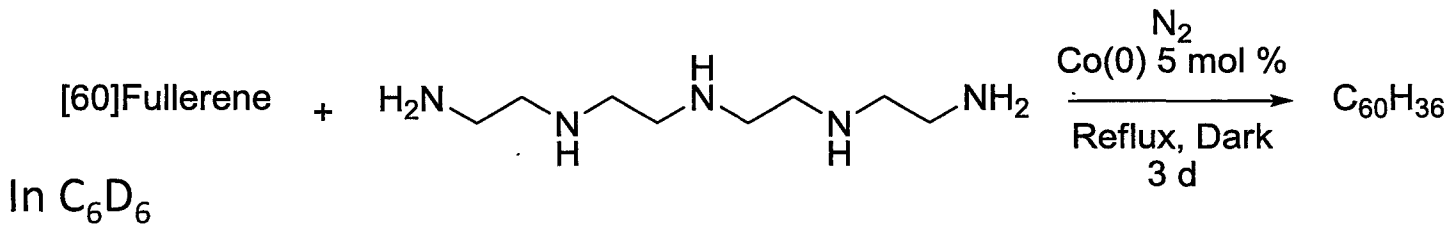
[60]Fullerene
+
H_2N
NH
NH
NH_2
N_2
Co(0) 5 mol %
Reflux, Dark
3 d
$C_{60}H_{36}$

In C_6D_6

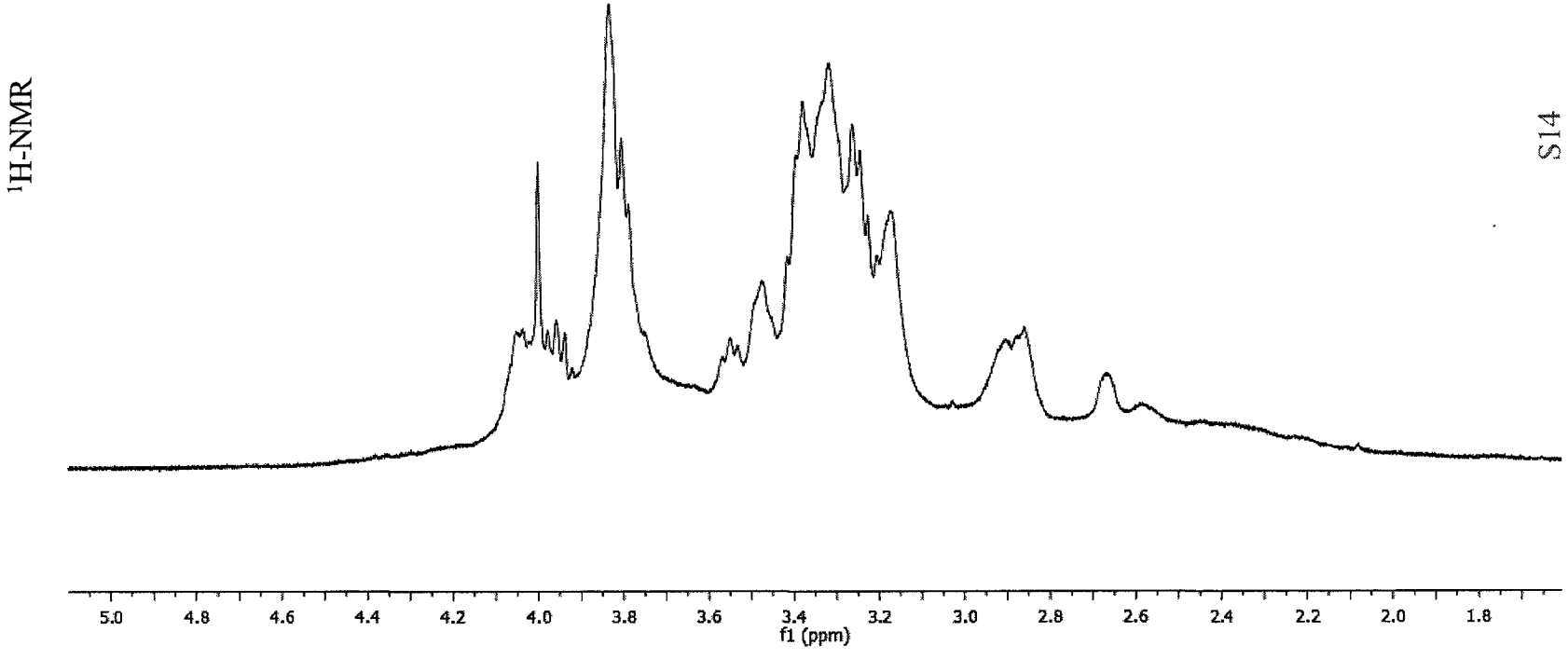
^{1}H-NMR
5.0
4.8
4.6
4.4
4.2
4.0
3.8
3.6
3.4
3.2
3.0
2.8
2.6
2.4
2.2
2.0
1.8
f1 (ppm)

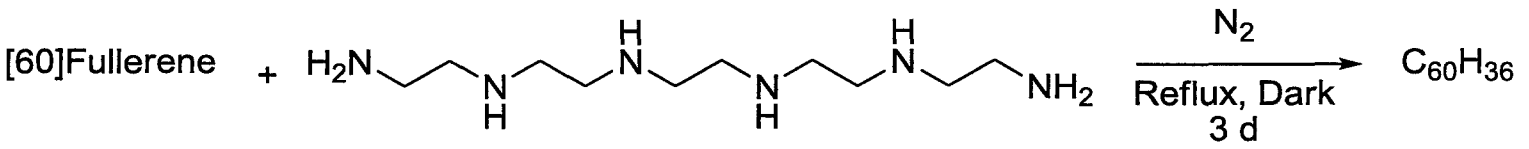

In C_6D_6

^{1}H-NMR

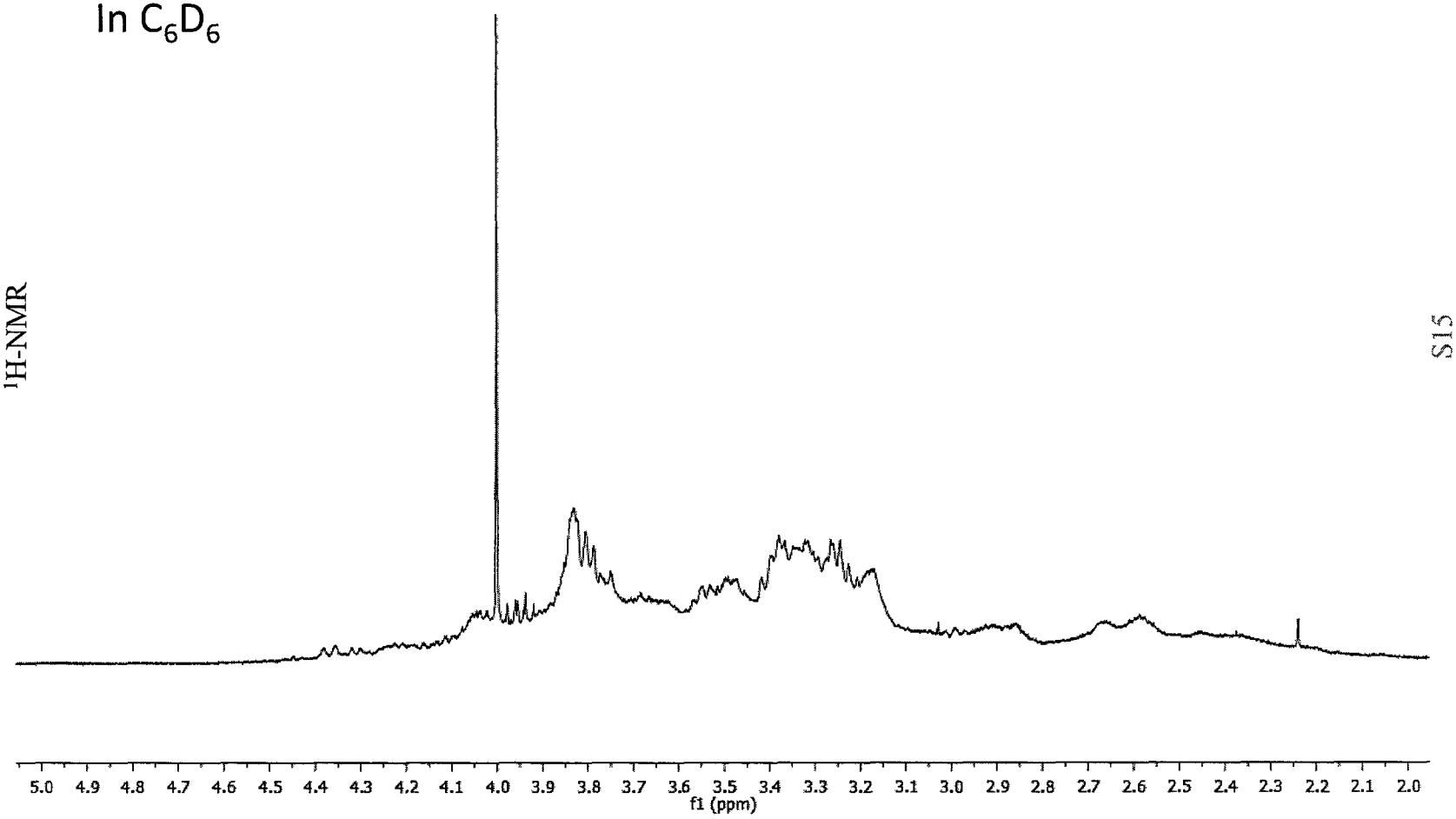

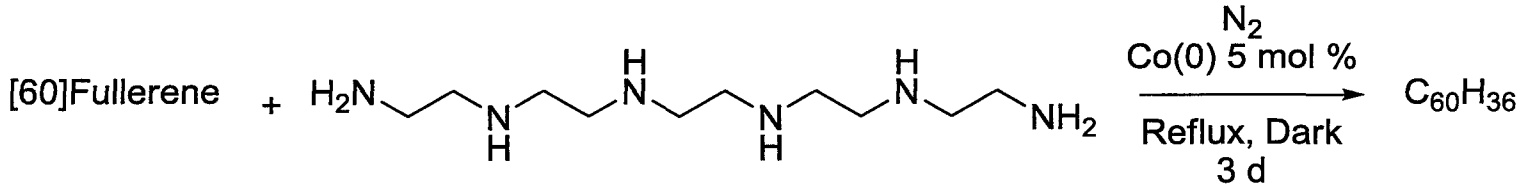
[60]Fullerene
+
H_2N
N
H
H
N
N
H
H
N
NH_2
N_2
Co(0) 5 mol %
Reflux, Dark
3 d
$C_{60}H_{36}$

In C_6D_6

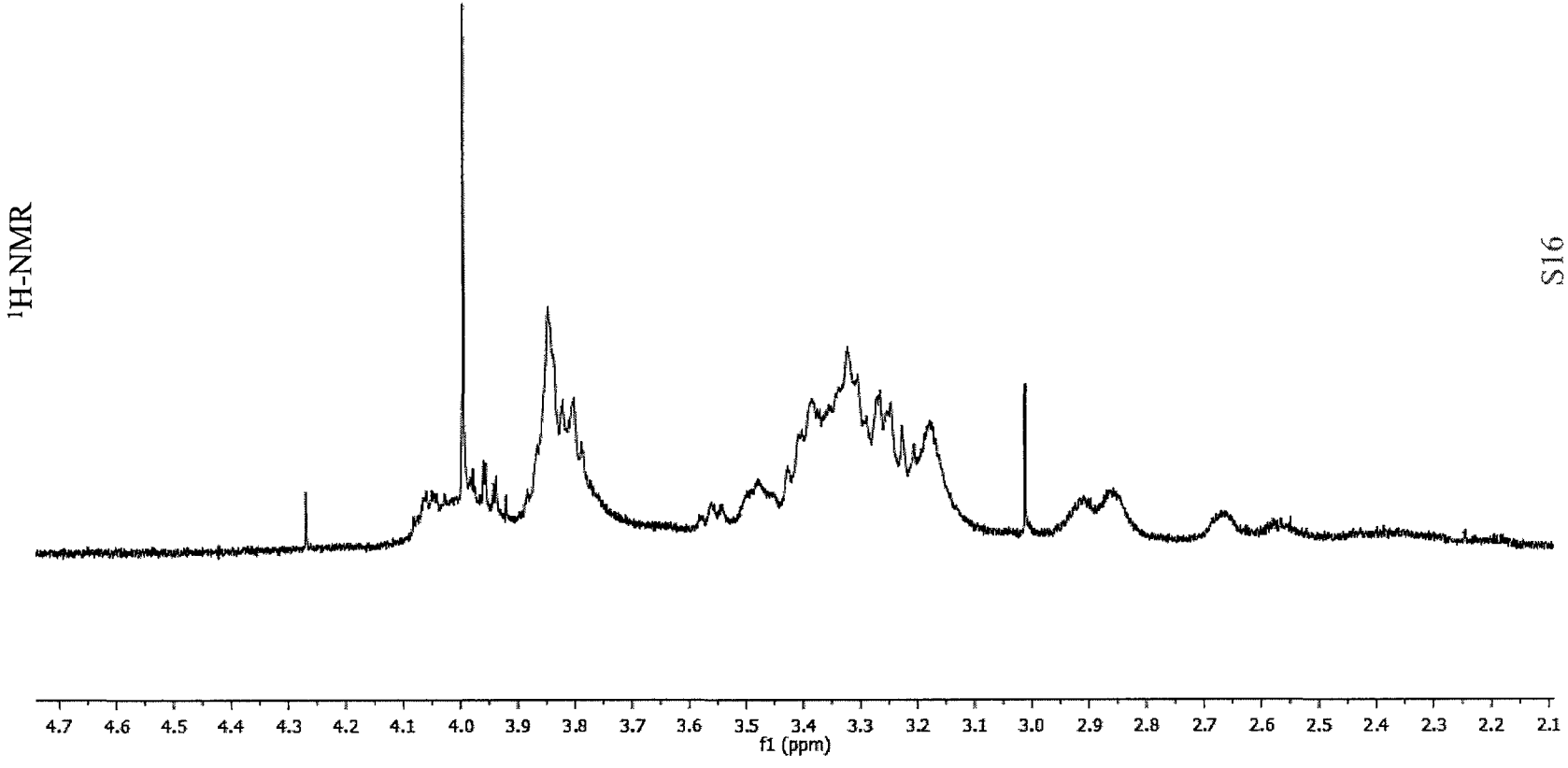
^{1}H-NMR
4.7
4.6
4.5
4.4
4.3
4.2
4.1
4.0
3.9
3.8
3.7
3.6
3.5
3.4
3.3
3.2
3.1
3.0
2.9
2.8
2.7
2.6
2.5
2.4
2.3
2.2
2.1
f1 (ppm)

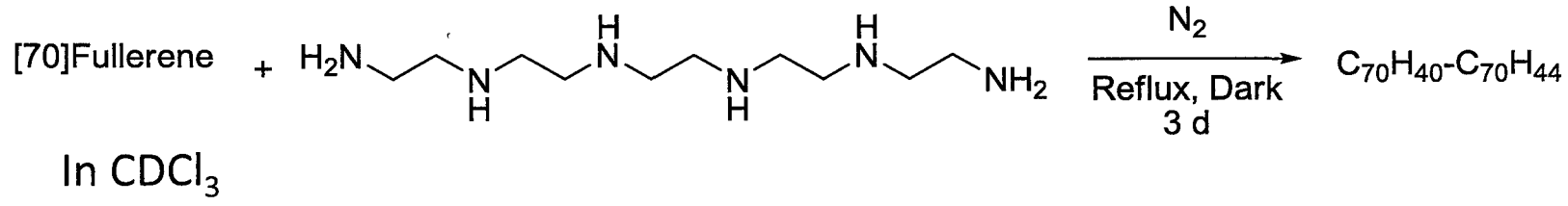
[70]Fullerene
+
H_2N
N
H
N
H
N
H
NH_2
N_2
Reflux, Dark
3 d
$C_{70}H_{40}$-$C_{70}H_{44}$

In $CDCl_3$

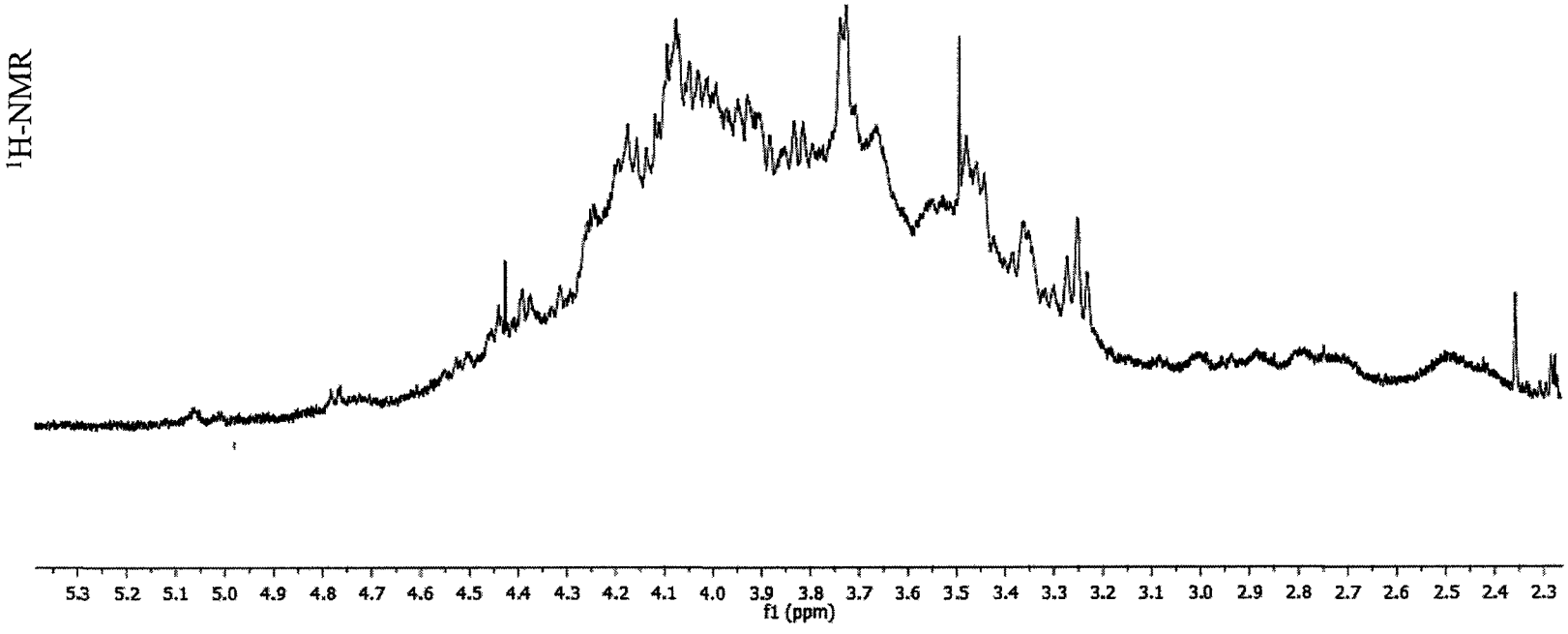
^{1}H-NMR
5.3 5.2 5.1 5.0 4.9 4.8 4.7 4.6 4.5 4.4 4.3 4.2 4.1 4.0 3.9 3.8 3.7 3.6 3.5 3.4 3.3 3.2 3.1 3.0 2.9 2.8 2.7 2.6 2.5 2.4 2.3
f1 (ppm)

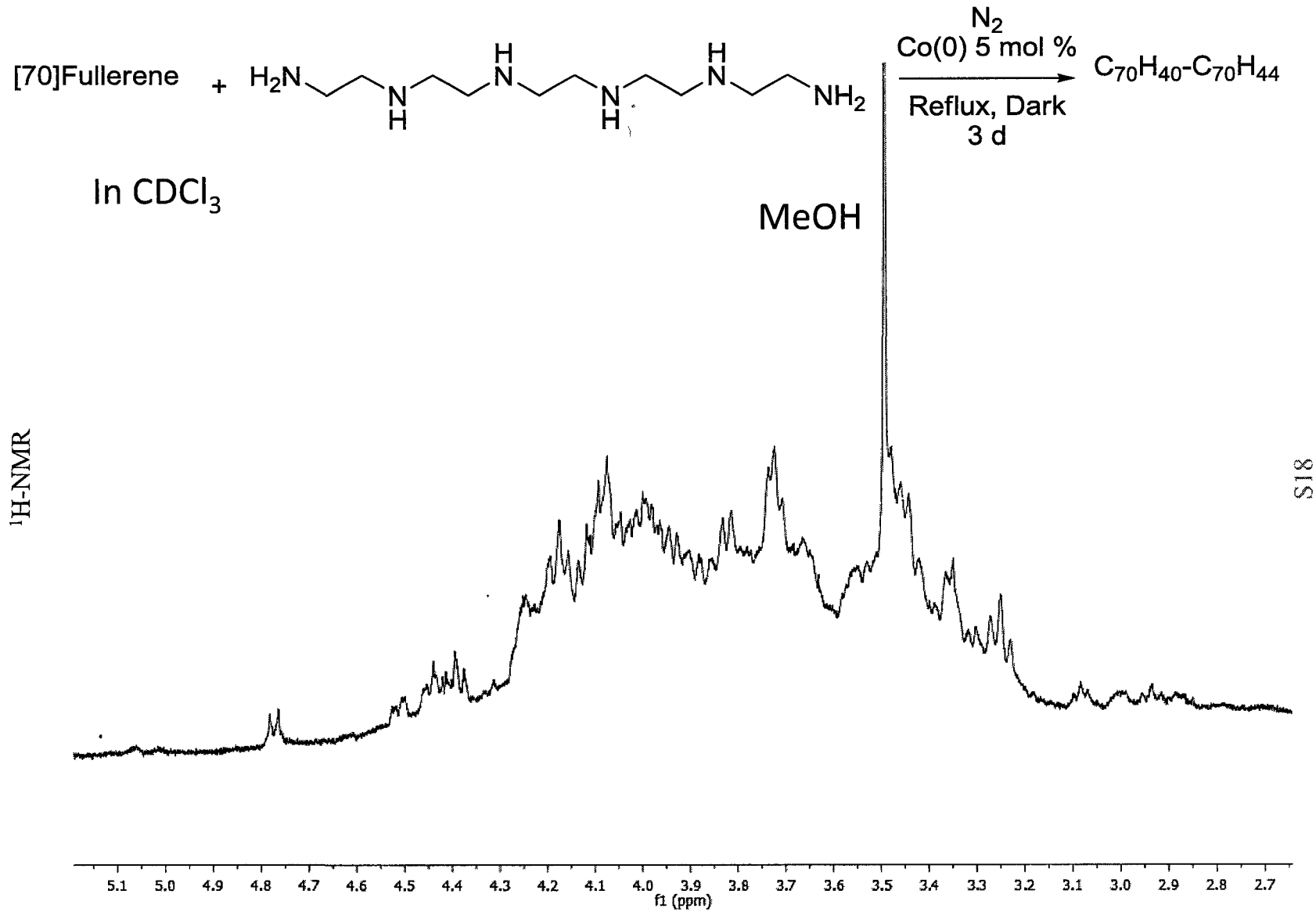
[70]Fullerene
+
H_2N
NH
NH
NH
NH_2
N_2
Co(0) 5 mol %
Reflux, Dark
3 d
$C_{70}H_{40}$-$C_{70}H_{44}$
In $CDCl_3$
MeOH
^{1}H-NMR
5.1 5.0 4.9 4.8 4.7 4.6 4.5 4.4 4.3 4.2 4.1 4.0 3.9 3.8 3.7 3.6 3.5 3.4 3.3 3.2 3.1 3.0 2.9 2.8 2.7
f1 (ppm)

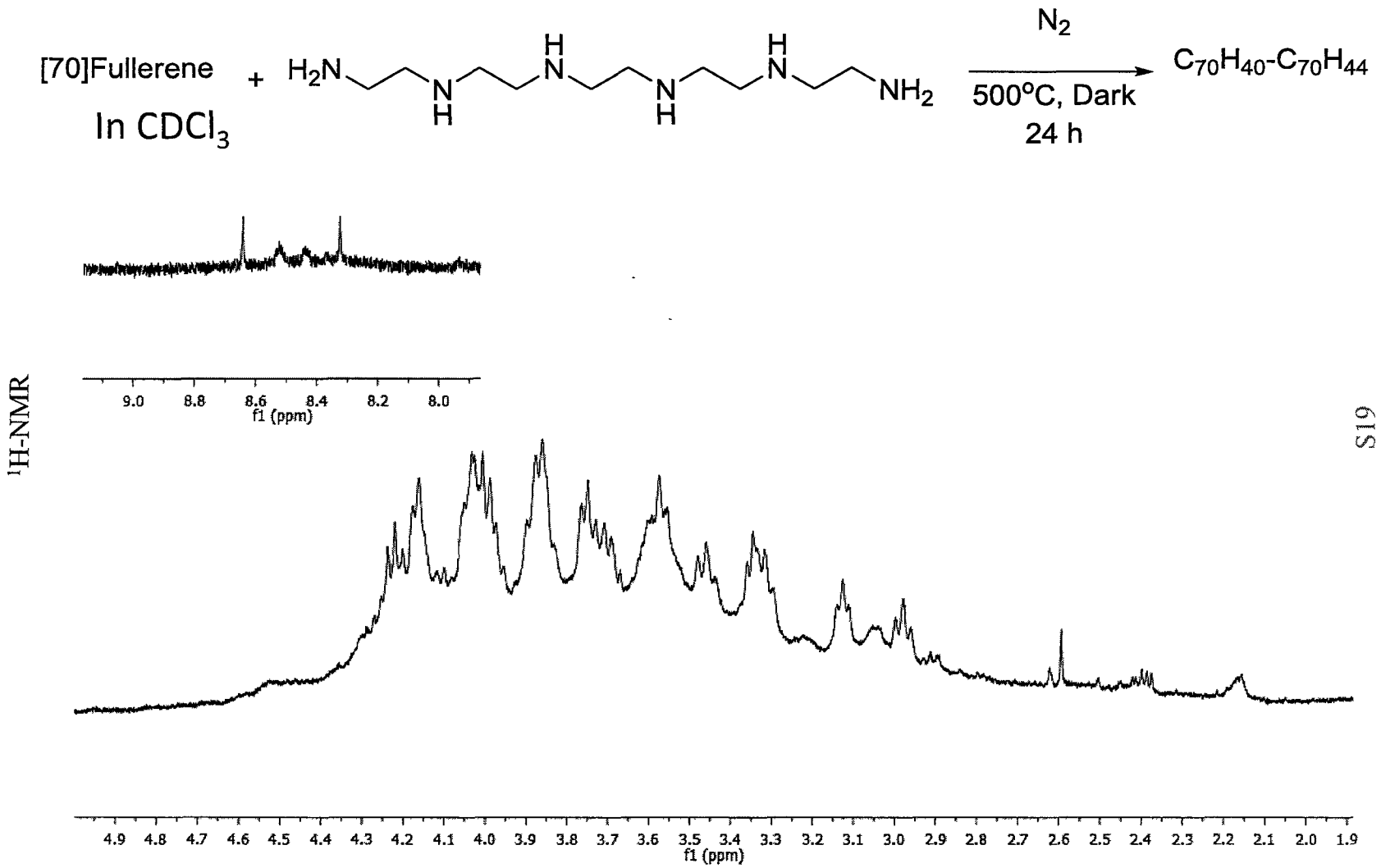
[70]Fullerene
In $CDCl_3$
+
H_2N
NH_2
N_2
500°C, Dark
24 h
$C_{70}H_{40}$-$C_{70}H_{44}$
^{1}H-NMR
9.0 8.8 8.6 8.4 8.2 8.0
f1 (ppm)
4.9 4.8 4.7 4.6 4.5 4.4 4.3 4.2 4.1 4.0 3.9 3.8 3.7 3.6 3.5 3.4 3.3 3.2 3.1 3.0 2.9 2.8 2.7 2.6 2.5 2.4 2.3 2.2 2.1 2.0 1.9
f1 (ppm)

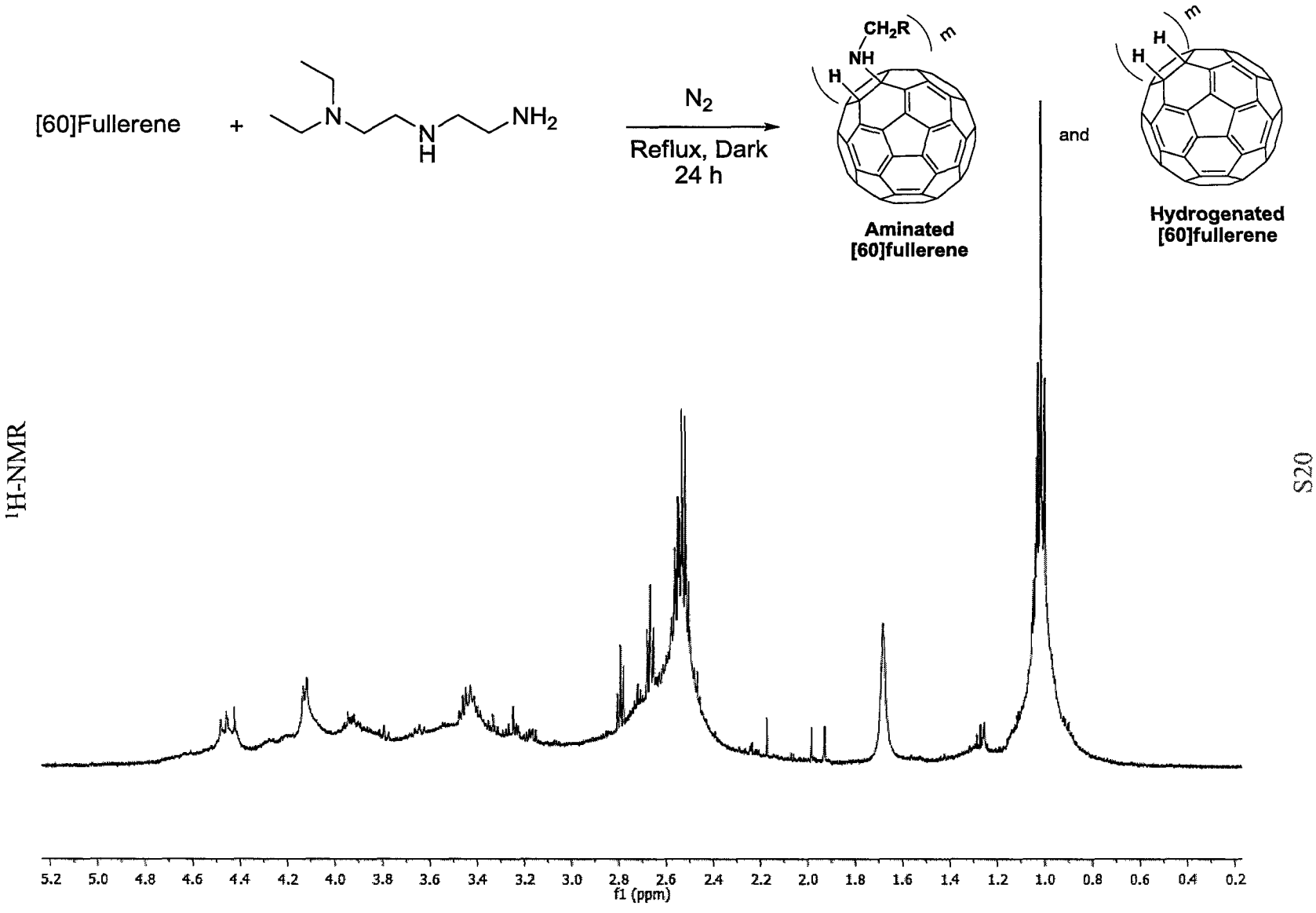
[60]Fullerene
+
N
N
H
NH2
N2
Reflux, Dark
24 h
CH2R
NH
H
m
Aminated
[60]fullerene
and
H
H
m
Hydrogenated
[60]fullerene
1H-NMR
5.2 5.0 4.8 4.6 4.4 4.2 4.0 3.8 3.6 3.4 3.2 3.0 2.8 2.6 2.4 2.2 2.0 1.8 1.6 1.4 1.2 1.0 0.8 0.6 0.4 0.2
f1 (ppm)

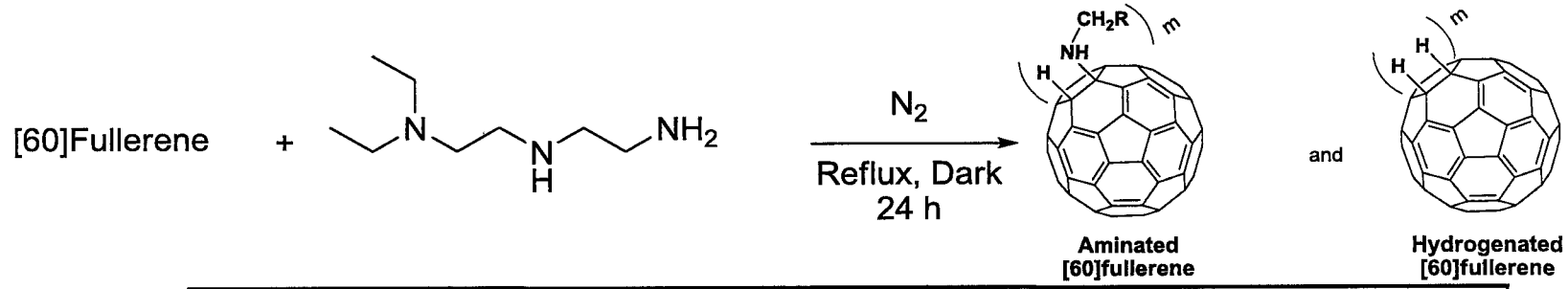
[60]Fullerene
+
N
N
H
NH2
N2
Reflux, Dark
24 h
CH2R
NH
H
m
and
H
H
m
Aminated
[60]fullerene
Hydrogenated
[60]fullerene

Mass Spec

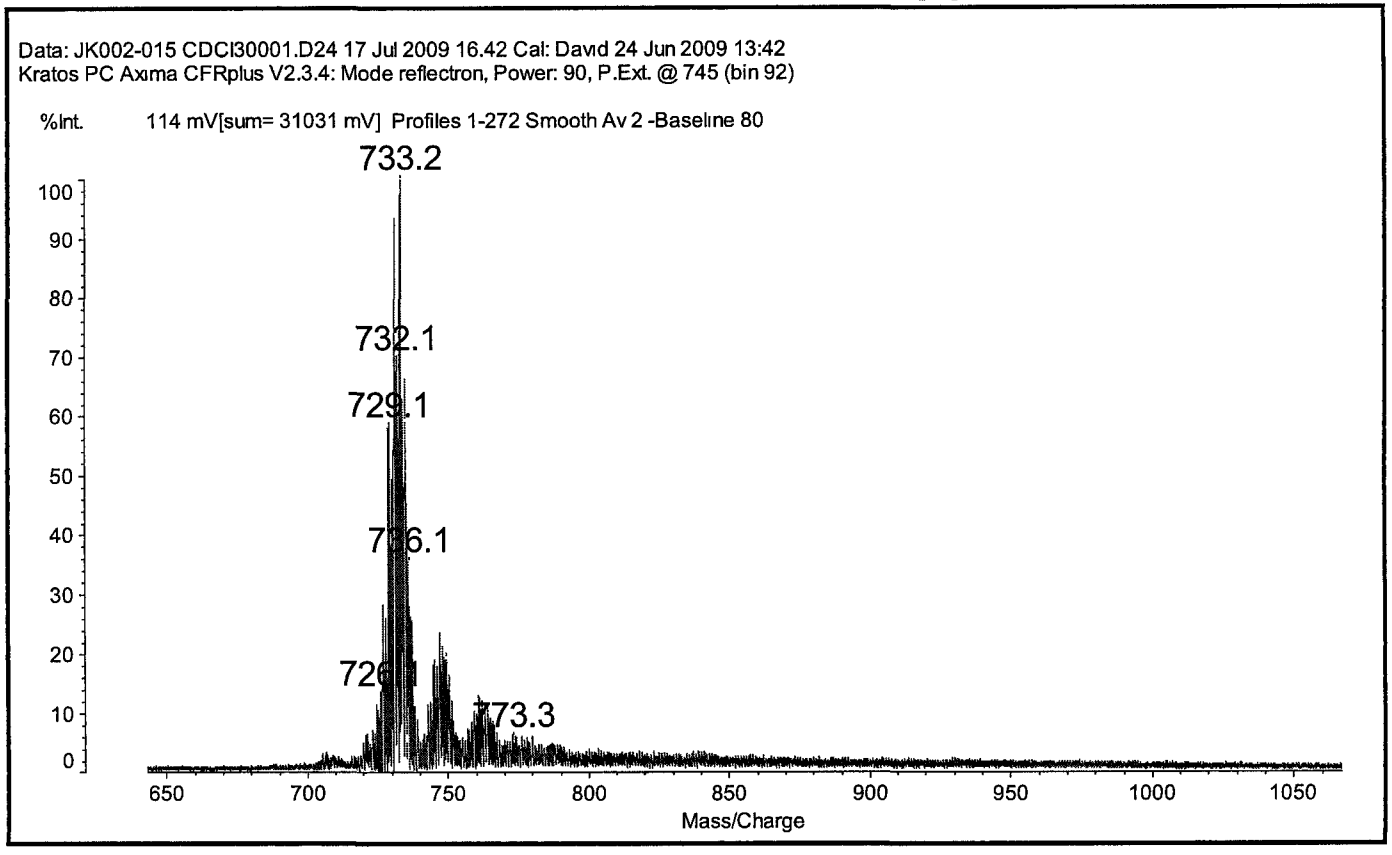
Data: JK002-015 CDCl30001.D24 17 Jul 2009 16.42 Cal: David 24 Jun 2009 13:42
Kratos PC Axima CFRplus V2.3.4: Mode reflectron, Power: 90, P.Ext. @ 745 (bin 92)
%Int.
114 mV[sum= 31031 mV] Profiles 1-272 Smooth Av 2 -Baseline 80
733.2
732.1
729.1
716.1
726.1
773.3
100
90
80
70
60
50
40
30
20
10
0
650
700
750
800
850
900
950
1000
1050
Mass/Charge

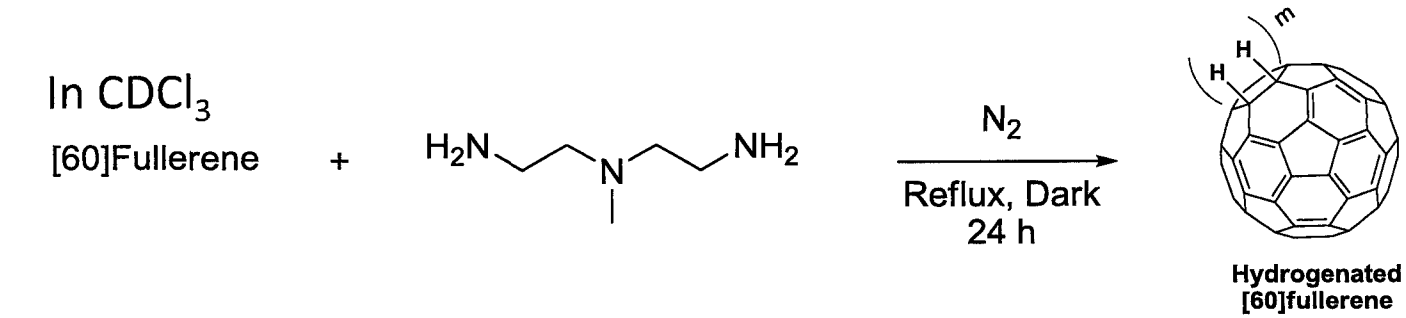
In $CDCl_3$
[60]Fullerene
+
H_2N
N
NH_2
N_2
Reflux, Dark
24 h
H
H
m
Hydrogenated
[60]fullerene

^{1}H-NMR

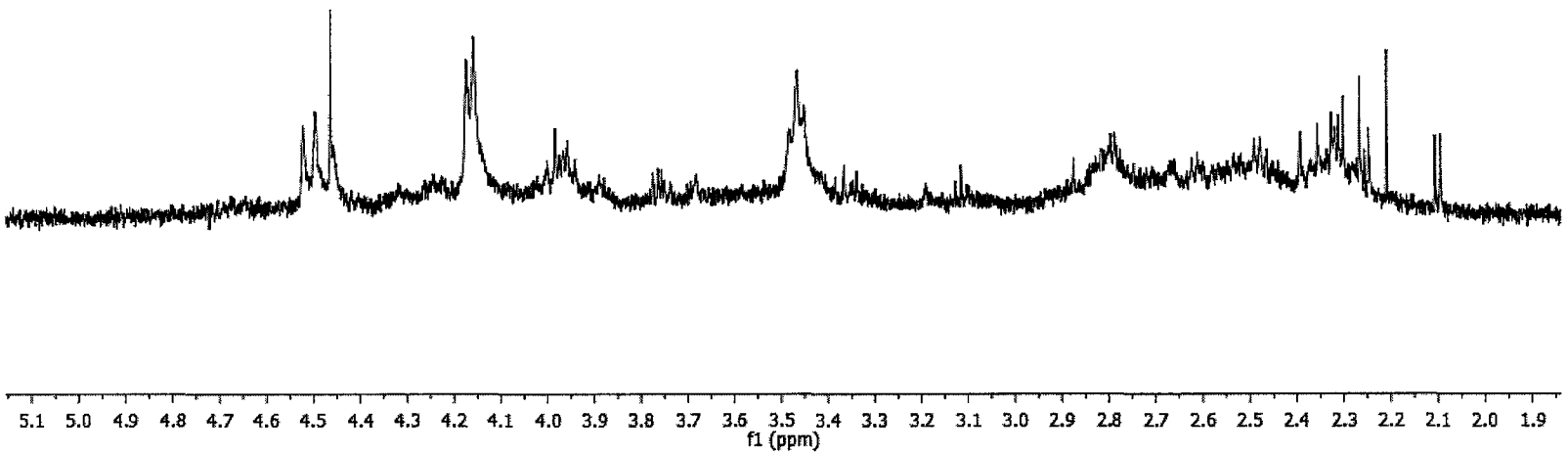
5.1 5.0 4.9 4.8 4.7 4.6 4.5 4.4 4.3 4.2 4.1 4.0 3.9 3.8 3.7 3.6 3.5 3.4 3.3 3.2 3.1 3.0 2.9 2.8 2.7 2.6 2.5 2.4 2.3 2.2 2.1 2.0 1.9
f1 (ppm)

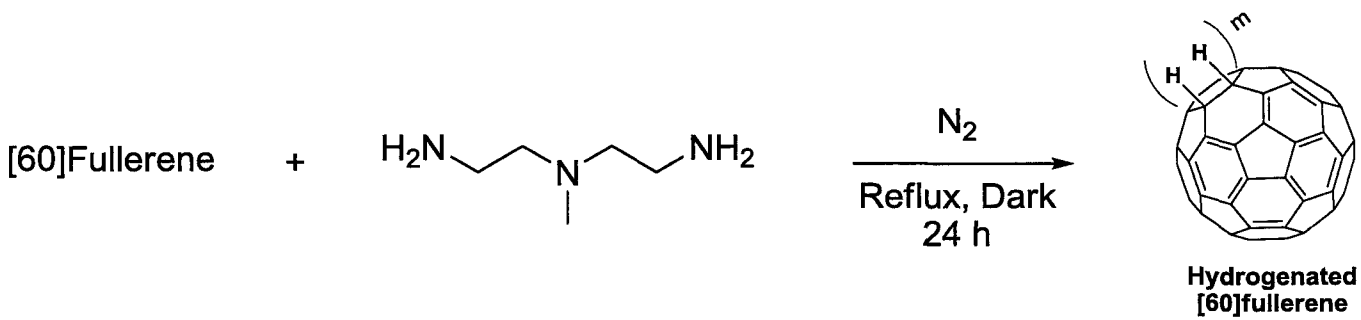
[60]Fullerene
+
H_2N
N
NH_2
N_2
Reflux, Dark
24 h
H
H
m
Hydrogenated
[60]fullerene

Mass Spec

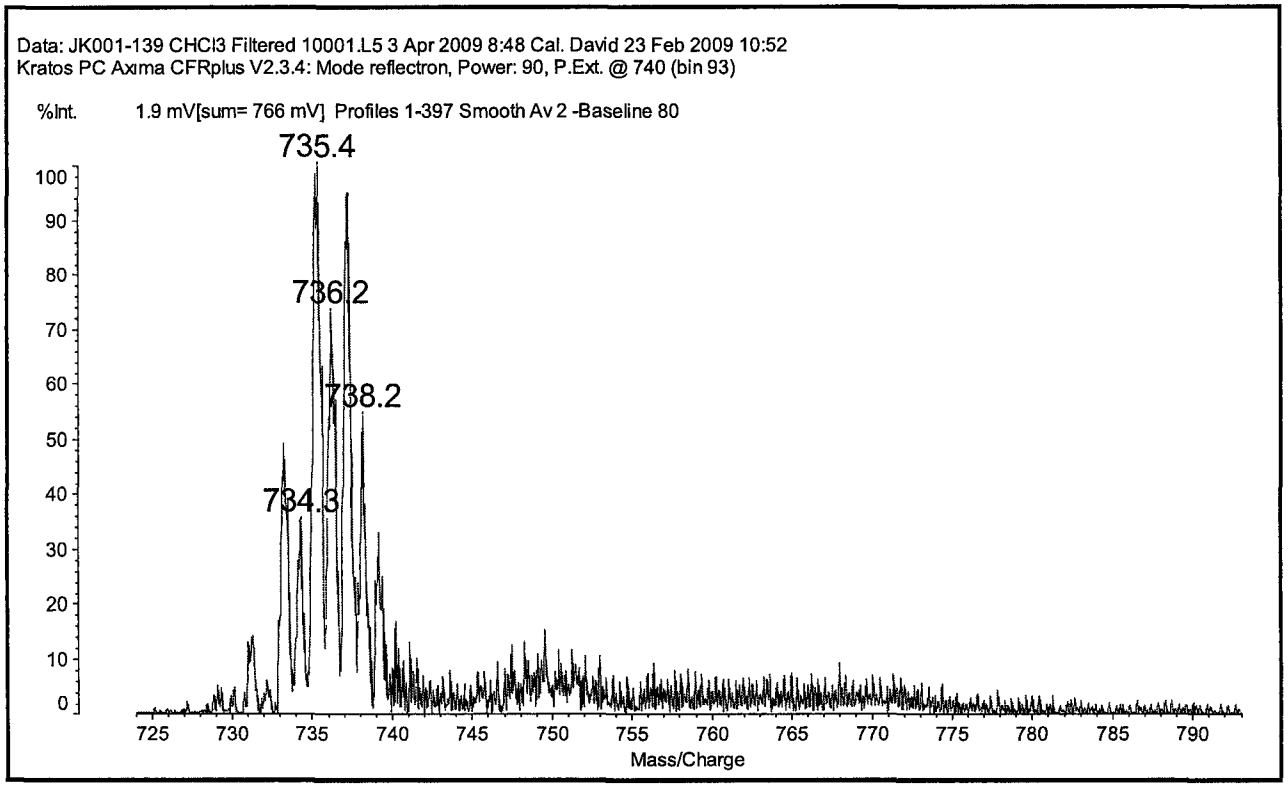
Data: JK001-139 CHCl3 Filtered 10001.L5 3 Apr 2009 8:48 Cal. David 23 Feb 2009 10:52
Kratos PC Axima CFRplus V2.3.4: Mode reflectron, Power: 90, P.Ext. @ 740 (bin 93)
%Int.
1.9 mV[sum= 766 mV] Profiles 1-397 Smooth Av 2 -Baseline 80
735.4
736.2
738.2
734.3
100
90
80
70
60
50
40
30
20
10
0
725
730
735
740
745
750
755
760
765
770
775
780
785
790
Mass/Charge

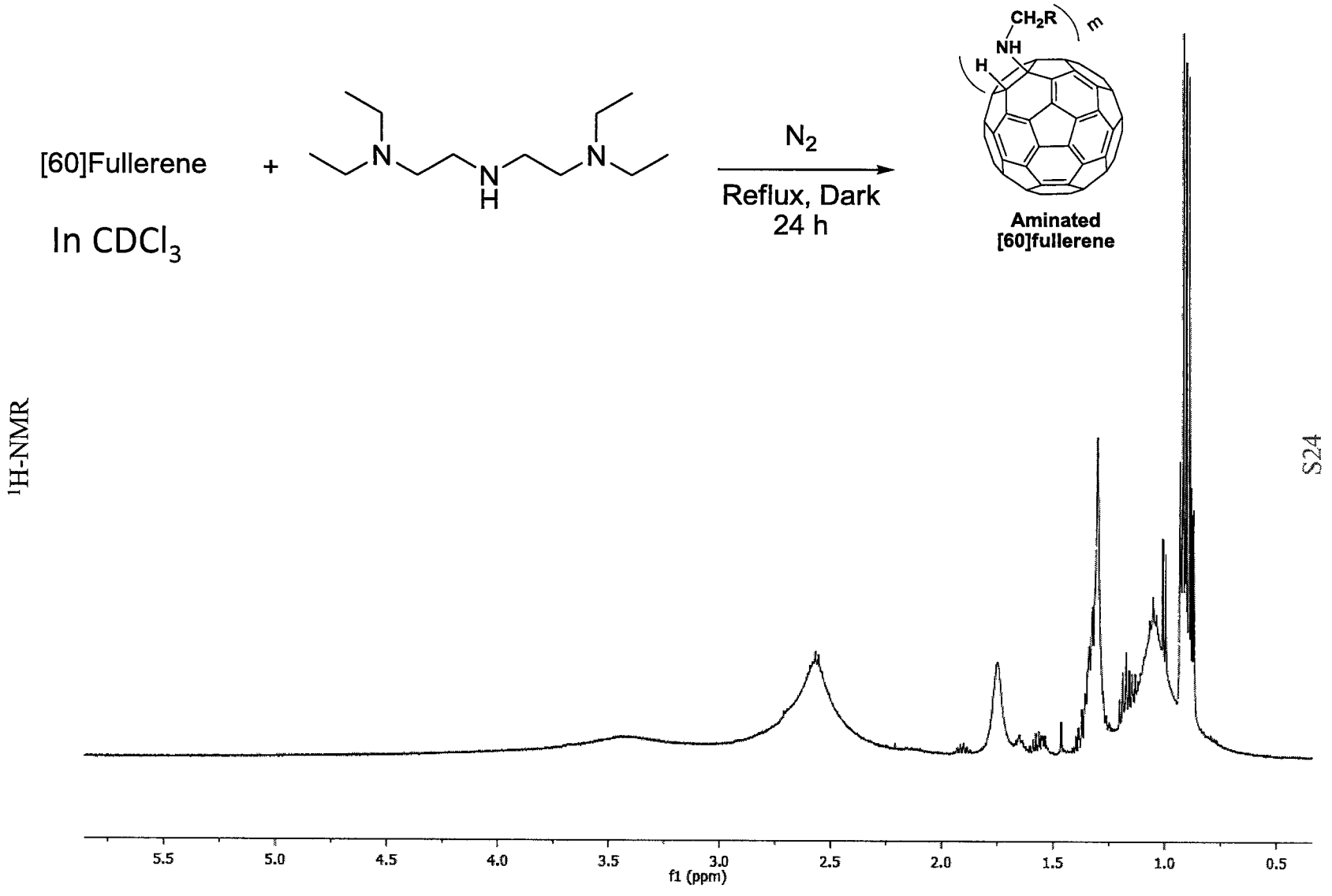
[60]Fullerene
+
In $CDCl_3$
N_2
Reflux, Dark
24 h
CH_2R
m
NH
H
Aminated
[60]fullerene
^{1}H-NMR
5.5
5.0
4.5
4.0
3.5
3.0
2.5
2.0
1.5
1.0
0.5
f1 (ppm)

Mass Spec

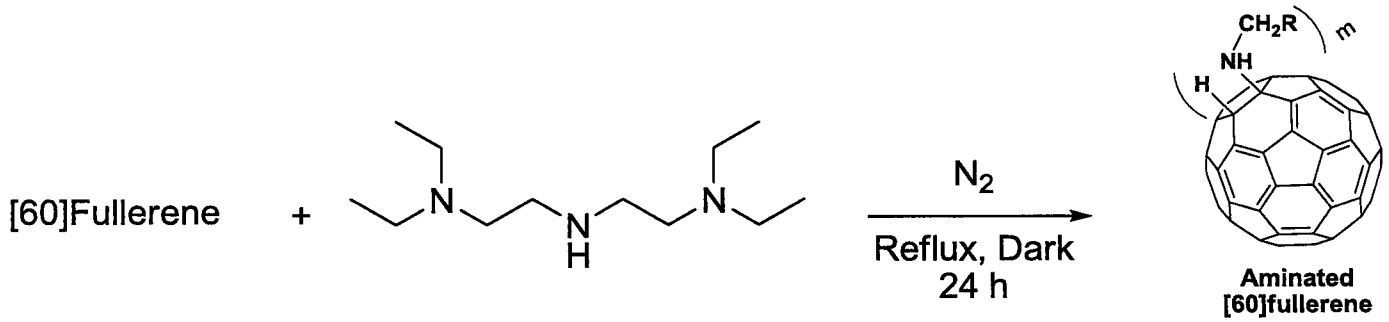
[60]Fullerene
+
N
N
H
N
N_2
Reflux, Dark
24 h
CH_2R
m
NH
H
Aminated
[60]fullerene

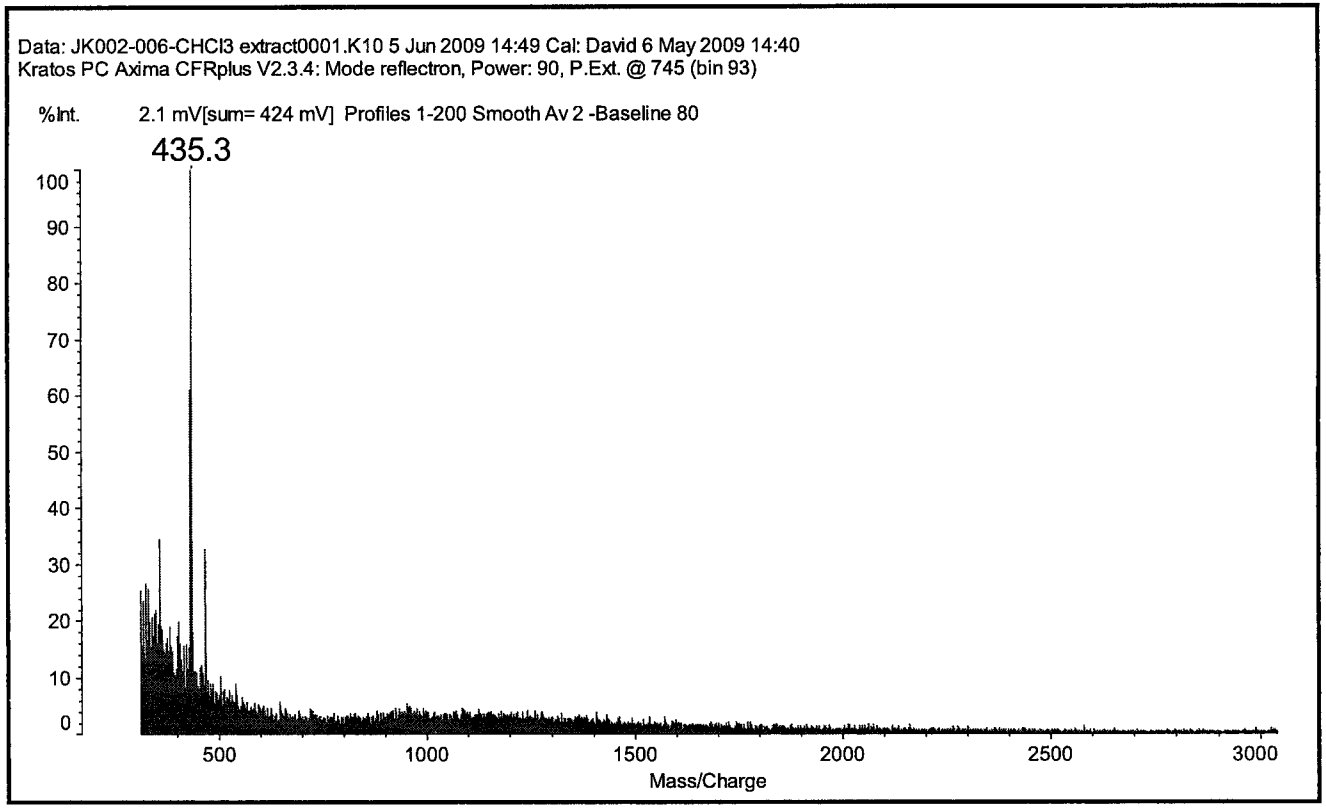
Data: JK002-006-CHCl3 extract0001.K10 5 Jun 2009 14:49 Cal: David 6 May 2009 14:40
Kratos PC Axima CFRplus V2.3.4: Mode reflectron, Power: 90, P.Ext. @ 745 (bin 93)
%Int.
2.1 mV[sum= 424 mV] Profiles 1-200 Smooth Av 2 -Baseline 80
435.3
100
90
80
70
60
50
40
30
20
10
0
500
1000
1500
2000
2500
3000
Mass/Charge

In d_6-Acetone

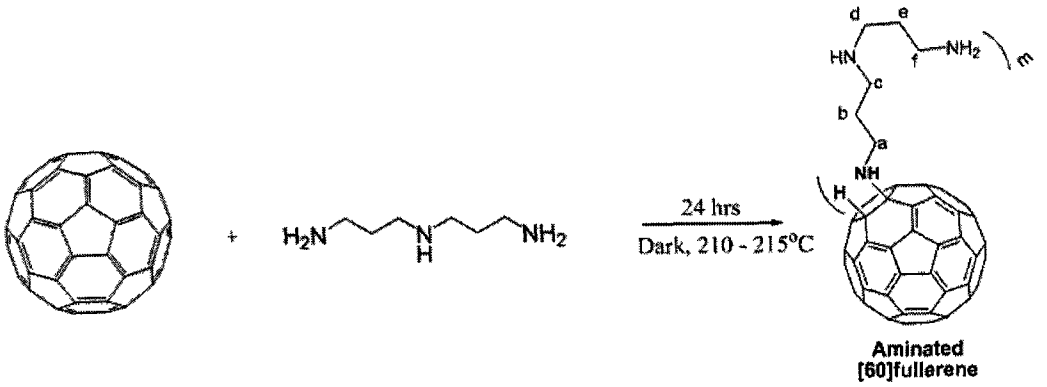

^{1}H-NMR

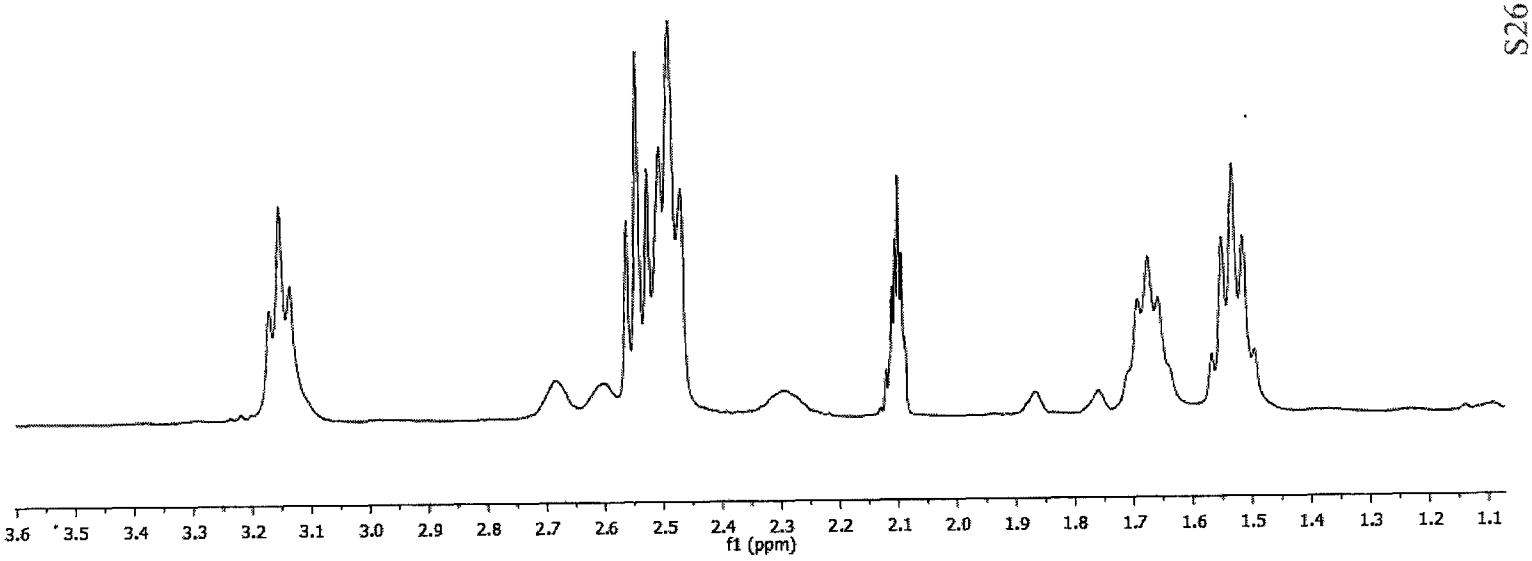

Mass Spec

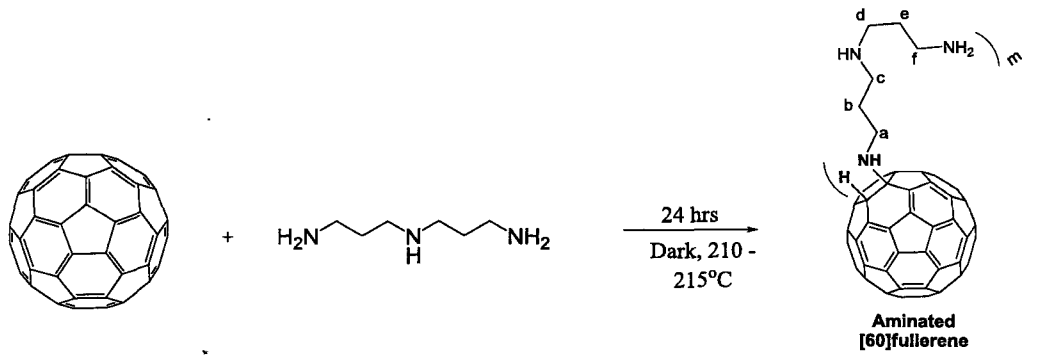
d
e
HN
f
NH2
n
c
b
a
NH
H
24 hrs
Dark, 210 - 215°C
Aminated [60]fullerene

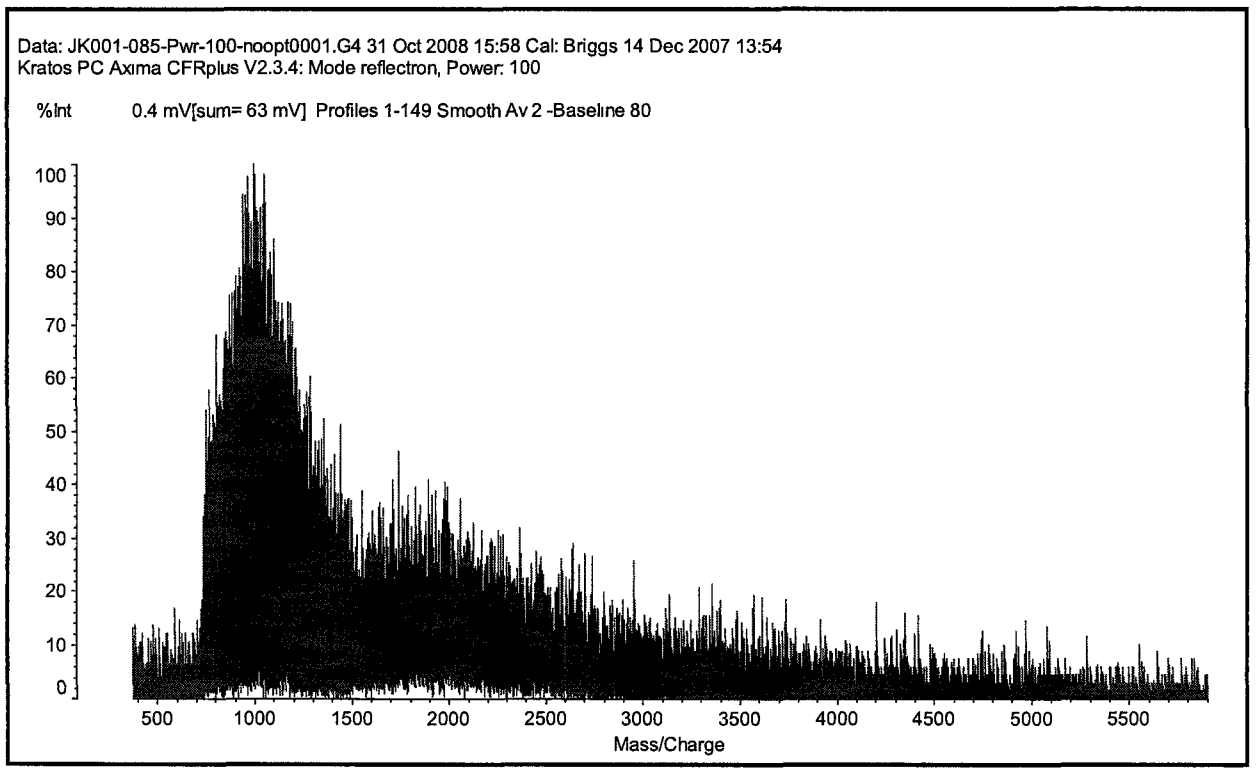
Data: JK001-085-Pwr-100-noopt0001.G4 31 Oct 2008 15:58 Cal: Briggs 14 Dec 2007 13:54
Kratos PC Axima CFRplus V2.3.4: Mode reflectron, Power: 100
%Int
0.4 mV[sum= 63 mV] Profiles 1-149 Smooth Av 2 -Baseline 80
100
90
80
70
60
50
40
30
20
10
0
500
1000
1500
2000
2500
3000
3500
4000
4500
5000
5500
Mass/Charge

Mass Spec

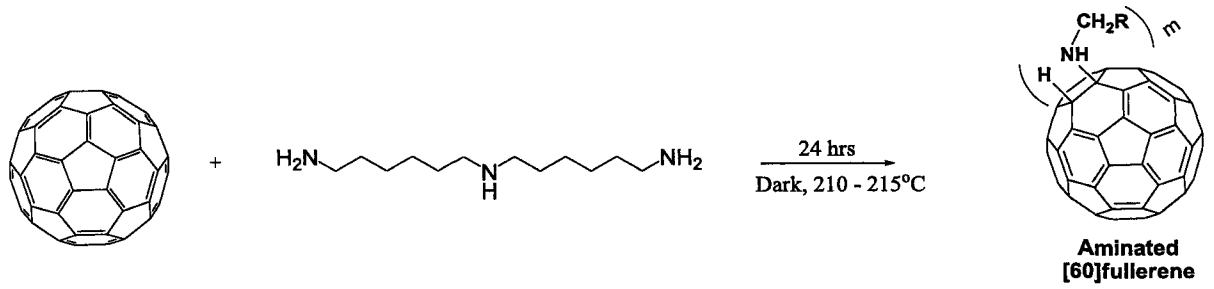
+
H_2N
N
H
NH_2
24 hrs
Dark, 210 - 215°C
CH_2R
m
NH
H
Aminated
[60]fullerene

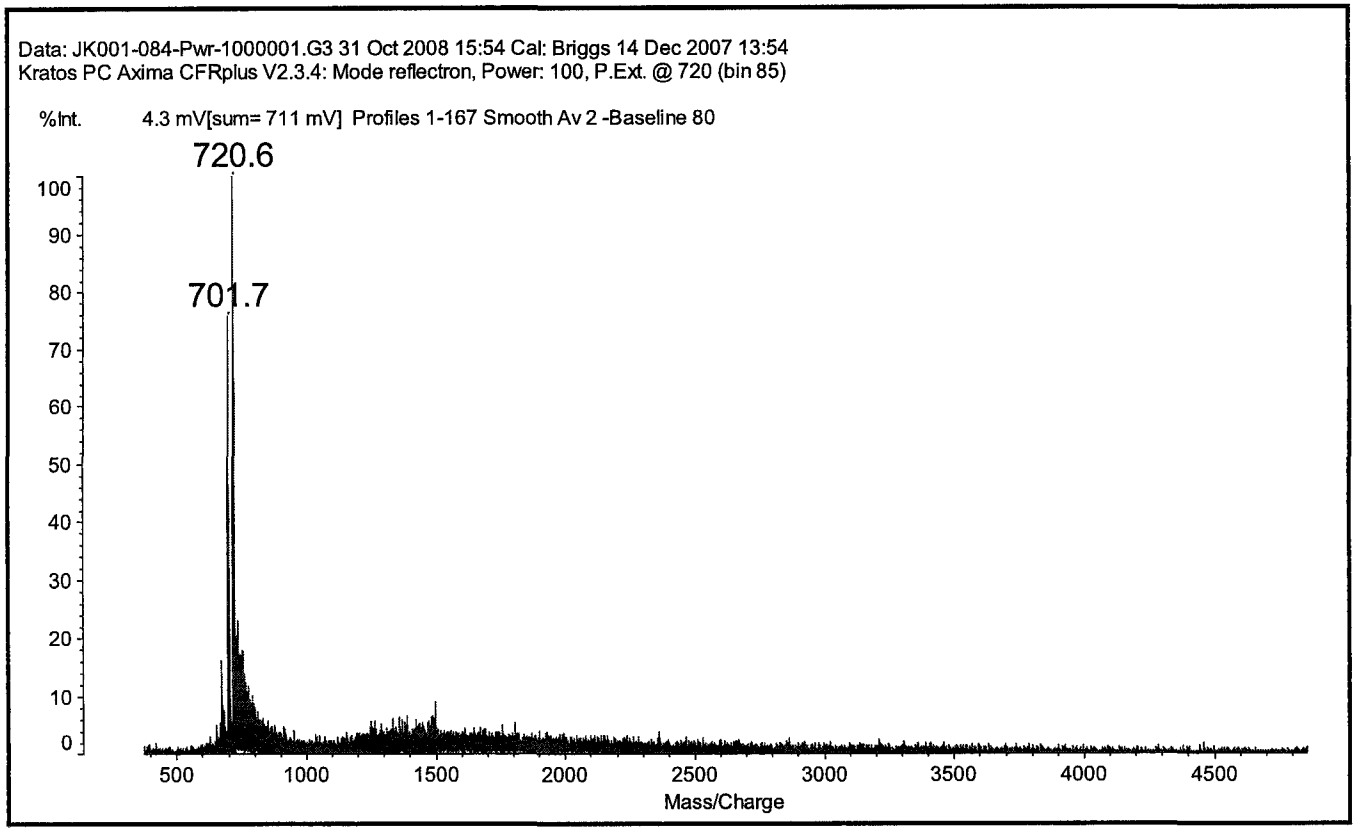
Data: JK001-084-Pwr-1000001.G3 31 Oct 2008 15:54 Cal: Briggs 14 Dec 2007 13:54
Kratos PC Axima CFRplus V2.3.4: Mode reflectron, Power: 100, P.Ext. @ 720 (bin 85)
%Int.
4.3 mV[sum= 711 mV] Profiles 1-167 Smooth Av 2 -Baseline 80
720.6
701.7
100
90
80
70
60
50
40
30
20
10
0
500
1000
1500
2000
2500
3000
3500
4000
4500
Mass/Charge

Mass Spec

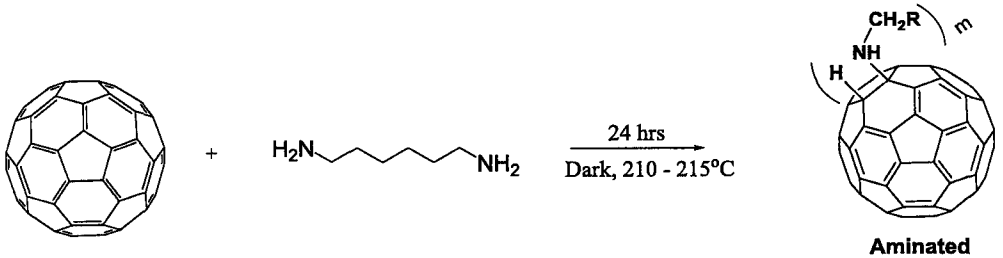

Aminated [60]fullerene

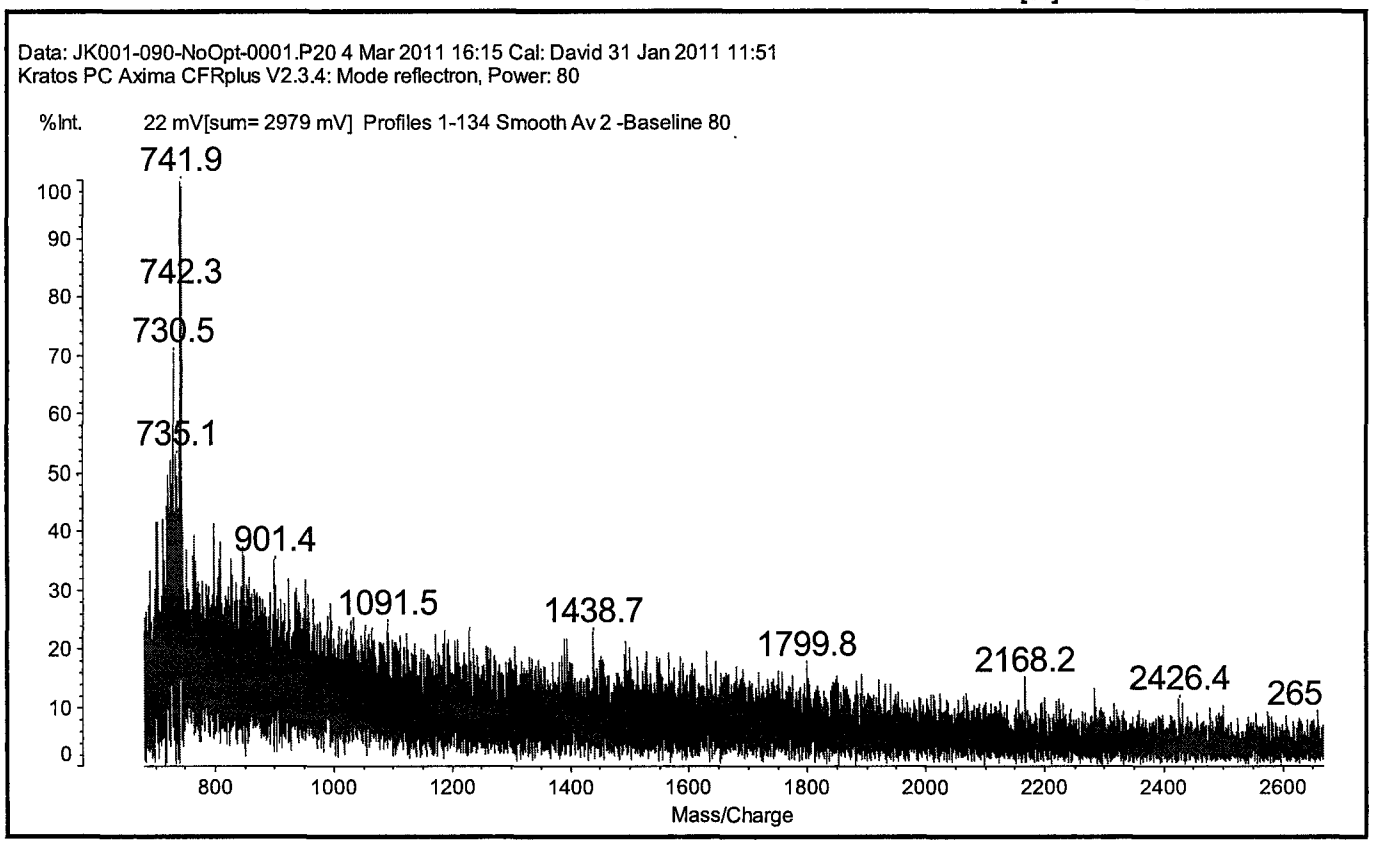

Mass Spec

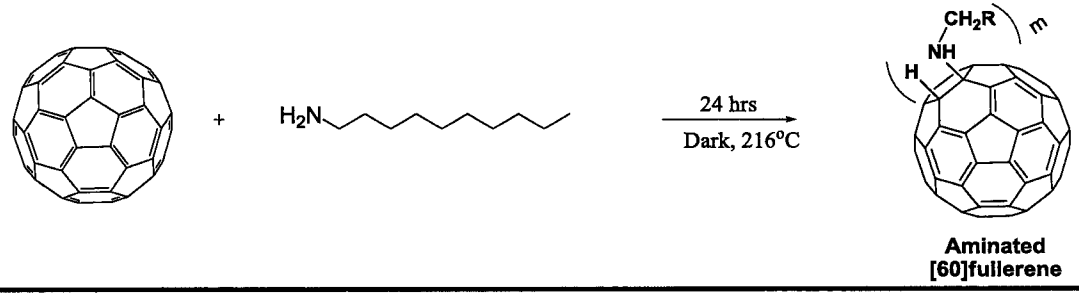

Aminated [60]fullerene

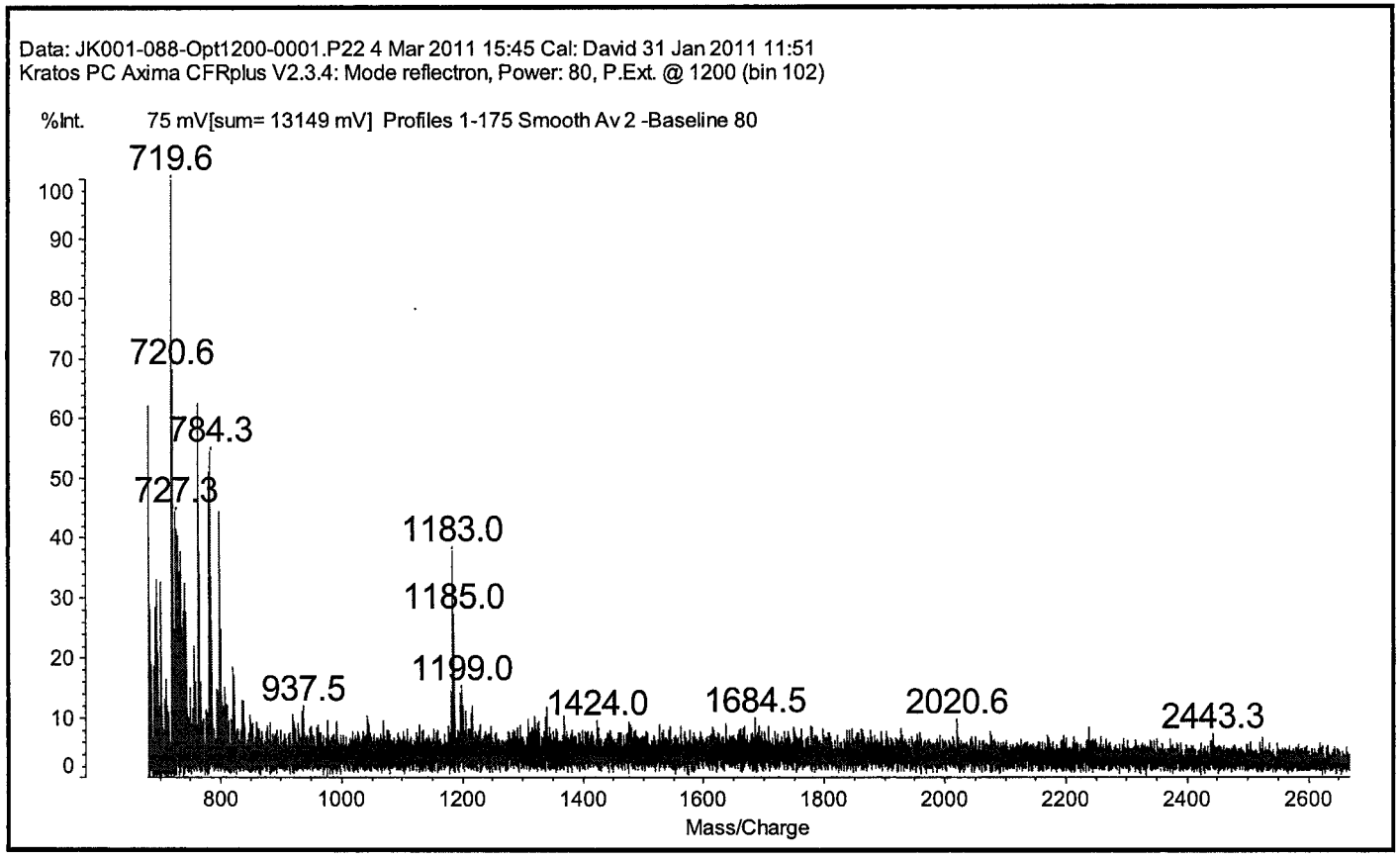

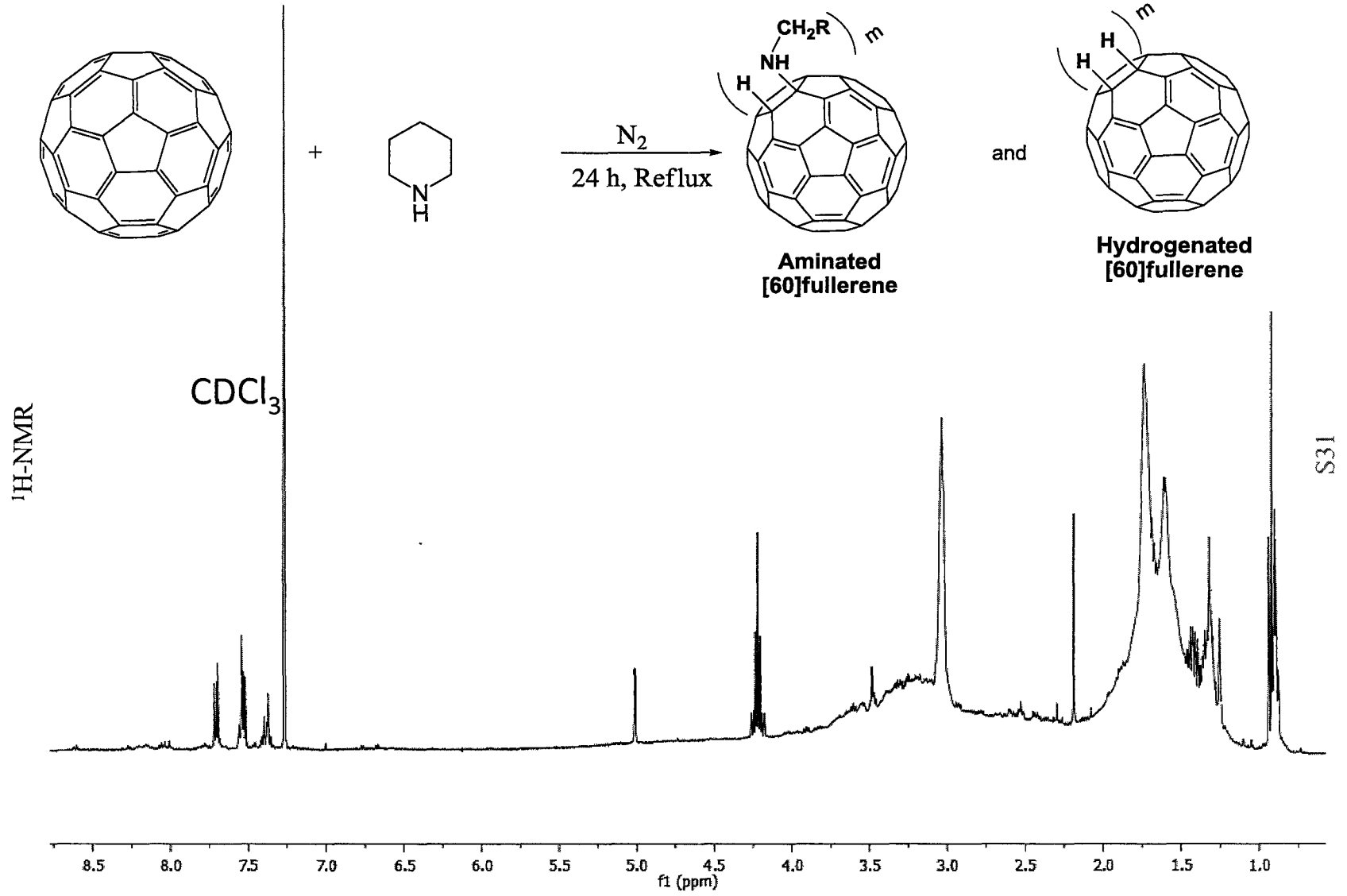
CH2R
m
NH
H
N2
24 h, Reflux
and
H
H
m
Aminated
[60]fullerene
Hydrogenated
[60]fullerene
CDCl3
1H-NMR
S31
8.5
8.0
7.5
7.0
6.5
6.0
5.5
5.0
4.5
4.0
3.5
3.0
2.5
2.0
1.5
1.0
f1 (ppm)

Mass Spec

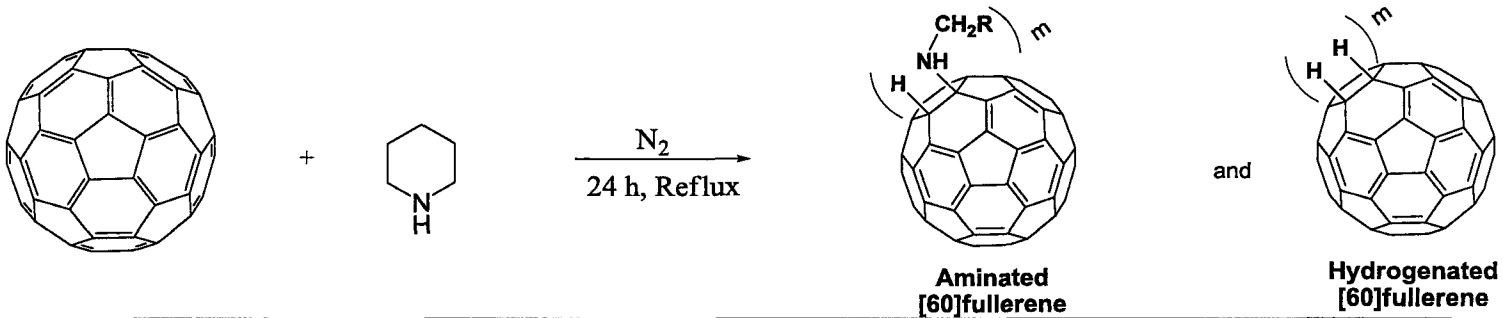

Aminated [60]fullerene

Hydrogenated [60]fullerene

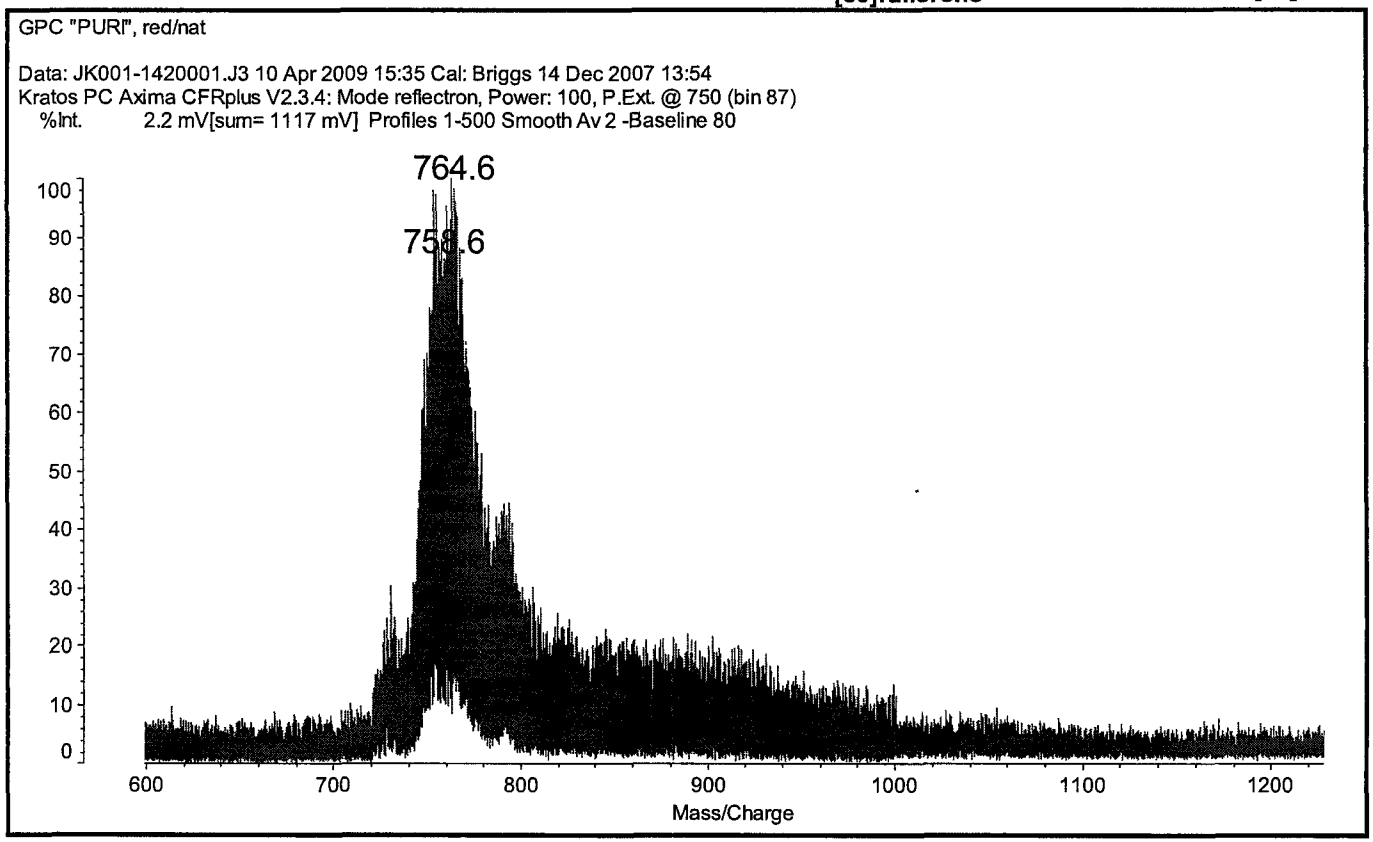

Mass Spec

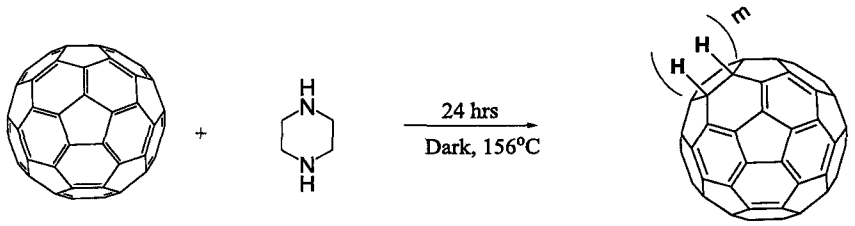

Hydrogenated [60]fullerene

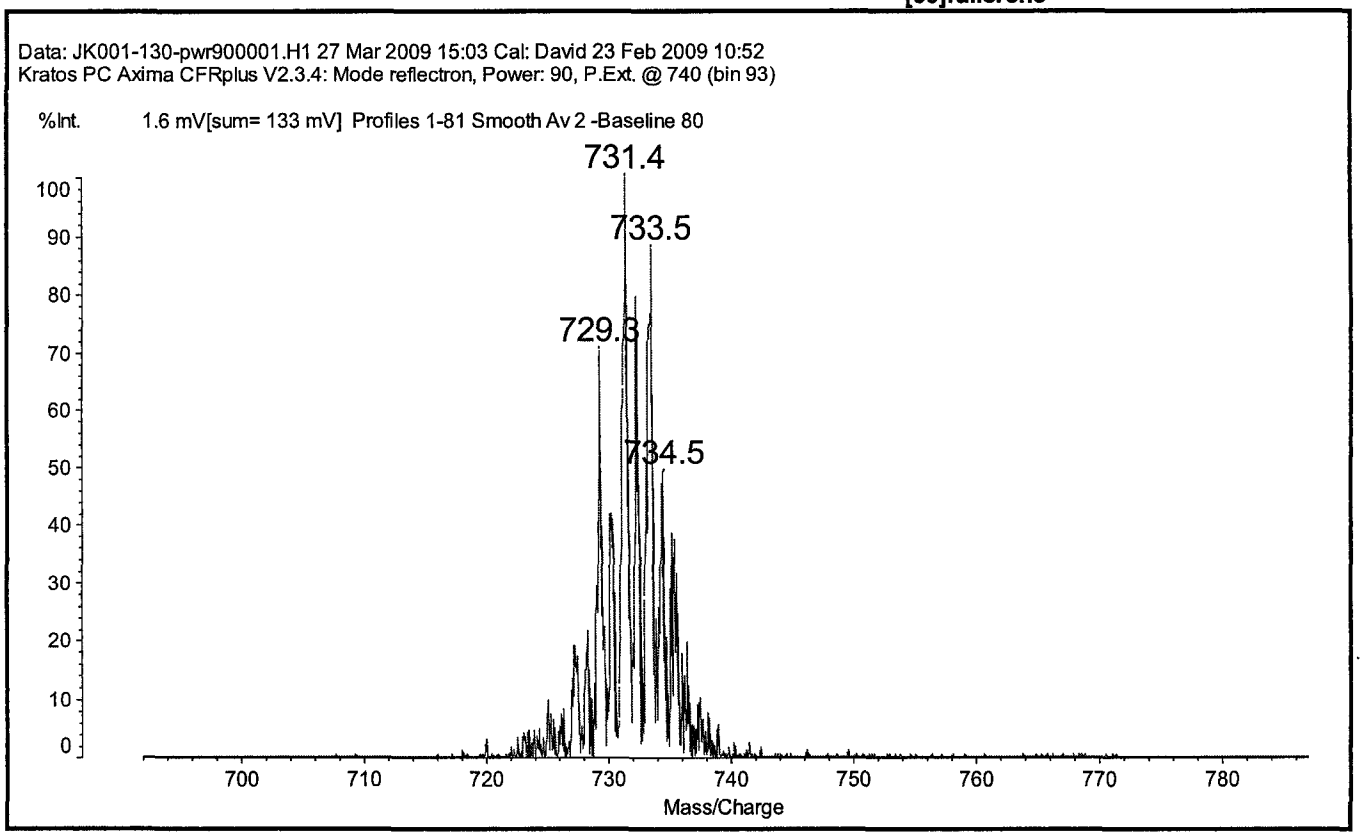

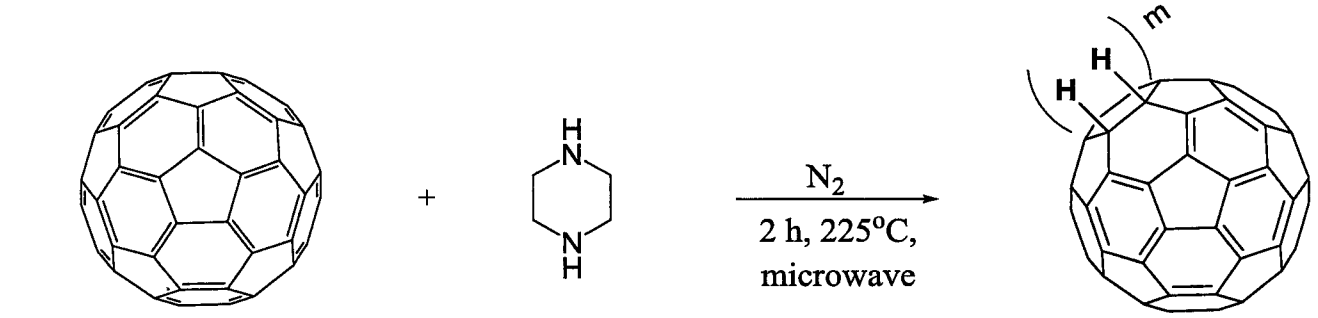
In $CDCl_3$
N_2
2 h, 225°C,
microwave
H
H
m
Hydrogenated
[60]fullerene

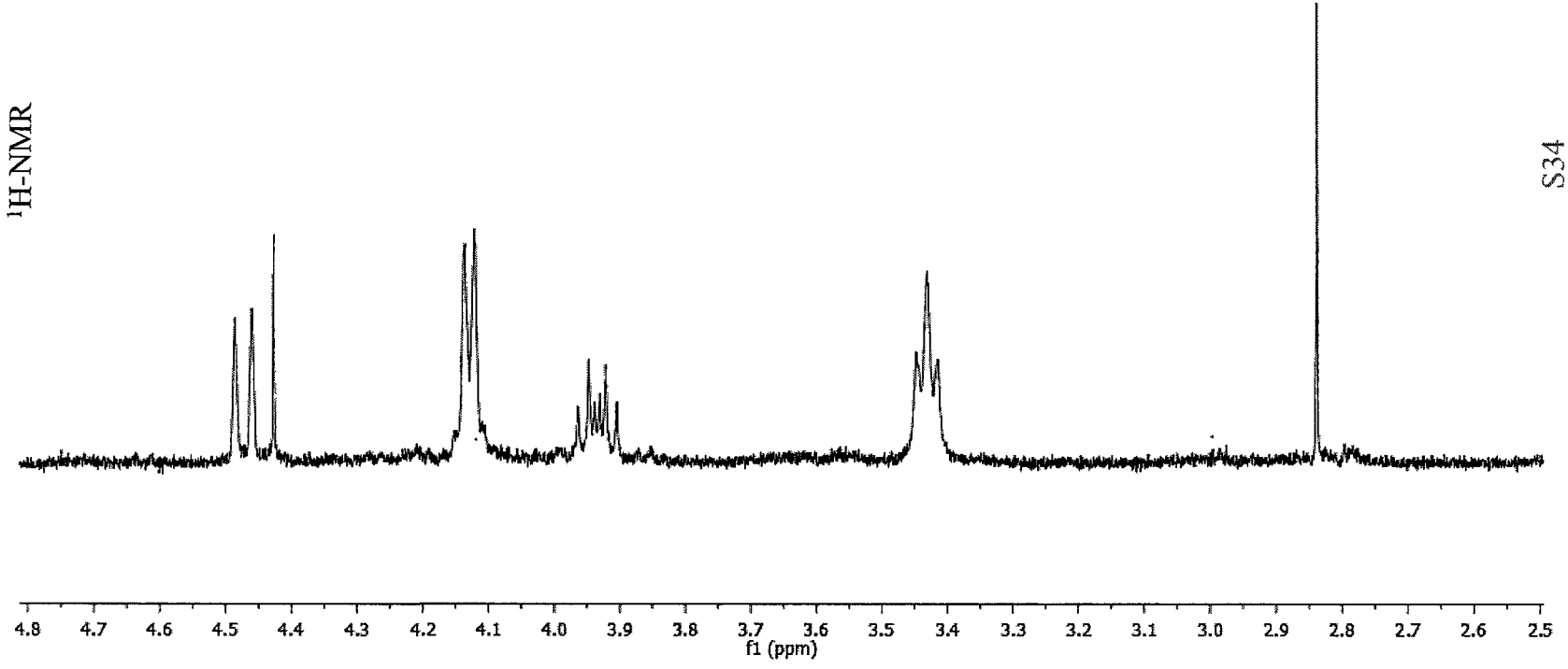
^{1}H-NMR
4.8 4.7 4.6 4.5 4.4 4.3 4.2 4.1 4.0 3.9 3.8 3.7 3.6 3.5 3.4 3.3 3.2 3.1 3.0 2.9 2.8 2.7 2.6 2.5
f1 (ppm)

TEM Image
Hydrogenated SWNTs

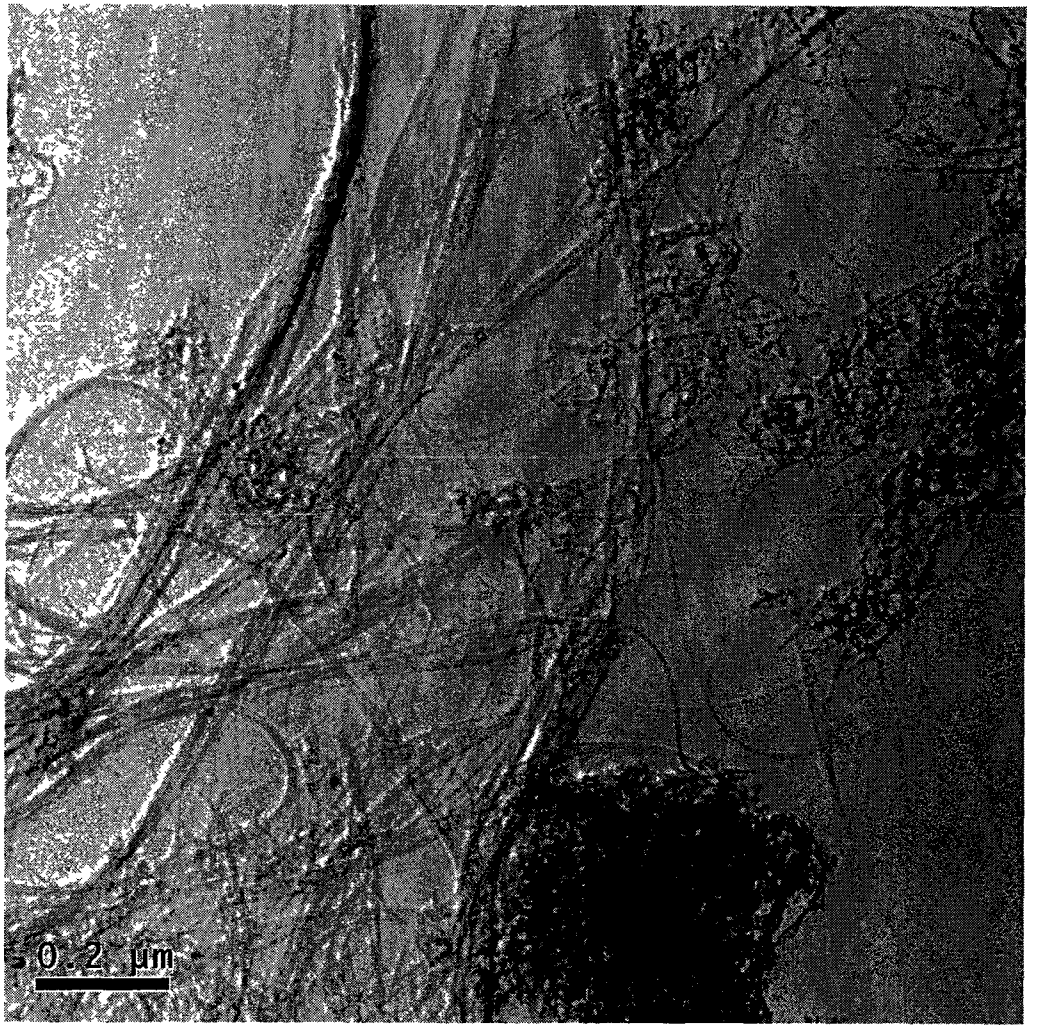

TEM Image
Hydrogenated SWNTs

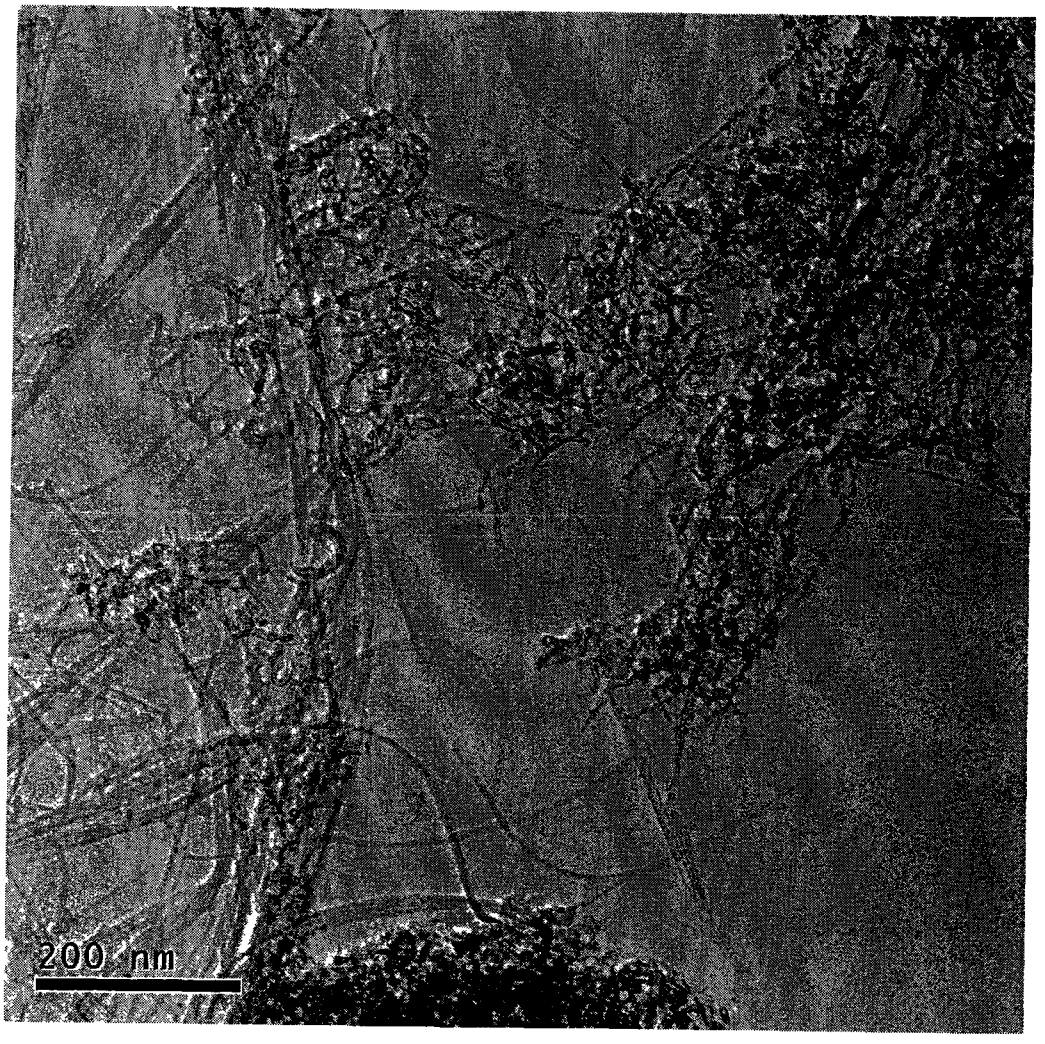

TEM Image
Hydrogenated SWNTs

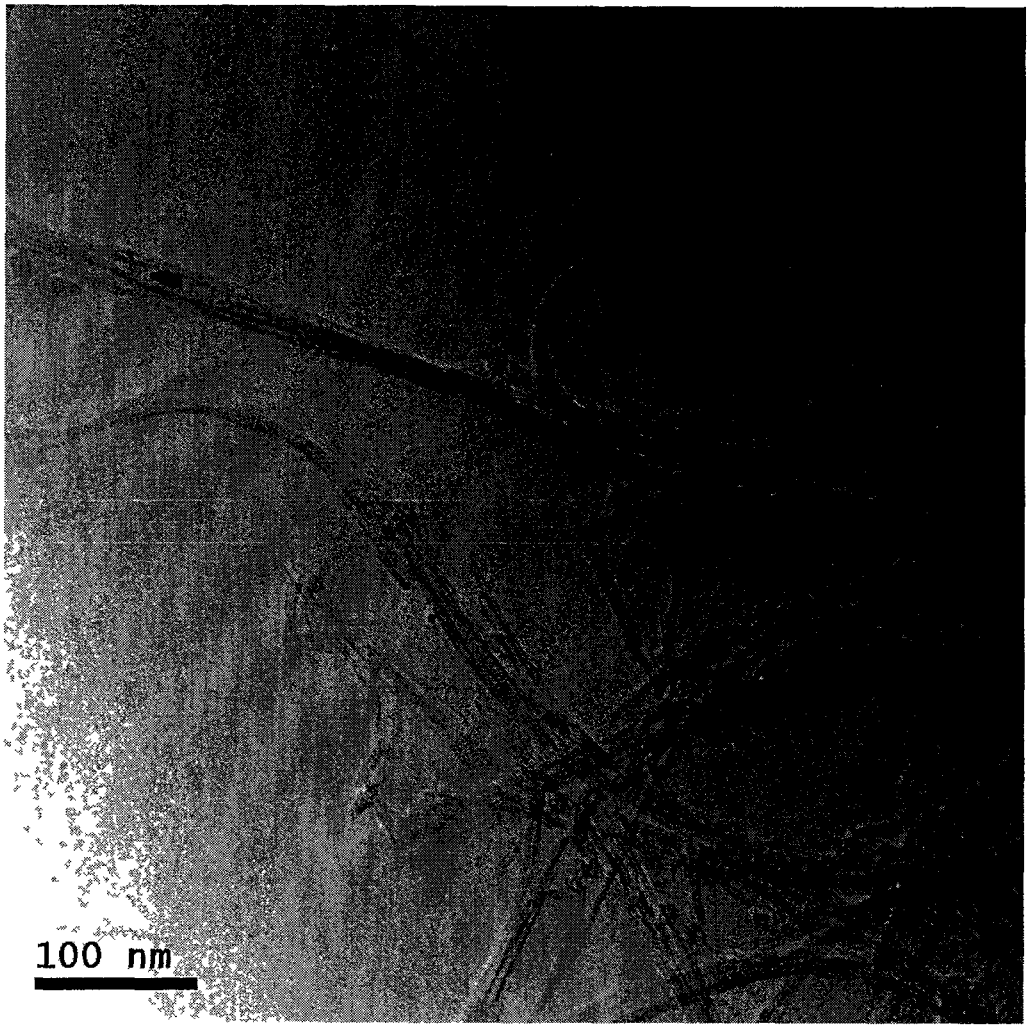

TEM Image
Hydrogenated SWNTs

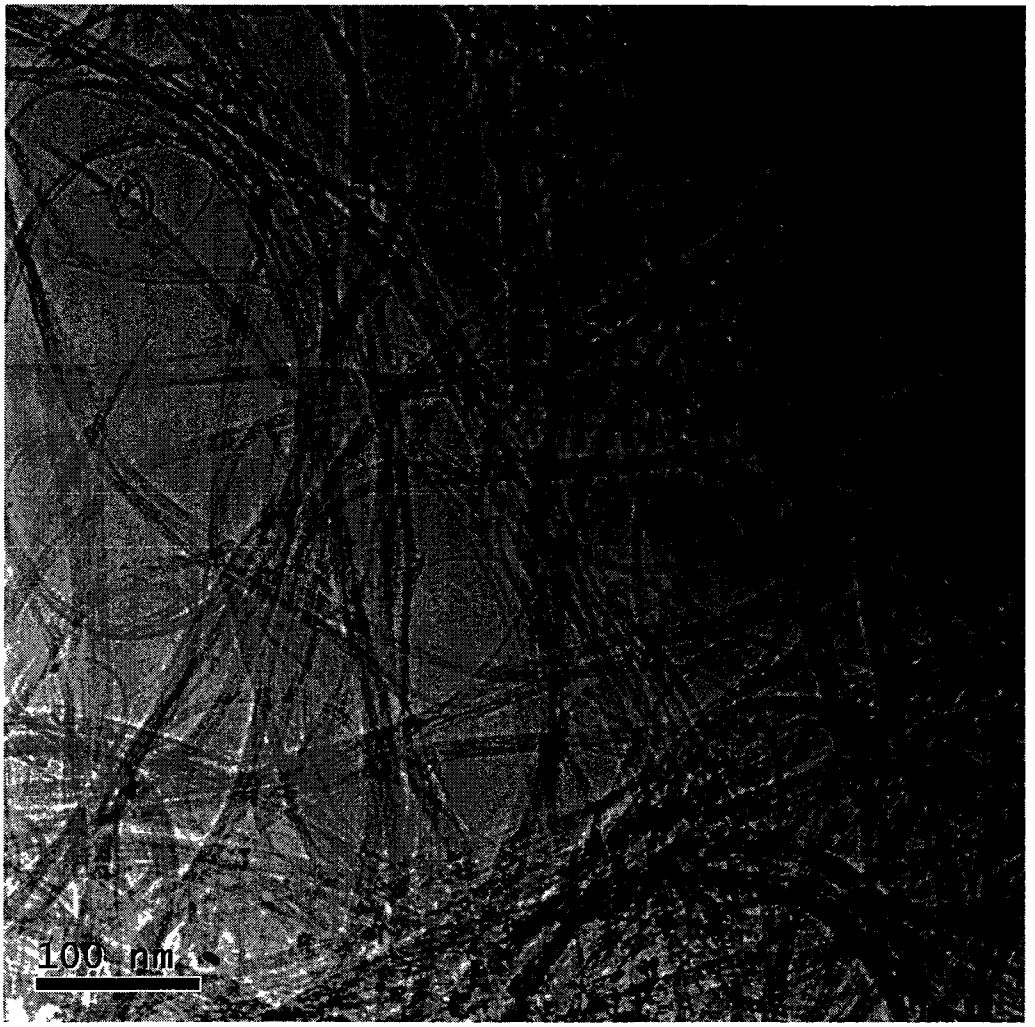

TEM Image
Hydrogenated SWNTs

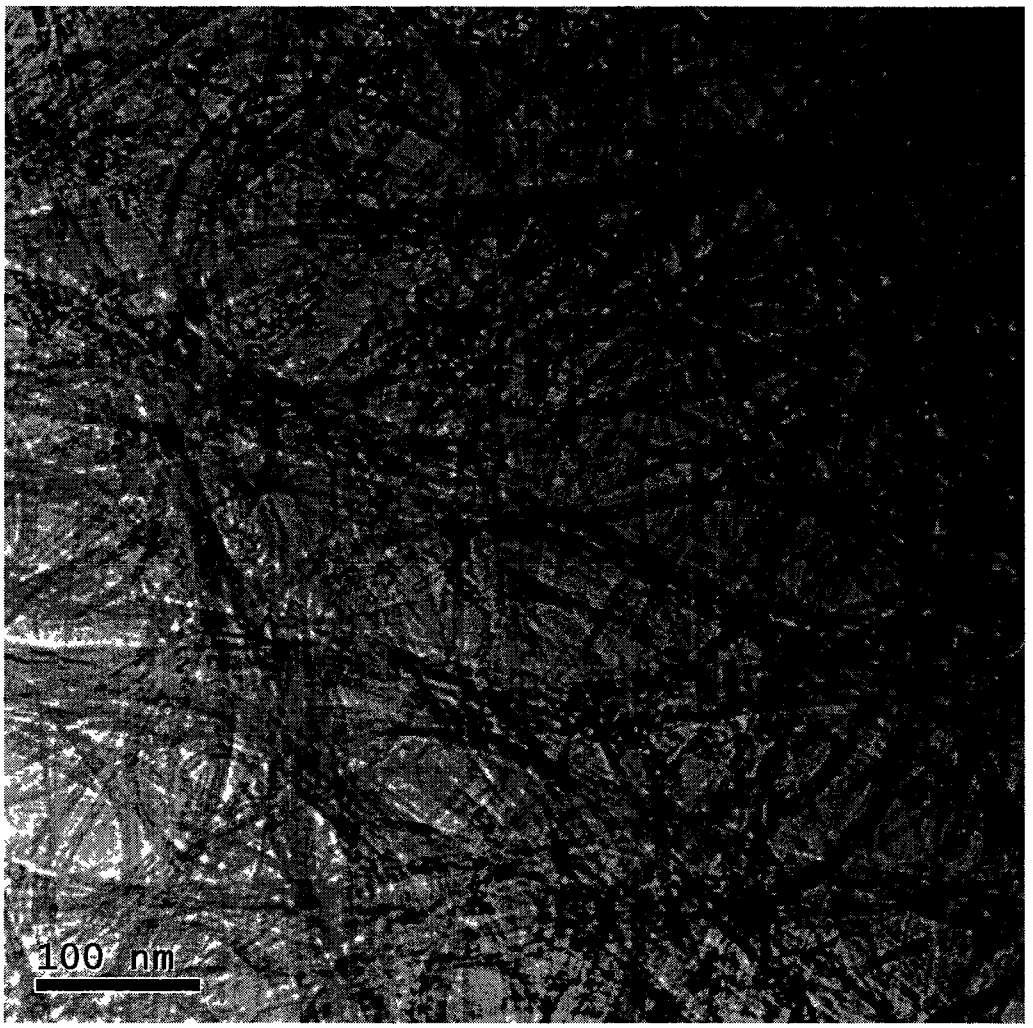

TEM Image
Hydrogenated SWNTs

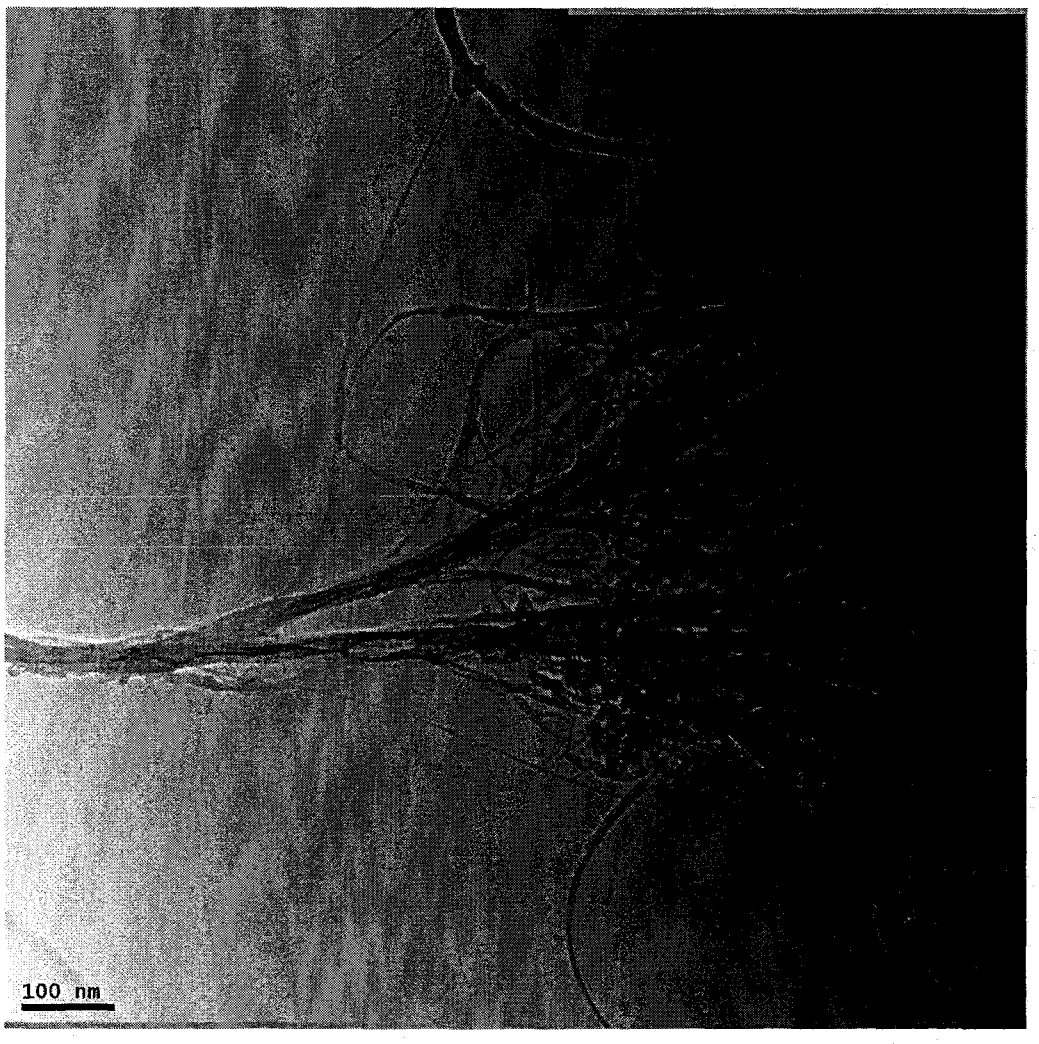

TEM Image
Hydrogenated SWNTs

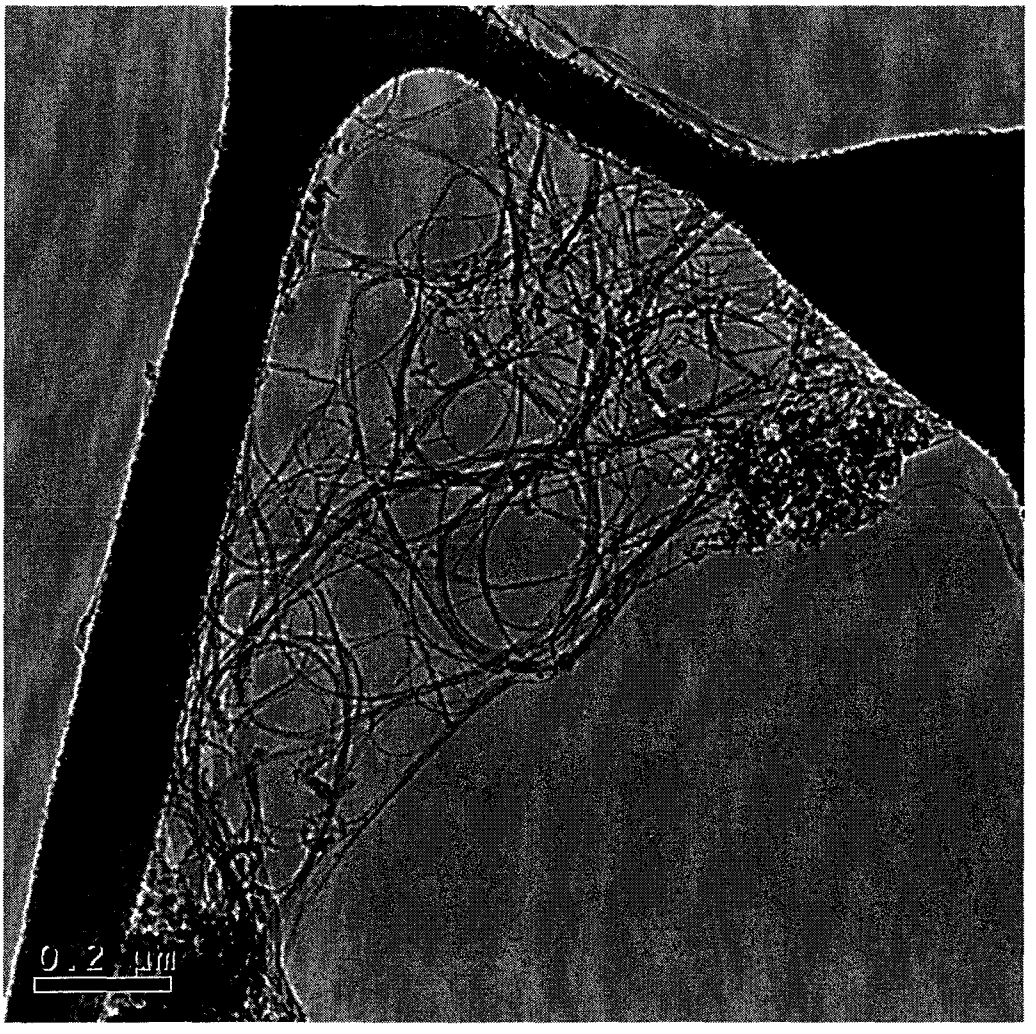

TEM Image
Hydrogenated SWNTs

TEM Image
Hydrogenated SWNTs after thermal annealing

TEM Image
Hydrogenated SWNTs after thermal annealing

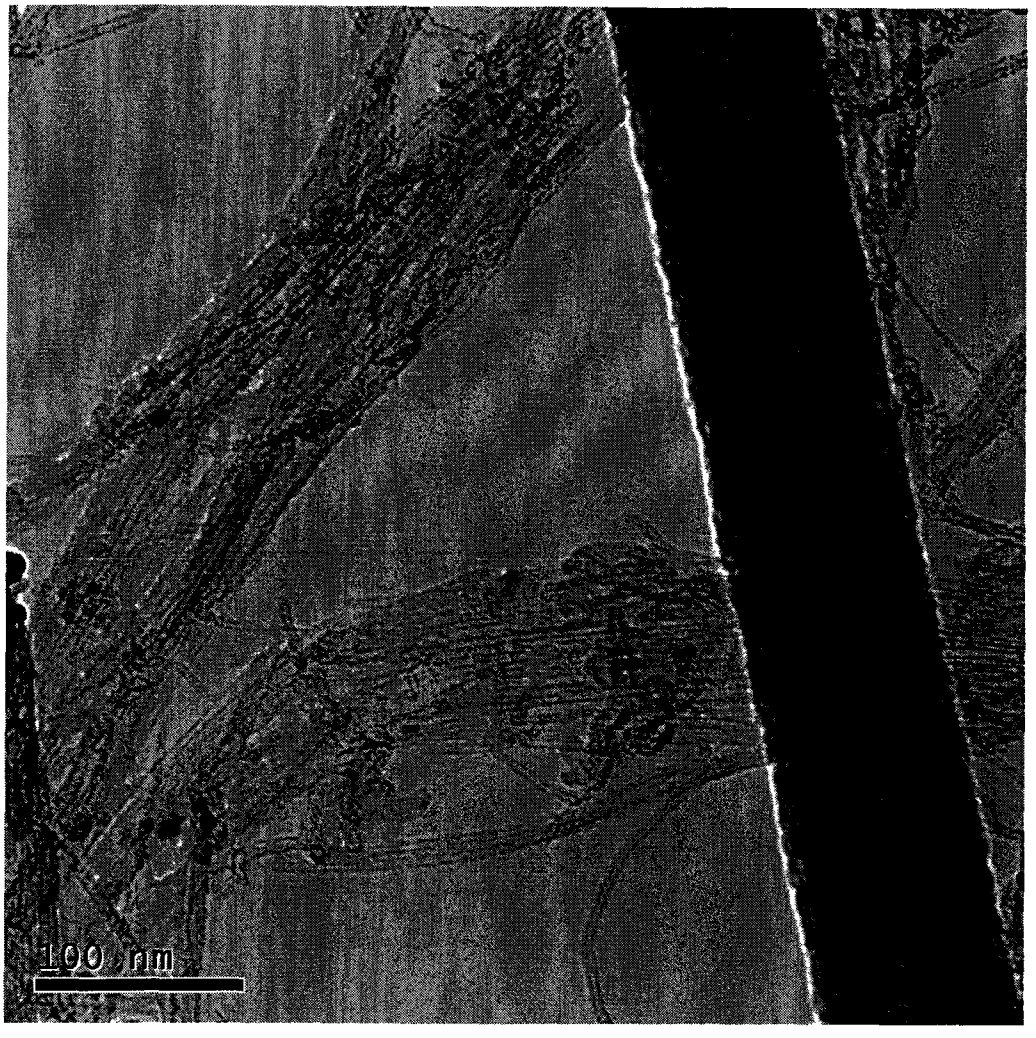

TEM Image
Single-Layer Graphane from the reaction of PEHA and as Purchased graphite

TEM Image
Single-Layer Graphane from the reaction of PEHA and as Purchased graphite

TEM Image
Single-Layer Graphane from the reaction of PEHA and as Purchased graphite

TEM Image
Single-Layer Graphane from the reaction of PEHA and as Purchased graphite

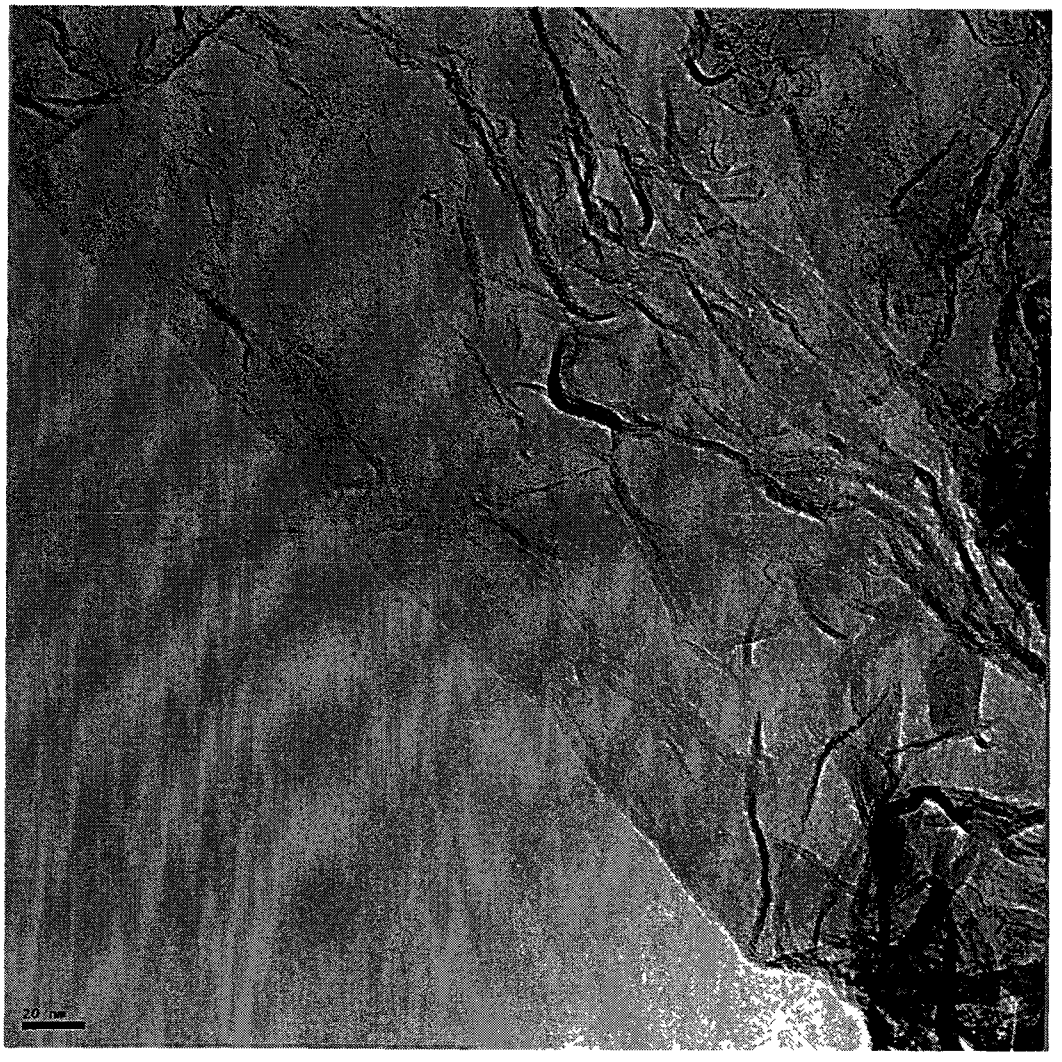

TEM Image
Multı-Layer Graphane from the reaction of PEHA and as Purchased graphıte

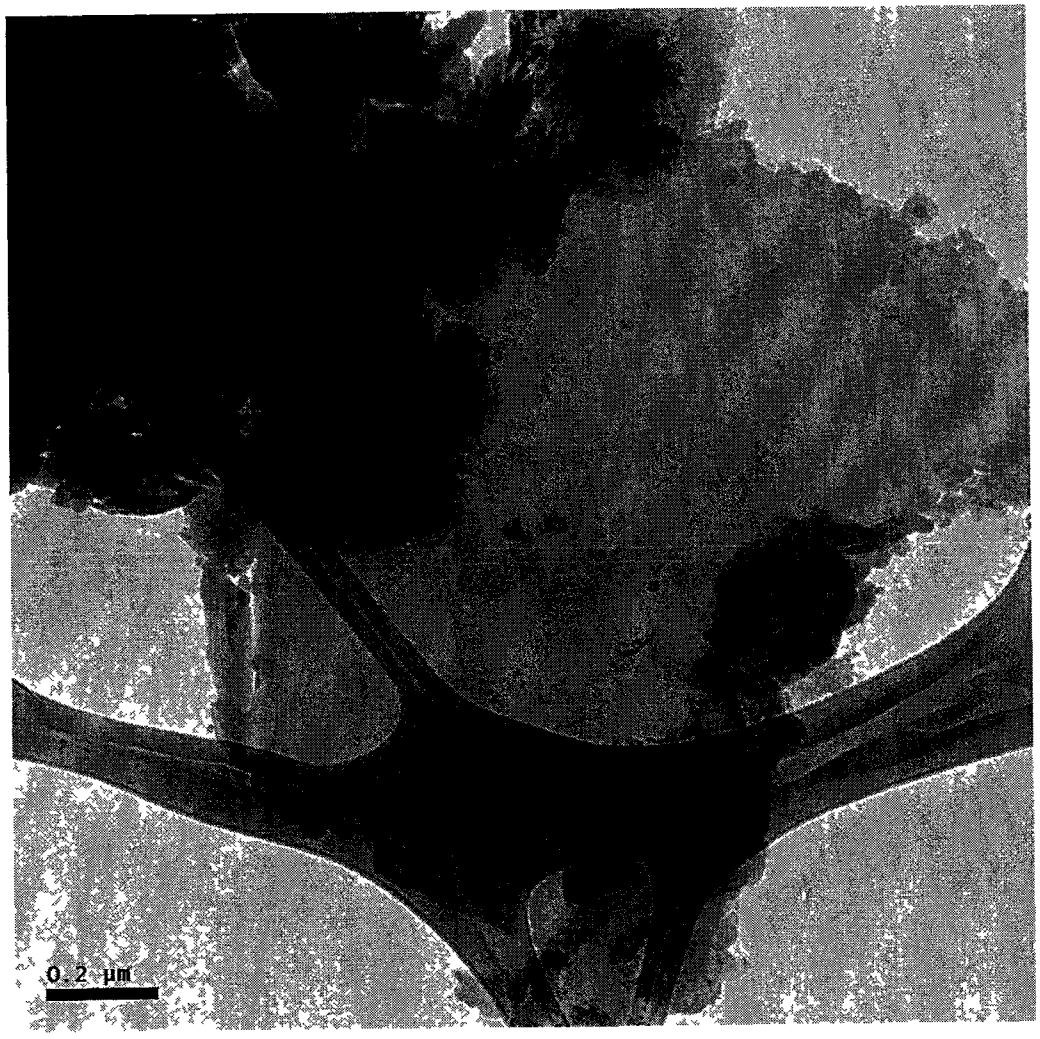

TEM Image
Multi-Layer Graphane from the reaction of PEHA and as Purchased graphite

TEM Image
Single-Layer Graphane from the reaction of PEHA and HOPG

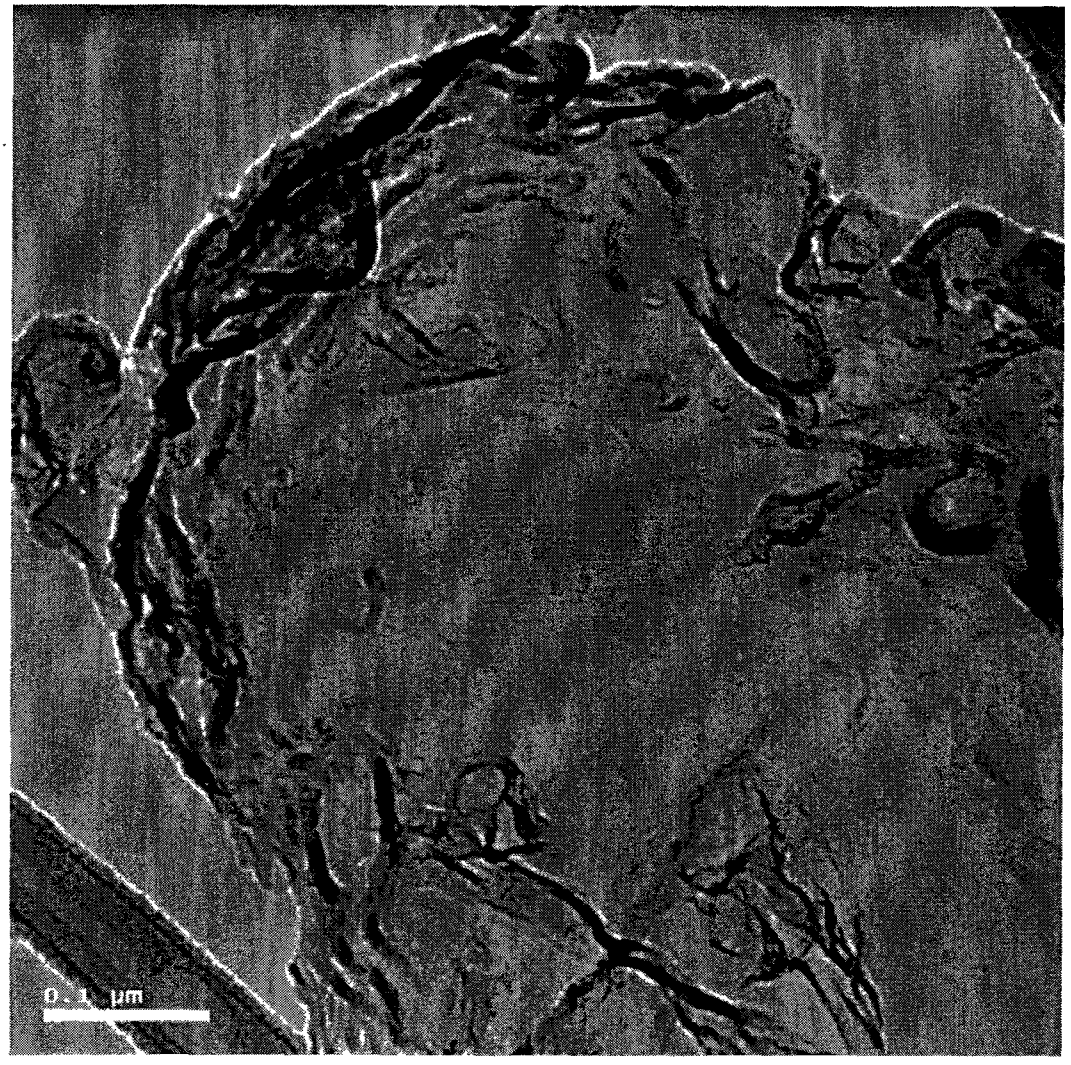

TEM Image
Single-Layer Graphane from the reaction of PEHA and HOPG

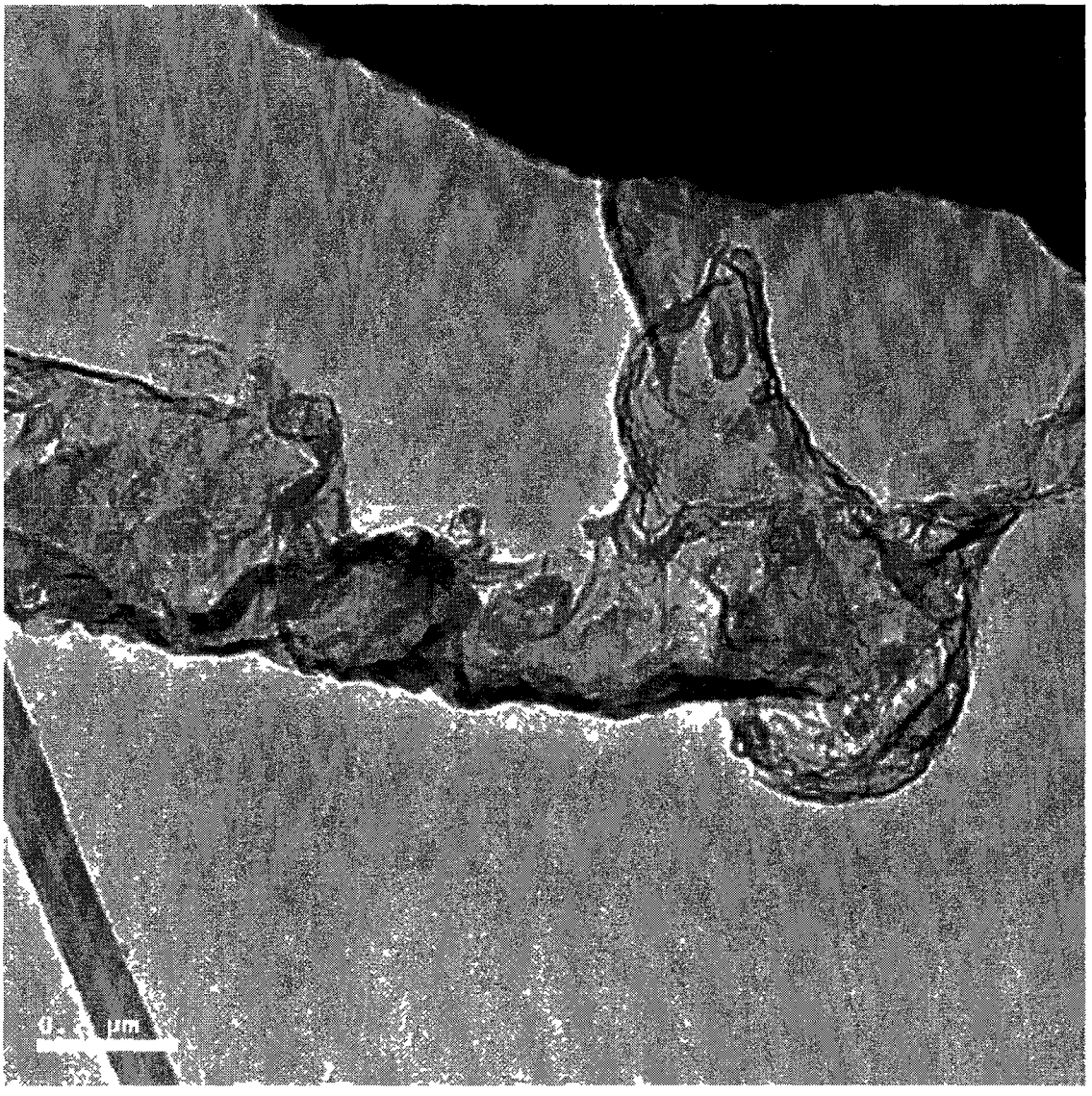

TEM Image
Multi-Layer Graphane from the reaction of PEHA and HOPG

TEM Image
Multi-Layer Graphane from the reaction of PEHA and HOPG

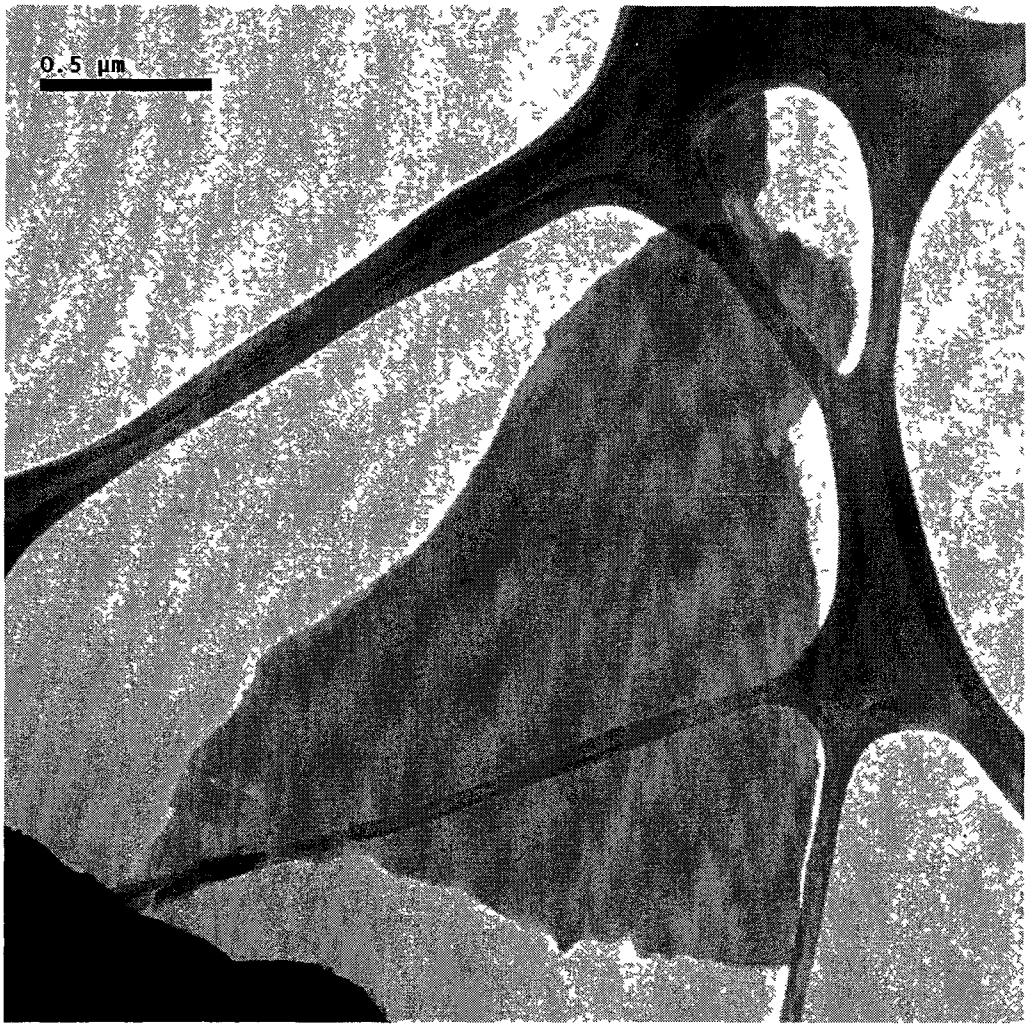

TEM Image
Multi-Layer Graphane from the reaction of PEHA and HOPG

TEM Image
Multi-Layer Graphane from the reaction of PEHA and HOPG

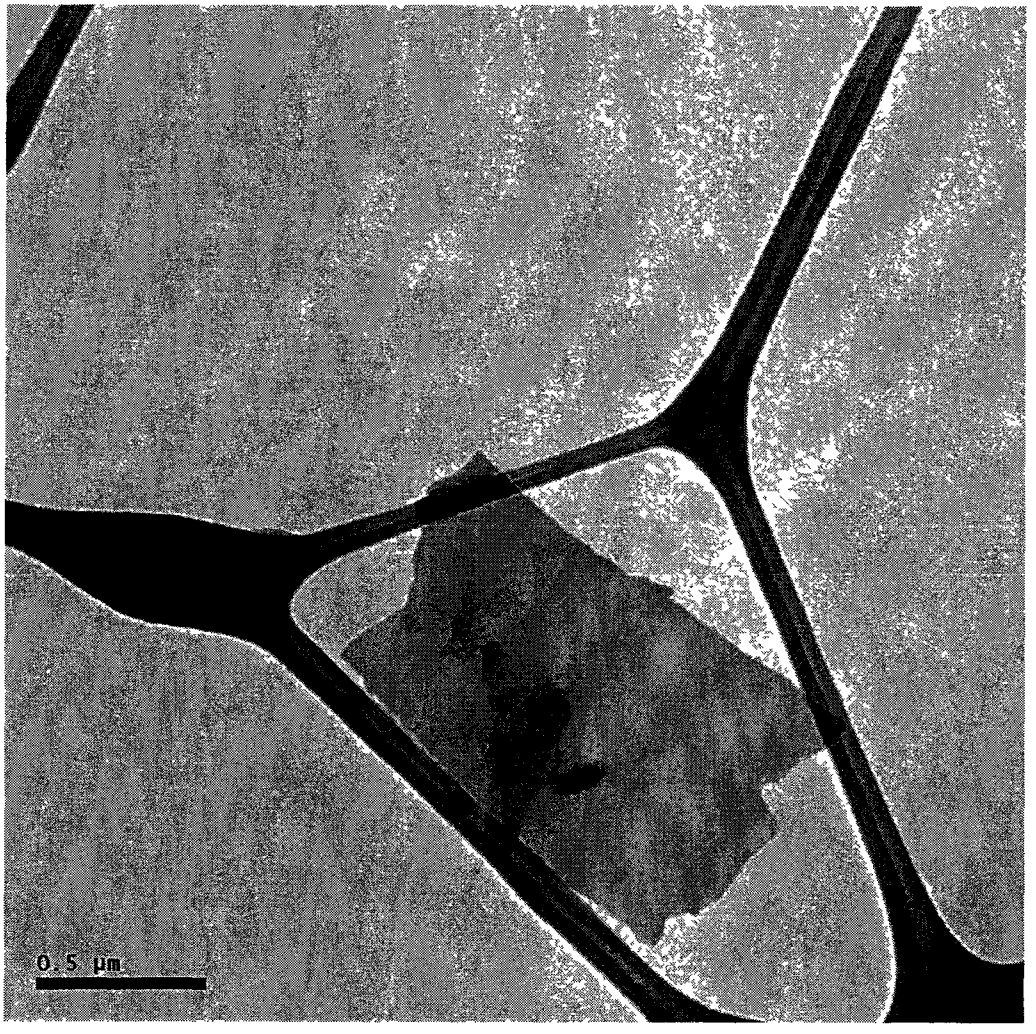

TEM Image
Single-Layer Graphene from the reaction of Naphthalene and HOPG

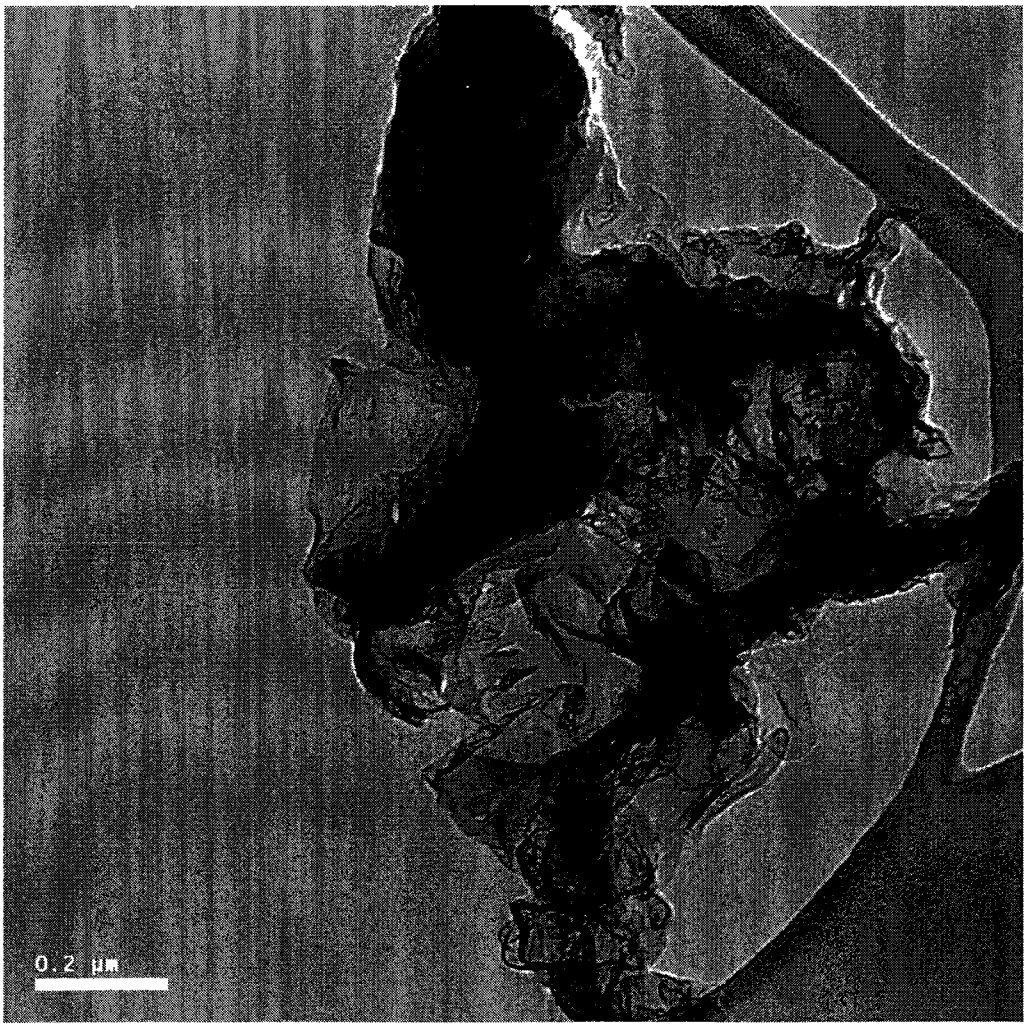

TEM Image
Single-Layer Graphene from the reaction of Naphthalene and HOPG

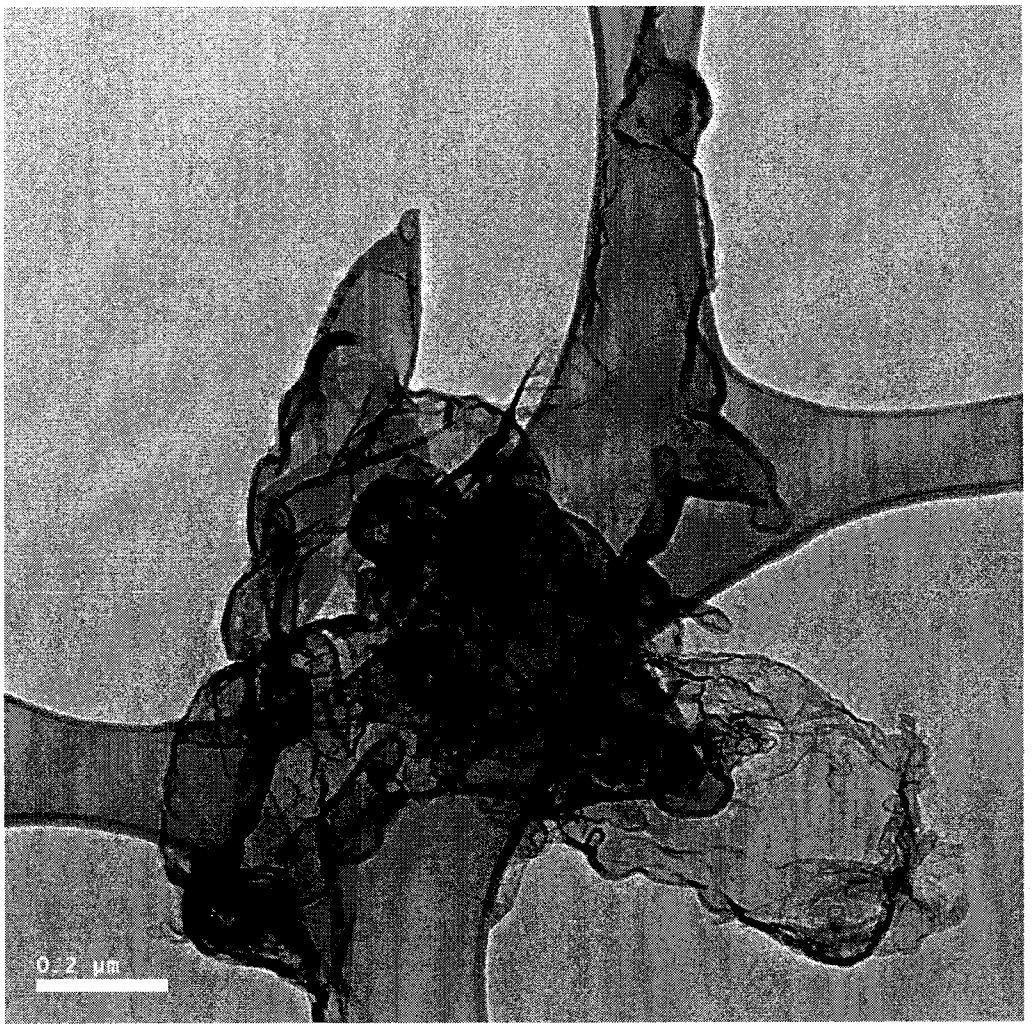

TEM Image
Multi-Layer Graphene from the reaction of Naphthalene and HOPG

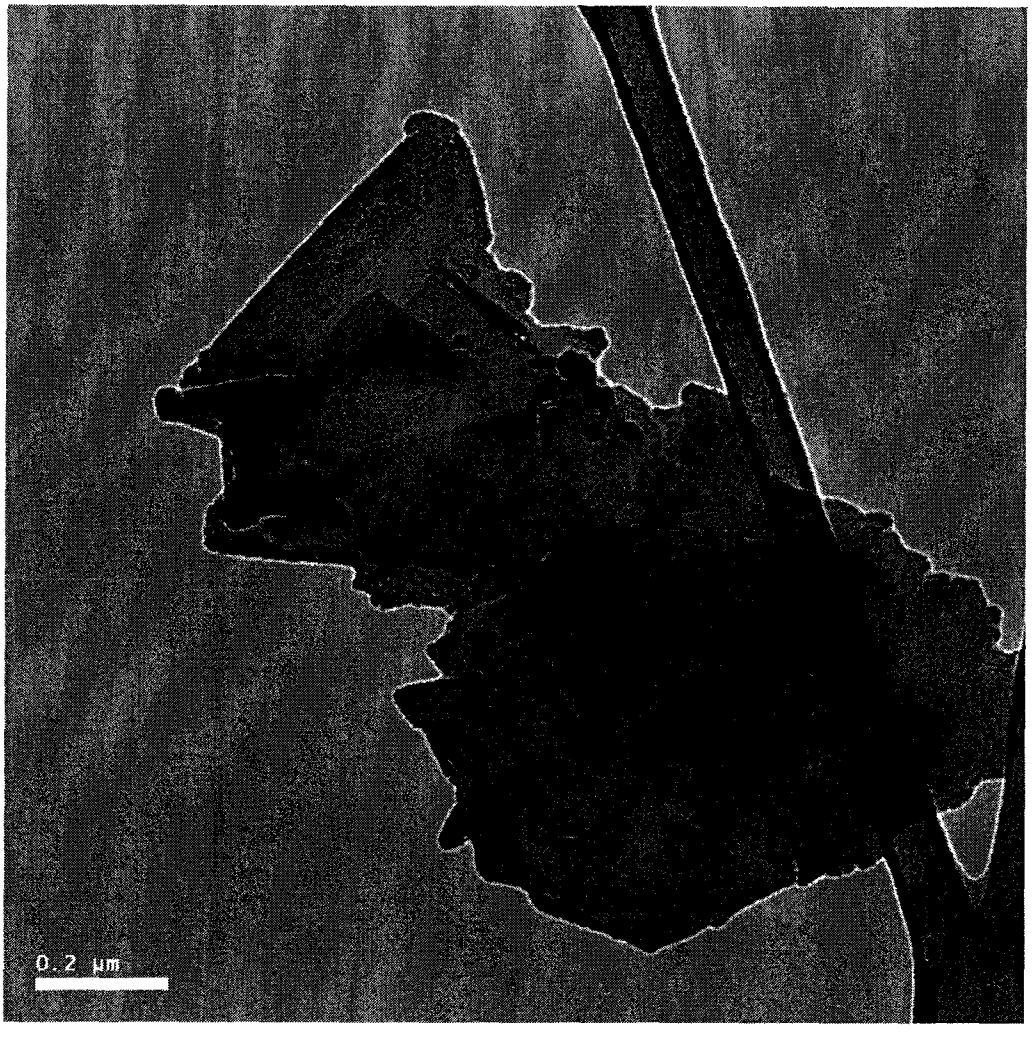

TEM Image
Multi-Layer Graphene from the reaction of Naphthalene and HOPG

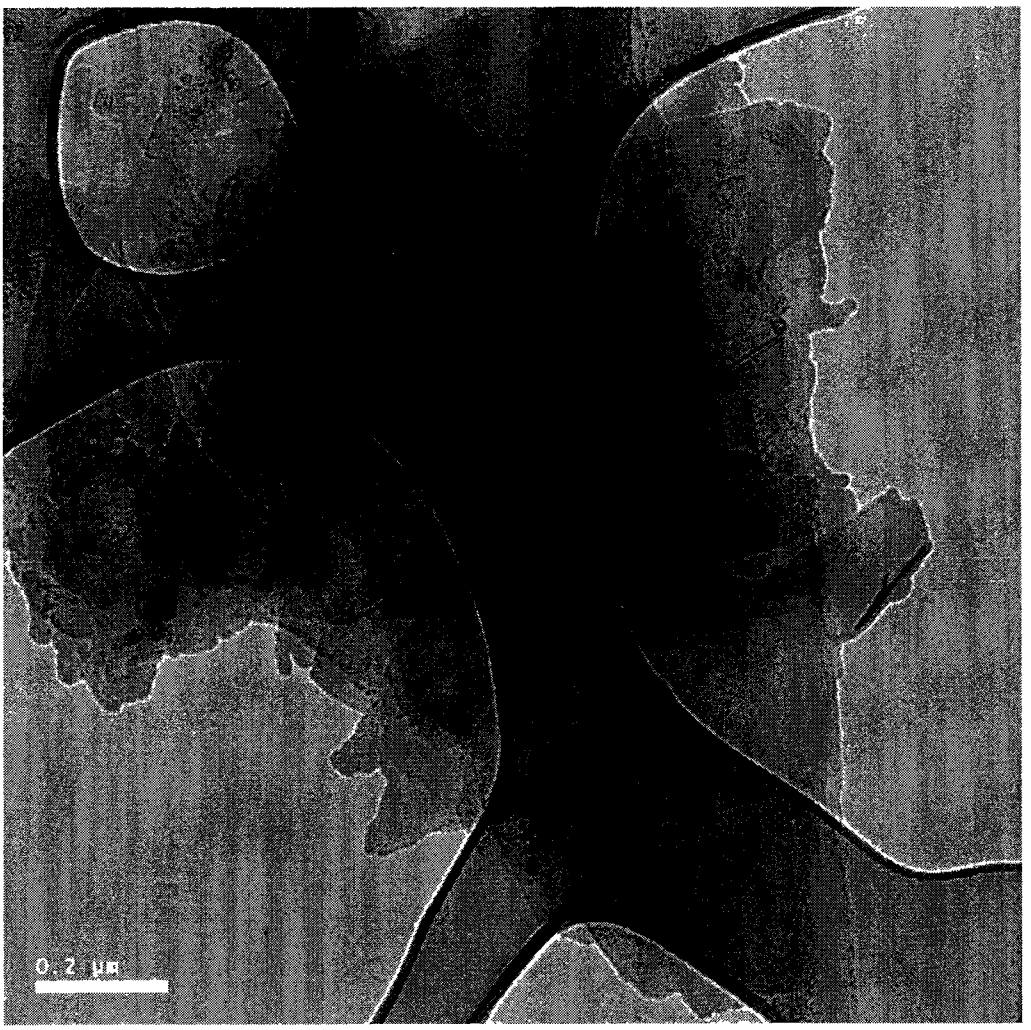

TEM Image
Single-Layer Graphene from the reaction of Adamantane and HOPG

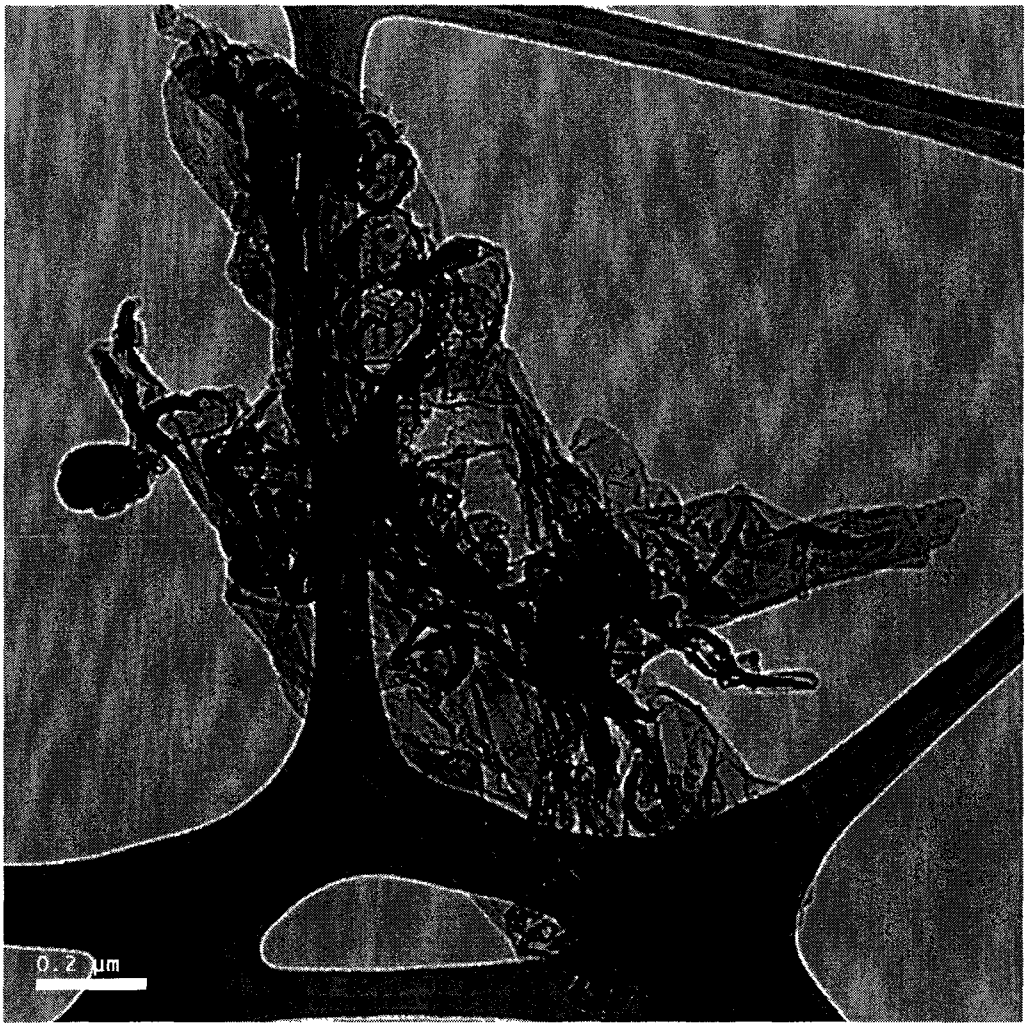

TEM Image
Single-Layer Graphene from the reaction of Adamantane and HOPG

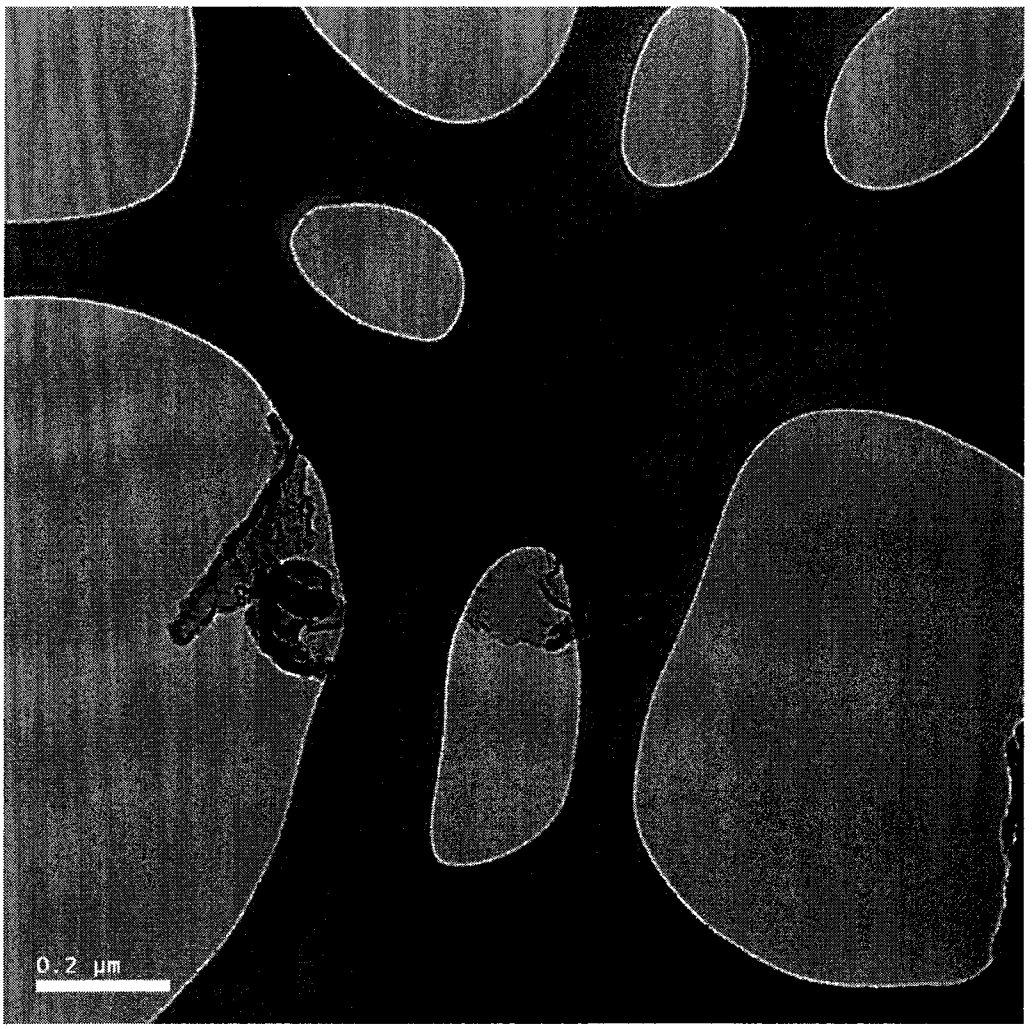

TEM Image
Multi-Layer Graphene from the reaction of Adamantane and HOPG

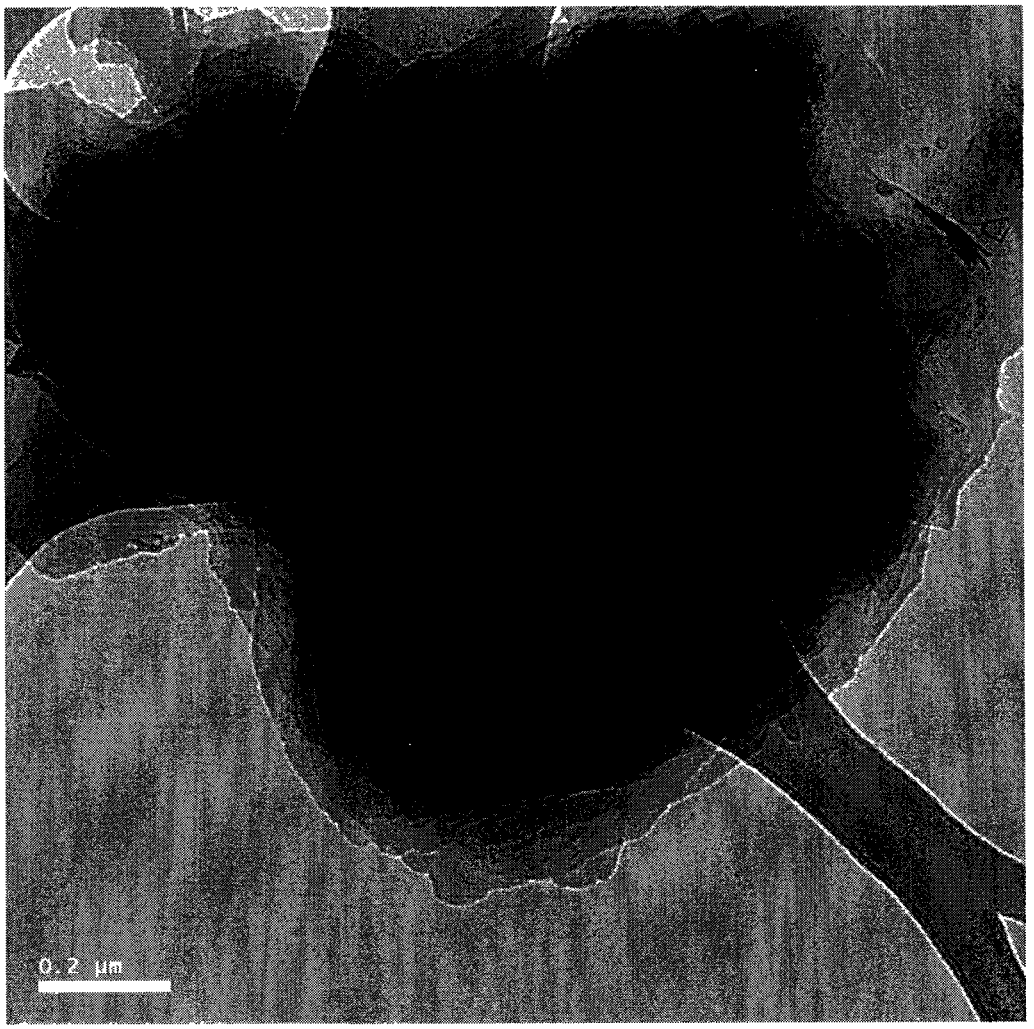

TEM Image
Multi-Layer Graphene from the reaction of Adamantane and HOPG

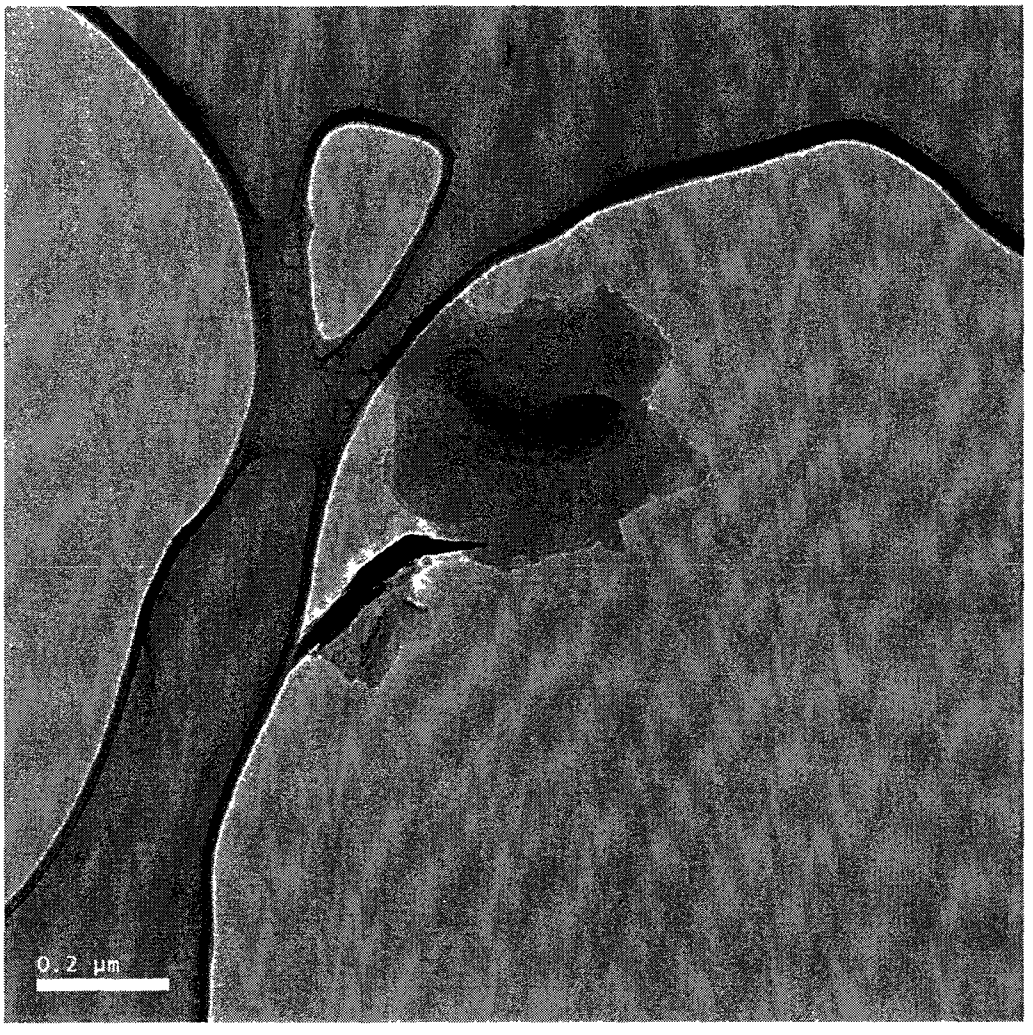

TEM Image
Single-Layer Graphene from the reaction of Chrysene and HOPG

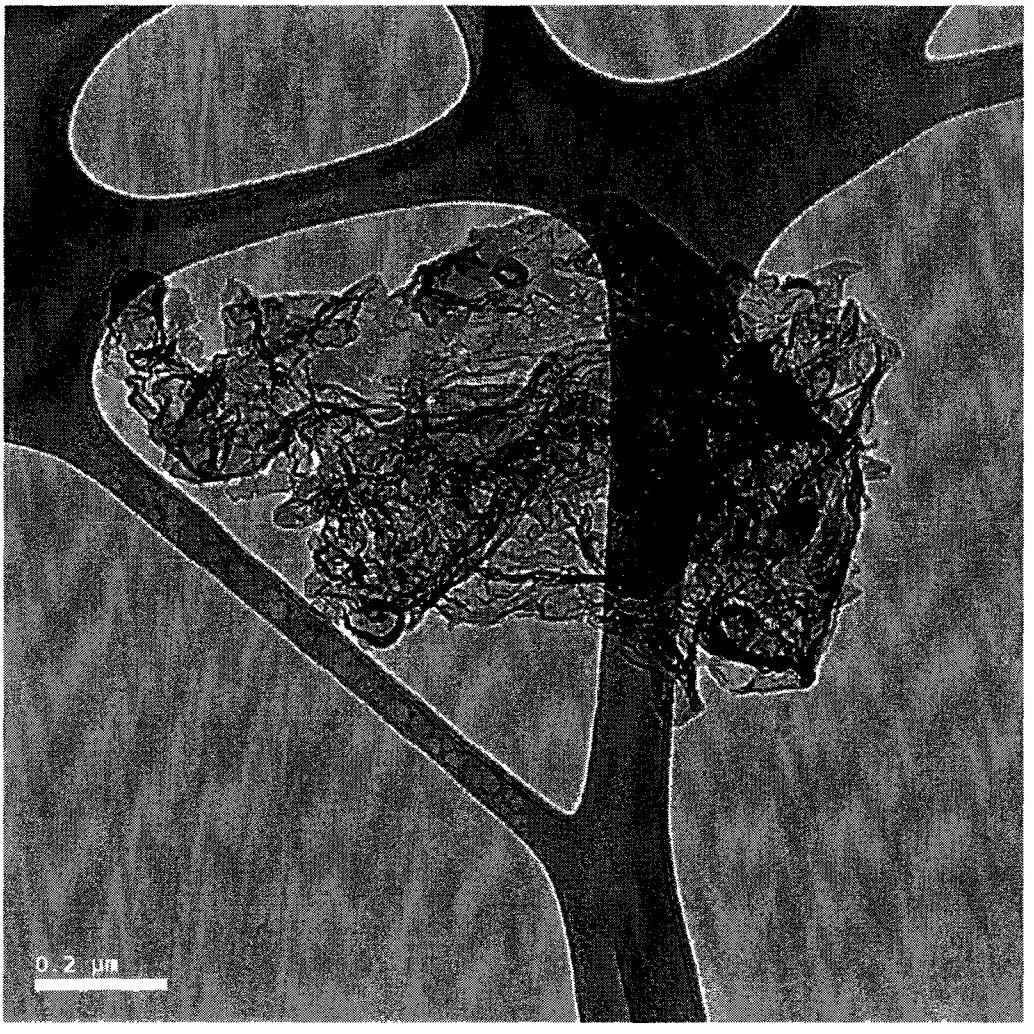

TEM Image
Single-Layer Graphene from the reaction of Chrysene and HOPG

TEM Image
Multi-Layer Graphene from the reaction of Chrysene and HOPG

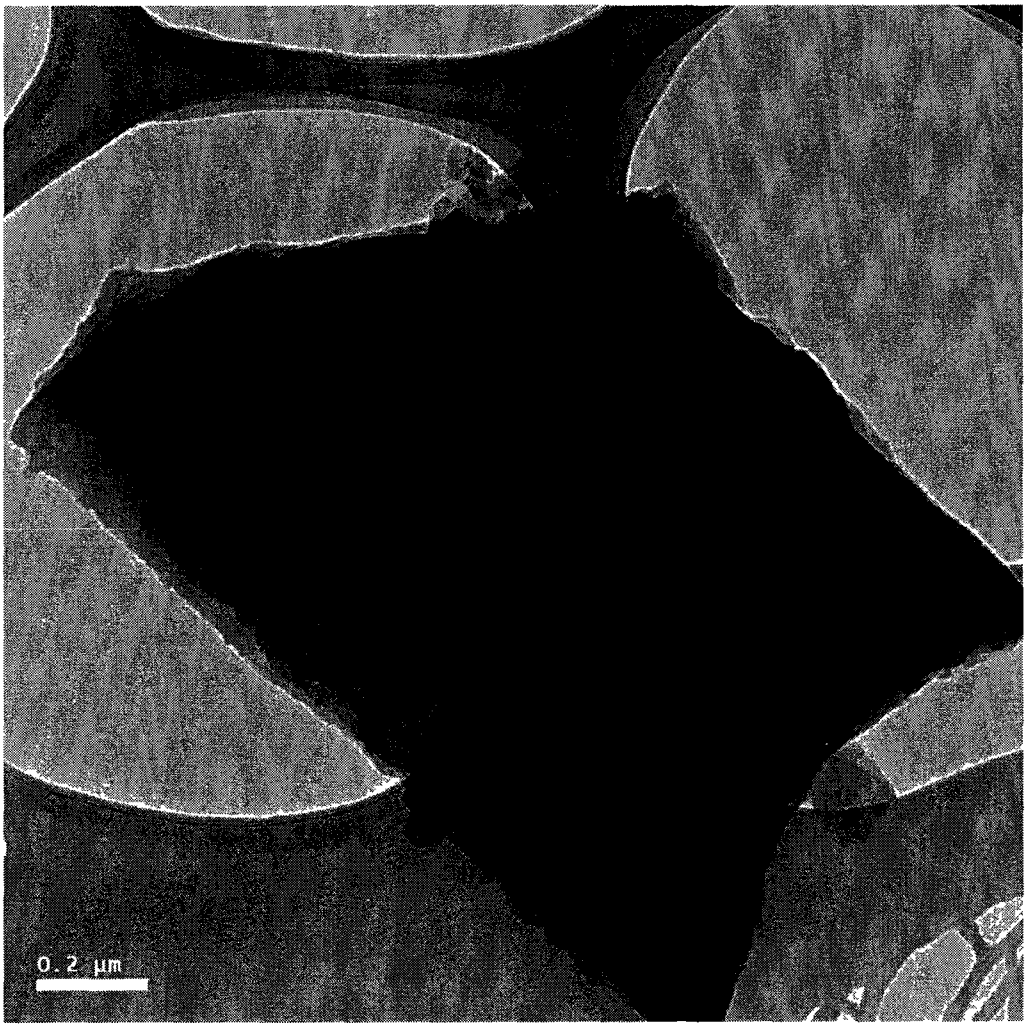

TEM Image
Multi-Layer Graphene from the reaction of Chrysene and HOPG

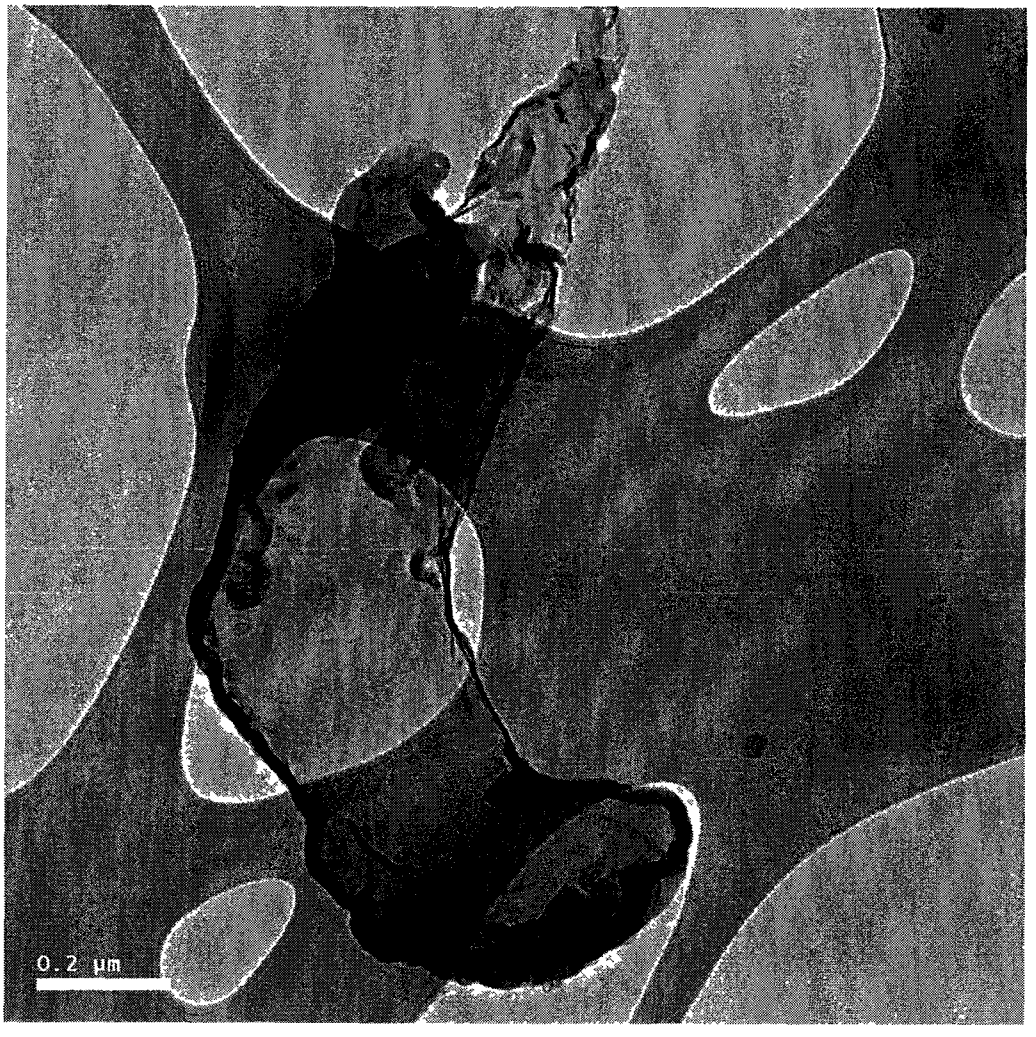

^{1}H-NMR

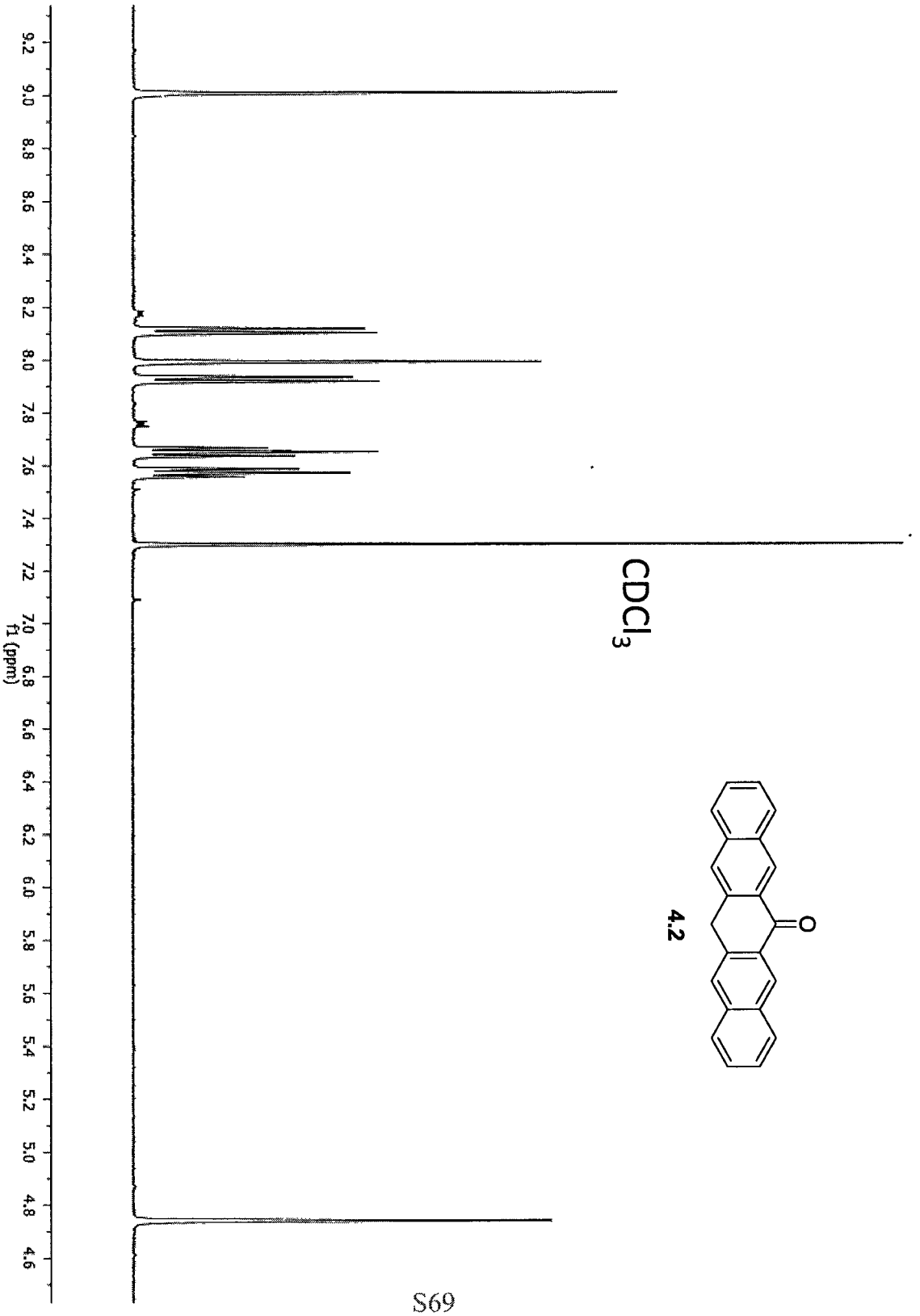
9.2
9.0
8.8
8.6
8.4
8.2
8.0
7.8
7.6
7.4
7.2
7.0
6.8
6.6
6.4
6.2
6.0
5.8
5.6
5.4
5.2
5.0
4.8
4.6
f1 (ppm)
CDCl3
O
4.2

^{13}C-NMR

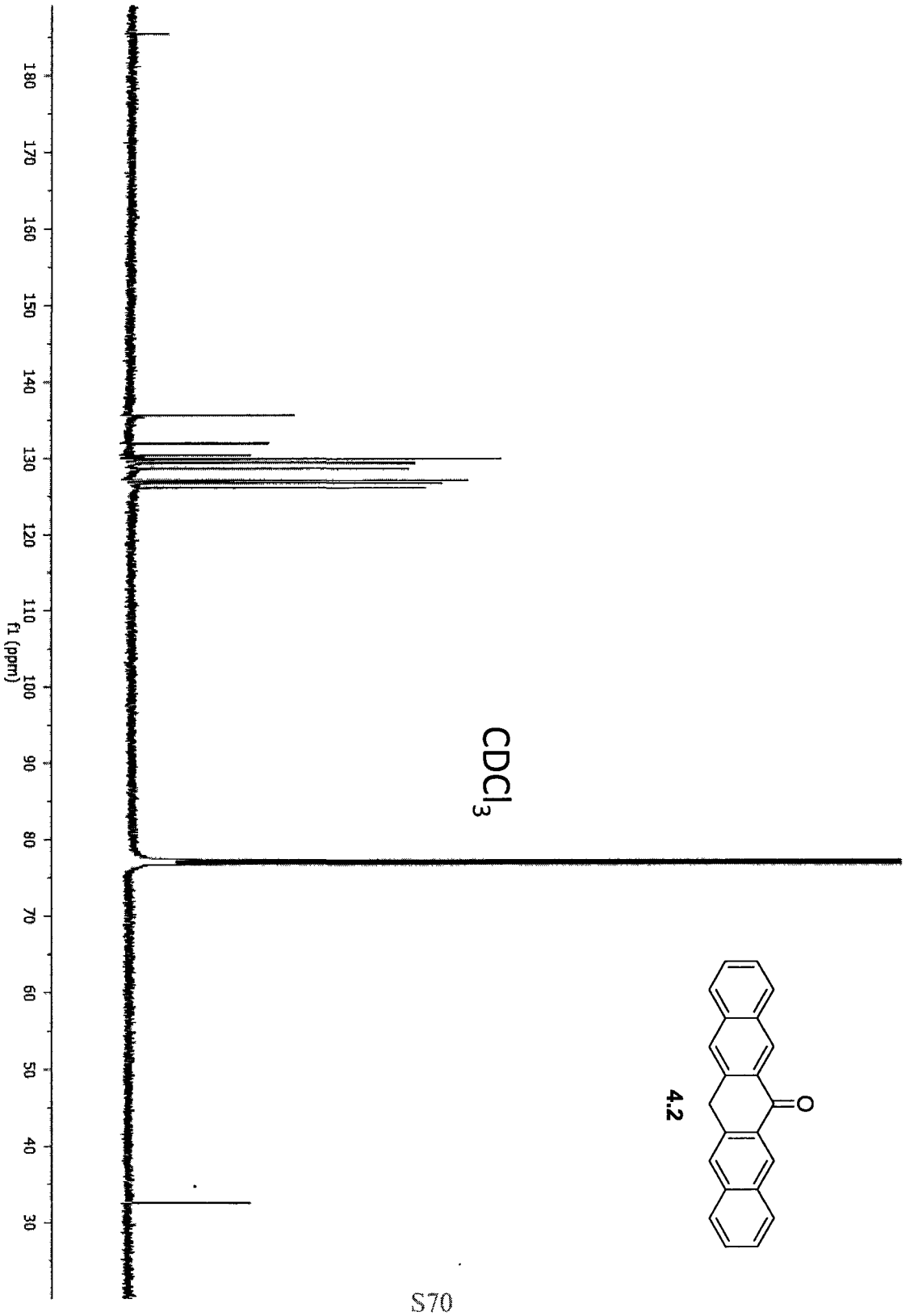
180
170
160
150
140
130
120
110
100
90
80
70
60
50
40
30
f1 (ppm)
CDCl3
4.2
O

^{1}H-NMR

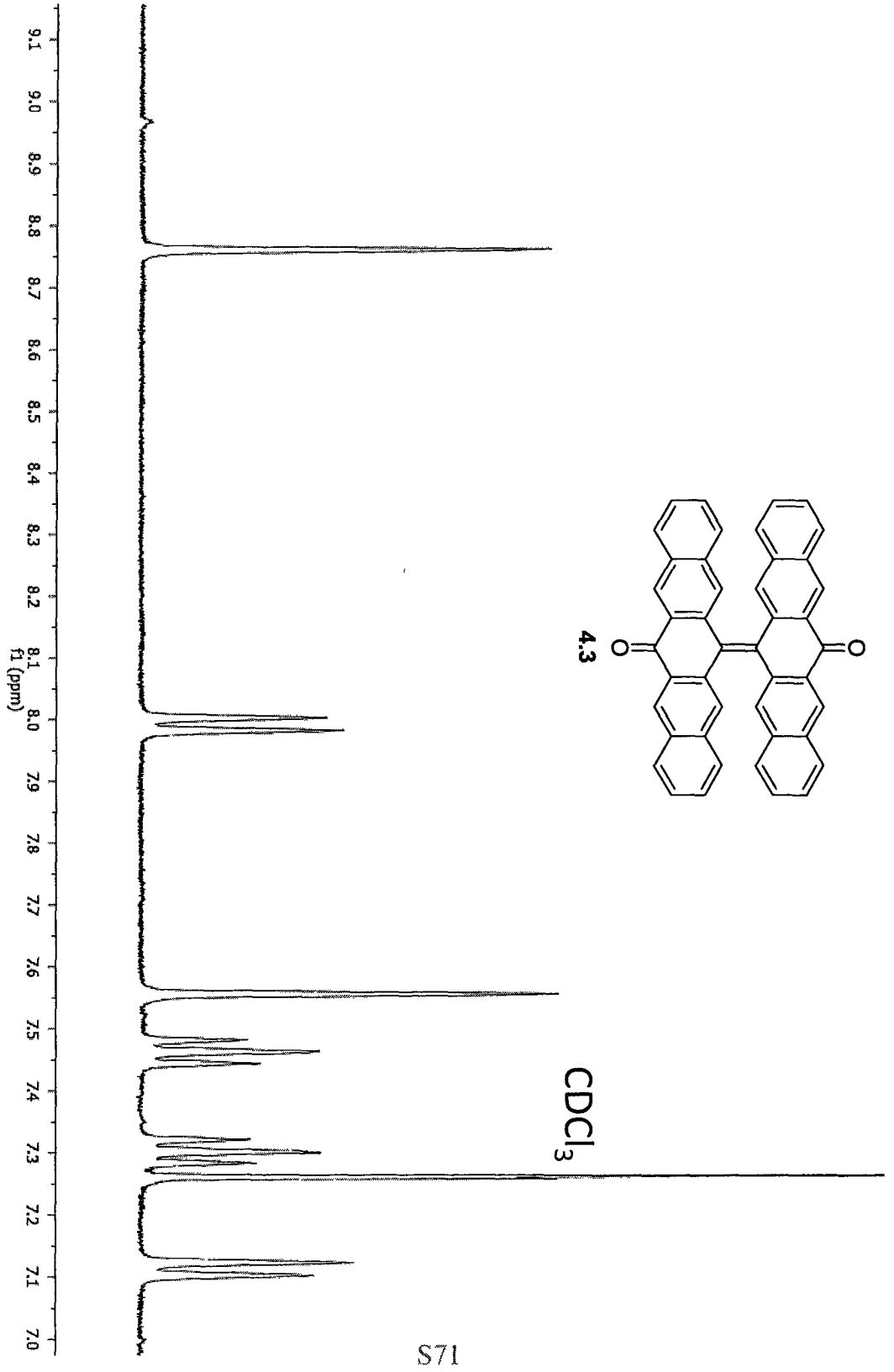
9.1
9.0
8.9
8.8
8.7
8.6
8.5
8.4
8.3
8.2
8.1
8.0
7.9
7.8
7.7
7.6
7.5
7.4
7.3
7.2
7.1
7.0
f1 (ppm)
4.3
O
O
CDCl3

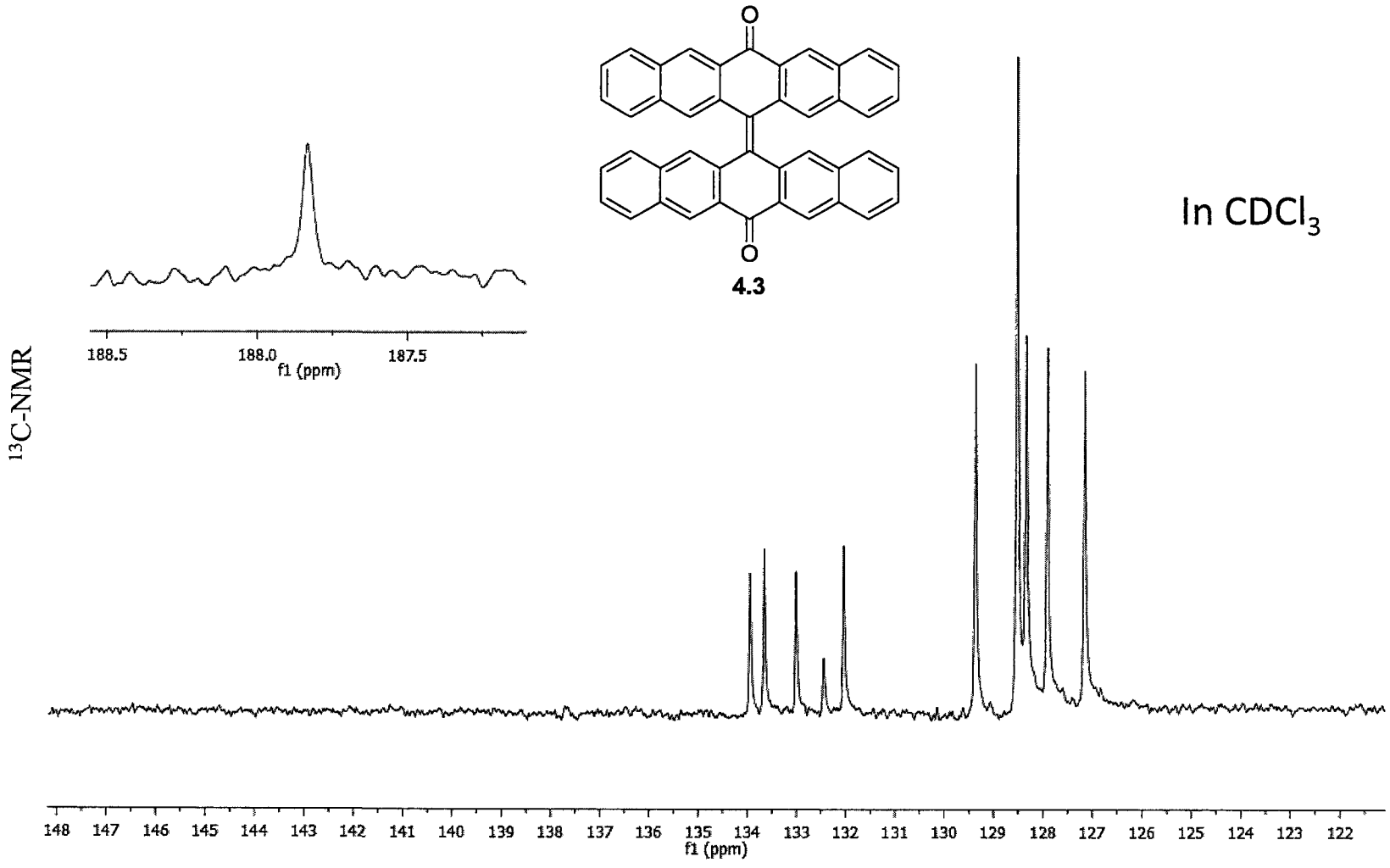
4.3
In $CDCl_3$
^{13}C-NMR
188.5
188.0
187.5
f1 (ppm)
148 147 146 145 144 143 142 141 140 139 138 137 136 135 134 133 132 131 130 129 128 127 126 125 124 123 122
f1 (ppm)

gCOSY-NMR

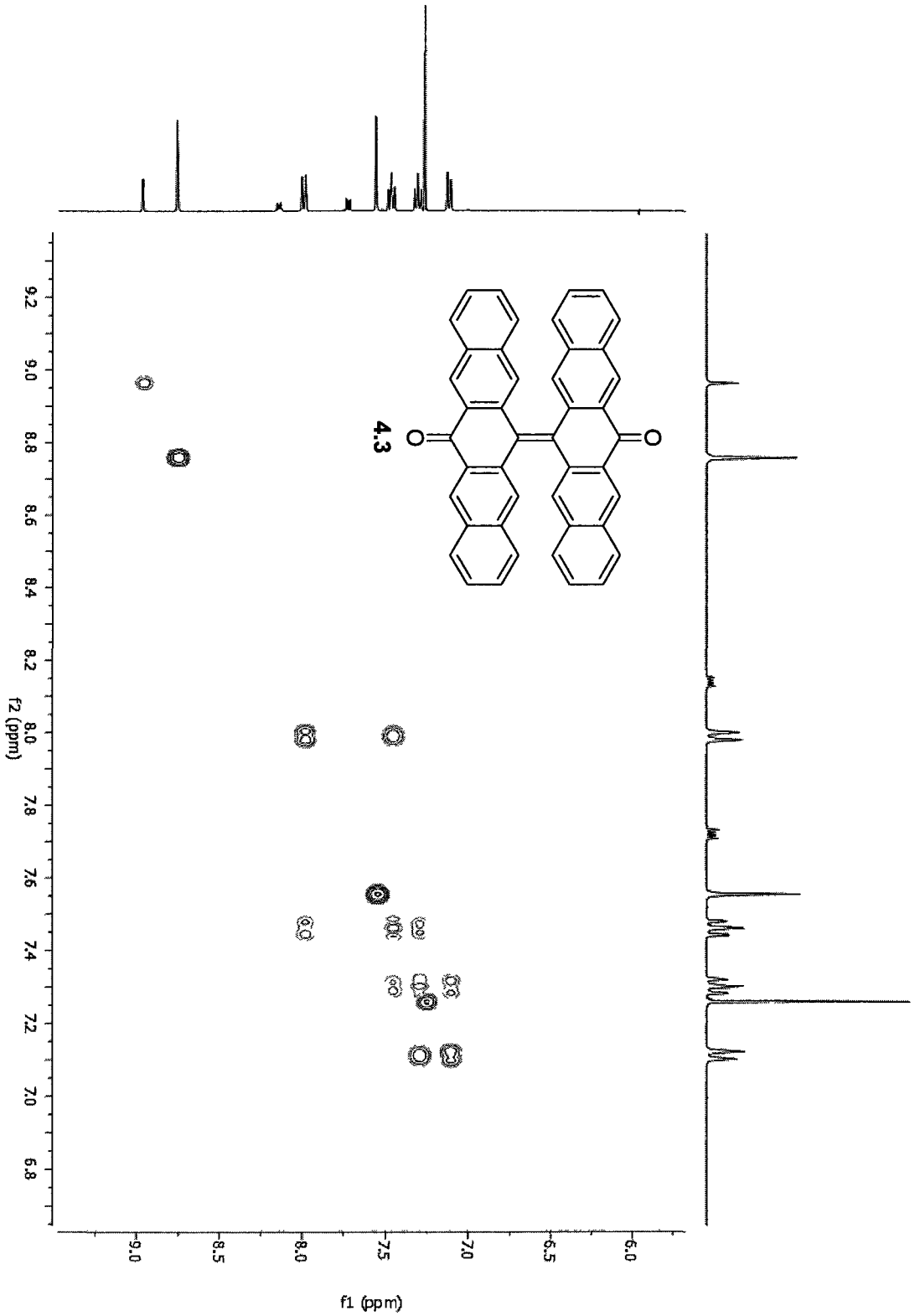
4.3
O
O
f2 (ppm)
f1 (ppm)
9.2
9.0
8.8
8.6
8.4
8.2
8.0
7.8
7.6
7.4
7.2
7.0
6.8
9.0
8.5
8.0
7.5
7.0
6.5
6.0

Mass Spec

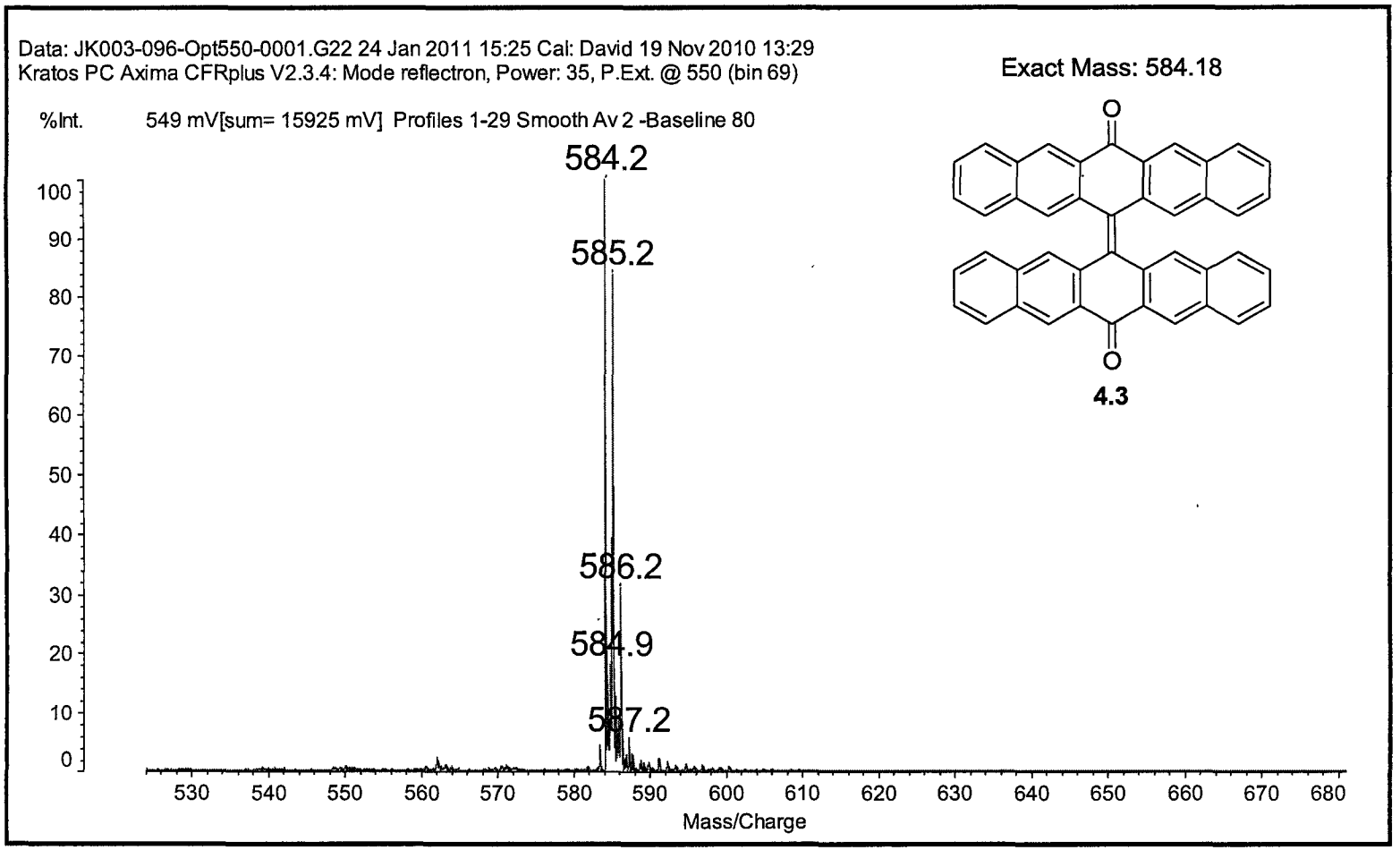
Data: JK003-096-Opt550-0001.G22 24 Jan 2011 15:25 Cal: David 19 Nov 2010 13:29
Kratos PC Axima CFRplus V2.3.4: Mode reflectron, Power: 35, P.Ext. @ 550 (bin 69)
%Int.
549 mV[sum= 15925 mV] Profiles 1-29 Smooth Av 2 -Baseline 80
584.2
585.2
586.2
584.9
587.2
100
90
80
70
60
50
40
30
20
10
0
530
540
550
560
570
580
590
600
610
620
630
640
650
660
670
680
Mass/Charge
Exact Mass: 584.18
O
O
4.3

X-Ray Crystal Structure of **4.3**

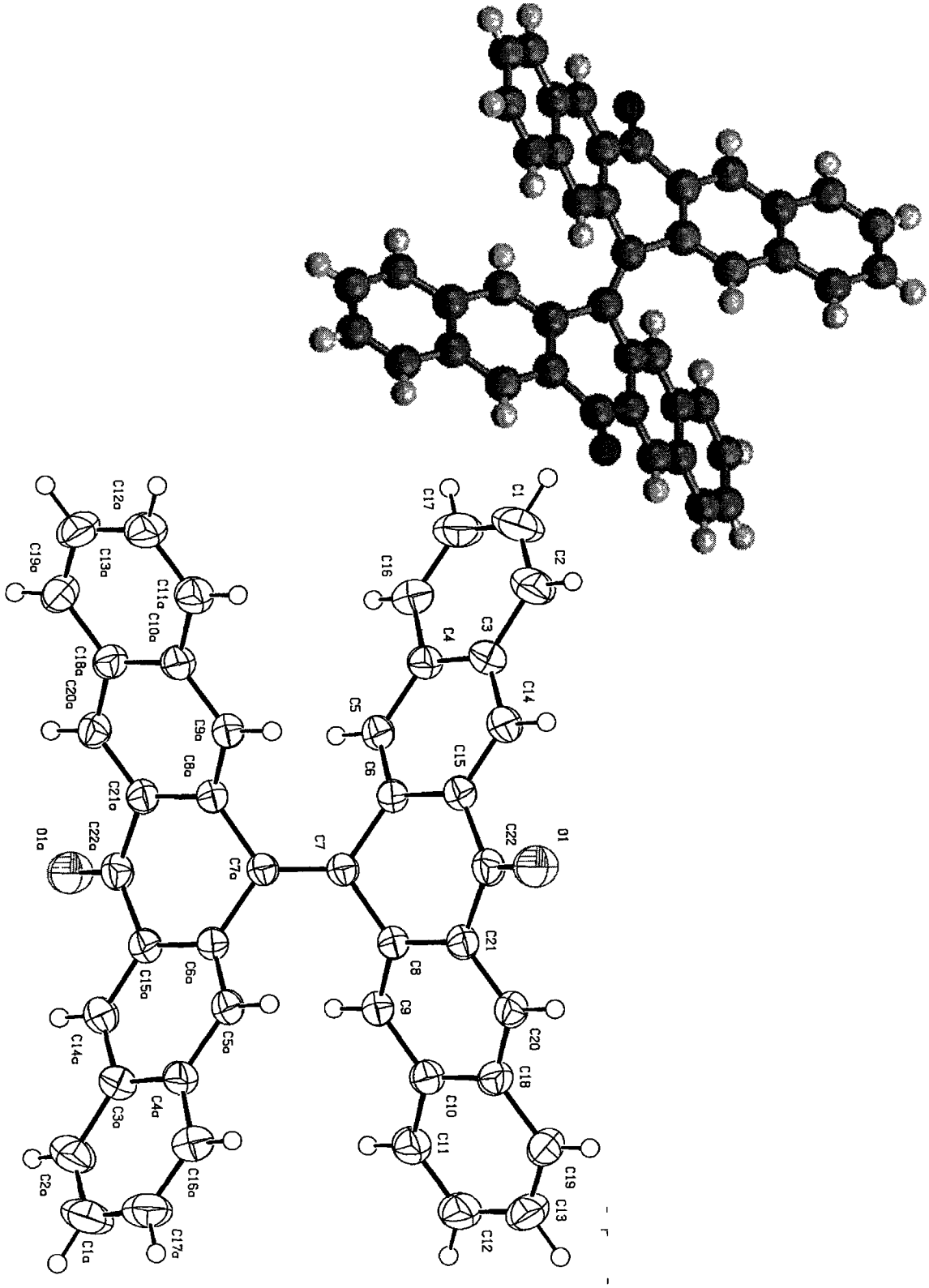

XYZ coordinates for the X-Ray Crystal Structure of **4.3**

O	6.683972	3.949194	9.247336
C	10.314478	1.193577	4.615082
H	11.233866	1.118546	4.490414
C	9.834312	1.906953	5.660650
H	10.426312	2.308660	6.253413
C	8.439954	2.046627	5.862942
C	7.545932	1.452378	4.928400
C	6.149678	1.644112	5.102935
H	5.560608	1.284769	4.478653
C	5.647509	2.343521	6.164028
C	4.196115	2.634758	6.358558
C	3.770076	2.379190	7.766252
C	2.611214	1.722260	8.098622
H	2.053339	1.416363	7.421297
C	2.246800	1.499821	9.448099
C	1.051670	0.824192	9.794818
H	0.487939	0.510214	9.124314
C	0.718480	0.629110	11.102542
H	-0.073958	0.191619	11.316596
C	1.562398	1.085070	12.125764
H	1.324759	0.943088	13.013732
C	7.904631	2.714984	6.982958
H	8.480268	3.087833	7.610652
C	6.543643	2.824068	7.164080
C	8.088312	0.692598	3.865661
H	7.518143	0.275885	3.261372
C	9.434917	0.564467	3.716529
H	9.774677	0.056562	3.015563
C	3.100032	1.974366	10.486728
C	2.728454	1.734958	11.834793
H	3.282915	2.022386	12.524468
C	4.297011	2.636259	10.125425
H	4.858113	2.962011	10.792048
C	4.648977	2.806869	8.805704
C	6.009832	3.311196	8.463454

XYZ coordinates for the X-Ray Crystal Structure of **4.3**

O	0.902984	1.822456	2.513832
C	-2.727522	4.578073	7.146086
H	-3.646910	4.653104	7.270754
C	-2.247356	3.864697	6.100518
H	-2.839356	3.462990	5.507755
C	-0.852999	3.725023	5.898226
C	0.041024	4.319272	6.832768
C	1.437278	4.127538	6.658232
H	2.026348	4.486881	7.282515
C	1.939447	3.428129	5.597140
C	3.390841	3.136892	5.402610
C	3.816880	3.392460	3.994916
C	4.975741	4.049390	3.662545
H	5.533617	4.355287	4.339871
C	5.340155	4.271829	2.313069
C	6.535286	4.947458	1.966350
H	7.099017	5.261436	2.636854
C	6.868476	5.142540	0.658625
H	7.660914	5.580031	0.444572
C	6.024558	4.686580	-0.364596
H	6.262196	4.828562	-1.252564
C	-0.317675	3.056666	4.778210
H	-0.893312	2.683817	4.150516
C	1.043313	2.947582	4.597088
C	-0.501356	5.079052	7.895507
H	0.068813	5.495765	8.499796
C	-1.847961	5.207183	8.044639
H	-2.187722	5.715088	8.745604
C	4.486924	3.797284	1.274440
C	4.858501	4.036692	-0.073625
H	4.304041	3.749264	-0.763300
C	3.289945	3.135391	1.635743
H	2.728843	2.809639	0.969120
C	2.937978	2.964781	2.955464
C	1.577124	2.460454	3.297714

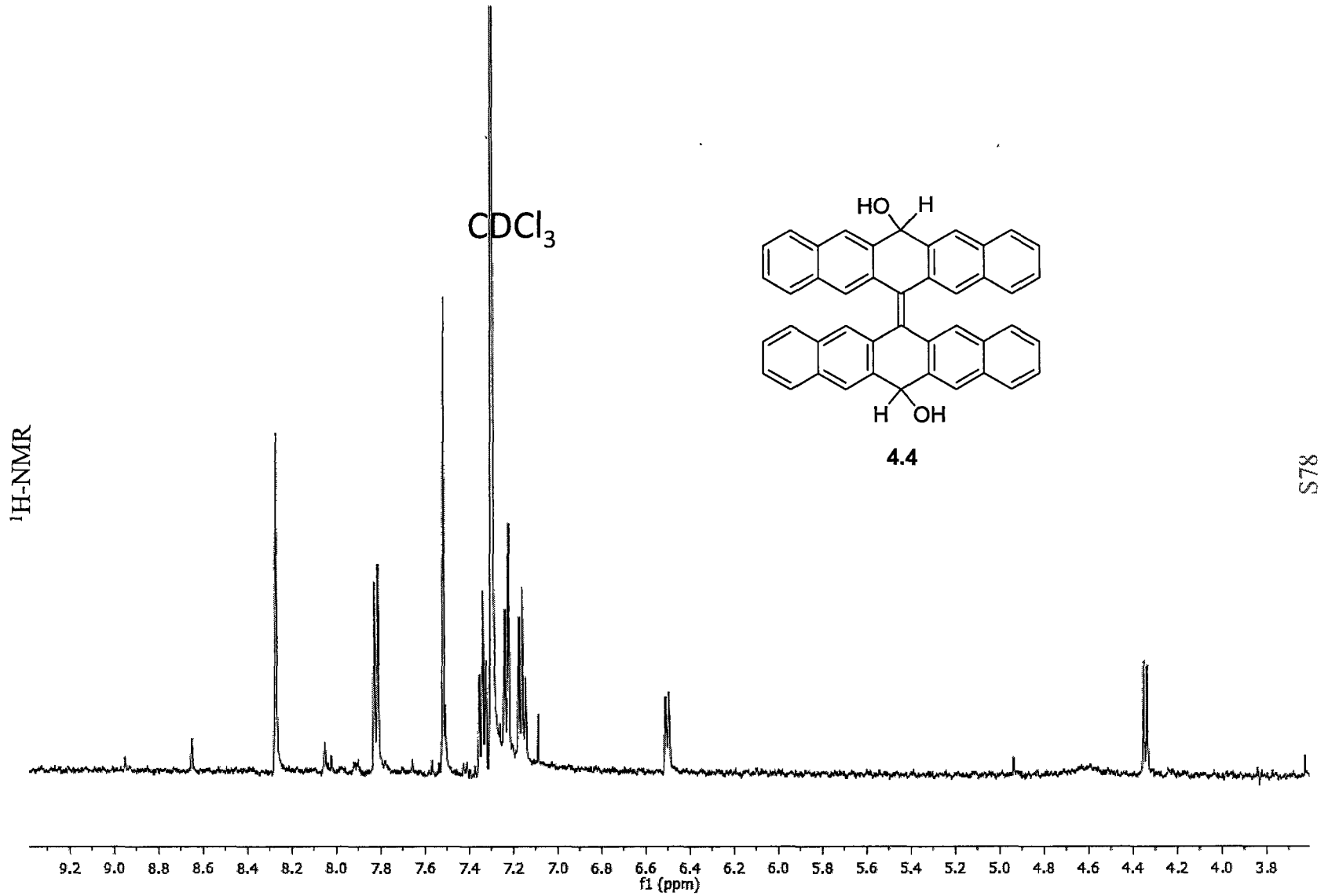
CDCl3
HO
H
H
OH
4.4
1H-NMR
9.2 9.0 8.8 8.6 8.4 8.2 8.0 7.8 7.6 7.4 7.2 7.0 6.8 6.6 6.4 6.2 6.0 5.8 5.6 5.4 5.2 5.0 4.8 4.6 4.4 4.2 4.0 3.8
f1 (ppm)

gCOSY-NMR

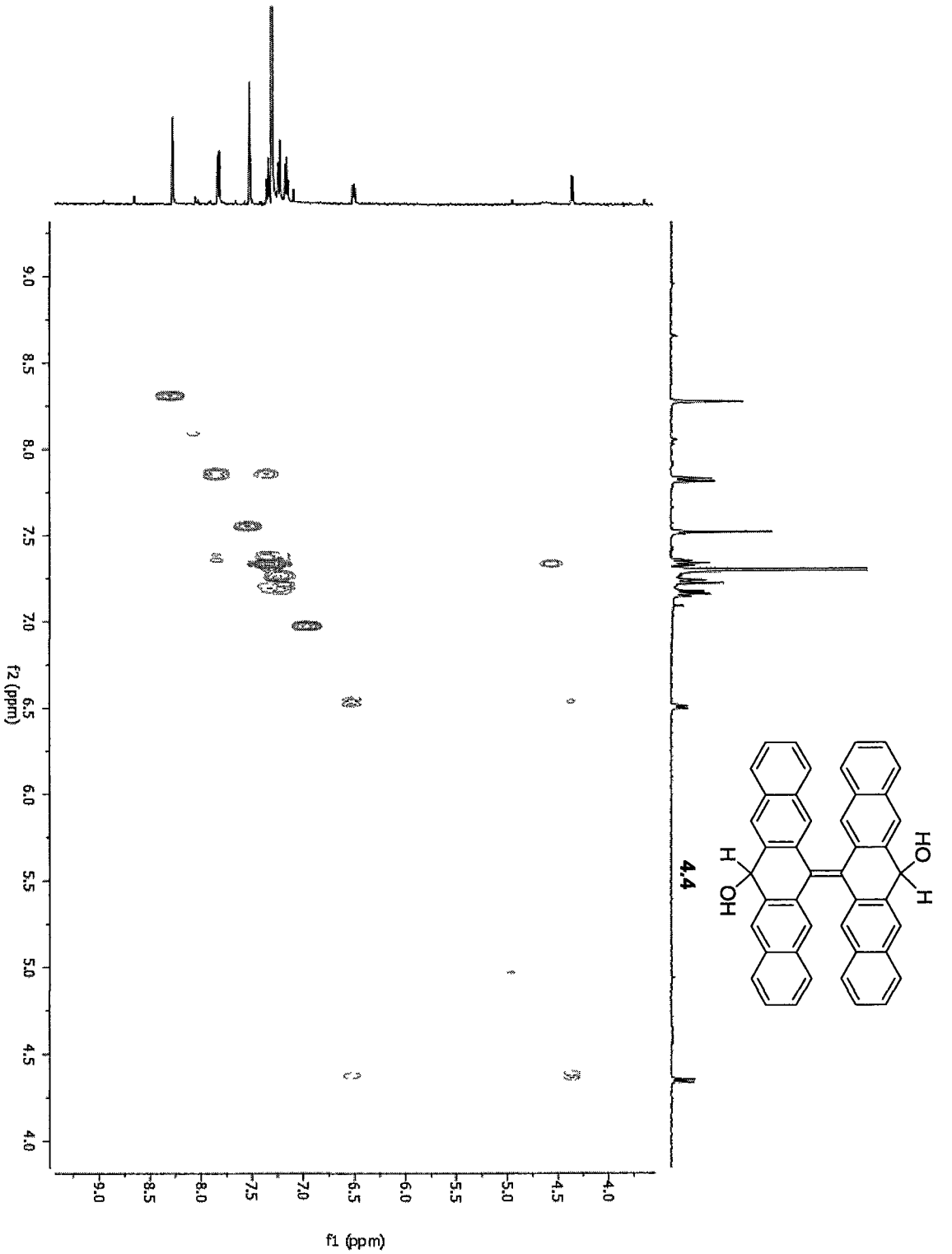

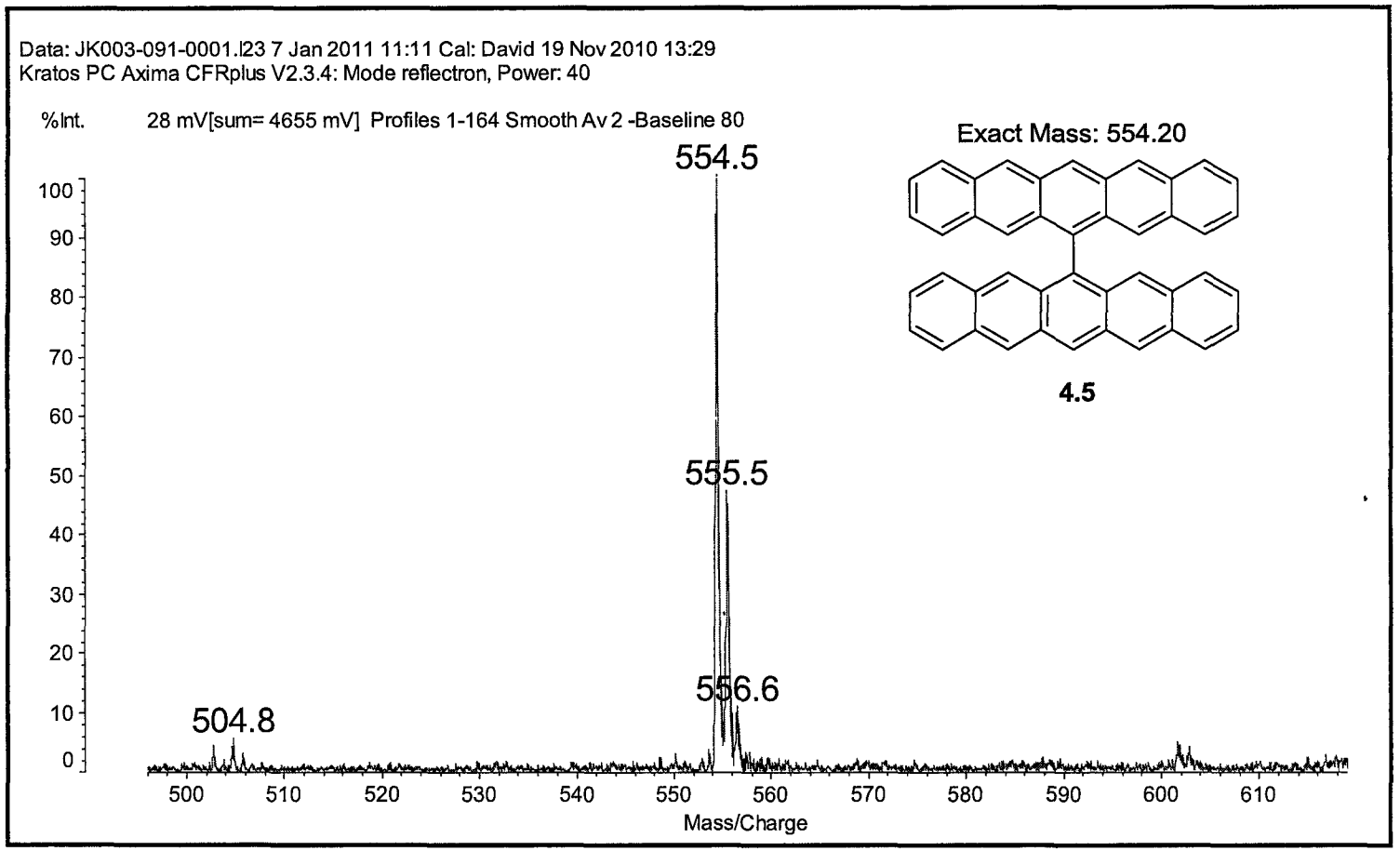
Data: JK003-091-0001.l23 7 Jan 2011 11:11 Cal: David 19 Nov 2010 13:29
Kratos PC Axima CFRplus V2.3.4: Mode reflectron, Power: 40
%Int.
28 mV[sum= 4655 mV] Profiles 1-164 Smooth Av 2 -Baseline 80
554.5
555.5
556.6
504.8
Exact Mass: 554.20
4.5
100
90
80
70
60
50
40
30
20
10
0
500
510
520
530
540
550
560
570
580
590
600
610
Mass/Charge

* 6,13-pentacenquinone

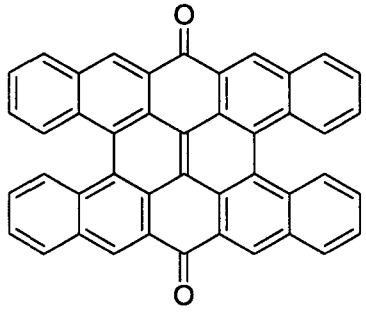

4.7

gCOSY-NMR

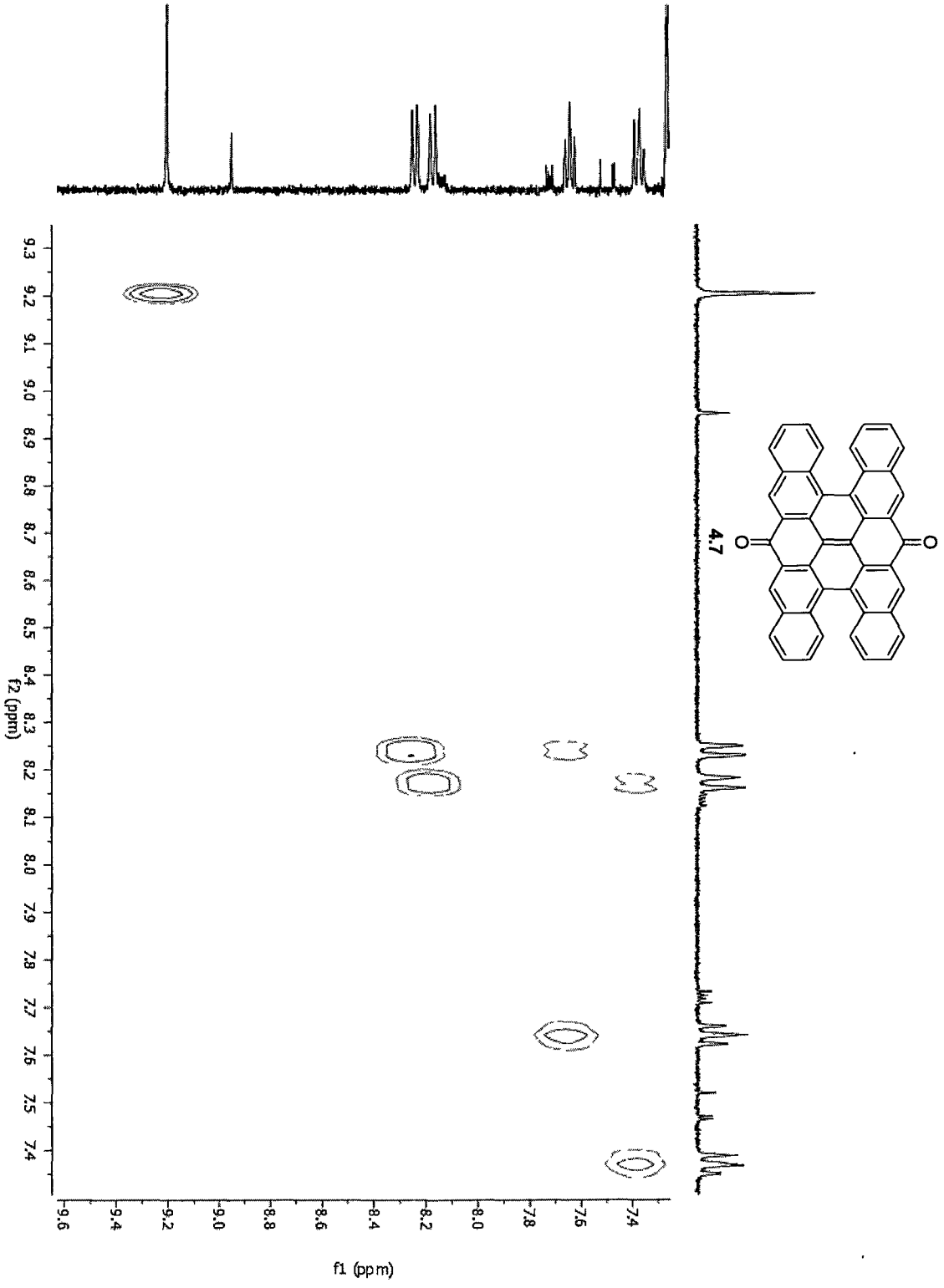

Mass Spec

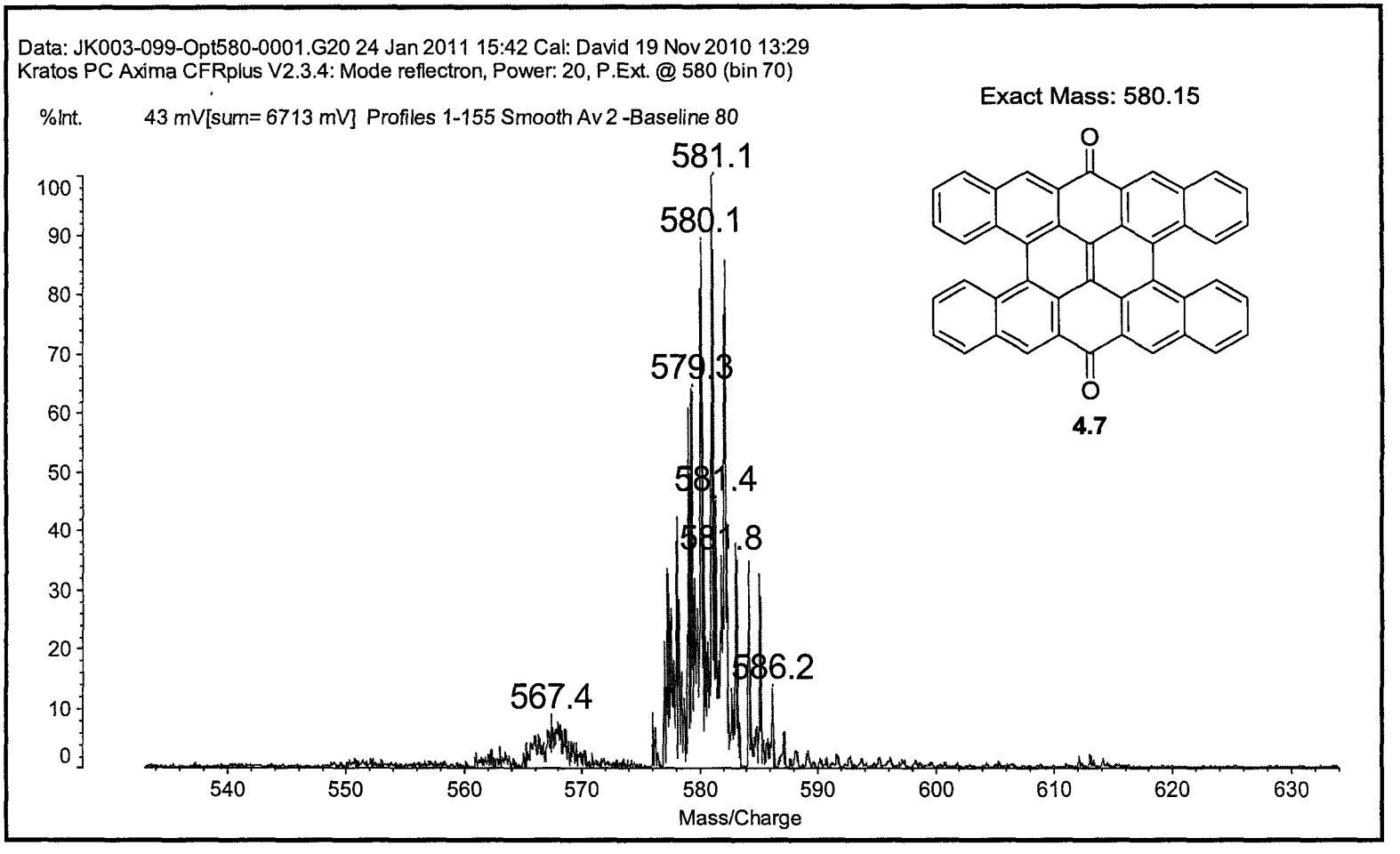
Data: JK003-099-Opt580-0001.G20 24 Jan 2011 15:42 Cal: David 19 Nov 2010 13:29
Kratos PC Axima CFRplus V2.3.4: Mode reflectron, Power: 20, P.Ext. @ 580 (bin 70)
%Int.
43 mV[sum= 6713 mV] Profiles 1-155 Smooth Av 2 -Baseline 80
581.1
580.1
579.3
581.4
581.8
586.2
567.4
100
90
80
70
60
50
40
30
20
10
0
540
550
560
570
580
590
600
610
620
630
Mass/Charge
Exact Mass: 580.15
O
O
4.7

UV/VIs

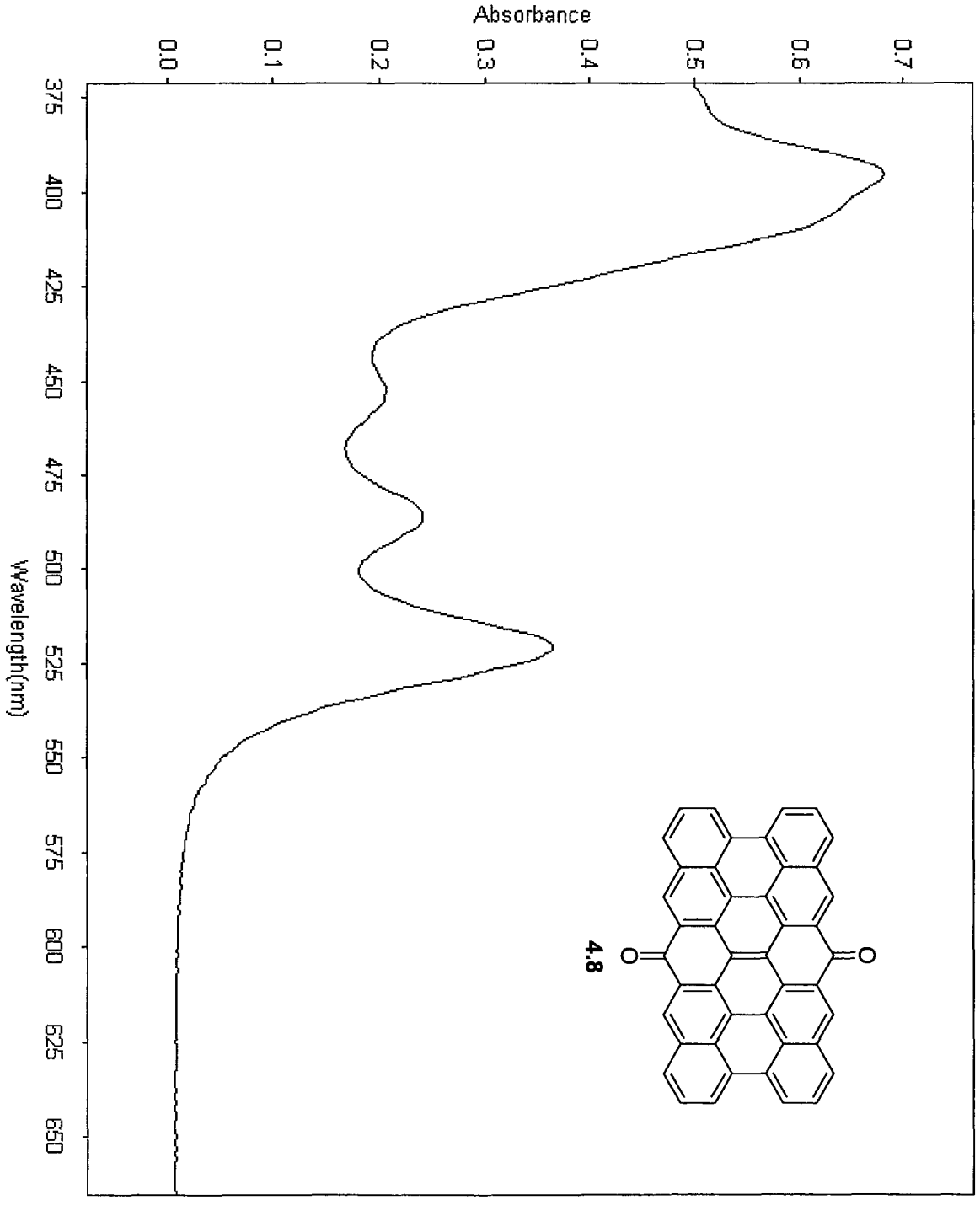
Absorbance
0.0
0.1
0.2
0.3
0.4
0.5
0.6
0.7
Wavelength(nm)
375
400
425
450
475
500
525
550
575
600
625
650
O
O
4.8

Mass Spec

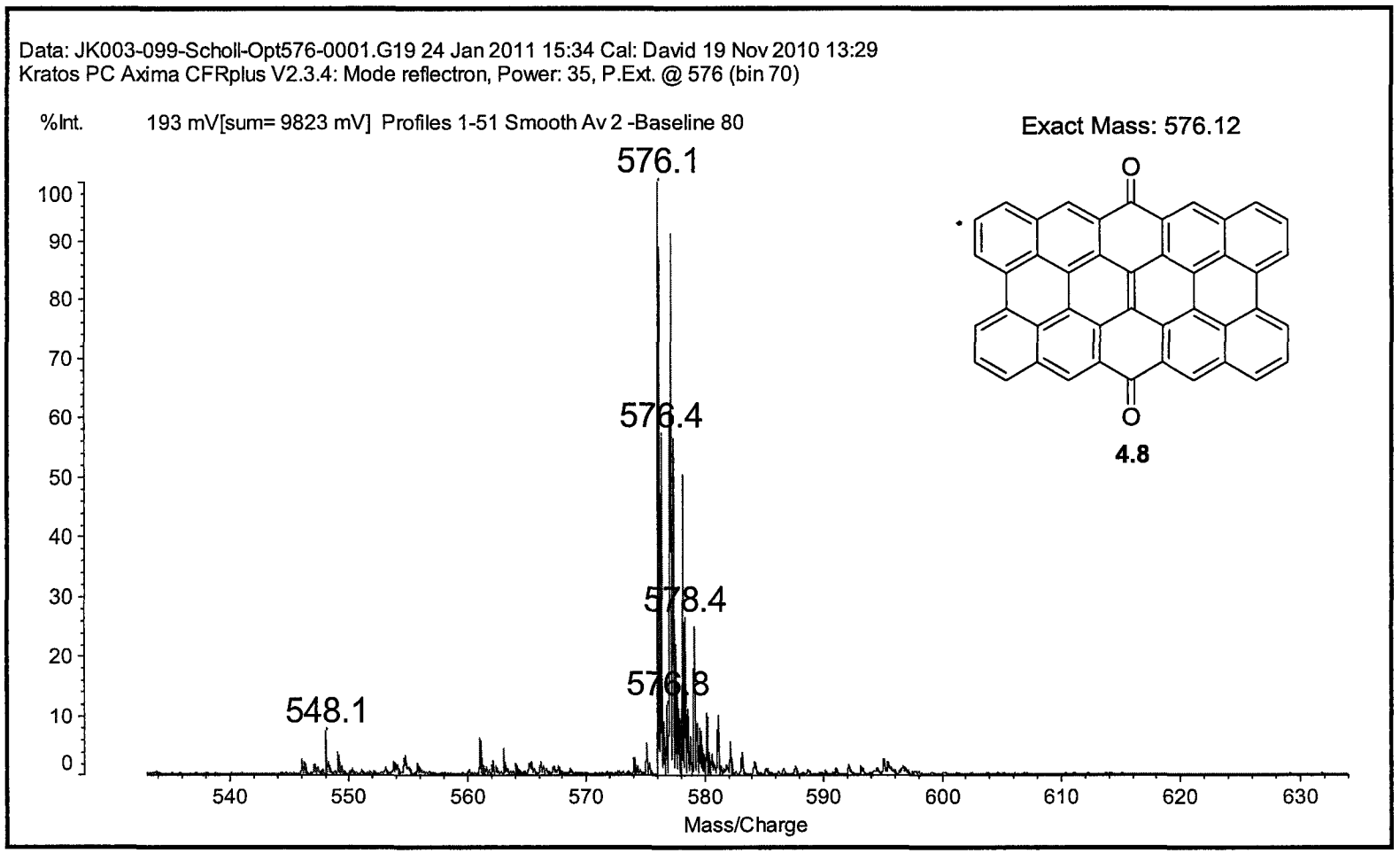
Data: JK003-099-Scholl-Opt576-0001.G19 24 Jan 2011 15:34 Cal: David 19 Nov 2010 13:29
Kratos PC Axima CFRplus V2.3.4: Mode reflectron, Power: 35, P.Ext. @ 576 (bin 70)
%Int.
193 mV[sum= 9823 mV] Profiles 1-51 Smooth Av 2 -Baseline 80
Exact Mass: 576.12
576.1
576.4
578.4
576.8
548.1
100
90
80
70
60
50
40
30
20
10
0
540
550
560
570
580
590
600
610
620
630
Mass/Charge
O
O
4.8

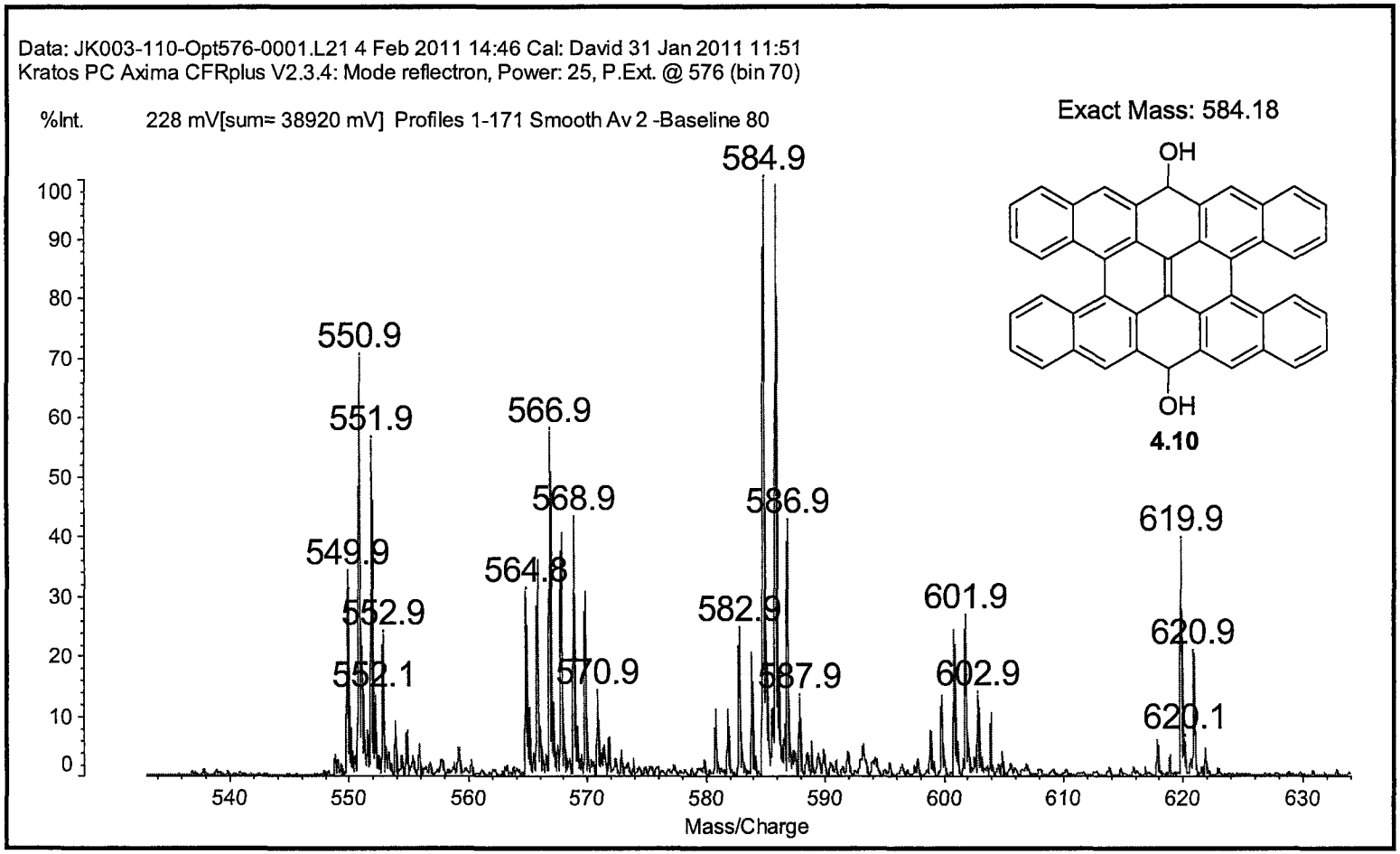
Data: JK003-110-Opt576-0001.L21 4 Feb 2011 14:46 Cal: David 31 Jan 2011 11:51
Kratos PC Axima CFRplus V2.3.4: Mode reflectron, Power: 25, P.Ext. @ 576 (bin 70)
%Int.
228 mV[sum= 38920 mV] Profiles 1-171 Smooth Av 2 -Baseline 80
Exact Mass: 584.18
OH
OH
4.10
584.9
550.9
551.9
566.9
568.9
586.9
619.9
549.9
564.8
552.9
582.9
601.9
620.9
552.1
570.9
587.9
602.9
620.1
100
90
80
70
60
50
40
30
20
10
0
540
550
560
570
580
590
600
610
620
630
Mass/Charge

Mass Spec

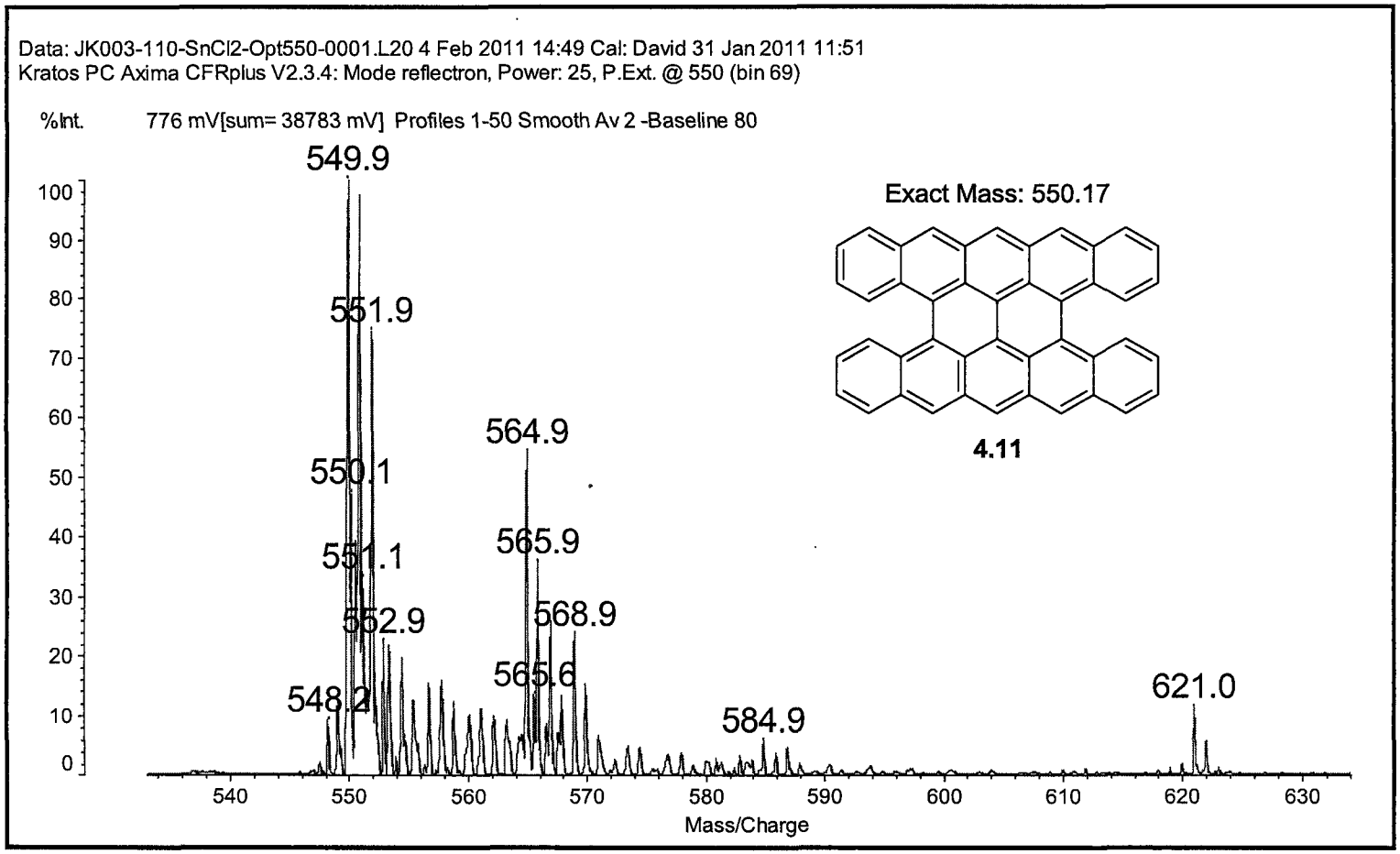
Data: JK003-110-SnCl2-Opt550-0001.L20 4 Feb 2011 14:49 Cal: David 31 Jan 2011 11:51
Kratos PC Axima CFRplus V2.3.4: Mode reflectron, Power: 25, P.Ext. @ 550 (bin 69)
%Int.
776 mV[sum= 38783 mV] Profiles 1-50 Smooth Av 2 -Baseline 80
549.9
551.9
550.1
564.9
551.1
565.9
552.9
568.9
548.2
565.6
584.9
621.0
Exact Mass: 550.17
4.11
Mass/Charge

^{1}H-NMR

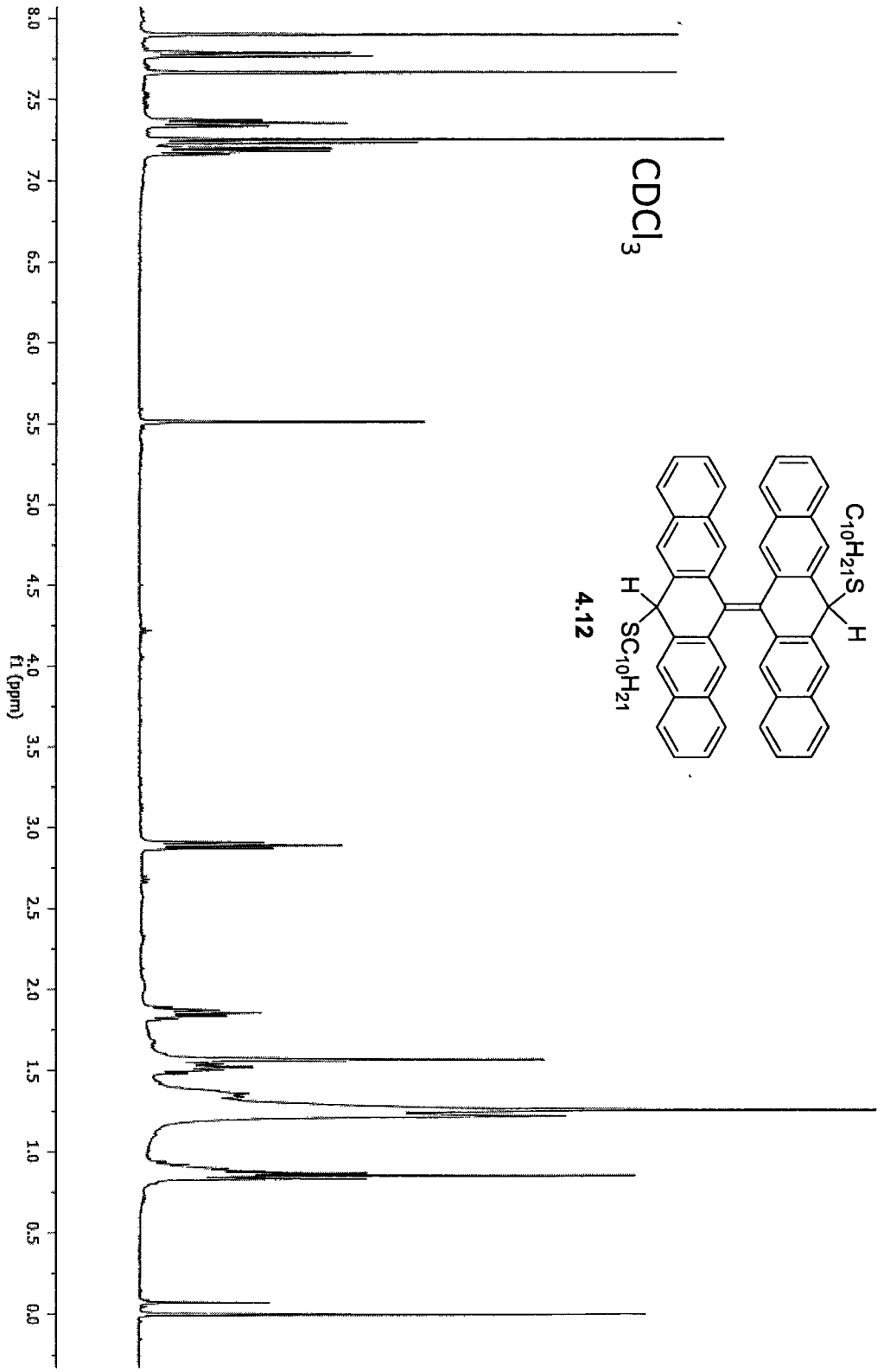
CDCl3
C10H21S
H
H
SC10H21
4.12
f1 (ppm)
8.0
7.5
7.0
6.5
6.0
5.5
5.0
4.5
4.0
3.5
3.0
2.5
2.0
1.5
1.0
0.5
0.0

^{13}C-NMR

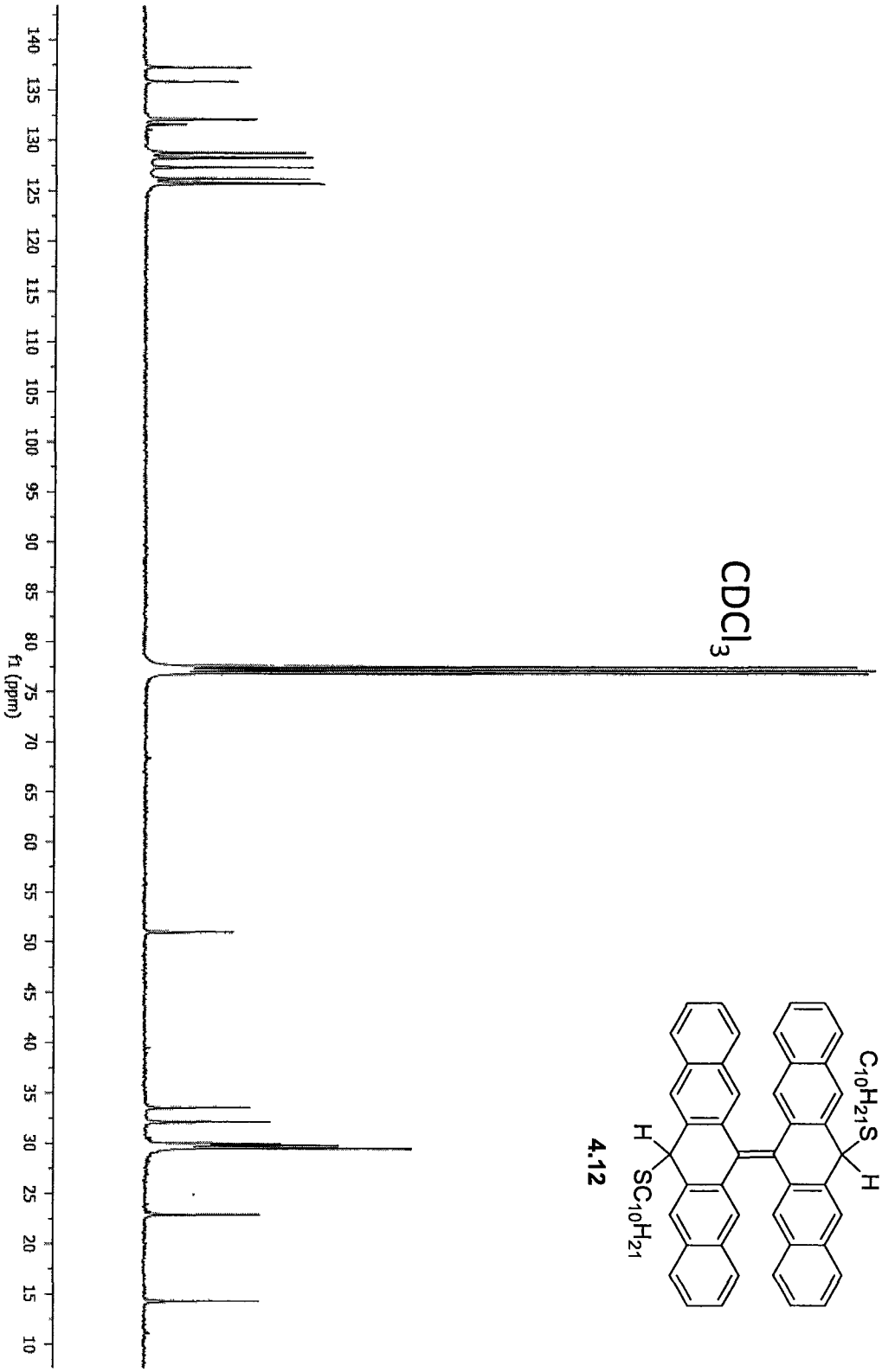

^{1}H-NMR

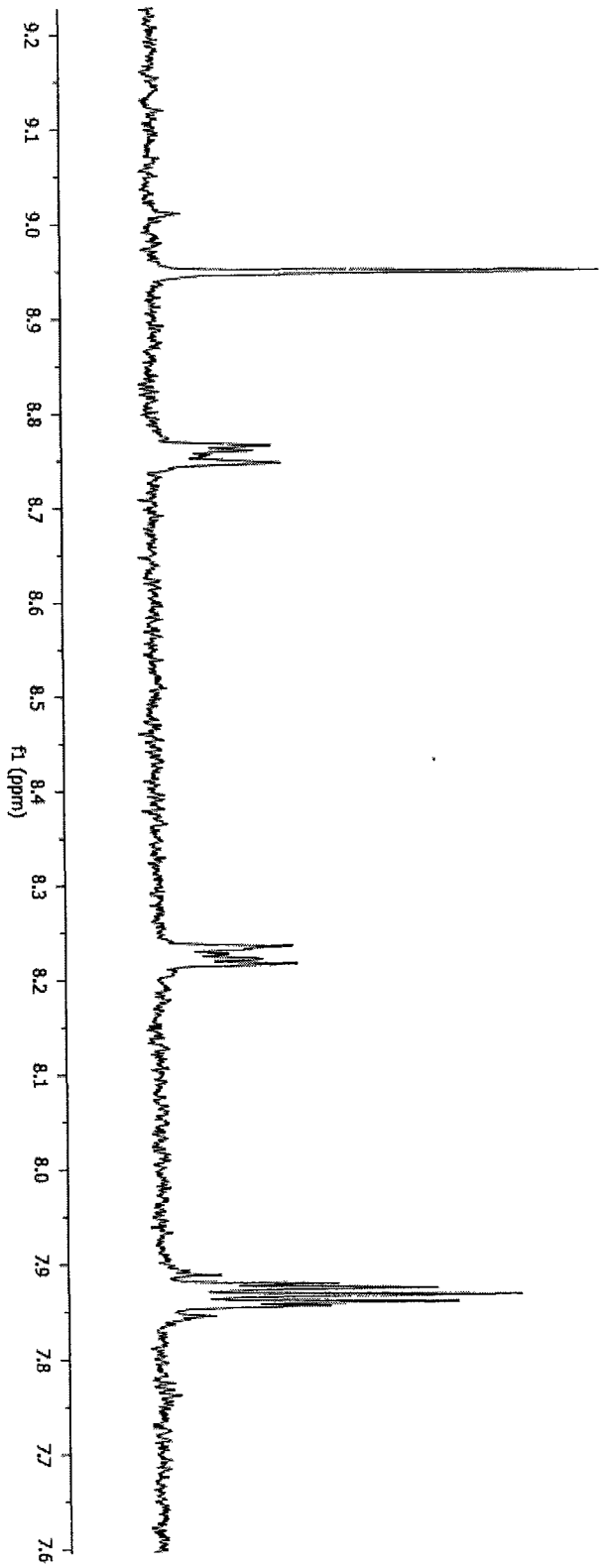

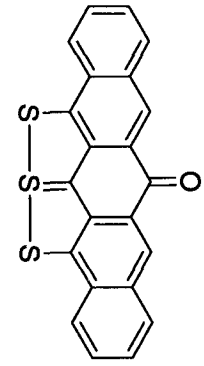

4.13

gCOSY-NMR

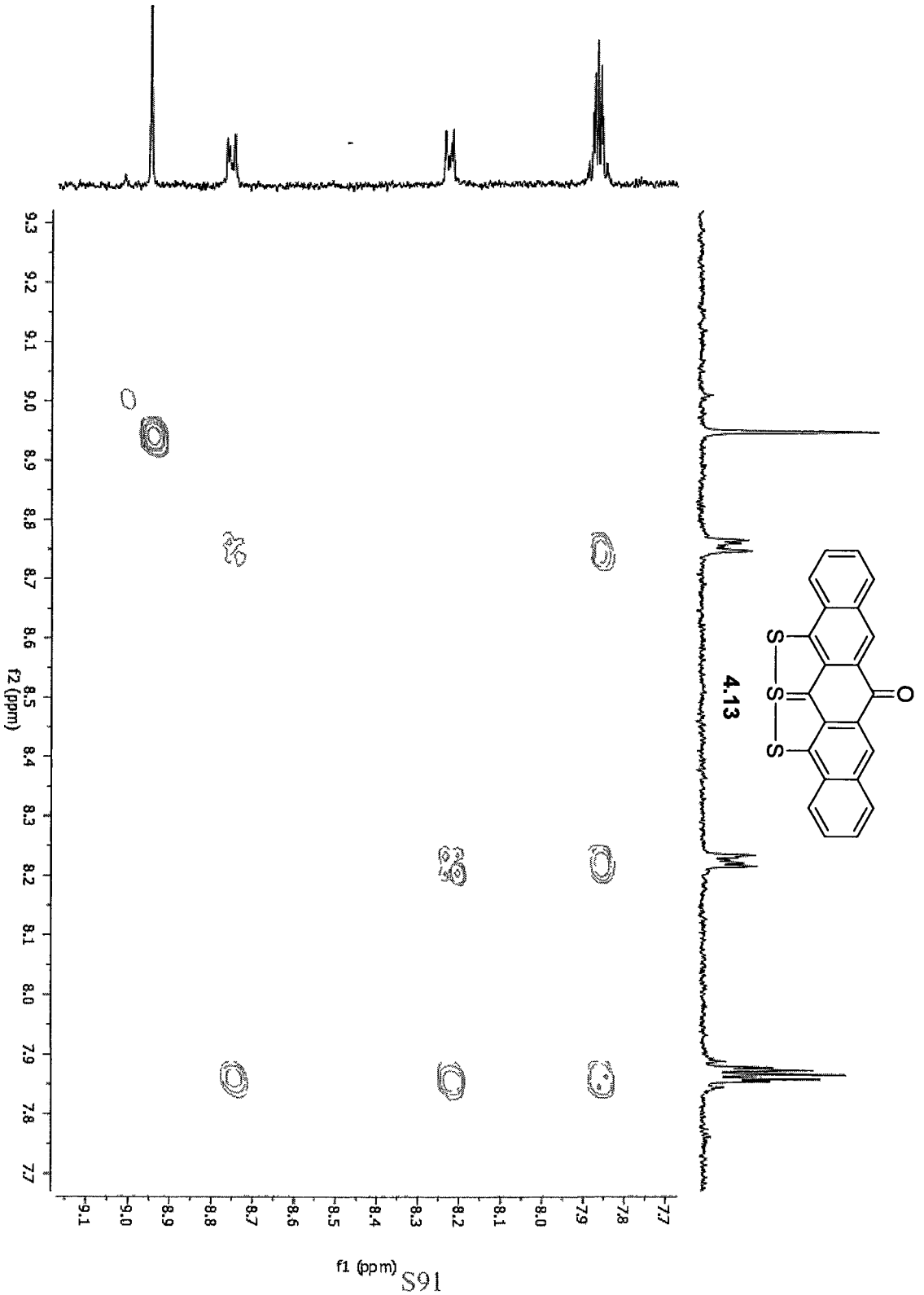

Mass Spec

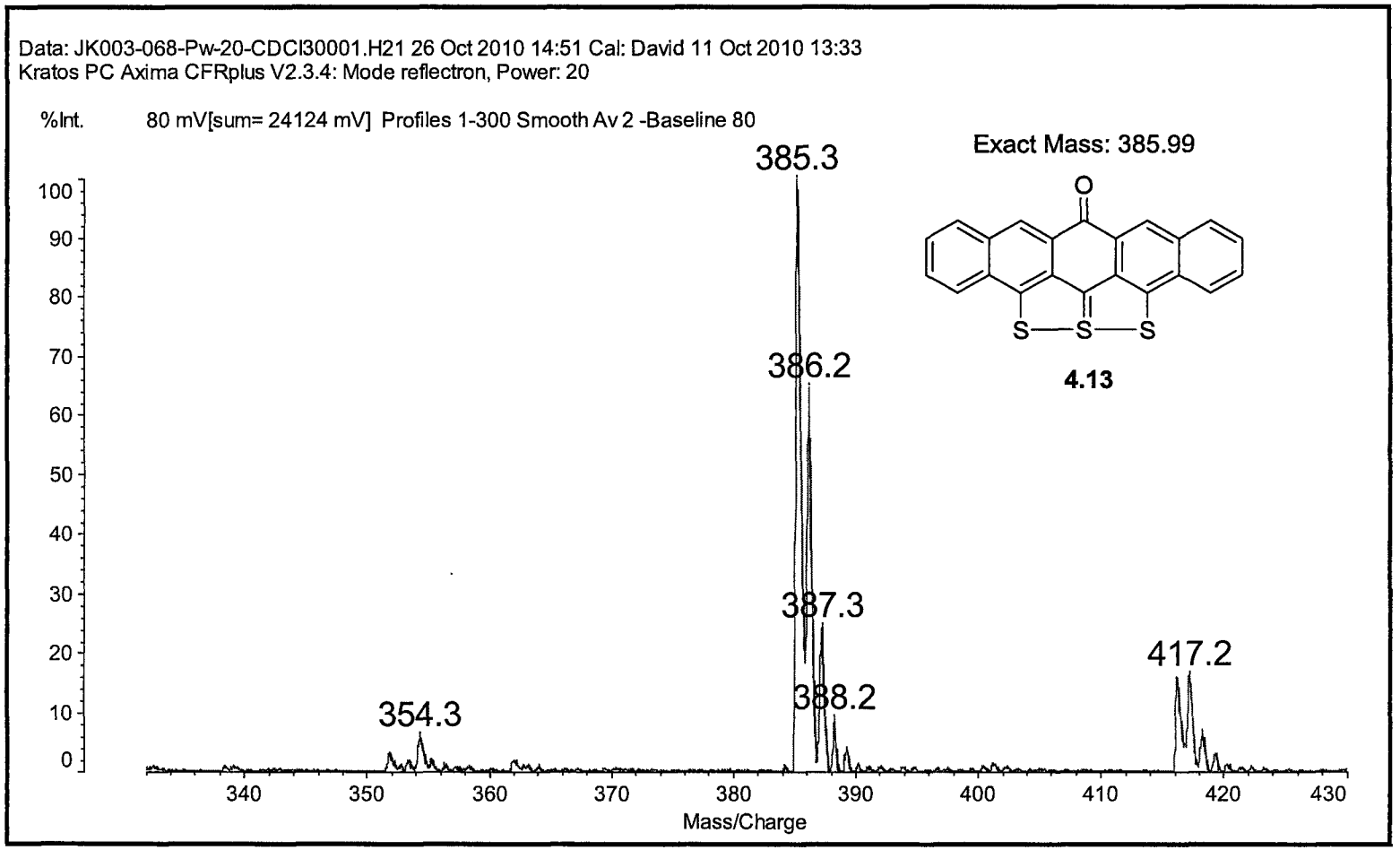
Data: JK003-068-Pw-20-CDCl30001.H21 26 Oct 2010 14:51 Cal: David 11 Oct 2010 13:33
Kratos PC Axima CFRplus V2.3.4: Mode reflectron, Power: 20
%Int.
80 mV[sum= 24124 mV] Profiles 1-300 Smooth Av 2 -Baseline 80
385.3
386.2
387.3
388.2
354.3
417.2
Exact Mass: 385.99
O
S
S
S
4.13
100
90
80
70
60
50
40
30
20
10
0
340
350
360
370
380
390
400
410
420
430
Mass/Charge

X-Ray Crystal Structure of **4.13**

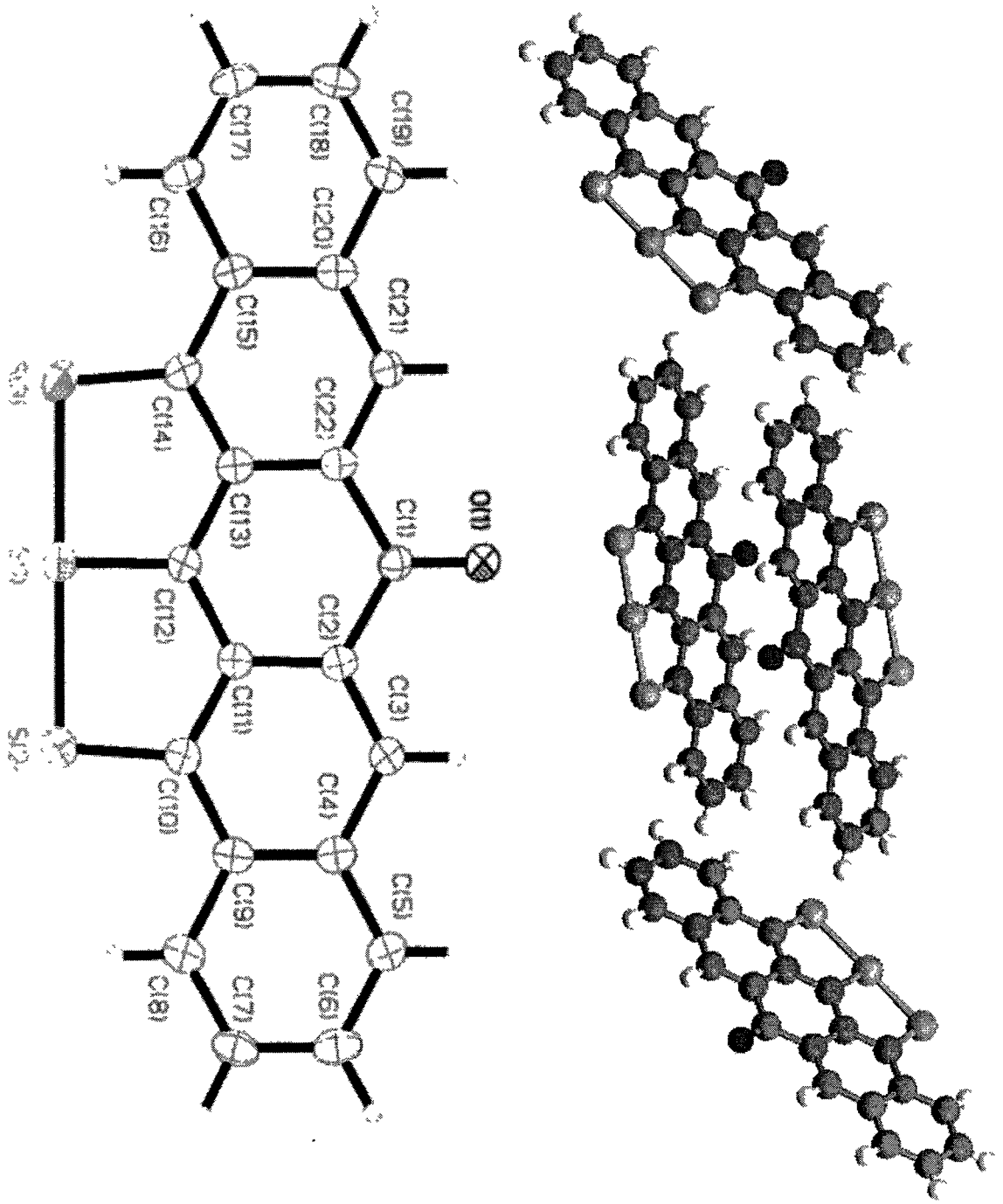

XYZ coordinates for the the X-Ray Crystal Structure of **4.13**

O	6.080382	1.199587	-0.707582
C	7.026419	1.218020	0.045650
C	6.919826	0.747622	1.450695
C	5.731645	0.245521	1.898964
H	4.995125	0.190961	1.301273
C	5.572825	-0.199071	3.245887
C	4.346567	-0.747622	3.684508
H	3.610952	-0.796284	3.087287
C	4.213707	-1.209172	4.965779
H	3.385632	-1.572661	5.254506
C	5.302163	-1.146501	5.858786
H	5.202460	-1.481236	6.741675
C	6.505328	-0.608272	5.468169
H	7.227178	-0.559611	6.082803
C	6.666687	-0.125341	4.144542
C	7.915908	0.404040	3.674389
C	8.046444	0.843471	2.342761
C	9.289199	1.358844	1.886022
C	9.455297	1.793851	0.537687
C	10.691335	2.294478	0.125892
C	10.876585	2.744968	-1.231856
C	12.109402	3.250018	-1.695419
H	12.855999	3.293519	-1.108317
C	12.231529	3.681339	-2.997869
H	13.062447	4.026395	-3.301421
C	11.148402	3.617194	-3.875581
H	11.248195	3.922436	-4.769764
C	9.943219	3.117304	-3.459785
H	9.216799	3.070854	-4.070889
C	9.770890	2.669763	-2.127451
C	8.523615	2.155865	-1.673535
H	7.790762	2.110153	-2.275462
C	8.361616	1.724545	-0.383558
S	10.629142	1.459707	2.957395
S	9.296062	0.536533	4.658697
S	11.925308	2.359655	1.282683

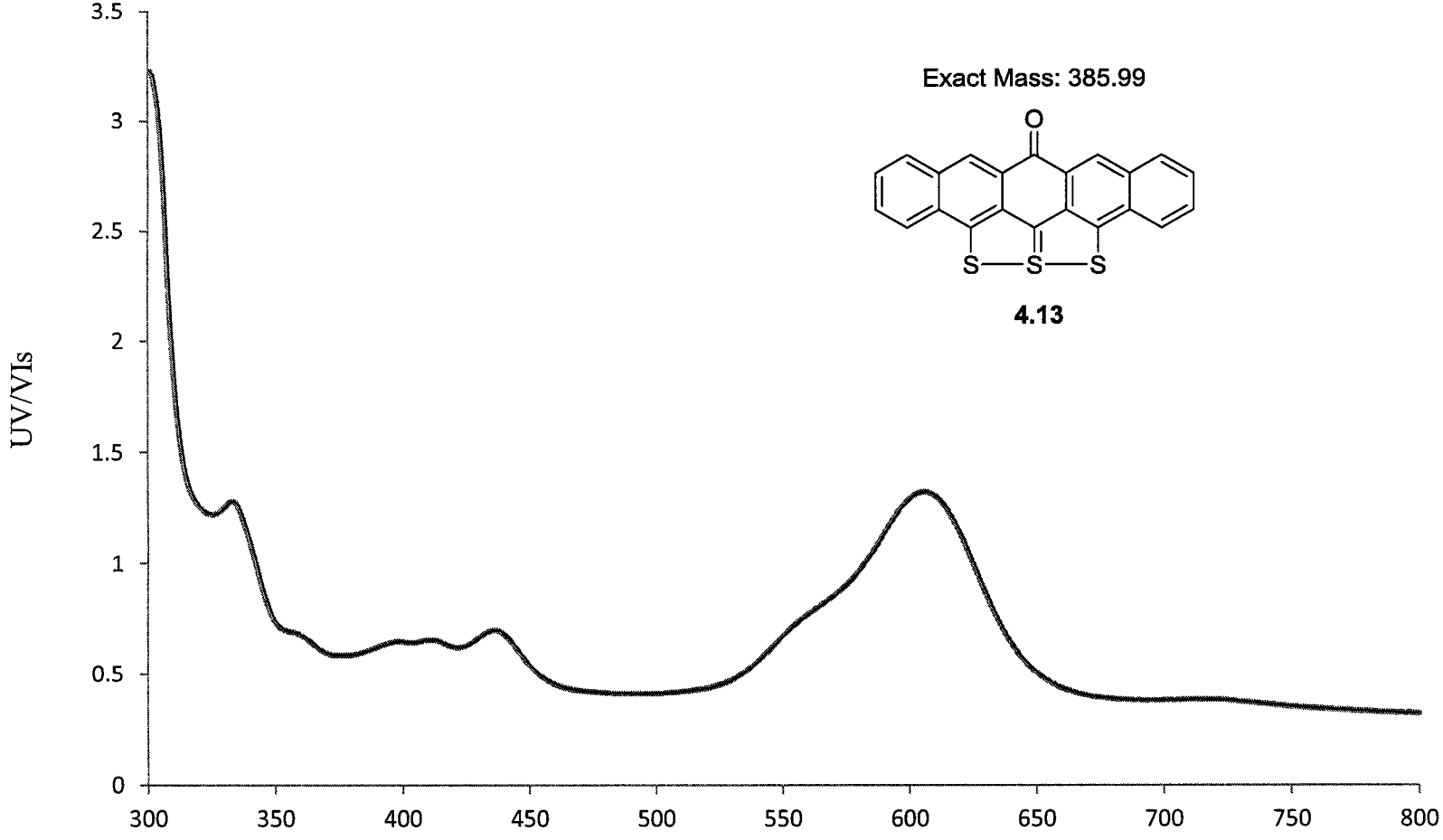
Exact Mass: 385.99
O
S
S
S
4.13
UV/VIs
3.5
3
2.5
2
1.5
1
0.5
0
300
350
400
450
500
550
600
650
700
750
800

TD- 3LYP/6-31+G(d,p) Calculations

Structure	Ground state	TD-B3LYP/6-311+G(d,p)// B3LYP/6-31G(d)		
		E_{HOMO}(eV)	E_{LUMO}(eV)	E_g(eV)
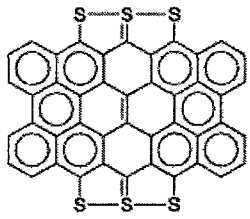	closed-shell	-5 25	-3 25	1 65
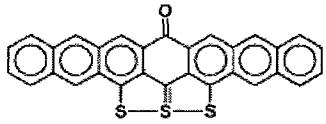	closed-shell	-5 73	-3 31	2 03
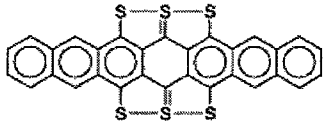	closed-shell	-5 45	-3 37	1 75
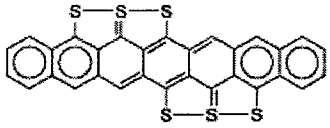	open-shell	–	couldn't optimize	–
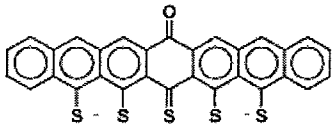	closed-shell	-5 39	-3 25	1 81
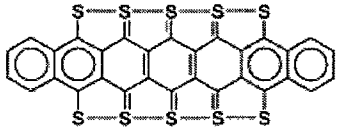	closed-shell	-4 95	-3 32	1 40
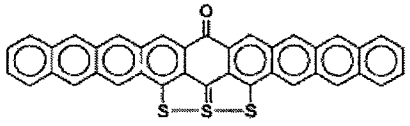	closed-shell	-5 44	-3 28	1 79
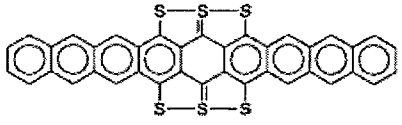	closed-shell	-5 29	-3 34	1 54

TD- 3LYP/6-31+G(d,p) Calculations

Structure	Ground state	TD-B3LYP/6-311+G(d,p)// B3LYP/6-31G(d)		
		E_{HOMO} (eV)	E_{LUMO} (eV)	E_g (eV)
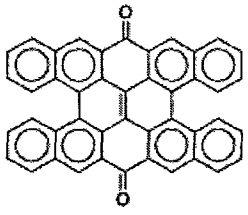	closed-shell	-5 98	-2 97	2 53
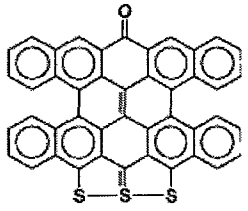	closed-shell	-5 62	-3 33	1 98
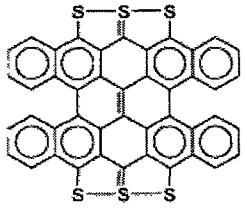	closed-shell	-5 39	-3 30	1 75
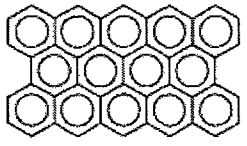	open-shell	-4 84	-3 10	1 28
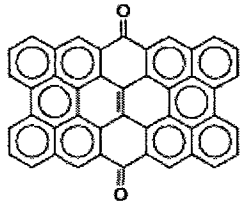	closed-shell	-5 64	-3 08	2 18
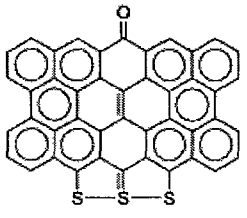	closed-shell	5 43	-3 23	1 82

TD- 3LYP/6-31+G(d,p) Calculations

Structure	Ground state	TD-B3LYP/6 311+G(d,p)// B3LYP/6-31G(d)		
		E_{HOMO} (eV)	E_{LUMO} (eV)	E_g (eV)
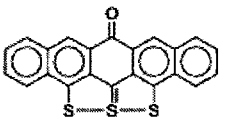	closed-shell	-6 04	-3 47	2 13
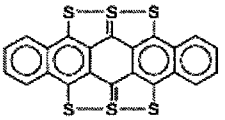	closed-shell	-5 62	-3 54	1 76
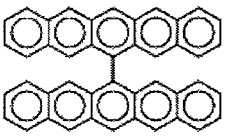	closed-shell	-5 00	-2 85	1 64
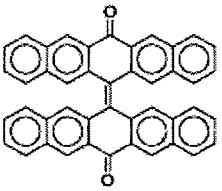	closed-shell	-5 90	-2 72	2 63
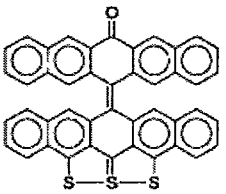	triplet	-5 20	-2 96	1 36
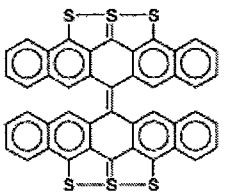	open-shell triplet	-5 32 -5 32	-3 72 -2 98	0 91 1 33
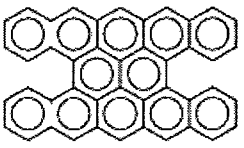	open-shell	-4 76	-3 07	1 14

^{1}H-NMR

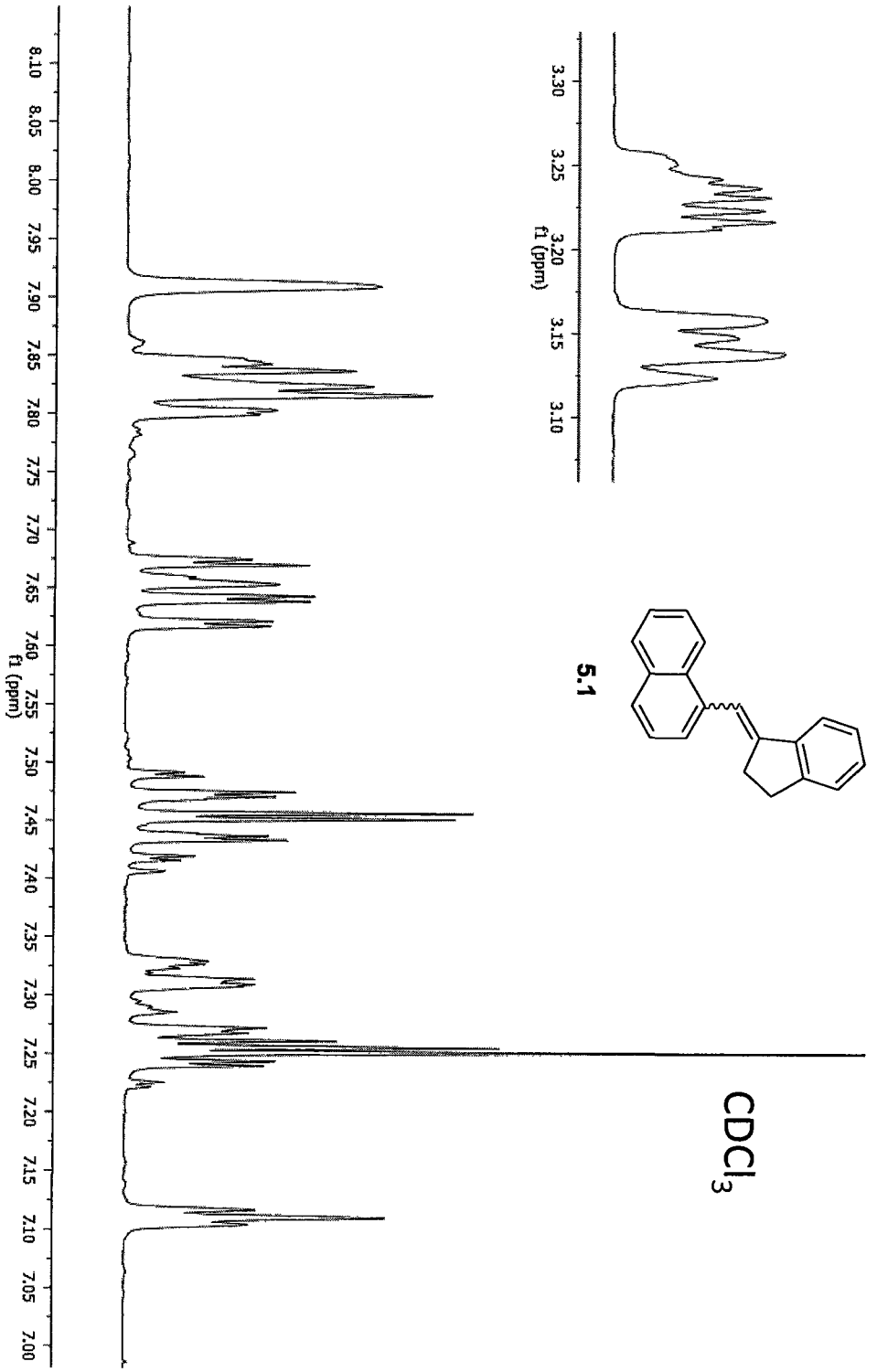
8.10
8.05
8.00
7.95
7.90
7.85
7.80
7.75
7.70
7.65
7.60
7.55
7.50
7.45
7.40
7.35
7.30
7.25
7.20
7.15
7.10
7.05
7.00
f1 (ppm)
3.30
3.25
3.20
3.15
3.10
f1 (ppm)
5.1
CDCl3

^{13}C-NMR

In $CDCl_3$

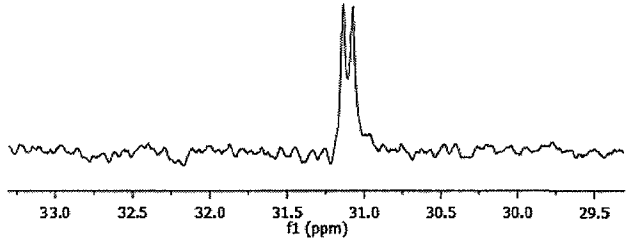

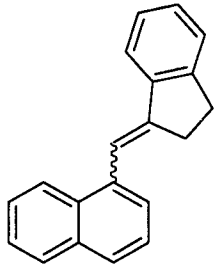

5.1

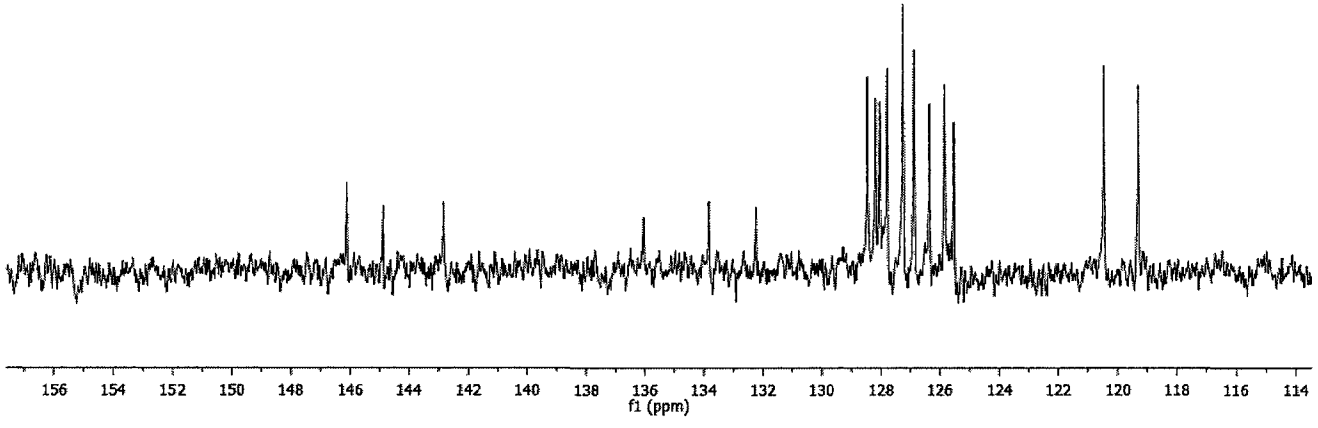

^{1}H-NMR

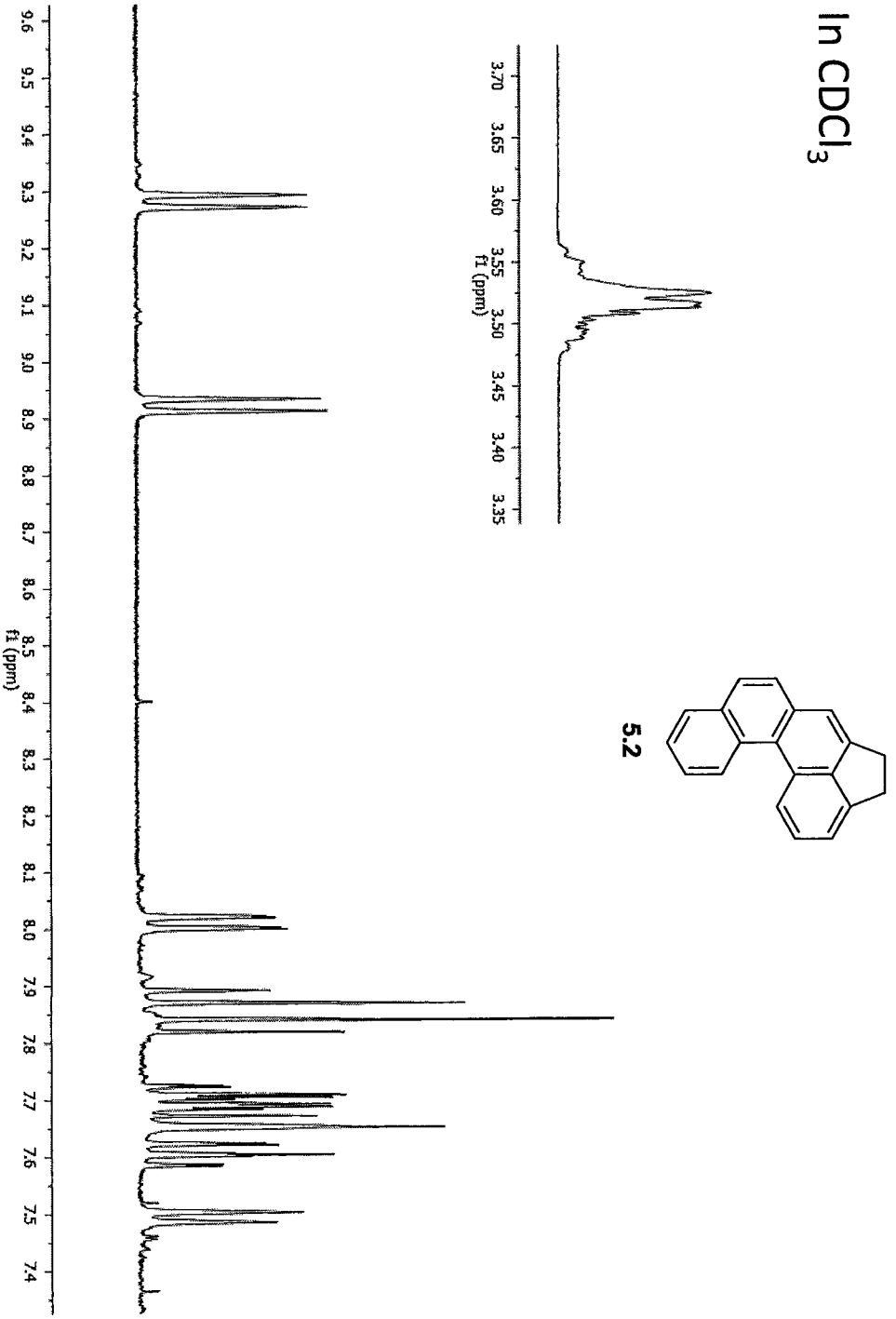

^{13}C-NMR

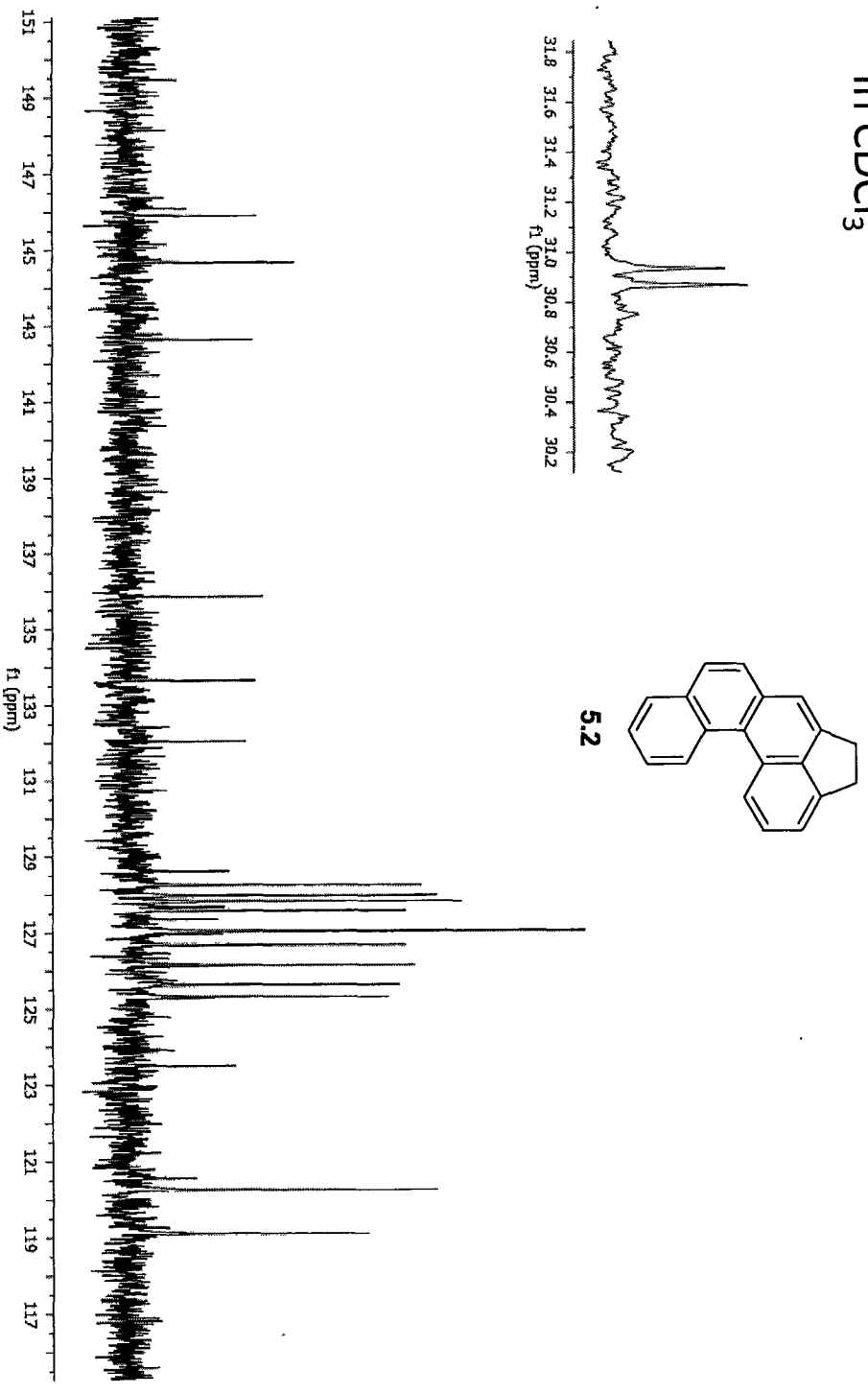

^{1}H-NMR

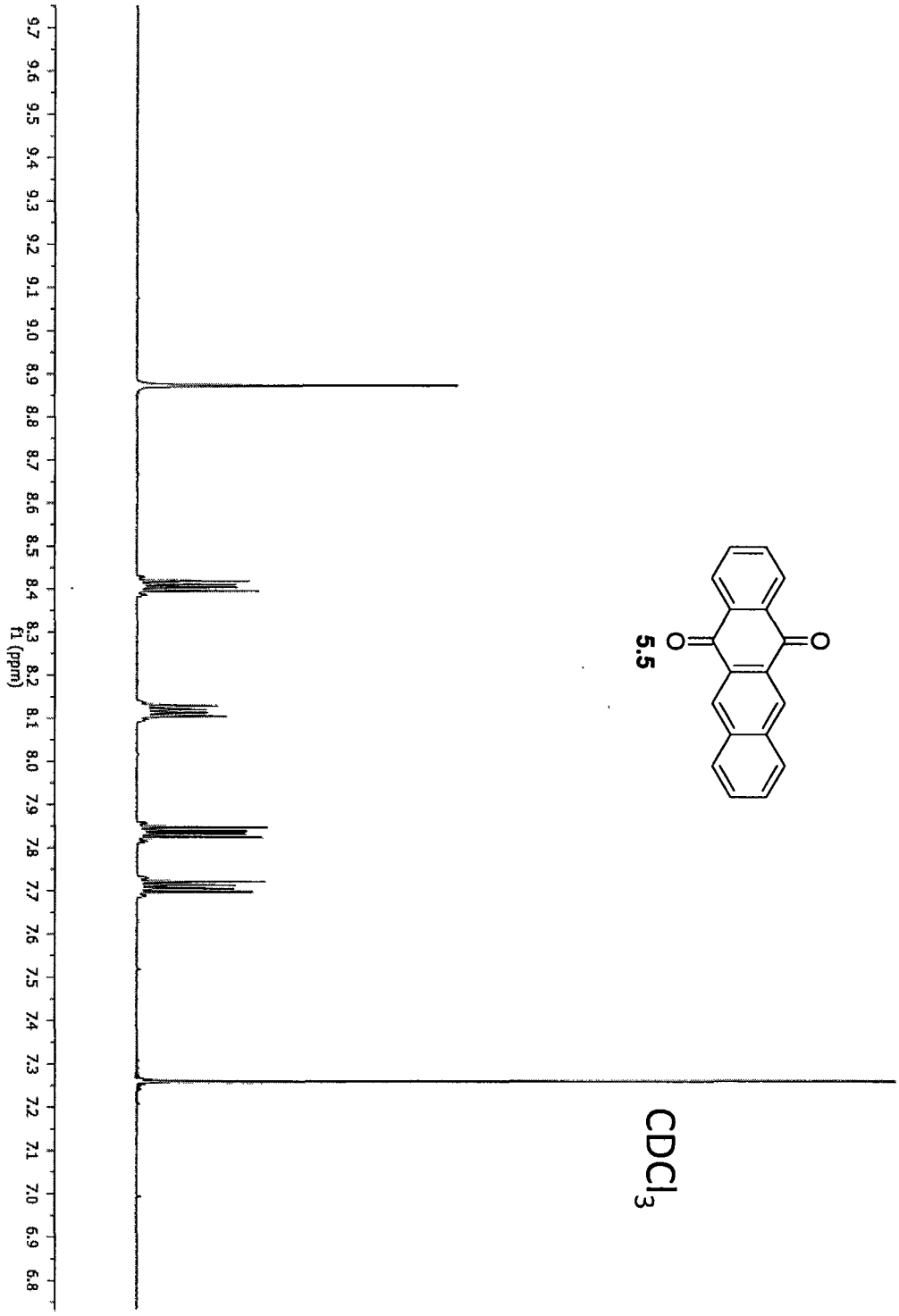
9.7 9.6 9.5 9.4 9.3 9.2 9.1 9.0 8.9 8.8 8.7 8.6 8.5 8.4 8.3 8.2 8.1 8.0 7.9 7.8 7.7 7.6 7.5 7.4 7.3 7.2 7.1 7.0 6.9 6.8
f1 (ppm)
5.5
CDCl3

^{13}C-NMR

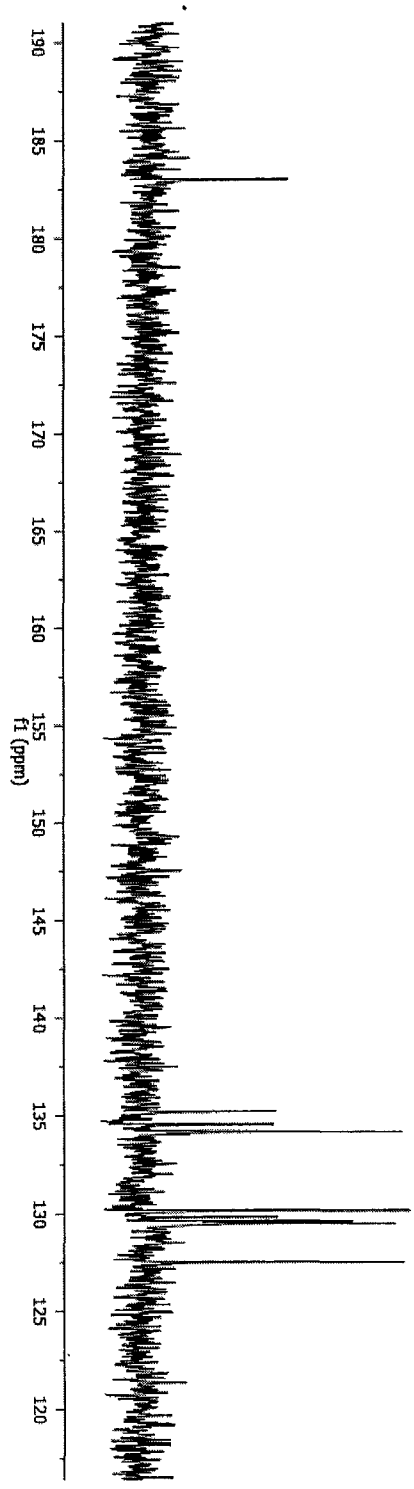
190
185
180
175
170
165
160
155
150
145
140
135
130
125
120
f1 (ppm)

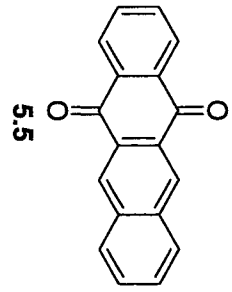
O
O

5.5

X-Ray Crystal Structure of **5.5**

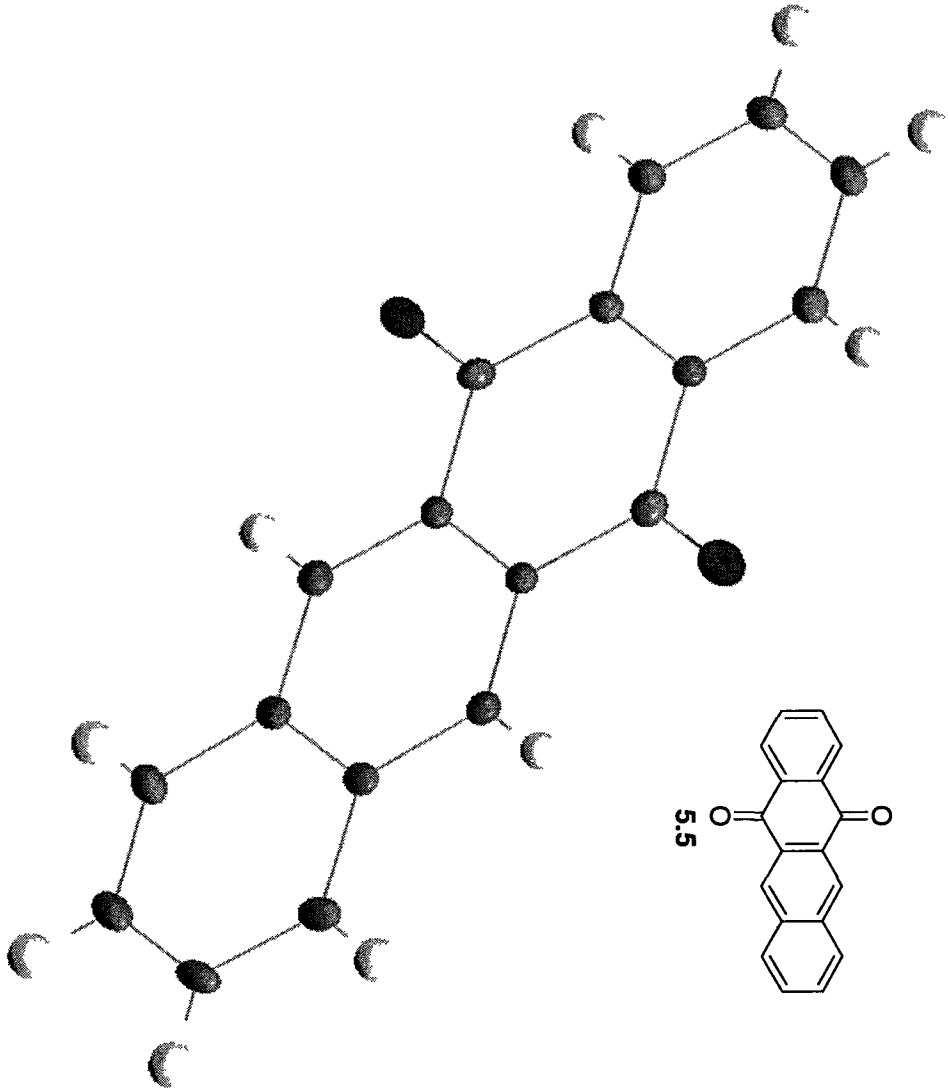

5.5

XYZ coordinates for the X-Ray Crystal Structure of **5.5**

O	3.950465	8.676621	14.658593
O	3.000138	3.409245	14.920943
C	5.800478	5.206959	20.440094
H	6.043401	4.733487	21.203407
C	5.183280	4.563333	19.417857
H	4.995351	3.655845	19.495192
C	4.819291	5.251347	18.230917
C	4.198927	4.622517	17.133058
H	4.025637	3.708864	17.175151
C	3.841269	5.316696	15.998245
C	3.203101	4.615119	14.873221
C	2.801527	5.394375	13.686525
C	2.185515	4.755681	12.624397
H	2.021325	3.840795	12.667225
C	1.815988	5.467122	11.509407
H	1.400961	5.034339	10.797488
C	2.058515	6.814791	11.442351
H	1.804118	7.290729	10.684912
C	3.058693	6.760539	13.613840
C	3.726929	7.470747	14.719531
C	4.111887	6.698889	15.919197
C	4.731854	7.332651	16.960523
H	4.916618	8.241372	16.891265
C	5.103360	6.640938	18.149911
C	5.721746	7.274700	19.258783
H	5.887914	8.189586	19.228436
C	6.073865	6.569424	20.359823
H	6.500365	6.998508	21.066358
C	2.670174	7.465815	12.476825
H	2.826848	8.381934	12.422495

^{1}H-NMR

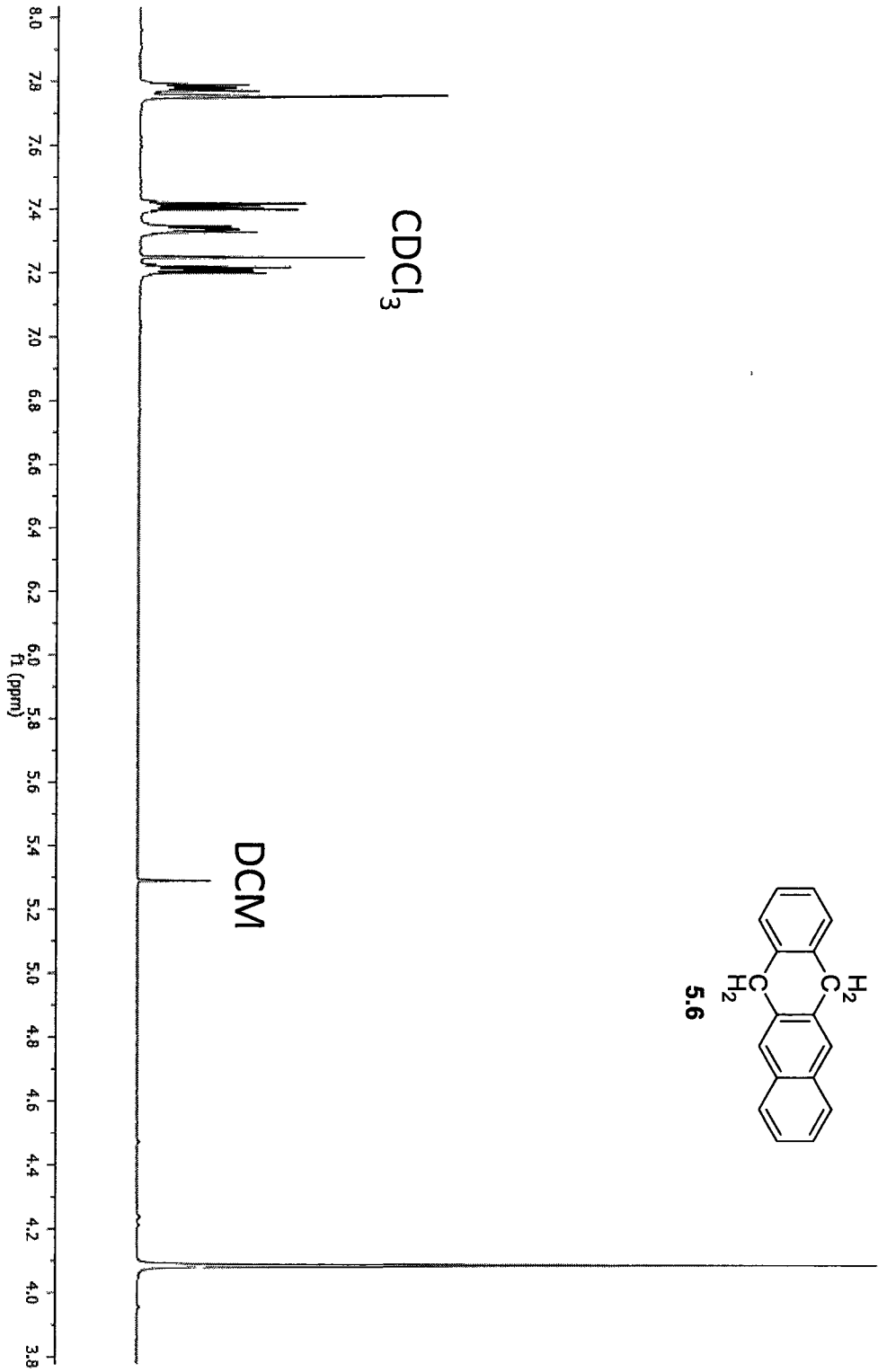
CDCl3
DCM
f1 (ppm)
8.0
7.8
7.6
7.4
7.2
7.0
6.8
6.6
6.4
6.2
6.0
5.8
5.6
5.4
5.2
5.0
4.8
4.6
4.4
4.2
4.0
3.8
H2
C
C
H2
5.6

X-Ray Crystal Structure of **5.6**

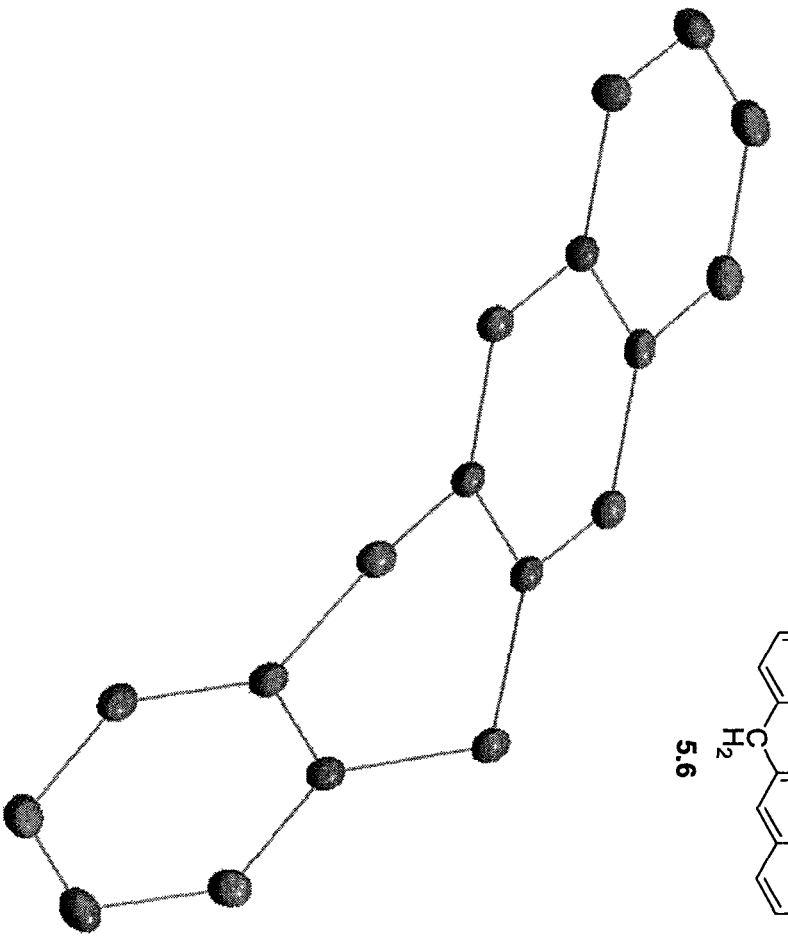

XYZ coordinates for the X-Ray Crystal Structure of **5.6**

C	3.566240	3.660843	11.752945
H	2.743638	3.235931	11.665928
C	4.437158	3.258174	12.742922
H	4.202304	2.567116	13.321054
C	5.662193	3.887105	12.872285
H	6.255445	3.615591	13.535368
C	6.006524	4.918707	12.017610
H	6.829737	5.340551	12.112631
C	5.135605	5.330581	11.018595
C	5.452414	6.454988	10.070190
H	6.407733	6.622959	10.075354
H	5.004111	7.263395	10.367132
C	5.005946	6.117512	8.663204
C	5.749652	6.405900	7.555999
H	6.572865	6.826211	7.658509
C	5.295844	6.078396	6.248424
C	6.049336	6.366784	5.081573
H	6.871938	6.793230	5.159036
C	5.580238	6.023939	3.847329
H	6.085420	6.215687	3.090774
C	4.339914	5.385037	3.714609
H	4.029832	5.154173	2.868713
C	3.587646	5.099717	4.803739
H	2.766878	4.676338	4.694258
C	4.032279	5.435658	6.111572
C	3.288573	5.142668	7.280231
H	2.466583	4.716222	7.198895
C	3.747273	5.470940	8.520930
C	2.983996	5.174115	9.793647
H	2.528354	5.977920	10.088265
H	2.312460	4.497629	9.615740
C	3.899562	4.691678	10.884584

^{1}H-NMR

In $CDCl_3$

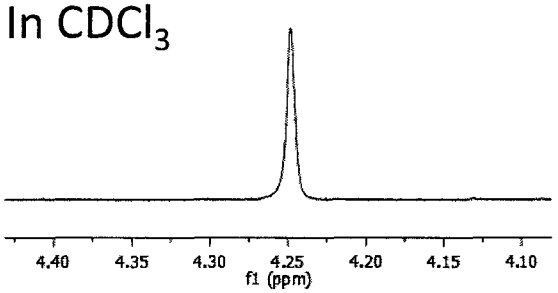

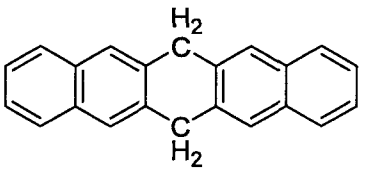

5.7

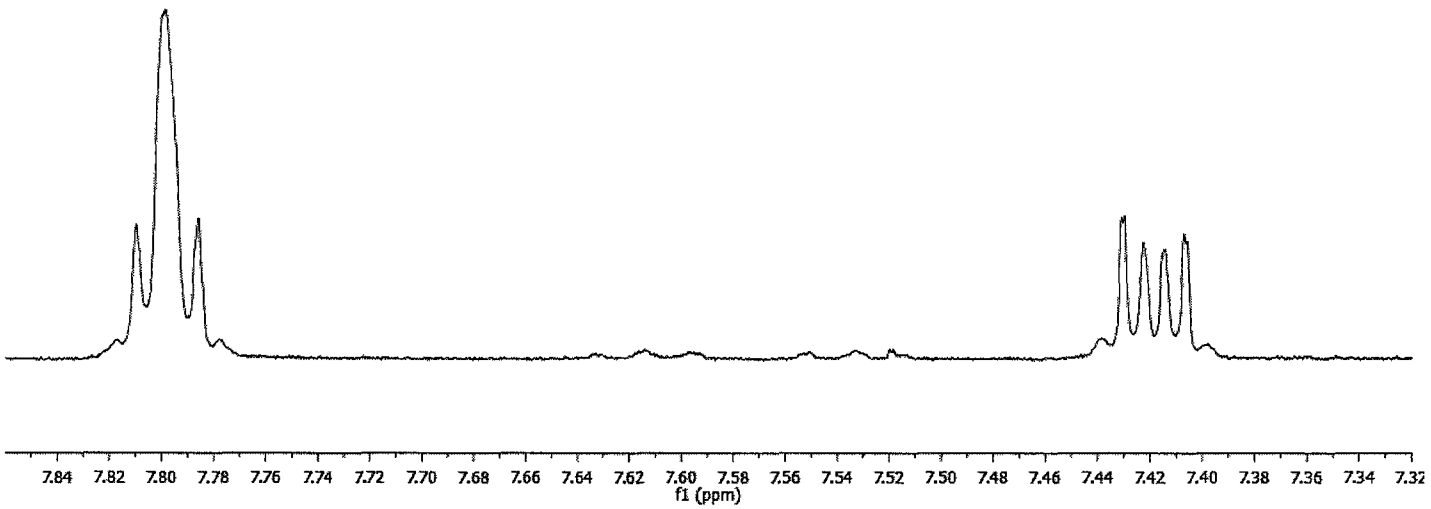

^{13}C-NMR

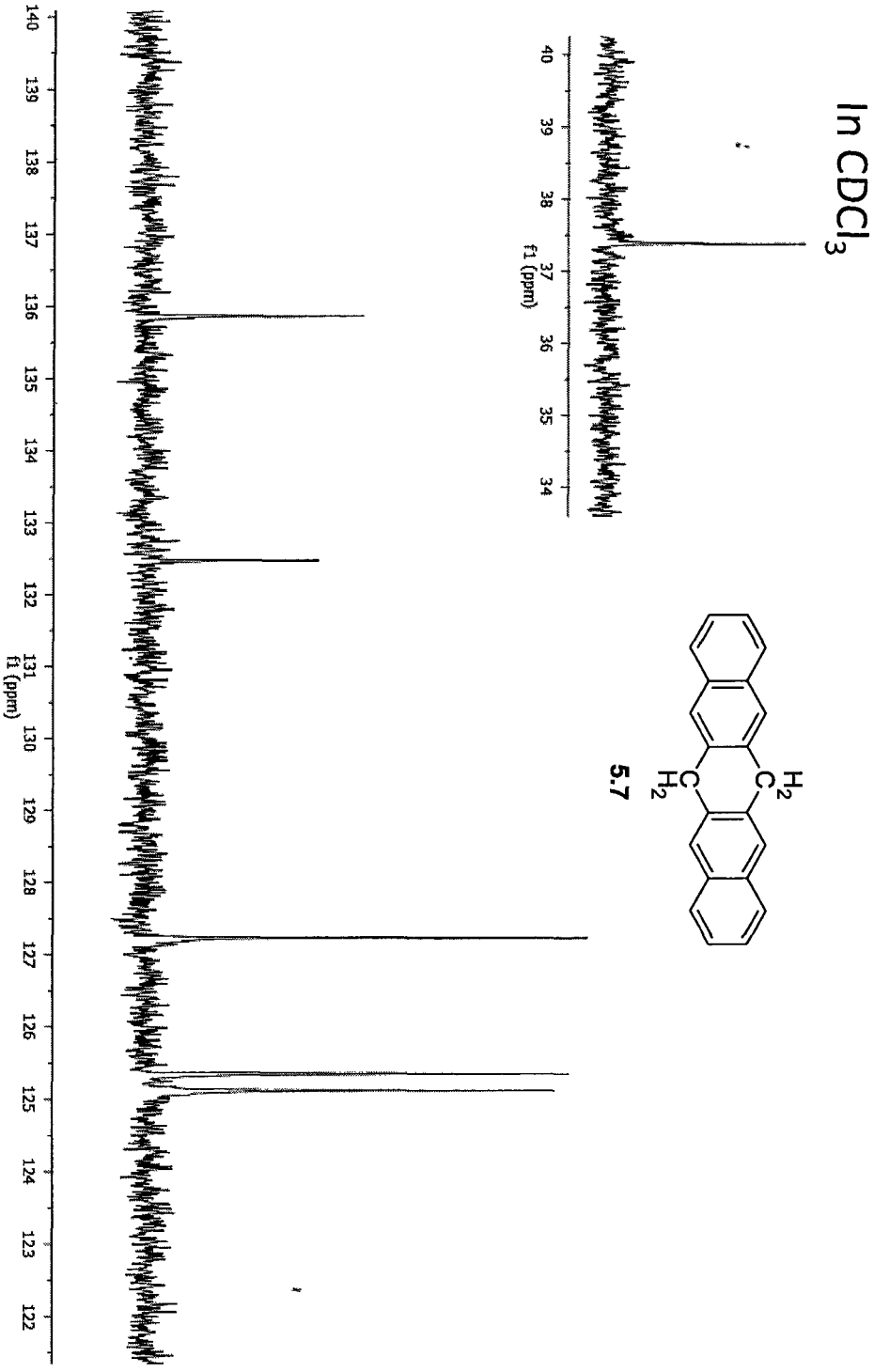

^{1}H-NMR

In $CDCl_3$

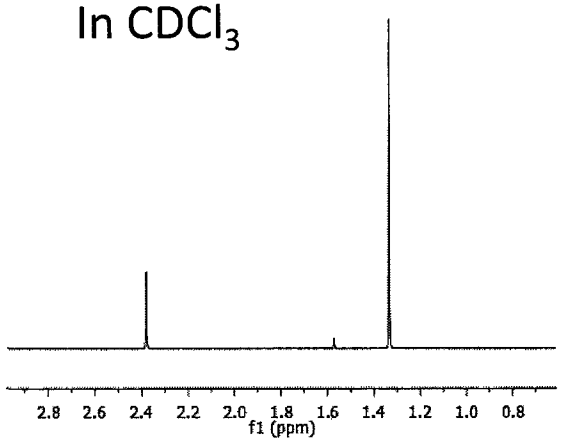

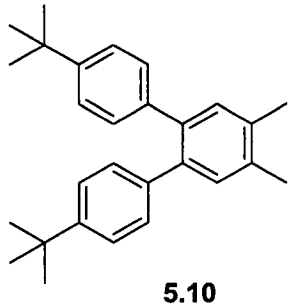

5.10

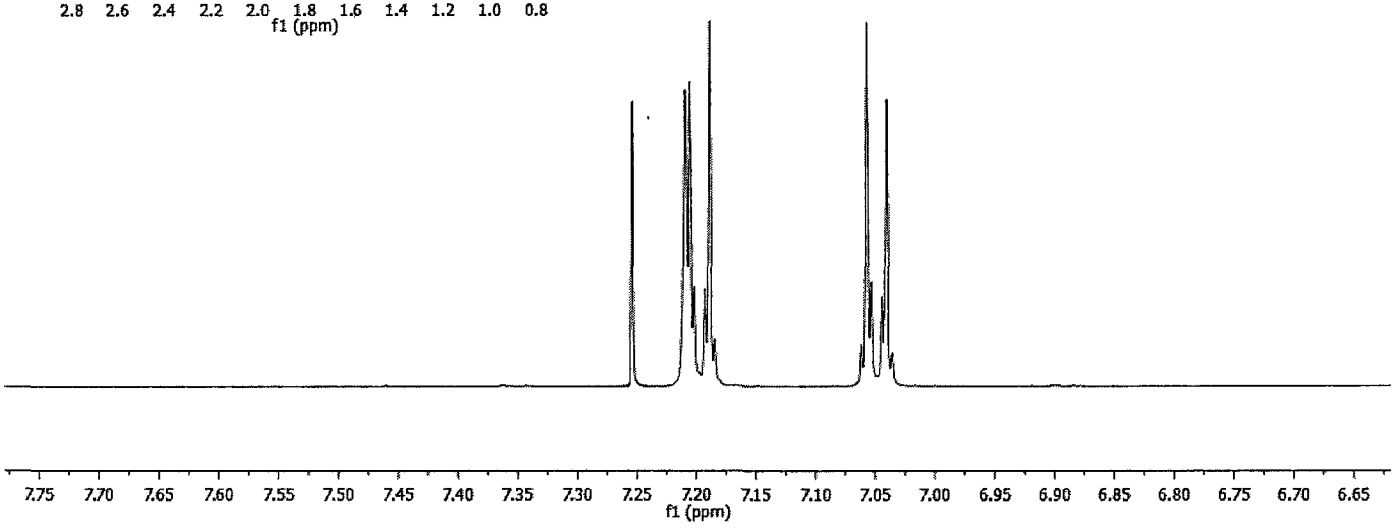

^{13}C-NMR

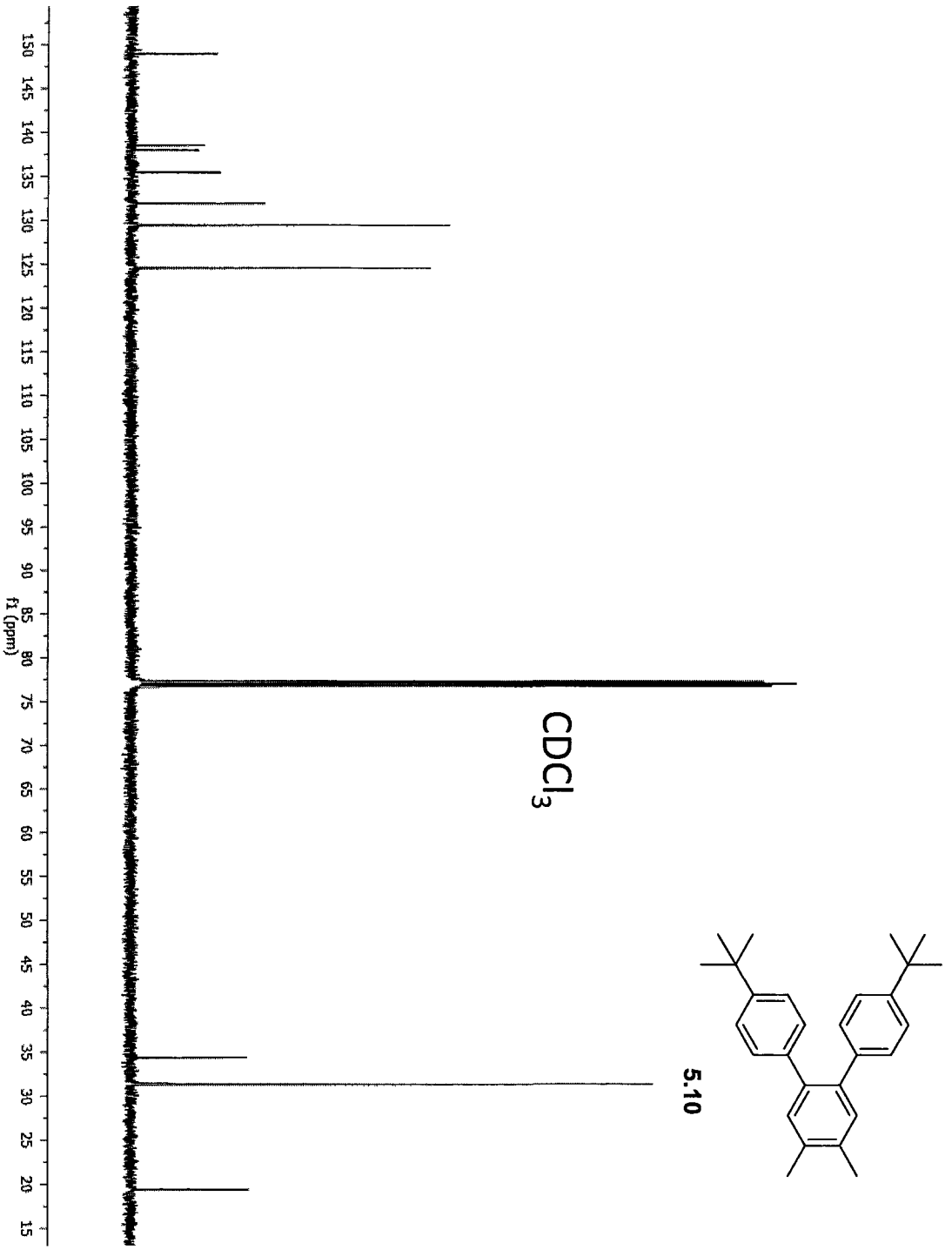
150 145 140 135 130 125 120 115 110 105 100 95 90 85 80 75 70 65 60 55 50 45 40 35 30 25 20 15
f1 (ppm)
CDCl3
5.10

^{1}H-NMR

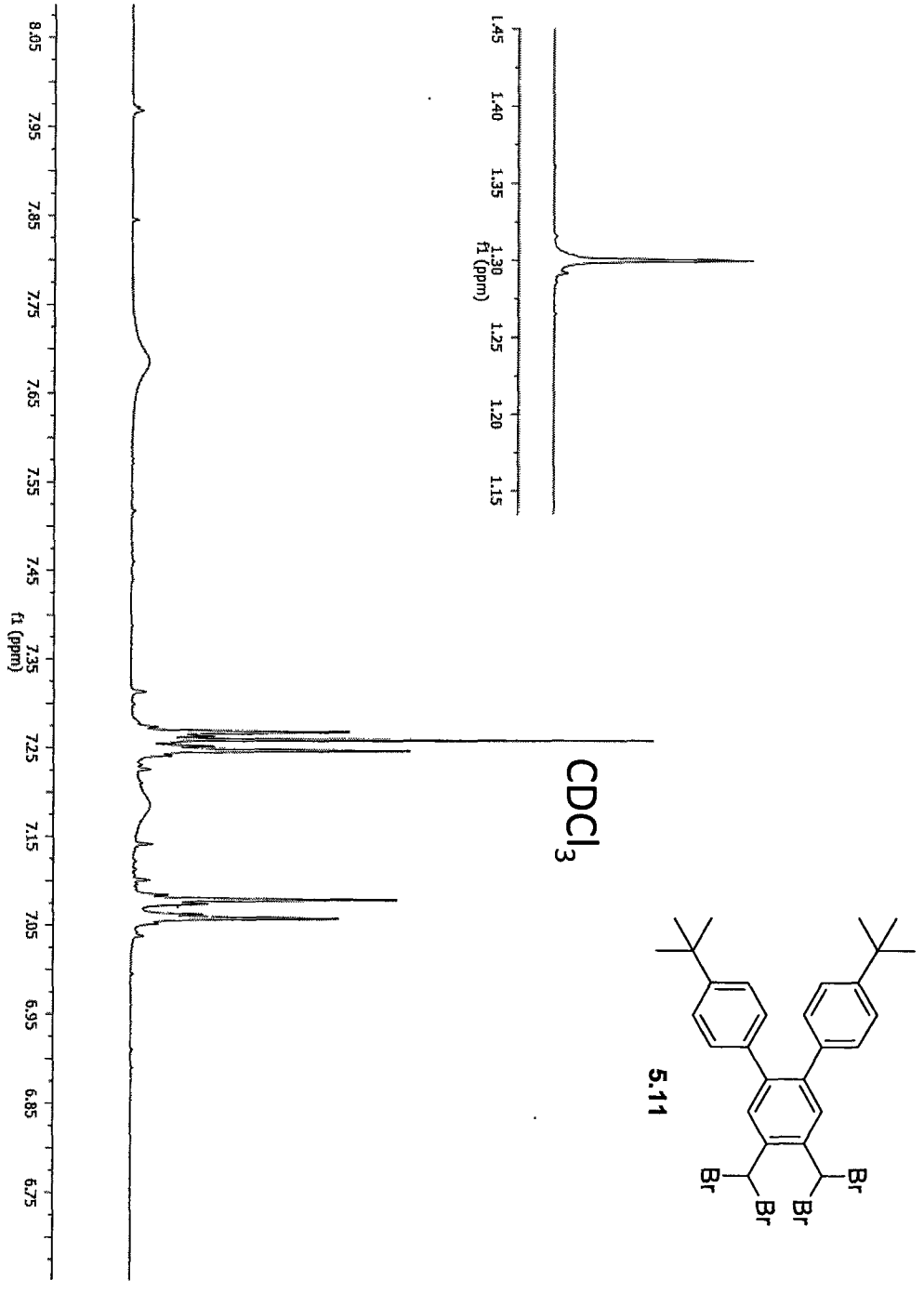
8.05
7.95
7.85
7.75
7.65
7.55
7.45
7.35
7.25
7.15
7.05
6.95
6.85
6.75
f1 (ppm)
1.45
1.40
1.35
1.30
1.25
1.20
1.15
f1 (ppm)
CDCl3
5.11
Br
Br
Br
Br

^{13}C-NMR

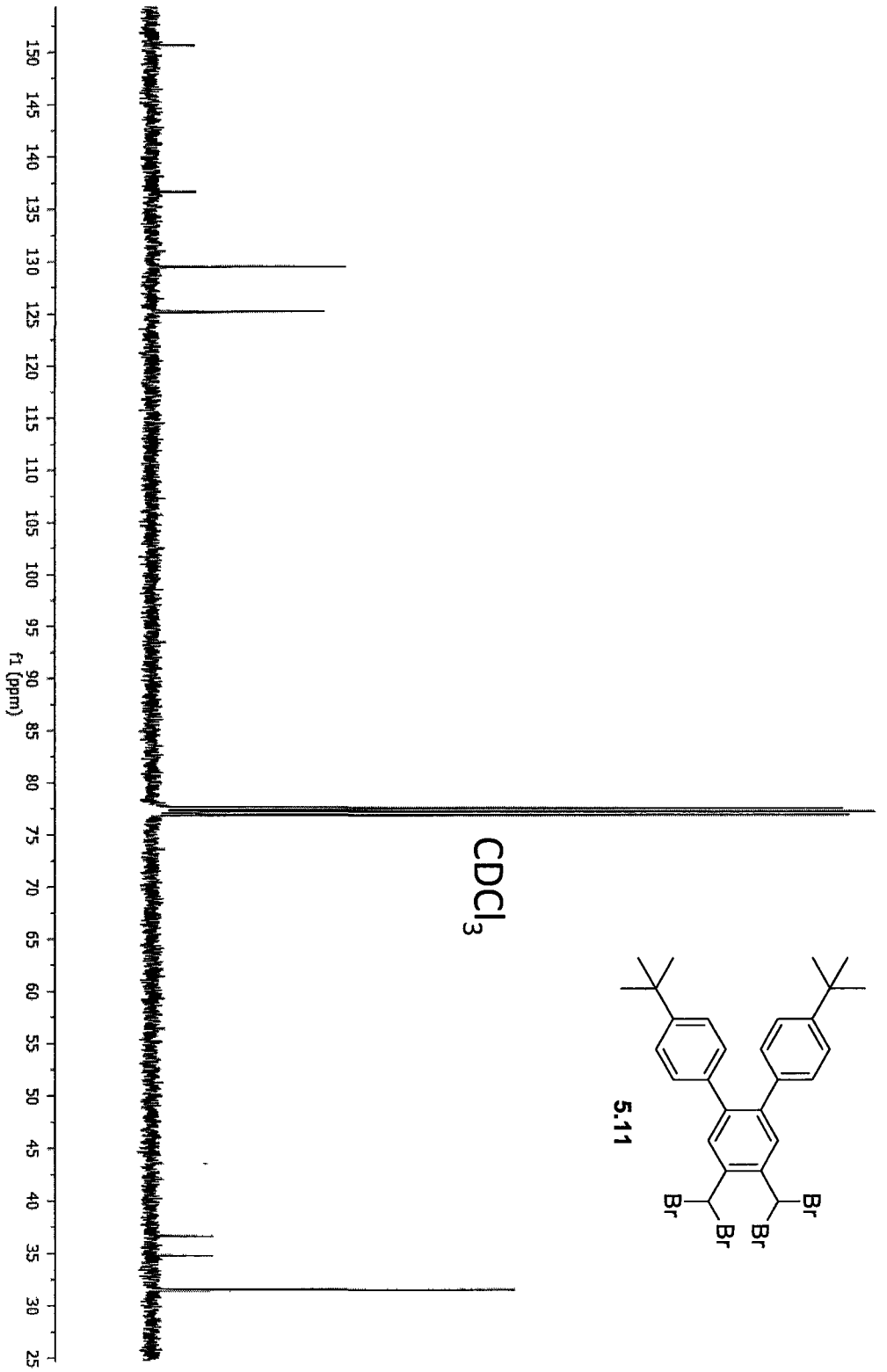
150 145 140 135 130 125 120 115 110 105 100 95 90 85 80 75 70 65 60 55 50 45 40 35 30 25
f1 (ppm)
CDCl3
5.11
Br
Br
Br
Br

^{1}H-NMR

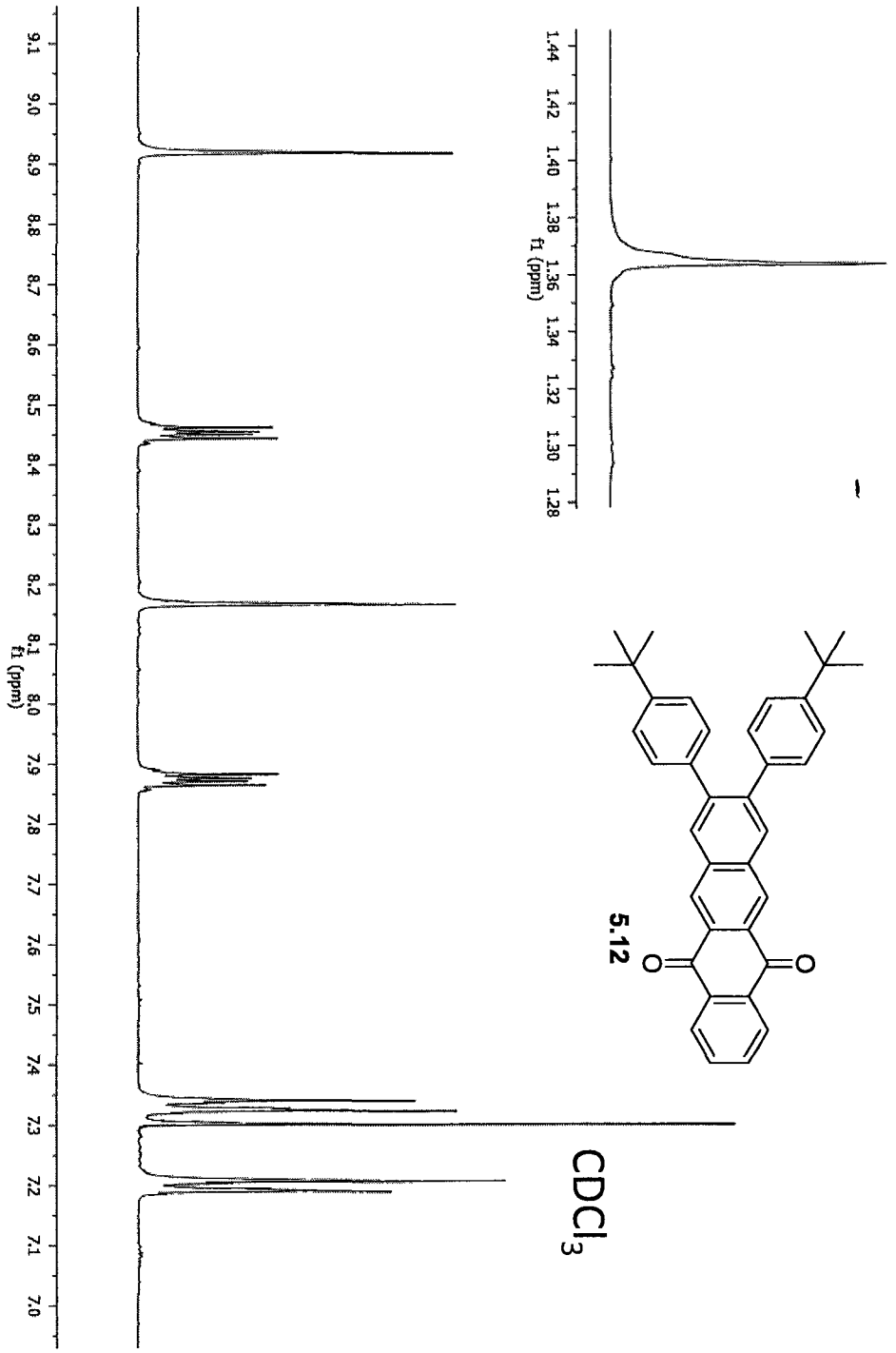
9.1
9.0
8.9
8.8
8.7
8.6
8.5
8.4
8.3
8.2
8.1
8.0
7.9
7.8
7.7
7.6
7.5
7.4
7.3
7.2
7.1
7.0
f1 (ppm)
1.44
1.42
1.40
1.38
1.36
1.34
1.32
1.30
1.28
f1 (ppm)
5.12
O
O
CDCl3

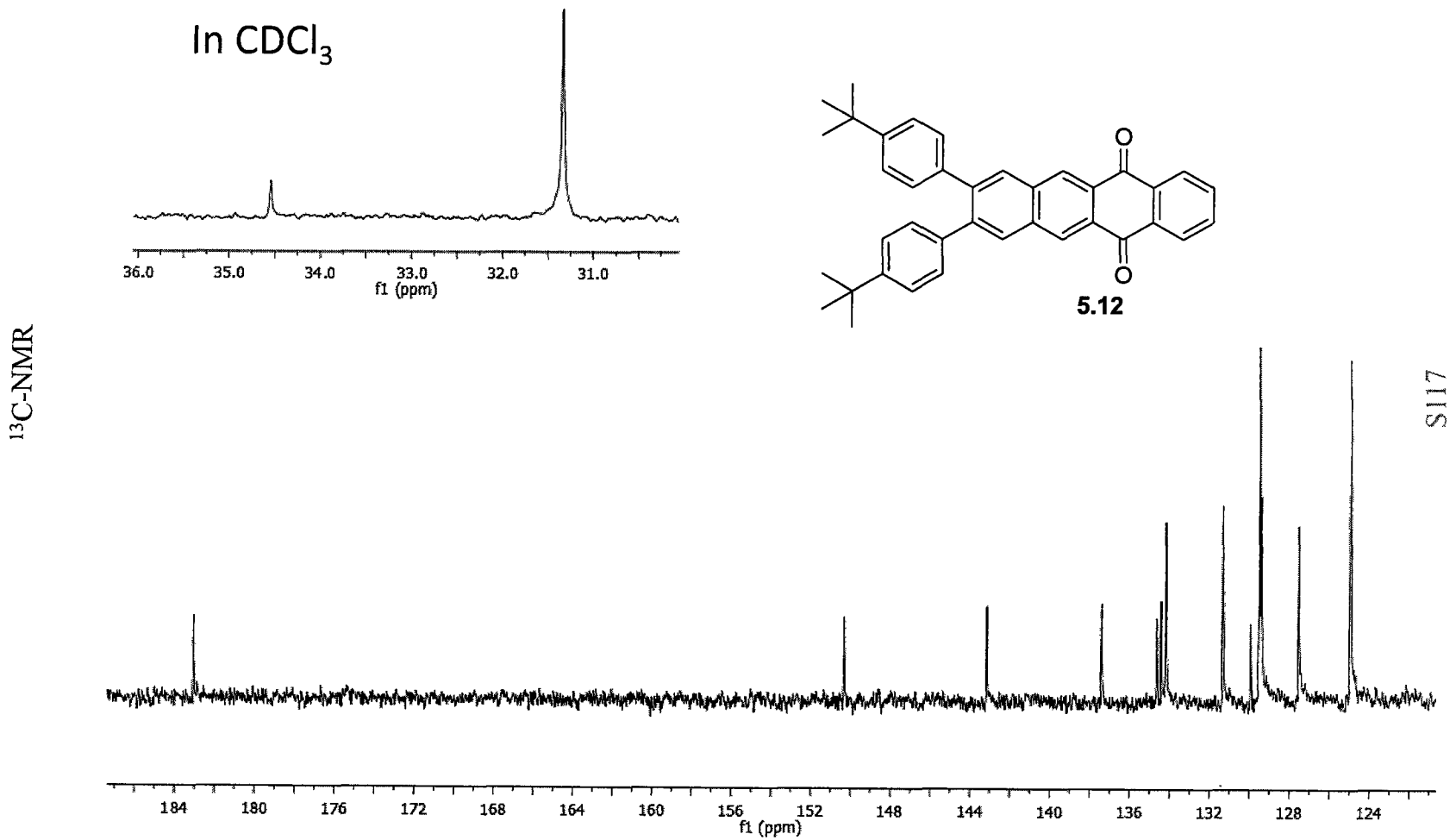
In $CDCl_3$
36.0
35.0
34.0
33.0
32.0
31.0
f1 (ppm)
O
O
5.12
^{13}C-NMR
S117
184
180
176
172
168
164
160
156
152
148
144
140
136
132
128
124
f1 (ppm)

^{1}H-NMR

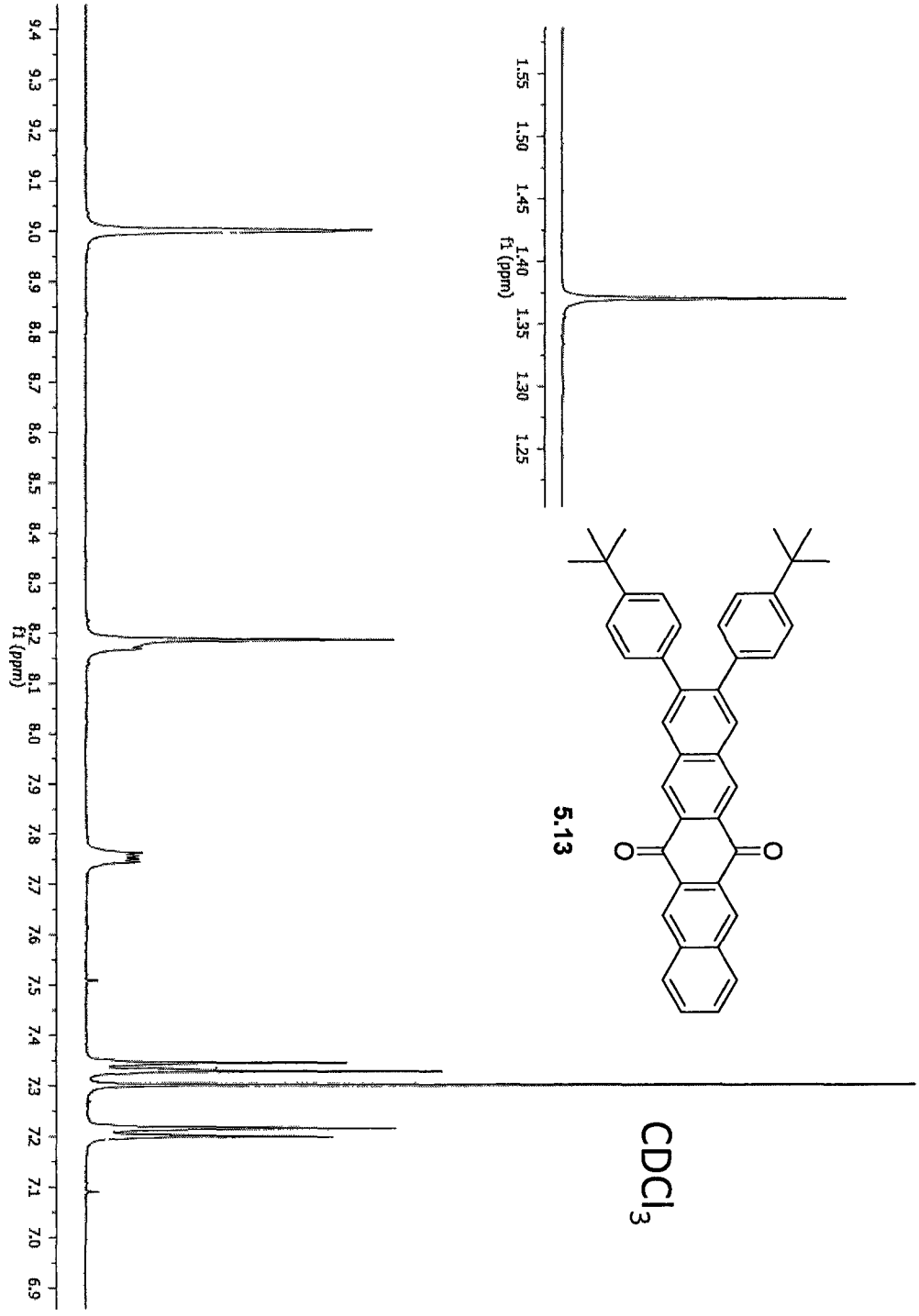
9.4
9.3
9.2
9.1
9.0
8.9
8.8
8.7
8.6
8.5
8.4
8.3
8.2
8.1
8.0
7.9
7.8
7.7
7.6
7.5
7.4
7.3
7.2
7.1
7.0
6.9
f1 (ppm)
1.55
1.50
1.45
1.40
1.35
1.30
1.25
f1 (ppm)
5.13
O
O
CDCl3

In $CDCl_3$

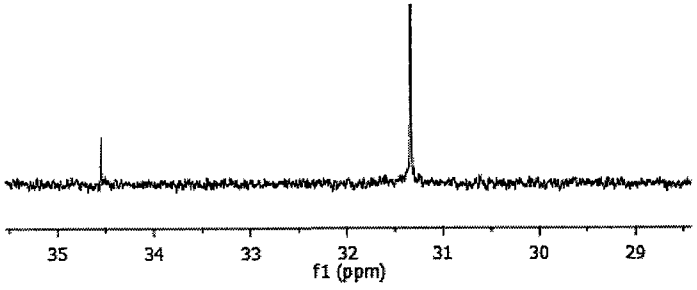

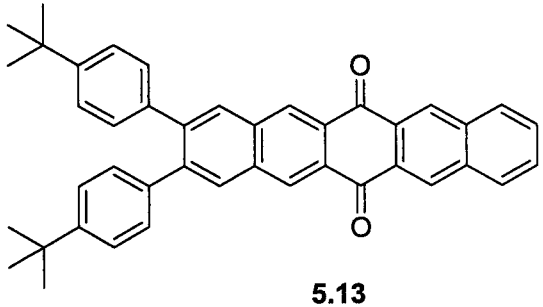

5.13

^{13}C-NMR

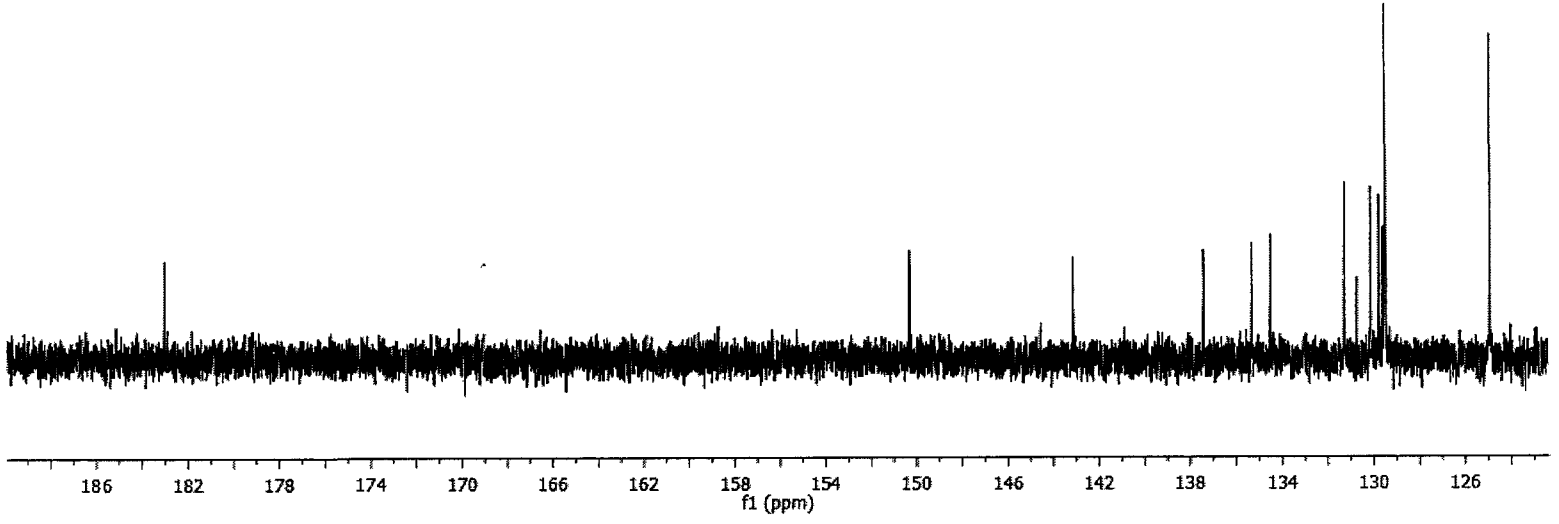

^{1}H-NMR

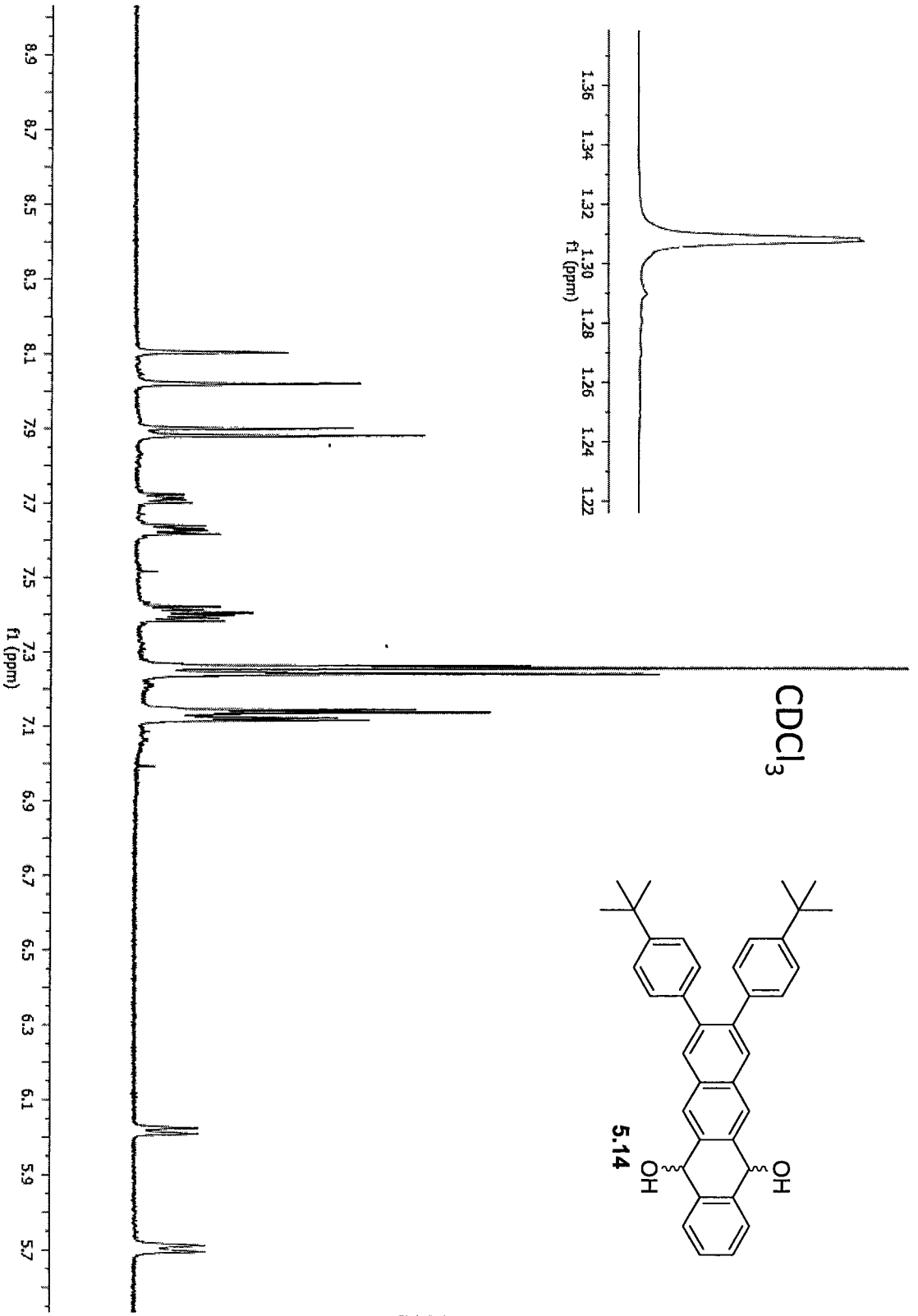

^{13}C-NMR

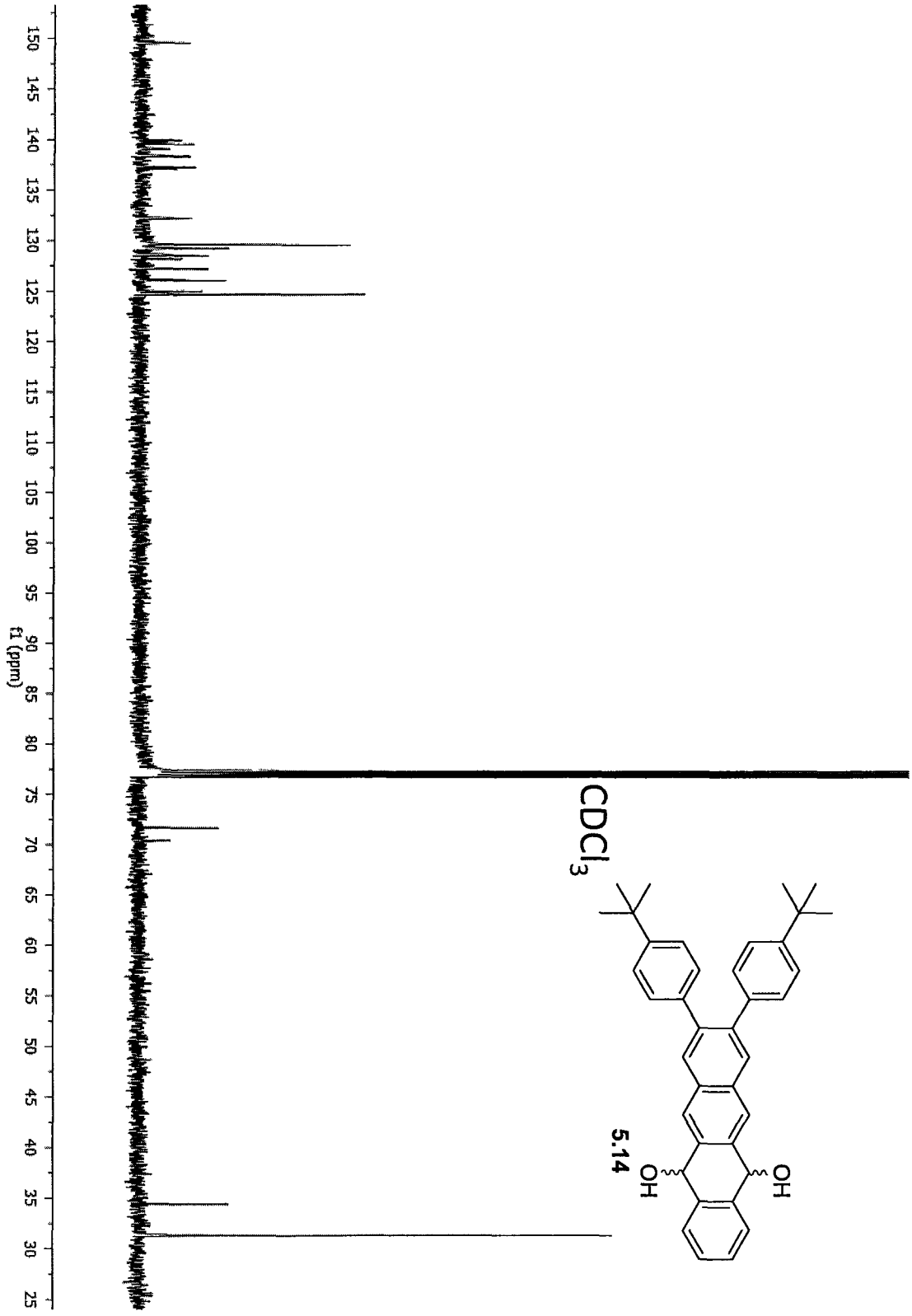
150
145
140
135
130
125
120
115
110
105
100
95
90
85
80
75
70
65
60
55
50
45
40
35
30
25
f1 (ppm)
CDCl3
5.14
OH
OH

^{1}H-NMR

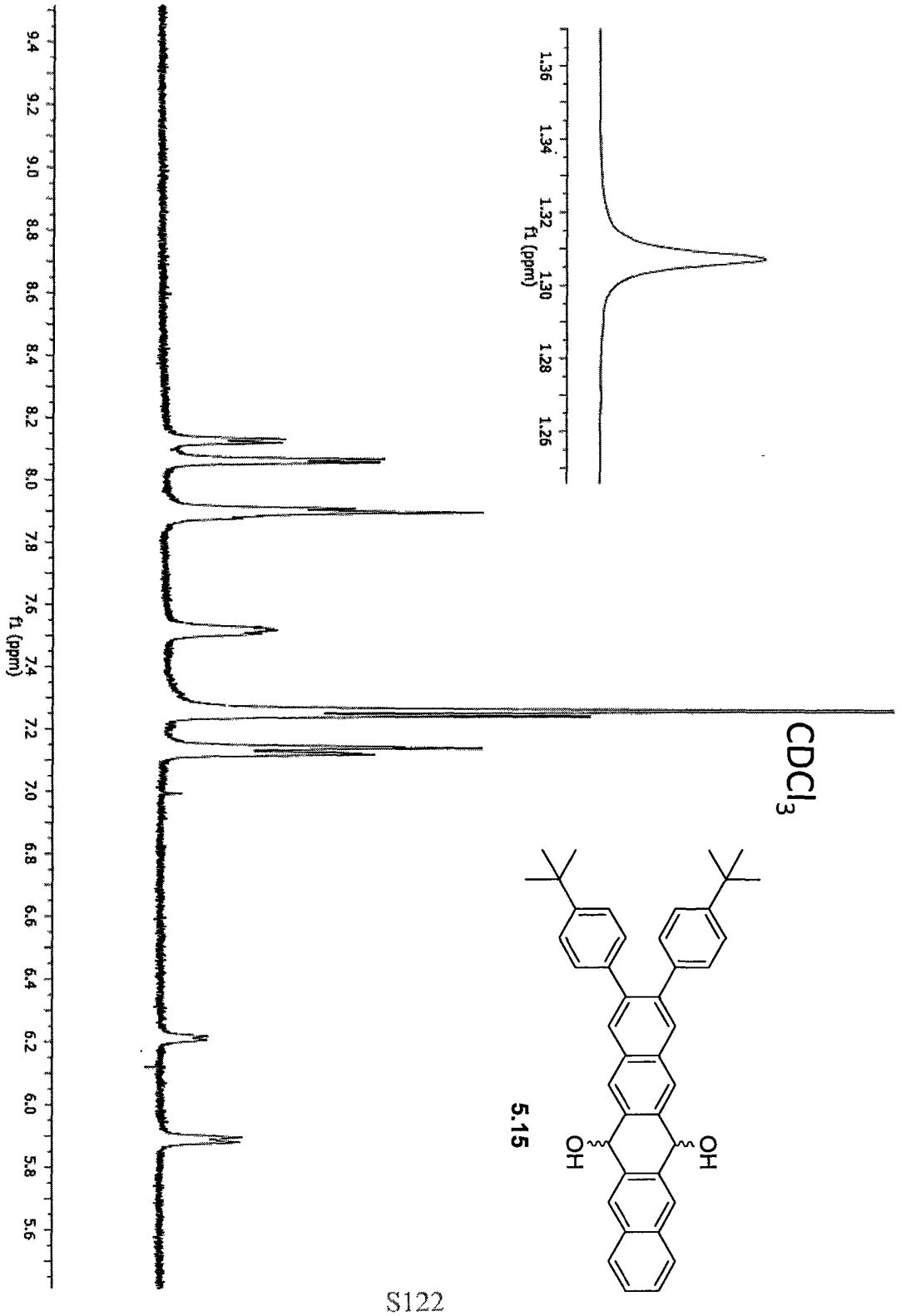

^{13}C-NMR

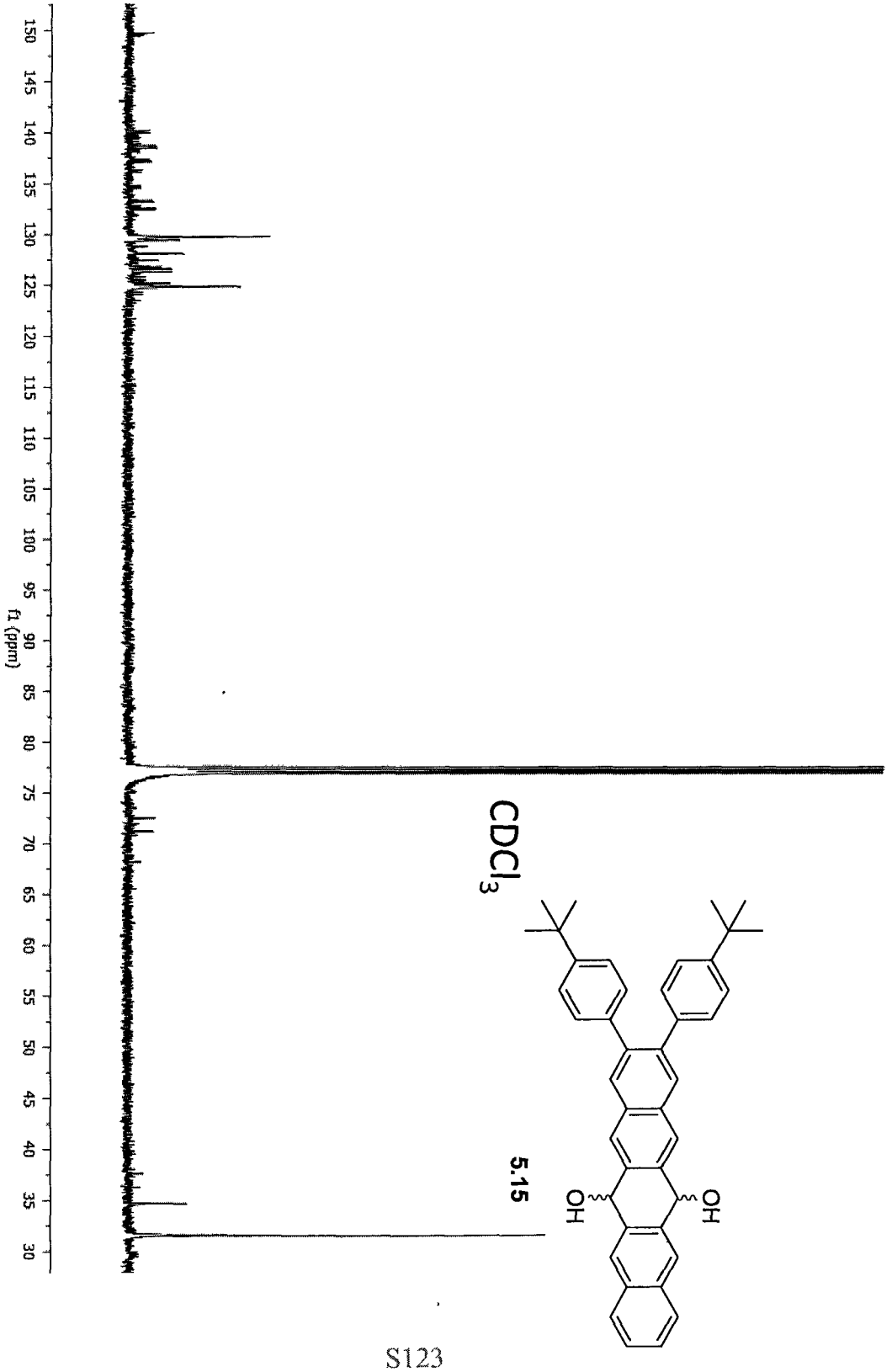
150
145
140
135
130
125
120
115
110
105
100
95
90
85
80
75
70
65
60
55
50
45
40
35
30
f1 (ppm)
CDCl3
5.15
OH
OH

^{1}H-NMR

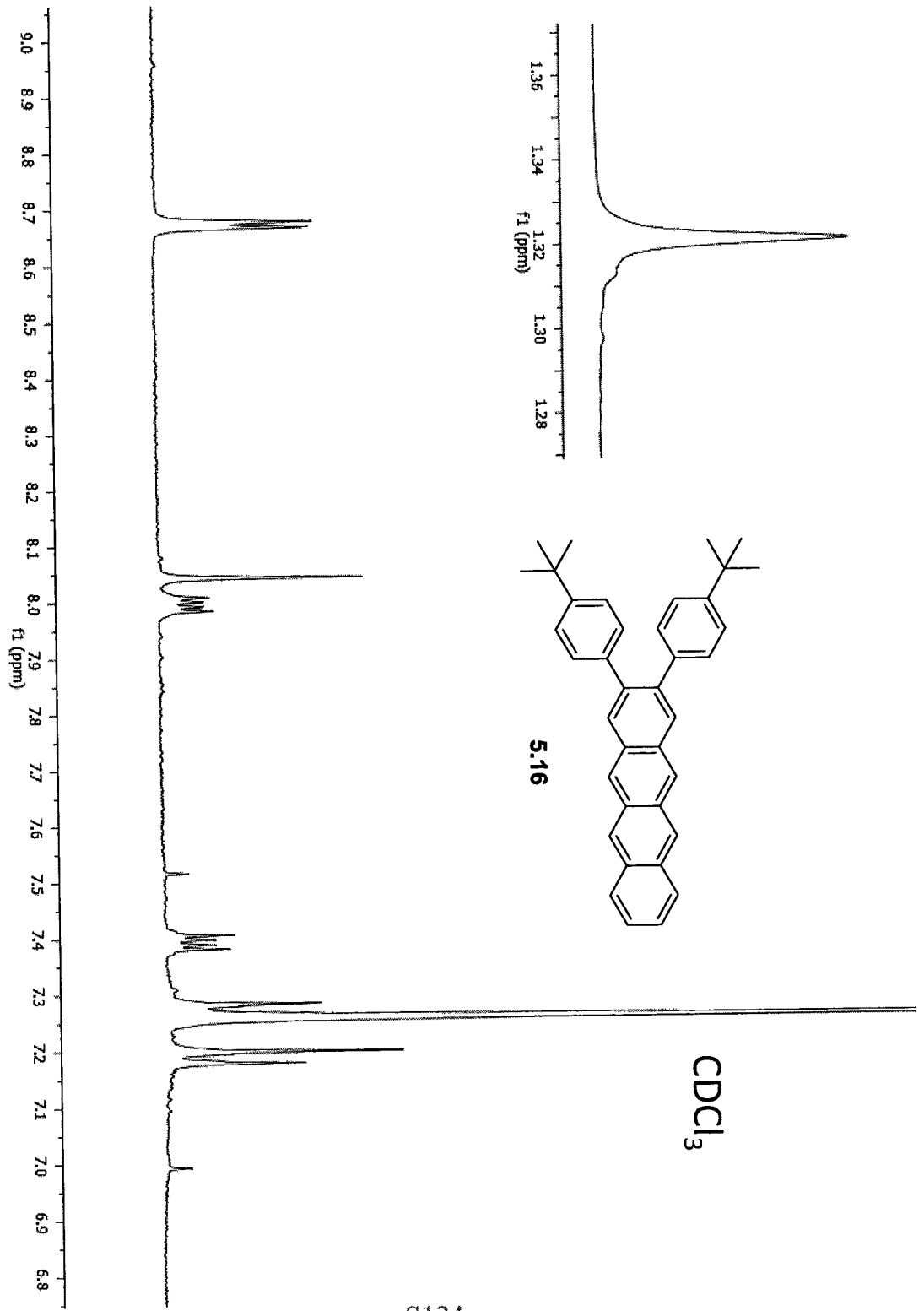
9.0
8.9
8.8
8.7
8.6
8.5
8.4
8.3
8.2
8.1
8.0
7.9
f1 (ppm)
7.8
7.7
7.6
7.5
7.4
7.3
7.2
7.1
7.0
6.9
6.8
1.36
1.34
1.32
f1 (ppm)
1.30
1.28
5.16
CDCl3

^{13}C-NMR

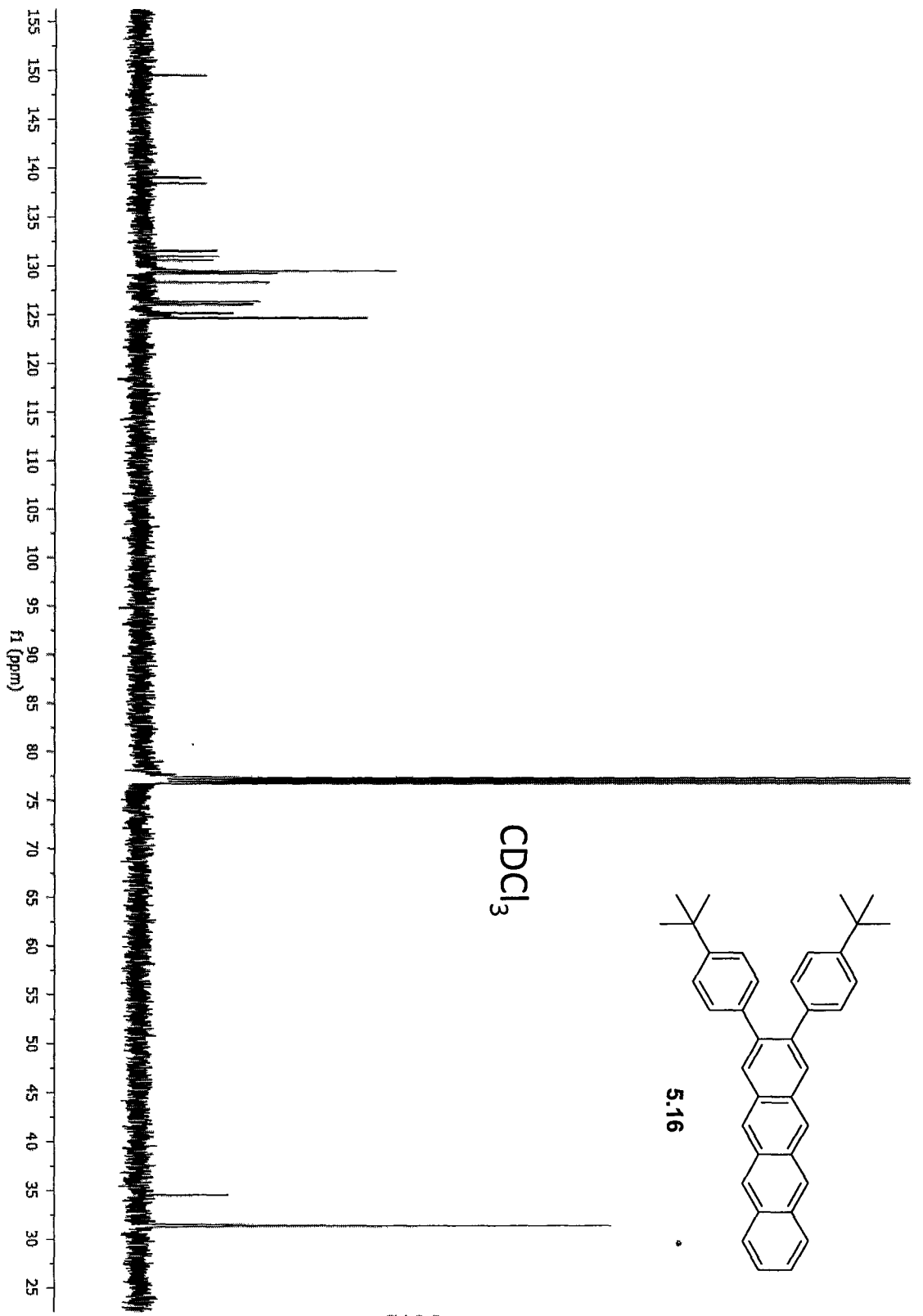
155 150 145 140 135 130 125 120 115 110 105 100 95 90 85 80 75 70 65 60 55 50 45 40 35 30 25
f1 (ppm)
CDCl3
5.16

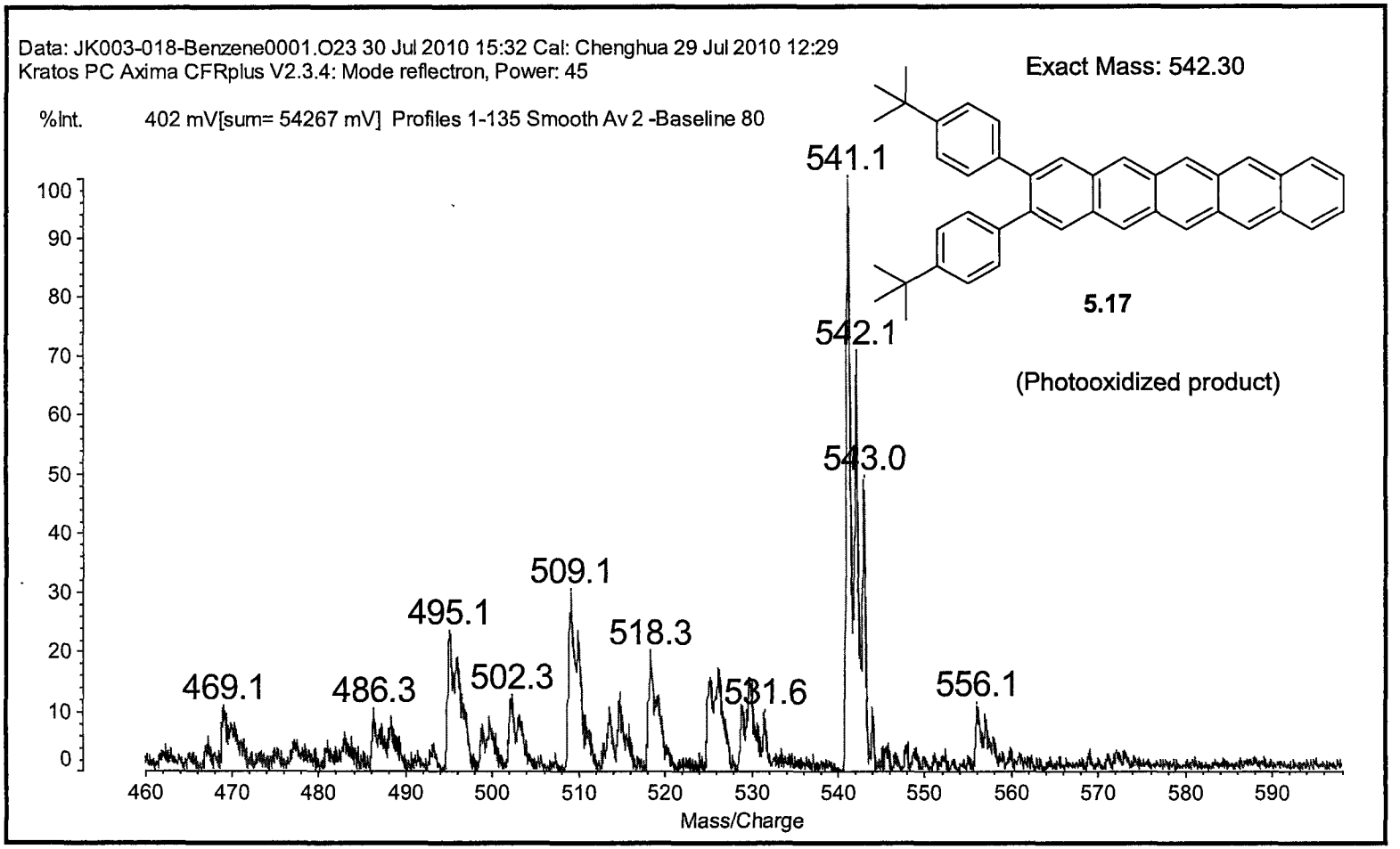
Data: JK003-018-Benzene0001.O23 30 Jul 2010 15:32 Cal: Chenghua 29 Jul 2010 12:29
Kratos PC Axima CFRplus V2.3.4: Mode reflectron, Power: 45
%Int.
402 mV[sum= 54267 mV] Profiles 1-135 Smooth Av 2 -Baseline 80
Exact Mass: 542.30
541.1
542.1
543.0
509.1
495.1
518.3
502.3
469.1
486.3
531.6
556.1
5.17
(Photooxidized product)
Mass Spec
Mass/Charge

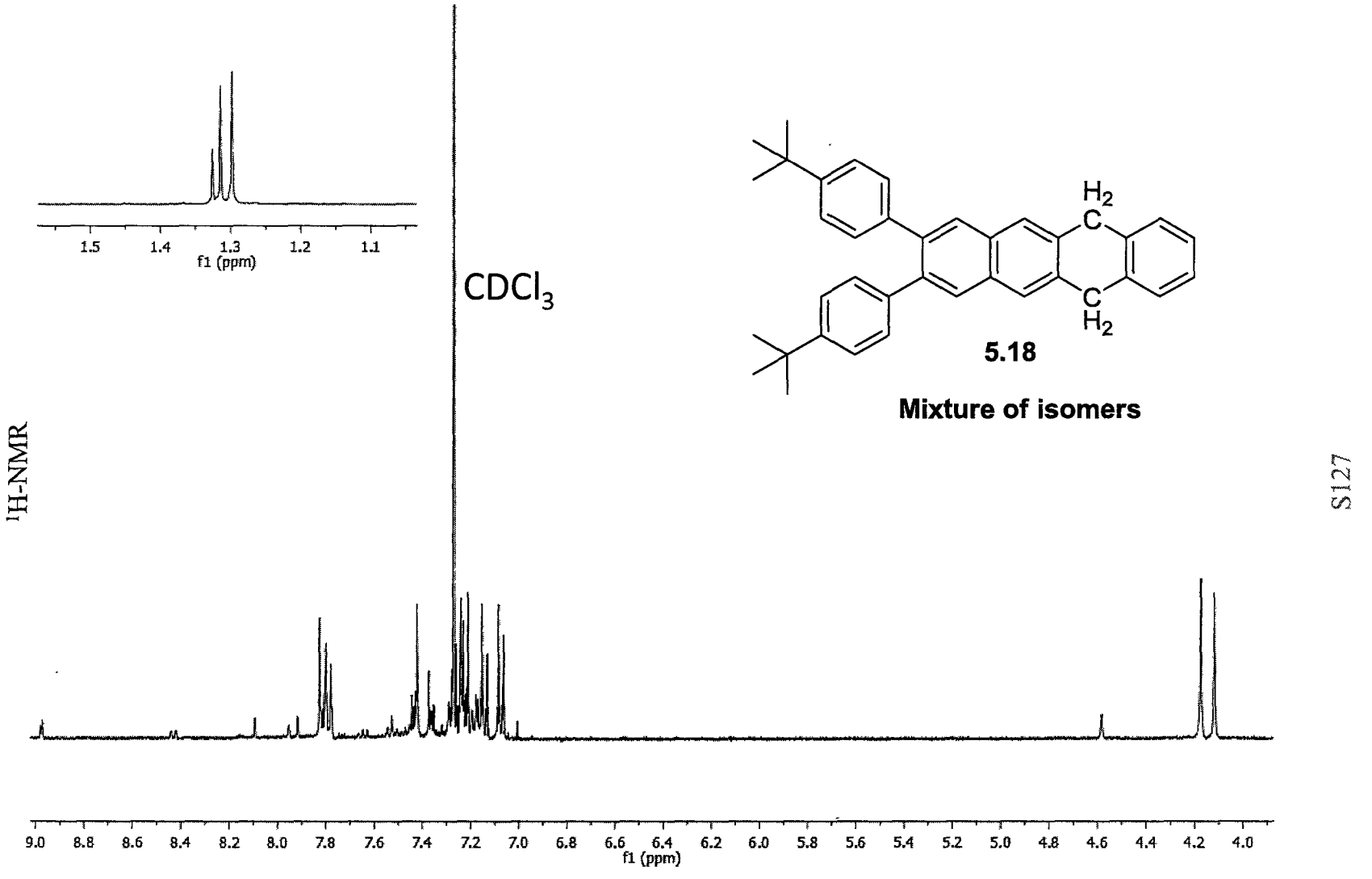
1.5
1.4
1.3
1.2
1.1
f1 (ppm)
CDCl3
H2
C
C
H2
5.18
Mixture of isomers
1H-NMR
9.0
8.8
8.6
8.4
8.2
8.0
7.8
7.6
7.4
7.2
7.0
6.8
6.6
6.4
6.2
6.0
5.8
5.6
5.4
5.2
5.0
4.8
4.6
4.4
4.2
4.0
f1 (ppm)

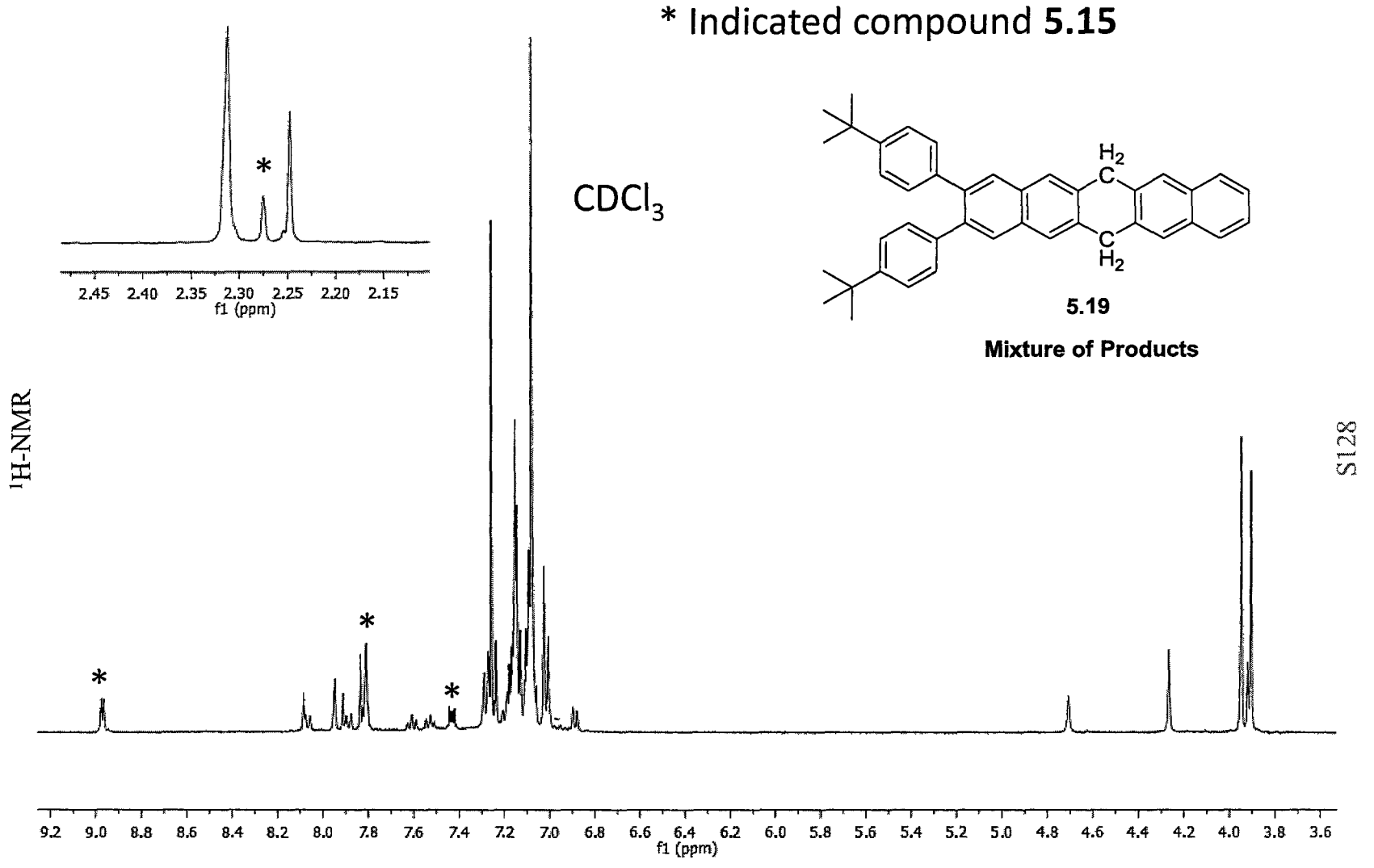
* Indicated compound 5.15
CDCl3
H2
C
C
H2
5.19
Mixture of Products
1H-NMR
S128
f1 (ppm)